

# Understanding the evolution of shell shape in snails

Jenny Larsson

A thesis submitted in partial fulfilment of the requirements for the degree of  
Doctor of Philosophy

**University of Sheffield**  
Faculty of Science  
Department of Animal and Plant Sciences

July 2021

## Acknowledgements

First, I want to thank my supervisors, Roger Butlin and Torbjörn Lundh, for their guidance, encouragement, and never ending optimism. I also want to thank all members of the multinational *Littorina* group for all the opportunities to learn new things, experience different scientific fields and methods, and communicate and collaborate across disciplines. In particular, a big thank you to Sean Stankowski for teaching me how to write better texts, and for all our interesting discussions.

I also want to thank all of my friends in Sheffield and around the world who made my time in Sheffield eventful and enjoyable. In particular, thanks to Martha Gibson for all the fun adventures, and for helping me keep my mind and body healthy. Also thank you to all the members of my Star Trek Adventures crew and my fellow Dungeons and Dragons adventurers, I have really been enjoying this new hobby of mine. And, as always, thank you to Ester Sandström for being a constant source of emotional support, as per agreement.

Last but not least, a big thank you to my parents for all their help and support throughout my life and this PhD, and for housing me during the pandemic years of 2020 and 2021.

## Abstract

The shape of snail shells is a complex and important factor contributing to their fitness, and needs to be adapted to different selection pressures in different environments. However, the link between form and function, and the evolutionary processes that create the wide diversity seen in the shell shape of gastropods, is still not fully understood. In order to connect the environmental adaptations of snail shells to phenotypic plasticity and genetics it is crucial to have quantification methods which relate to biologically relevant components. I therefore developed a high-throughput snail shell quantification method building on the classic ideas of Raup, which is able to describe the variability in shape and growth within two ecotypes of the intertidal snail species *Littorina saxatilis*. This method was also used to gain new insights into the genetic architecture involved in different aspects of shell shape in *L. saxatilis*, including detecting and describing allometric growth. As the quantification method directly describes how to construct computer generated shell models, I investigated whether and how shape affects the hydrodynamic properties of the shells. I performed flume experiments with both real shells and 3D printed shell models in water flow as well as computational fluid dynamics simulations. The results from the fluid dynamics analysis gave some new insight into how shape affects the optimal orientation against a steady current, but also suggests that foot size has a larger influence on attachment ability, and that the hydrodynamic efficiency of the shell is likely secondary to having a shape which can accommodate a large enough foot. In conclusion, a better quantification of shape and growth can lead to an improved understanding of how and why snail shells have the shape that they do, and how the shape relates to evolutionary processes such as local adaptation and speciation.

# Contents

|          |   |           |
|----------|---|-----------|
| <b>1</b> | <b>Introduction</b>   | <b>1</b>  |
| 1.1      | General Introduction . . . . .  | 1         |
| 1.2      | Modelling shells . . . . .  | 1         |
| 1.2.1    | Shape quantification . . . . .  | 5         |
| 1.3      | Littorina saxatilis . . . . .   | 9         |
| 1.4      | Adaptations, functions and fitness . . . . .  | 11        |
| 1.4.1    | Predator adaptations . . . . .  | 11        |
| 1.4.2    | Flow adaptations . . . . .  | 12        |
| 1.4.3    | Other adaptations . . . . .   | 15        |
| 1.5      | Shape: Genetics vs. plasticity . . . . .  | 15        |
| 1.6      | Summary . . . . .   | 17        |
| 1.7      | Thesis overview . . . . .   | 17        |
| 1.7.1    | Chapter 2 - Quantifying Shape in Shells . . . . .                                     | 17        |
| 1.7.2    | Chapter 3 - Genetic architecture of Shell Shape . . . . .                             | 18        |
| 1.7.3    | Chapter 4 - Hydrodynamical Effects of Shell Shape . . . . .                           | 18        |
| 1.7.4    | Chapter 5 - Discussion . . . . .  | 19        |
| 1.7.5    | Appendix E . . . . .  | 19        |
| 1.7.6    | Appendix F . . . . .  | 19        |
| <b>2</b> | <b>A developmentally descriptive method for quantifying shape in gastropod shells</b> | <b>20</b> |
| 2.1      | Introduction . . . . .  | 21        |
| 2.2      | The model . . . . .   | 23        |
| 2.3      | Sample collection and shell photography . . . . .                                     | 25        |
| 2.4      | Parameter Approximation Method . . . . .  | 26        |
| 2.5      | Statistical analysis . . . . .  | 29        |
| 2.6      | Results . . . . .   | 30        |
| 2.7      | Discussion . . . . .  | 35        |
| 2.8      | Acknowledgements . . . . .  | 38        |
| <b>3</b> | <b>Investigating the genetic architecture of shell shape</b>                          | <b>39</b> |
| 3.1      | Introduction . . . . .  | 40        |
| 3.2      | Methods . . . . .   | 42        |
| 3.2.1    | The F2 setup and genetic analysis . . . . .   | 42        |
| 3.2.2    | Geometric Morphometrics . . . . .   | 43        |

|          |  |            |
|----------|--|------------|
| 3.2.3    | Growth based method . . . . .  | 45         |
| 3.2.4    | Comparison of methods . . . . .  | 47         |
| 3.3      | Results . . . . .  | 47         |
| 3.3.1    | Geometric morphometrics . . . . .  | 47         |
| 3.3.2    | Growth parameters . . . . .  | 47         |
| 3.3.3    | Comparison of the shape descriptions . . . . .   | 52         |
| 3.4      | Discussion . . . . .   | 54         |
| <b>4</b> | <b>Hydrodynamical effects of shell shape for snails in flow with variable directionality</b> | <b>59</b>  |
| 4.1      | Introduction . . . . .   | 60         |
| 4.2      | Methods . . . . .  | 62         |
| 4.2.1    | Data . . . . .   | 62         |
| 4.2.2    | Simulations . . . . .  | 63         |
| 4.2.3    | Experimental setup . . . . .   | 66         |
| 4.2.4    | Statistics . . . . .   | 67         |
| 4.3      | Results . . . . .  | 68         |
| 4.3.1    | Foot size . . . . .  | 68         |
| 4.3.2    | Simulations . . . . .  | 69         |
| 4.3.3    | Experiment . . . . .   | 71         |
| 4.4      | Discussion . . . . .   | 75         |
| <b>5</b> | <b>Discussion</b>  | <b>80</b>  |
| 5.1      | Summary of findings . . . . .  | 80         |
| 5.1.1    | Chapter 2 - Quantifying Shape in Shells . . . . .  | 80         |
| 5.1.2    | Chapter 3 - Genetic architecture of Shell Shape . . . . .                                    | 81         |
| 5.1.3    | Chapter 4 - Hydrodynamical Effects of Shell Shape . . . . .                                  | 81         |
| 5.2      | Future work . . . . .  | 81         |
| 5.2.1    | Shell quantification . . . . .   | 81         |
| 5.2.2    | The 3D shell models . . . . .  | 82         |
| 5.2.3    | Future implications for <i>Littorina</i> research . . . . .                                  | 82         |
| 5.2.4    | Wider implications . . . . .   | 83         |
| 5.3      | Conclusion . . . . .   | 83         |
|          | <b>Bibliography</b>  | <b>83</b>  |
|          | <b>Appendices</b>  | <b>104</b> |
|          | <b>A ShellShaper</b>   | <b>105</b> |
|          | <b>B Chapter 2 supplementary material</b>  | <b>106</b> |
|          | <b>C Chapter 3 supplementary material</b>  | <b>107</b> |
|          | <b>D Chapter 4 supplementary material</b>  | <b>113</b> |

- E** Quantitative measures and 3D shell models reveal interactions between bands and their position on growing *Cepaea* shells 119
- F** Genetic variation for adaptive traits is associated with polymorphic inversions in *Littorina saxatilis* 146

# Chapter 1

## Introduction

### 1.1 General Introduction

Humans have long had a fascination for snail shells with their often self-similar shapes and intricate structure and patterns (figure 1.1). Despite their apparent complexity, it is possible to generate realistic-looking shell models displaying much of the diversity of shapes found in nature by taking advantage of relatively simple mathematical formulas which approximate the biological construction process. Gastropod shells have an accretionary growth method, meaning that the shell is constructed by the snail depositing shell material at the current aperture as it grows, which incrementally increases the protected living space within the shell. This is typically done in a roughly self-similar spiral growth pattern, making it possible for the snail to keep growing inside a shell which increases in size but stays roughly the same shape, while taking advantage of the previously constructed parts and minimising the material needed for further construction. Not only does the final shape contain information about the ontogenetic growth process, shells also preserve well as fossils, making them a unique resource for studying developmental processes and how they vary over evolutionary time scales (Hammer and Bucher, 2005; Giokas et al., 2014).

Investigations of the functionality of shell shape in relation to ecology require a biologically relevant quantification (Løvtrup and Løvtrup, 1988; Hammer and Bucher, 2005), which needs to be accessible to a wide range of conchologists without requiring a strong mathematical background (Liew and Schilthuizen, 2016). A good quantification of morphology should be able to distinguish between different components of shape and growth in a biologically relevant way, and thus improve the understanding of trade-offs between adaptations to different ecological features, since there tend to be multiple different natural selection processes acting at any one time (DeWitt et al., 2000; Tandler et al., 2015).

### 1.2 Modelling shells

Describing gastropod shell growth by a logarithmic helico-spiral with a generating curve has a long history, and can be traced back to Moseley in the mid 1800's (Moseley, 1838), where some formulas for area and volume of the shells were derived. The spiral growth of shells is also described in D'Arcy Thompson's famous book 'On Growth and Form' (figure 1.2a) (Thompson, 1917), in which he also suggested that the same accretionary growth pattern can



**Figure 1.1:** A cross-section of a *Neptunea antiqua* (red whelk) shell, showing its internal structure. The size of each consecutive whorl increases by a constant factor throughout its growth, giving the shell its characteristic self-similar spiral shape.

be found in e.g. animal horns. In the same book Thompson also introduced the shape transformation grids which were the precursor to what is now known as geometric morphometrics (figure 1.2b).

With the emergence of computers, the ability to construct and visualise a wide variety of shell forms using the logarithmic helico-spiral growth became possible. Raup made good use of this early on, with his famous parametric description and quantification during the 1960's, which led to the introduction and investigation of the morphospace (figure 1.3) (Raup, 1966). The morphospace, or shape space, is not just useful for quantifying and comparing the shapes found in nature, it is also helpful in finding which combinations of parameters give shapes that are not present in the wild, which helps in understanding the limiting factors for these types of shape.

Further additions to Raup's growth parameter models were developed, and were able to describe and visualise a larger range of shell types (Savazzi, 1985). An important addition to the shell models was to use apertures that are not perpendicular to the vertical axis, but instead to use the Frenet frame to define the apertural plane perpendicular to the growth direction (figure 1.4a) (Illert, 1989). The true orientation of the apertures is often constructed by the snails to be parallel to the substrate and not defined by the growth direction (Linsley, 1977), but using the Frenet frame gives a more realistic representation for most shells than the previously used orientation with the apertures parallel with the coiling axis. A large extension to Raup's description is the 16 parameter model of Cortie, which also allows shell sculptures, different aperture tilts and elliptical apertures of varying eccentricity and orientation, or even freely defined aperture shapes (Cortie, 1989). In addition to modelling the general shape and growth, realistic colour and ornamental patterns, such as those found in *Conus* shells (figure 1.4b), can be simulated by including a reaction-diffusion system (Meinhardt and Klingler, 1987; Fowler et al., 1992). Models with many parameters, such as Cortie's can be used to generate an impressive range of shapes, but that also means that they are less practical

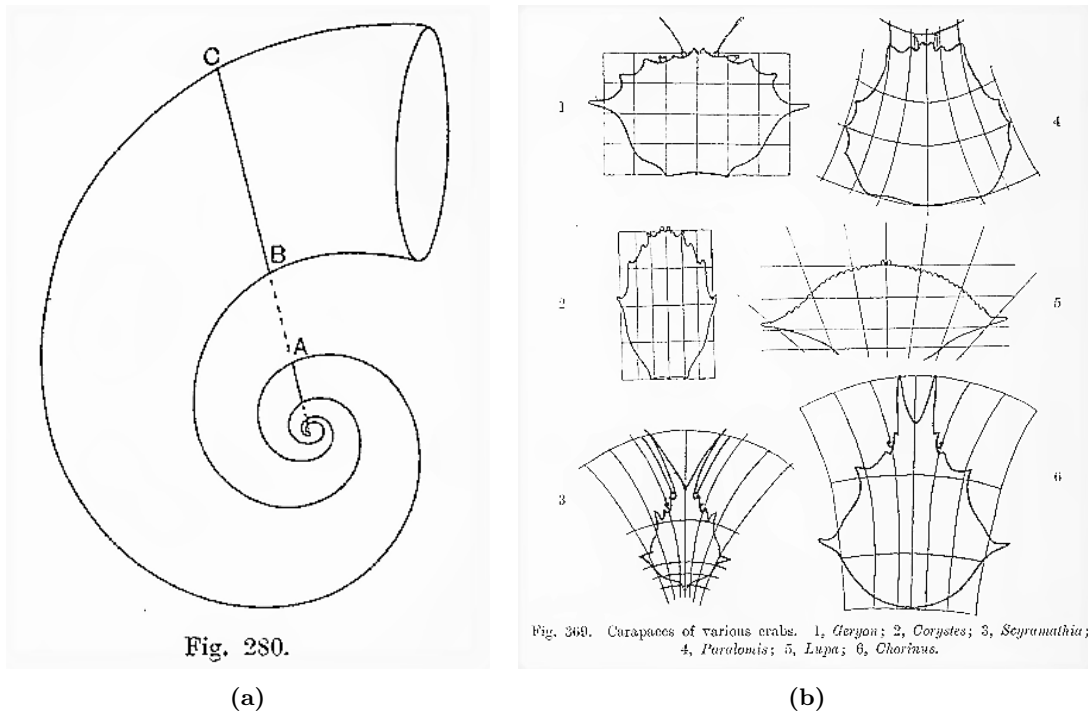
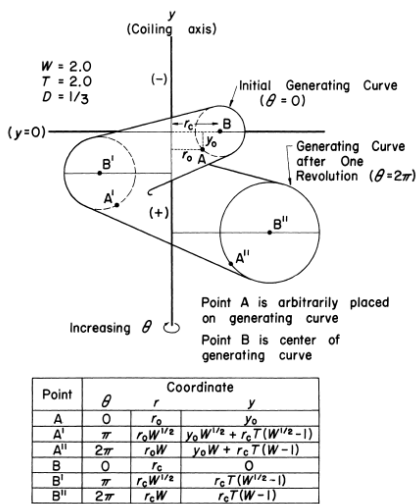
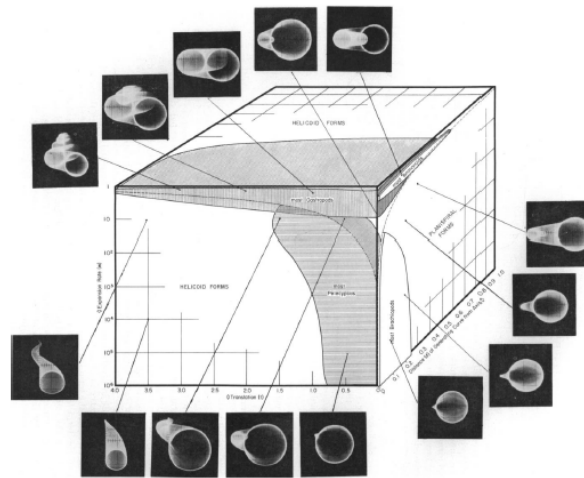


**Figure 1.2:** Images from Thompson’s 1917 book (Thompson, 1917). (a) A representation of growth along a logarithmic spiral trajectory. (b) Transformation grids showing the variation in carapace shape between different species of crabs. (Public domain images, copyright expired.)



TEXT-FIG. 1.—One whorl of a hypothetical coiled shell in cylindrical coordinates.

(a)



TEXT-FIG. 4.—Three dimensional block illustrating the spectrum of possible shell forms. The shape of the generating curve is assumed to be constant. The regions occupied by the majority of species in four taxonomic groups are outlined in the block. Species of these groups are not commonly found in the blank regions of the block.

(b)

**Figure 1.3:** Raup made the first systematic quantification of shell shape in terms of growth (Raup, 1966). (a) A visual description of the shape parameters. (b) Visualisations of various shell shapes, and their position in the morphospace. Images reproduced with permission from publisher.

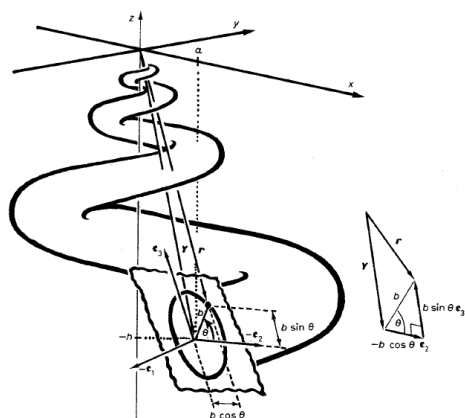
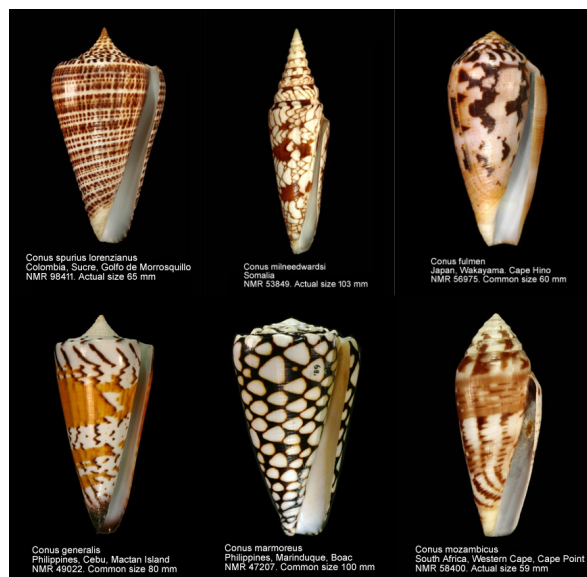


Fig. 4. – Frenet coordinates provide a natural way of describing orthoconical growth rings on tubular coiled seashell surfaces. Equation (6), for the shell aperture which lies in the  $(\mathbf{e}_2, \mathbf{e}_3)$ -plane, is a simple vectorial addition;  $\mathbf{r} = Y - b \cos \theta \mathbf{e}_2 + b \sin \theta \mathbf{e}_3$ .

(a)



(b)

**Figure 1.4:** Additions to computer visualisations of shells. (a) Illert suggested using the Frenet frame for more realistic aperture orientations perpendicular to the direction of growth. Image from Illert (1989) reproduced with permission from publisher. (b) A set of photos of *Conus* shells showcasing their variability in colour patterns and spire profiles. Examples of concave, straight, and convex growth patterns from left to right in both rows. Reaction-diffusion systems can be used to model pattern formation on the shell surfaces, see examples in Fowler et al. (1992). Photos obtained from the WoRMS open access database (WoRMS Editorial Board, 2021), reproduced under CC-BY-NC-SA licence.

to use for shape quantification, as inferring the values of a larger number of convoluted parameters increases the risk of over-fitting and decreases the accuracy and replicability of the inferred parameter values.

Developmental allometry is the study of how shape, or other biological traits, vary with size as an organism grows, and is of great interest in developmental biology in general, and in modelling the growth of shells in particular (Urdu et al., 2010b; Schindel, 1990; Urdu et al., 2010a). Not all shells conform to a true logarithmic helicospiral growth, and already in his 1917 book Thompson noted that some grew in a convex or concave fashion (Thompson, 1917). To be able to capture different types of shape variation during growth, several possible options to extend the abilities of Raup’s original models have been introduced. A common idea first presented by Raup himself (Raup, 1961), is to let the growth parameter vary in different ways during the construction, while another method is to introduce more growth parameters describing different components of growth, i.e. vertical and radial growth, but keep their values constant (Ashline et al., 2009; Fowler et al., 1992; Van Osselaer and Grosjean, 2000), or combining the two approaches and both including more parameters as well as letting them vary throughout growth (Schindel, 1990; Stone, 1995). Depending on the study species, and the properties of interest, different models could be used in different cases, but it is clear that to understand variation in shell shape, an investigation into allometric changes needs to be

included.

Most of the growth based modelling of snail shells can be described as one of two different types: The fixed reference frame models with a global growth quantification and coordinate system, and the moving reference frame models with local growth quantification and coordinate system at the current aperture (Urdu et al., 2010a). The modelling methods build on Raup's models described above are examples of using a fixed reference frame, which assumes a predefined coiling axis and logarithmic spiral growth relative to this axis. In contrast, a local quantification does not describe growth relative to an external structure, but is defined by the local growth trajectories relative to the current aperture, and this reference frame therefore moves as the shell construction progresses. Despite the coiling axis being an artificial construction not representing an actual biological structure (Okamoto, 1996), it can still emerge together with the logarithmic growth patterns as features under certain conditions of the local growth modelling (Moulton and Goriely, 2014; Savazzi, 1990).

Different versions of local growth models include the growing tube model, which uses a theoretical internal reference point for the aperture growth (Okamoto, 1988b; Savazzi, 1990), and the growth vector model which describes the growth locally at each point of the aperture (Hammer and Bucher, 2005; Urdu et al., 2010b). Local growth can be quantified by translation, dilation, and rotation of the aperture (Ackerly, 1989; Moulton and Goriely, 2014), and has been suggested to be more biologically representative than the fixed reference frame since this better describes the construction process from the viewpoint of the animal inside (Urdu et al., 2010a; Rice, 1998). It has also been shown to have greater flexibility in the types of shells it can describe, including e.g. the complex growth patterns of heteromorph ammonites (Okamoto, 1988a; Savazzi, 1990), since it does not rely on a fixed reference frame. These models can also be used to model the emergence of spines through mechanical interactions between shell and snail (Chirat et al., 2013) and they allow for allometric variations such as convex and concave growth patterns (Rice, 1998; Urdu et al., 2010a).

There are of course other examples of shell modelling methods, often specific to a certain type of visualisation or for investigating a specific aspect of shell growth, and comparisons of many of the existing models can be found in the reviews (Stone, 1996; Dera et al., 2008; Urdu et al., 2010a). An interesting example of a different shell modelling procedure is the road-holding model which is built on the idea that the shape of the previous whorl determines the growth of the next whorl (Hutchinson, 1989). The road-holding method has some support from experimental results showing that the snail reacts to the shape or patterns of the previous whorl when constructing its shell (Checa et al., 1998; Boettiger et al., 2009).

### 1.2.1 Shape quantification

Quantifying shape accurately and in a way that is relevant to a particular field of study is one of the current problems in biology in general, and quantitative genetics in particular (Klingenberg, 2010; Fu et al., 2018). Shape itself is a complex trait, and can be affected by many different genetic and environmental factors. Hence finding an informative quantification which connects to the formation and functions should improve the ability to draw conclusions across the fields of ecological, evolutionary, and developmental biology.

The most commonly used shape quantification methods for gastropod shells are landmark-based geometric morphometrics (GM) (Bookstein, 1992; Dryden and Mardia, 1998; Rohlf and Slice, 1990), outline analysis (Kuhl and Giardina, 1982), and linear measurements and

ratios, which includes different versions of growth based methods. The GM method analyses how a set of homologous points, i.e. points representing the same biological position, vary between a set of specimens. The outline analysis instead quantifies the variation of the entire outline of the structure, removing the need for finding homologous points, but cannot say anything about variation within the outline or how specific points vary between specimens. The linear measurements method is methodologically the simplest of the methods discussed here, as it only requires the measurement of a set of linear distances of each specimen, from these measurements it is easy to calculate ratios, which can be used as approximations of parameters introduced by Raup.

The general conclusion in comparisons between the accuracy and practicality of the methods above has been that they all are able to quantify and describe the main shape variation for the shells, and one should therefore choose the method which best fits the purpose of a study, and the information required (Stone, 1996, 1998; Walker and Grahame, 2011; Dommergues et al., 2003). For example, some studies are mainly about finding the largest differences between samples to characterise the distinguishing features or to classify specimens into distinct groups. However, a good developmentally informative quantification method should be able to do more, and will likely improve both analyses and interpretations since it describes the shell in a way that relates to its biological growth process (Løvtrup and Løvtrup, 1988; Hammer and Bucher, 2005; Cortie, 1992). Currently, such a method of quantifying shell shapes consistently for large data sets is lacking, in particular when apertures have variable and non-circular shapes, which is why I developed the method presented in chapter 2.

Despite the benefits of a model which describes both shape and development, which is possible for gastropod shells, growth-based quantifications have not been the standard method used for empirical studies. The method of choice has instead been landmark-based geometric morphometrics. This method uses Procrustes superposition to do rigid translation, rotation and scaling of the set of landmark points of each specimen to minimise the overall distance between the corresponding landmarks (Bookstein, 1992), and projects the data to the tangent space (Dryden and Mardia, 1998). The projection is usually followed by a principal component analysis to summarise the shape variability into a small number of factors explaining most of the variation (figure 1.5), or analysed through regression against a specific known trait or an environmental factor. A standard software for acquisition of landmark data from 2D images is tpsDig2 (Rohlf, 2015), and common examples of software for the analysis of landmark data are the various programs of the tps series, e.g. tpsUtil, (Rohlf, 2015), the free-standing and versatile program MorphoJ (Klingenberg, 2011), and the R package geomorph (Adams et al., 2019). The GM method is widely used in different fields within biology because it is so generally applicable, and it has paved the way for many interesting results where quantitative traits are investigated.

The main reasons for choosing this method over a growth based one is the shorter learning curve needed since the user does not need as much mathematical proficiency, and the fact that it is already implemented to consistently handle large data sets. Current research often needs very high throughput methods in order to quantitatively link phenotype with genotype in e.g. QTL-analyses, and such a method has been lacking in the case of growth-based quantification of shells.

The three biggest problems with using the standard 2D GM methods to analyse gastropod shells specifically are: 1) the lack of truly homologous points on shells, 2) issues relating to correctly accounting for different allometric effects (Urduy et al., 2010a), and 3) the general

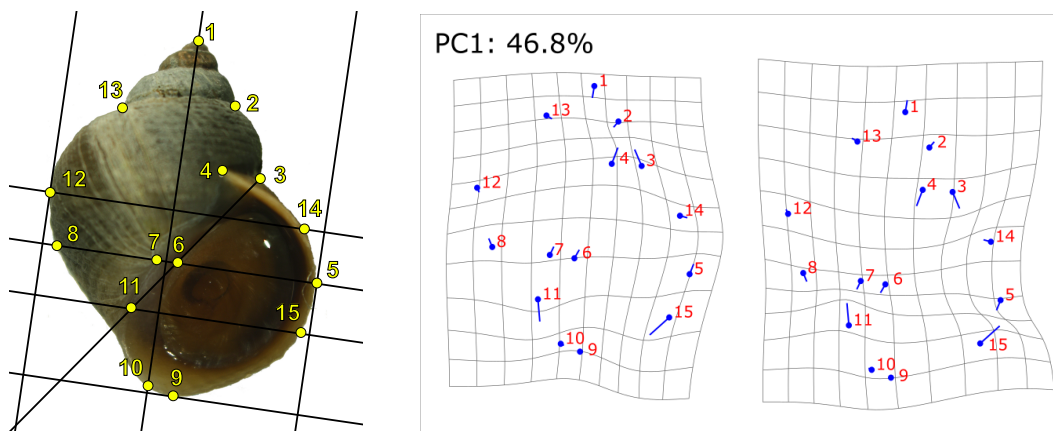


**Figure 1.5:** Example of landmark positions used for GM analysis of gastropod shells, and the transformation grids visualising the shape variation corresponding to the first principal component which explain almost half of the total variation in landmark position found in the analysed set.

problem that describing any 3D growth pattern by variations in a 2D plane will likely miss important details (Cardini, 2014). GM works best for expansive growth, where homologous points follow growth trajectories largely within the 2D imaging plane, but snail shells famously do not conform to this method of growth. A 3D GM method would not solve the two first problems since it does not provide additional homologous structures, and the landmarks would be even harder to define consistently on the shell surface due to the extra dimension. The inherent incompatibilities of using the GM method to account for the growth pattern of shells could be solved by replacing this method with a well constructed growth-based quantification. Further, the results from a GM method are defined relative to the mean landmark position of all shapes included in the analysed set, and then usually involve a PCA to quantify the largest correlated variations, which results in components which are not necessarily describing distinct or functional shape traits (Cooke and Terhune, 2015). Since the scores from a GM PCA for a given specimen will vary depending on the data set as a whole, it is not straightforward to compare results between data sets. A growth-based method has the additional advantage that the shape data are intrinsically described, meaning that each parameter consistently describes the same thing independently of the data set, i.e. the shape parameters inferred for a shell will have the same values independently of the rest of the data set, and results are thus comparable directly between samples.

Raup's parameters, or versions thereof, have been used to describe shape variation in several species of snail shells (Vermeij, 1971; Newkirk and Doyle, 1975; Kohn and Riggs, 1975; Verduin, 1982; Ekaratne and Crisp, 1983; Urabe, 1998; Walker and Grahame, 2011). The morphospace associated with these parameters has been explored and some general conclusions have been drawn, e.g. about which parts of the space are occupied by certain types of shells, and which parameter combinations do not give rise to biologically feasible shapes (figure 1.3b). One important point is that growth parameters are likely to be highly correlated, as otherwise the shells can become detached from the previous whorl, or obtain other non-functional or non-optimal shapes (Schindel, 1990). The connectedness of the shell is not a universal

constraint, however, since for example shells like those of the heteromorph ammonites exist (Okamoto, 1988b), which are neither attached to previously constructed material nor have a fixed coiling axis. There are also examples of inferring growth parameters from shells in 3D, e.g. from  $\mu$ -CT scans (Monnet et al., 2009; Liew and Schilthuizen, 2016), which can be used when few samples are investigated in great detail, but is not currently applicable to investigate large data sets due to the cost and time consumption of acquiring and analysing 3D data.

The reason snail shells can be quantified using logarithmic helicospirals is that many are very close to self-similar, which is one of the reasons they are so fascinating. However, the departure from perfect self-similarity is also something that can be quantified and studied (Urduy et al., 2010a), and, when present, could relate to different biological functions or ecological factors. With a growth based method it is possible to account for some specific types of allometry, the simplest being variable degrees of convex or concave spire profiles.

A shorter spire could give a stronger shell because the smaller and weaker whorls are more hidden (Seeley, 1986). This is an example of where a convex growth pattern could emerge as an adaptation, especially when overall growth is large, so that the previous whorls are much smaller and thinner than the more recent ones. In contrast, increased aperture area combined with a taller spire has been suggested as a plastic allometric response to an increased availability of food (Saura et al., 2012), which could be due to a more concave growth pattern. However, more analyses would be needed to specifically investigate if the allometric variation in different species can be explained by a convex/concave growth pattern. In this thesis I therefore investigate the possibility for a convex/concave growth pattern in *L. saxatilis*, and if it can be attributed to a genetic component (chapter 3).

In addition to having a more biologically relevant shape and growth description of snail shells, a growth based method can yield 3D models which in turn can be used for further analysis. Such models have been used to investigate how internal space, allometry and stability depend on different parameter values and aperture tilts (Noshita et al., 2012; Urduy et al., 2010b), how shell thickness affects what shape requires the least amount of material to produce (Heath, 1985; Okabe and Yoshimura, 2017), or used in simulations for measuring the shell strength (Rajabi et al., 2014; Shojaei et al., 2012). It is also possible to use the parameters generating the 3D models as a step towards a local growth description at the aperture (Noshita, 2014), as the local description is less straight-forward to obtain from 2D images. The local growth quantification describes construction of the shells from the viewpoint of the snail, which could give additional insights into development, and has been used to relate gene expression in the mantle to shell growth (Noshita et al., 2016).

One of the current aims of quantitative genetics is finding biologically relevant descriptions in order to better relate phenotypes with genotypes. The goal is to be able to consistently quantify distinct aspects of form and development to use as the connection between biological functions, environmental adaptations, and the underlying genetics. Since a growth-based method allows for a developmentally descriptive quantification in the case of gastropod shells, unlike the current GM method, its implementation should improve the ability to answer questions regarding the interaction between various morphological components and different evolutionary processes, such as speciation, local adaptation, and the emergence and persistence of biological diversity.



**Figure 1.6:** The size and shape difference between the crab (left) and wave (right) ecotypes of the *L. saxatilis* species.

### 1.3 *Littorina saxatilis*

In this thesis I am using the intertidal snail *Littorina saxatilis*, the rough periwinkle, as the study species. This common snail is a great example of extreme morphological variation due to local adaptation to distinct adjacent environments (Grahame et al., 2006; Johannesson et al., 1993; Butlin et al., 2014). The most investigated variation within this species is the differentiation between two environmentally adapted morphs known as the crab and wave ecotypes (figure 1.6), which can be abundantly found on many of the rocky shores of the North Atlantic Ocean. The divergence between the two ecotypes has been investigated as a possible example of ongoing speciation with gene flow (Butlin et al., 2014), and is being analysed both on smaller and larger geographical scales (Westram et al., 2014; Morales et al., 2019).

The high natural shape variability in *L. saxatilis* makes it an ideal candidate to investigate how genetics and plasticity can affect the development of the shells. Previous analysis has described the main shape differences between the crab and wave ecotypes as variation in globosity (Grahame and Mill, 1989; Ravinet et al., 2016) or, when analysed using a growth based method, as variation in growth parameter values (Walker and Grahame, 2011; Clarke et al., 1999). The crab ecotype is much larger and more elongated with a taller spire, a thicker shell and a narrower aperture, all of these traits are known to improve the snail's ability to survive crab predation (figure 1.6). In contrast, the wave shell is much smaller and globular, with a thin shell and a large round aperture which fits a larger foot relative to its size. It has been shown that the wave snails are better at resisting hydrodynamic forces, which has mainly been attributed to its larger foot. In order to better understand if there are any direct effects of shape on the snails fitness in the wave swept environment, I conducted both a set of computational fluid dynamics simulations and measured the corresponding drag forces in a flume experiment (chapter 4).

In *L. saxatilis*, some allometric changes have been detected with several different quantification methods (Newkirk and Doyle, 1975; Walker and Grahame, 2011; Conde-Padín et al., 2009; Carvajal-Rodríguez et al., 2005; Johannesson and Johannesson, 1996; Hollander et al., 2006a; Boulding and Hay, 1993; Rolán-Alvarez et al., 2015), and have been suggested to vary between different growth stages for different ecotypes and sexes both within *L. saxatilis* (Hol-

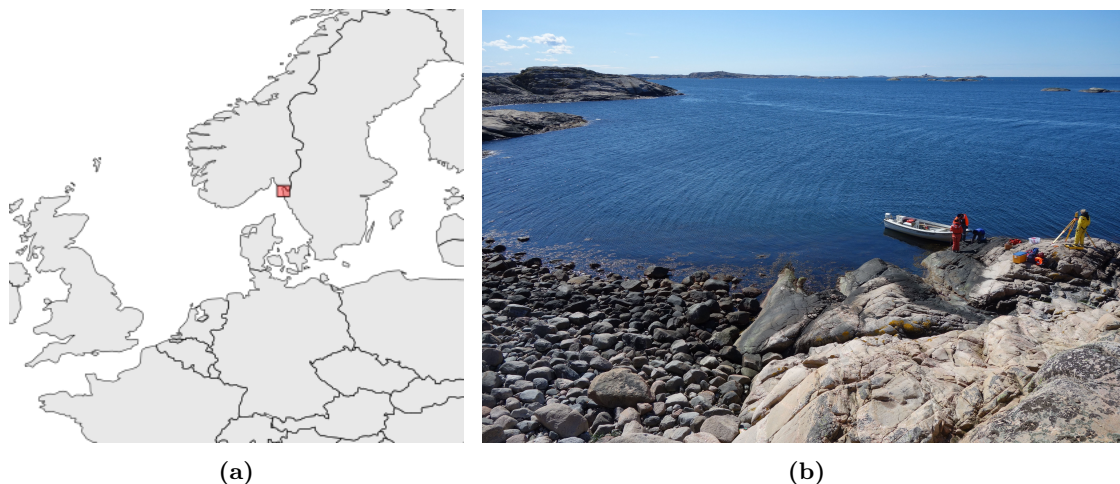


**Figure 1.7:** (a) All snails analysed in this thesis were collected in the Koster archipelago on the Swedish west coast. (b) The environment consists of alternating boulder fields and smooth rock faces with sharp habitat transitions.

lander et al., 2006a), and for a larger group of *Littorina* species (Lowell et al., 1994). Analysis does not, however, support the idea that allometry would be the main reason for the crab and wave ecotype shape differences, since even as newly hatched juveniles, their shapes were different (Hollander et al., 2006a). Important to note here is that the GM method can classify a self-similar logarithmic growth pattern as allometric variation, due to the way the landmark points are only defined for the apex and the most recently constructed whorls, not taking into account that the number of whorls will change throughout growth since the spiral pattern does not go on indefinitely, which also affects the centroid size obtained for shells at different times throughout growth (Urdu et al., 2010b). The growth trajectories obtained for perfect logarithmic growth would affect the position of landmarks similar to the way (Hollander et al., 2006a) suggested that *L. saxatilis* varies (Urdu et al., 2010b). This highlights the need for more growth based analysis of allometry, to get some clarity into whether and how the growth pattern of *L. saxatilis*, and other species, differs from a perfect logarithmic helicospiral. Although the ontogenetic shape variability is much smaller than the ecotypic differences, it is still an interesting topic which could improve the understanding of the growth and form of snail shells. To investigate the possible allometry in *L. saxatilis*, the convexity measure from chapter 2 was included as one of the quantitative shape traits in a genetic analysis with the goal of finding the genetic basis of different aspects of shell shape chapter 3.

The data used in this thesis were collected from transects across contact zones between crab and wave ecotype habitats in the Koster archipelago on the Swedish west coast (figure 1.7a). The shoreline in this almost atidal area consists of a patchwork of wave exposed smooth cliffs and protected boulder fields, hence the crab and wave ecotypes occur in alternating patches along the shore, with narrow hybrid zones in between (figure 1.7b). This makes them a great study species for understanding the replicability of local adaptation and speciation.

## 1.4 Adaptations, functions and fitness

How well a specimen or species can survive in a particular environment is determined by trade-offs between a complex combination of external and internal factors (DeWitt et al., 2000). I am interested in understanding how shell shape fits into this network of components for gastropods, and how it is affected by and affects other traits. Examples of trade-offs in shape include the negative relation between structural rigidity against available living space depending on how tightly coiled the shell is. In this section I introduce adaptive traits as separate factors. However, the optimal shape will depend on the relative importance of the traits for overall survival and fitness.

Mollusc shells are very useful for understanding long term evolutionary processes such as speciation and adaptation for several important reasons: 1) There is a rich fossil record of mollusc shells, as they both preserve well and have been around for a very long time. 2) Shells have the useful property of telling us something about both the development of the individual shells and the evolution of shell forms over time (Hammer and Bucher, 2005). 3) It is possible to extract genetic material from shells for some time after the snail itself has died (Ferreira et al., 2020). This means that mollusc shells, both fossils and contemporary, can be used to understand how the environment has changed over very large time-scales, how the molluscs have developed and adapted historically (Allmon, 1994), and how repeatable these evolutionary trends are (Tendler et al., 2015).

A common theme of divergent adaptations in intertidal snails is the evolution of a crab-wave dimorphism, which generates large morphological differences and can be found within several distinct species, e.g. *Nucella lapillus* (Gibbs, 1993; Guerra-Varela et al., 2009; Large and Smee, 2013), *Littorina sitkana* (Yamazaki and Goshima, 2012), and as diverged traits for separate species within the *Lepsiella* genus (Kitching and Lockwood, 1974), in addition our study species *Littorina saxatilis* (figure 1.6) (Carvajal-Rodríguez et al., 2005; Johannesson et al., 2010; Westram et al., 2016). Since the crabs themselves tend to do badly in wave swept environments, this divergence can easily become a dichotomy when the snails are present in both types of environment, and the survival rate of snails is lower in the opposing environment (Heller, 1976; Janson, 1983; Seeley, 1986; Etter, 1989; Raffaelli, 1982; Boulding and Van Alstyne, 1993).

### 1.4.1 Predator adaptations

Different predators will attack snails in different ways, but it is usually one or both of the following types; Either the predators crush the shells if they are large and strong enough, or they enter the shell through the aperture, possibly by breaking off the leading edge, if they e.g. have suitable claws, and the snails are counter-adapted thereafter (Edgell et al., 2008; Rochette et al., 2007; Konuma and Chiba, 2007; DeWitt et al., 2000; Johannesson, 1986; Bertness and Cunningham, 1981; Kitching et al., 1966; Heller, 1976; Raffaelli, 1982; Crothers, 1983; Atkinson and Newbury, 1984; Large and Smee, 2013).

A common adaptation to resist predation is to construct shells that are thicker and tougher, to make them harder to crush, which increases the survival from attacks using both predation methods mentioned above (Boulding et al., 1999; Edgell et al., 2008; Seeley, 1986; Trussell, 2000; Johannesson, 1986; Trussell, 1997a; Bourdeau and Padilla, 2019). Ridging and spines has been suggested to be accomplishing similar results using less material, which is especially

useful if the predator has limitations in the size of shells they can handle, e.g. due to claw or jaw size (Rolán-Alvarez et al., 1997; Palmer, 1979). A particular set of varices in the shell of the snail *Ceratostoma foliatum* was also found to increase survival against predatory fish as it increased the probability of landing aperture down when dropped onto the ocean floor from above (Palmer, 1977).

In addition to increased shell thickness, predator defences can also include factors such as shape. While more globular and larger shells are harder to crush, elongated shells are more entry resistant (DeWitt et al., 2000; Seeley, 1986; Rochette et al., 2007). An elongated shell shape would have a relatively smaller aperture due to the spiralling growth pattern, and the snail would more easily retract further into the shell as it does not decrease in available volume per whorl as quickly as a rounder shell shape normally does. Both factors help to avoid being eaten by shell-entering, or aperture-peeling predators (Edgell et al., 2008). Retracting further into the shell, as well as a more cautious behaviour, i.e. staying retracted for longer after being disturbed, would also increase survival against predators (Johannesson, 1986). Other adaptations to predators include a frequency dependent difference in chirality when predators are asymmetrical, e.g. snakes with asymmetric jaws, or crabs with dimorphic claws (Dietl and Hendricks, 2006; Hosono et al., 2010), as well as shell sculpture (Bertness and Cunningham, 1981).

#### 1.4.2 Flow adaptations

The ability to stay attached to the substrate despite strong water flow is crucial for survival in aquatic environments (Johannesson, 2003; Rolán-Alvarez et al., 1997; Trussell, 1997b; Grahame and Mill, 1986; Tendler et al., 2015; Trussell, 1997a). Understanding how the different forces are acting on snail shells is necessary for drawing conclusions about the ecological and evolutionary importance of shape (Koehl, 1996). It is hard to quantify the magnitude of wave exposure (Carrington Bell et al., 1994), but the type of flow will result in different optimal morphologies, as the relative importance of e.g. drag, lift, rotational forces, and the consistency of flow direction will vary, and it is impossible to be optimally adapted to all of them simultaneously (Verhaegen et al., 2019, 2018a,b; Vergara et al., 2017; Haase, 2003; Kistner and Dybdahl, 2014). In addition, the snails need to withstand both high force peaks and large variations in magnitude and direction over long periods of time due to the chaotic flow on topographically complex rocky shores. However, the parallel phenotypic trends of different species on similar gradients in wave exposure (Cuña et al., 2011), would suggest that some shell morphologies, such as being globular with large apertures, are advantageous even in such an unpredictable environment.

River snails, on the other hand, are in general subjected to a constant unidirectional flow, making it more likely that streamlining is the target shape to reduce the forces the shells are subjected to (Yang et al., 2007). A large foot and enough internal space, without increasing the external volume, are, however, still desirable traits in most types of flow, but their importance relative to the effect of streamlining could differ between snails in rivers and those on wave swept shores. In general, river snails have been found to have more globular shapes and larger apertures in faster flows (Lam and Calow, 1988; Minton et al., 2008, 2018; Verhaegen et al., 2018a,b; Haase, 2003; Kistner and Dybdahl, 2014; Cazenave and Zanatta, 2016). Comparisons between *Nucella* shells from a river and the sea found even larger foot size with thinner shells in the sea, providing larger internal volume available despite no difference in external size

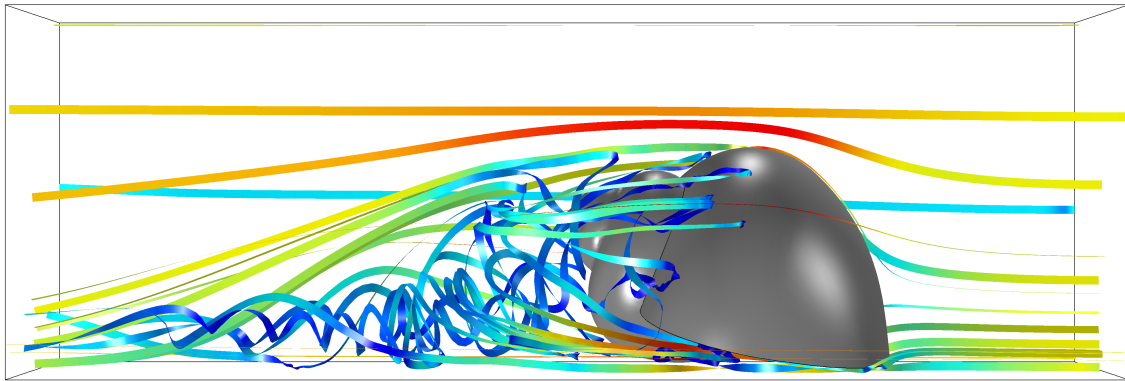


**Figure 1.8:** Example of water flow trajectories around a computer model of a shell. Ribbons indicate the trajectories of the water, and colour represent the local flow speed, red indicates higher, and blue lower velocities.

(Kitching et al., 1966). The movement of river snails upstream has also been suggested to be at least partially a result of mechanical effects for some snails, where the torque would orient the shell upstream (Huryn and Denny, 1997). By gaining a better understanding of the effects of morphological variation in shells for snails subjected to different types of flow, I aim to provide insight into what aspects of shape and development improve survival in wave swept environments through analysis of computer simulations (figure 1.8) and experimental measurements (chapter 4).

Size has been suggested as a large component of survival on rocky shores (Denny et al., 1985; Vermeij, 1972; Etter, 1989; Prowse and Pile, 2005). One suggestion for size limitations was that accelerational forces scale with volume, in contrast to drag and lift forces, which scale with area. However, the time-scales of the intense bursts of acceleration in waves are too short to affect a large enough portion of the animal at once when they are large enough for the acceleration forces to become dominant (Gaylord, 2000). Even without acceleration as a constraining factor, size could still be influencing survival, with a smaller size giving access to more crevices (Atkinson and Newbury, 1984; Johannesson et al., 1997), or allowing a larger portion of the shell to be contained within the boundary layer since the flow speed is decreased near the substrate (Le Pennec et al., 2017). However, the risk of dislodgement was not found to scale with shell size in adult *L. saxatilis* (Le Pennec et al., 2017), or *L. obtusata* (Trussell, 1997a).

Shape is an important factor which can have a large effect on the hydrodynamical forces a shell is subjected to. However, the optimal shape for a given species of snail will depend on many factors, and a streamlined shape is only favourable when alignment with the direction of flow is possible (Koehl, 1977). The general trend for intertidal gastropods on rocky shores is to become more globose while simultaneously squatter, and to have a larger aperture and thin shell compared to less exposed sites (Heller, 1976; De Wolf et al., 1999; Trussell, 1997a; Trussell et al., 1993; Trussell, 1997b; Forrester et al., 2016; Kitching et al., 1966). In limpets, the hydrodynamically optimal shape was not actually found in nature, suggesting that there are also other factors involved (Denny and Blanchette, 2000). There is a possibility of the optimal shape also depending on size, e.g. depending on how much of the shell is contained

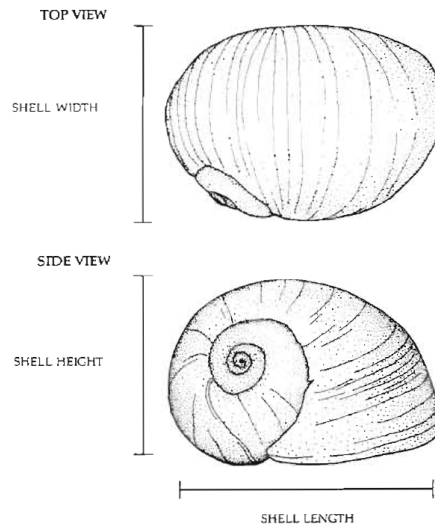


**Figure 1.9:** The optimal orientation against the flow is assumed to minimise the front-facing area. In the case of *Littorina obtusata*, and similar short-spined shells, this means an alignment as pictured, when the flow comes from the right hand side. Image from Trussell et al. (1993), reproduced under CC-BY licence.

within the boundary layer of the flow, or the relative size of the foot needed to resist the fluid forces, which could potentially favour an allometric growth pattern.

Another factor which has been shown to matter in mollusc shells is ornamentation, where spines affect the hydrodynamics by inducing a boundary layer transition at lower Reynolds numbers, to decrease drag (Chamberlain and Westermann, 1976). In contrast, barnacles and algae growing on shells were found to increase drag forces (Wahl, 1996). Varices, i.e. axial ridges, have also been found to matter in terms of increasing the probability of landing with the right side up when falling through the water column (Palmer, 1977).

In combination with shape, orientation should also be taken into account, as snails tend to orient themselves with the flow when possible (Boulding and Van Alstyne, 1993; Verhaegen et al., 2019). The relative effect of forces acting depending on orientation of different gastropod shells is important to understand why some shapes are more common than others. Alignment with the flow by minimising the front facing area should in general decrease the forces (Koehl, 1984). However, in the unpredictable waves of rocky shores, it might not be possible to align, and thus the largest area against the flow could be more informative to estimate the relevant forces for survival (figure 1.9) (Trussell et al., 1993). In chapter 4 I investigated how shape and orientation interact, and found some variation in optimal alignment within the shape variability found in *L. saxatilis*.

Several species of *Littorina* have been found to hide in crevices and empty barnacle shells, suggesting that this helps them withstand stronger wave action (Raffaelli and Hughes, 1978; Janson, 1983; Johannesson and Johannesson, 1996; Hughes and Roberts, 1981; Emson and Faller-Fritsch, 1976). This is not necessarily due to the crevices themselves lowering the water speeds: snails can wedge themselves into cracks and transfer the forces through to the rock, and provide shelter to each other when the concentration of shells is high. Crevices can also make the water flow more predictable in direction (O'Donnell and Denny, 2008) and provide

shelter from heat and desiccation during low tide (Atkinson and Newbury, 1984; Johannesson et al., 1997).

Despite the above factors affecting the survival on wave swept shores, the main factor contributing to decreasing the risk of detachment has been found to be the relative foot size (Le Pennec et al., 2017; Hohenlohe, 2003; Etter, 1988; Trussell, 1997a; Atkinson and Newbury, 1984; Johannesson et al., 1997). In general, foot size has a large plastic component (Etter, 1988; Trussell, 1997a), and aperture size is not necessarily a good proxy for foot size (Verhaegen et al., 2019).

Comparing experimental data with simulations should provide useful information into how important the factor of shape is and how it matters. Simulations are particularly useful when investigating a single factor separately, removing confounding effects, or to see how different factors interact with each other. However, results need to be validated with experiments. In chapter 4, I compare the results from flow simulations with empirical data, to investigate whether and how shape is important, and if this changes with varying conditions.

### 1.4.3 Other adaptations

Terrestrial snails are subjected to different environmental pressures than aquatic snails. They tend to be restricted in their possible morphologies due to gravity and lower availability of shell construction materials. Terrestrial snail shell shape variation have been characterised as bimodal, divided into elongated shells for snails mainly living on vertical surfaces, and flattened for snails mainly living on horizontal surfaces (Okajima and Chiba, 2009, 2013). Snails also need to keep a certain level of moisture, which is particularly restrictive for those that are terrestrial or intertidal. Two different types of strategy have been found in the *Albinaria* family; Either by active retention or resistance to loss (Giokas et al., 2014), reflecting the fact that there are different ways of adapting to the same environmental factors. Adaptations to heat also include behaviour (Ng et al., 2017; Chapperon et al., 2017), and shell colour (Cowie and Jones, 1985).

## 1.5 Shape: Genetics vs. plasticity

The question of how much of the morphological variation can be attributed to genetics or plasticity is a common research focus when it comes to adaptive traits, including shell shape (Kistner and Dybdahl, 2014). Within the gastropods, various levels of morphological plasticity have been found (Bourdeau et al., 2015), hence species-specific analysis is needed to fully understand how and why shell shape plasticity affects the fitness and functionality of different gastropods.

In addition to traits adapted to specific environments or general biological improvements, there is a possibility that variations found are non-adaptive, such as neutral traits, or those that arise as side effects of environmental or developmental problems. Some human-induced factors which could affect the shape, both due to adaptations or adverse affects, are pollution, climate change, and farming (Sousa et al., 2020). The problems of constructing shells in more acidic and polluted environments have been well documented, making shells less thick or changing the material composition (Nuñez et al., 2012; Füllenbach et al., 2014; Cross et al., 2019; Oliveira et al., 2020; Márquez et al., 2011), and thus making them less sturdy and more likely to break. Shape of both snails and limpets has also been shown to be

affected by pollution and ocean acidification (Márquez et al., 2017; Gouveia et al., 2019; Hellberg et al., 2001; Harayashiki et al., 2020). Understanding how animals are affected by, and how they can adapt to, changing climate or pollution levels is important to understand the severity of impacts and help mitigate their effects. Research into variation in fossil shell shape and composition could inform us about long term evolutionary processes such as speciation (Allmon and Smith, 2011), but also give insight into the environmental conditions of the past (Escobar et al., 2010; Goodwin et al., 2003). A better understanding of how gastropods adapt to various environmental pressures, both plastically and genetically, and how the adaptations can change over short and long time scales with changing conditions, would also be useful for understanding how shells are being affected by current climate change.

Most of the shape variation in *L. saxatilis* shells has been attributed to genetics (Carballo et al., 2001; Conde-Padín et al., 2009, 2007; Hollander et al., 2006b; Boulding and Hay, 1993; Newkirk and Doyle, 1975; Janson, 1982), where chromosomal inversions have been suggested to play a significant role in maintaining the ecotype dimorphism (Westram et al., 2018; Faria et al., 2019b), as well as clustering of sex-related traits (chapter F). However, some plasticity has also been found (Hollander and Butlin, 2010; Hollander et al., 2006b). There is some evidence that the heritability of shape, at least when quantified by GM, differs between the ecotypes (Conde-Padín et al., 2007). It was also found that the genetic basis involved in divergence between ecotypes was not invariant over larger geographical scales (Westram et al., 2014), hence separate analyses at different sites would be needed to see if the genetics of shape is consistent between sites. There is evidence of a complex genetic architecture of shape, involving both a few large effect loci and many of small effect in Spanish *L. saxatilis* (Kess and Boulding, 2019), and I investigate this for Swedish snails in chapter 3 to find if this conclusion is consistent across larger geographical scales.

In chapter 3 I investigated how the new growth-based quantification method of chapter 2 improves the ability to determine the genetic basis of shell shape in the Swedish population of *L. saxatilis*, and estimated heritability of the different shape components. I identified some parts of the genome which are related to certain aspects of shape, and found that some variation in shape could be linked with the sex determining region. There is likely, however, also some plasticity involved in several shape components, particularly in shell thickness, but future analyses would be needed to better understand their relative effects, and to see how consistent these results are across the Atlantic and across species.

In *L. littorea*, plastic allometry has been linked to growth rate in a linear measurement analysis (Kemp and Bertness, 1984). Another species of *Littorina* showed correlation between food availability, high growth rates and more elongated shells using Raup-like growth parameters (Boulding and Hay, 1993). How both these allometric trends relate to a convex/concave situation would be informative to understand what is actually going on during growth, and covariation between overall growth and convexity in *L. saxatilis* was also found and discussed with respect to genetics and plasticity in chapter 3. It is possible that convexity might have some adaptive component to it, which could be independent of the wave exposure gradient and present in several species.

One of the main focuses in recent research into gastropod shell traits, is the chirality (Abe and Kuroda, 2019; Davison et al., 2016; Shimizu et al., 2013, 2011). Most snail species consist of shells which are only either coiling clockwise (dextral) or counter-clockwise (sinistral) when viewed from the apex, but some are able to maintain populations with shells of both chiralities, possibly due to e.g. frequency dependent selection when co-evolving with predators that are

better adapted to eat snails of one chirality than the other (Dietl and Hendricks, 2006; Hosono et al., 2010). Despite the problems with inter-chiral matings, due to e.g. sexual organs on opposite sides, this is not a trait that necessarily leads to speciation because of the maternal effects of chirality inheritance (Davison et al., 2005). Chirality is an important aspect of growth and development in snails, and investigations into the causes involved in determining chirality could also lead to a better understanding of the development of other growth related traits. Chirality has not been a focus in *Littorina* research, since this species complex is generally dextral, with only incredibly rare sinistral specimens. Since dextral and sinistral shells are mirror images of each other, it is easy to incorporate into a growth based model by including a well placed minus sign.

Another shell trait which is of interest from a genetic and evolutionary point of view, is the formation of bands and other colour patterns found on the shells (Williams, 2017; Kozminskii et al., 2010), which can be modelled using reaction-diffusion systems (Meinhardt and Klingler, 1987), and is expected to be affected by the shells external geometry (Fowler et al., 1992). In, for example, different species of *Cepaea* the presence and placement of bands have been investigated and found to conform to the expectations of a convex growth pattern chapter E, and affected crush resistance (Rosin et al., 2013). In *L. saxatilis* there have also been some investigations of how colour variation can affect their fitness in different environments, and discussion of possible genetic components (Ekendahl and Johannesson, 1997; Johannesson and Butlin, 2017). In the sister species *L. obtusata* colour variation showed patterns varying with a thermal gradient (Phifer-Rixey et al., 2008), and has been found to have a single genetic locus which controls the presence or absence of a band (Kozminsky, 2016).

## 1.6 Summary

The choice of quantification is crucial in order to understand the connections between form, function, and adaptation, as well as to identify the relevant biological traits correctly, and to draw accurate conclusions about genetics and developmental processes. Gastropod shells provide a great possibility to study the combination of development and evolution, as their shape and growth can be described by a set of informative parameters. Despite this possibility, a high-throughput method for such a quantification has been lacking. Therefore, I developed a quantification method for analysing the shapes of large data sets of shells from a growth-based perspective. Using this method, I aimed to improve the understanding of the diversity found in *L. saxatilis*, the fitness effect of different shape factors in various environments, and how this relates to genetic and plastic effects.

## 1.7 Thesis overview

### 1.7.1 Chapter 2 - Quantifying Shape in Shells

In chapter 2 I develop a quantitative method for inferring growth-based shape parameters from a set of landmarks on 2D standardised shell images of *L. saxatilis* (figure 1.10a). This method is specifically constructed to be able to account for the type of variability in aperture shape which is found in *L. saxatilis* (figure 1.6). I compare the results from the growth-based method with a classical GM analysis, implementing a Procrustes superposition and

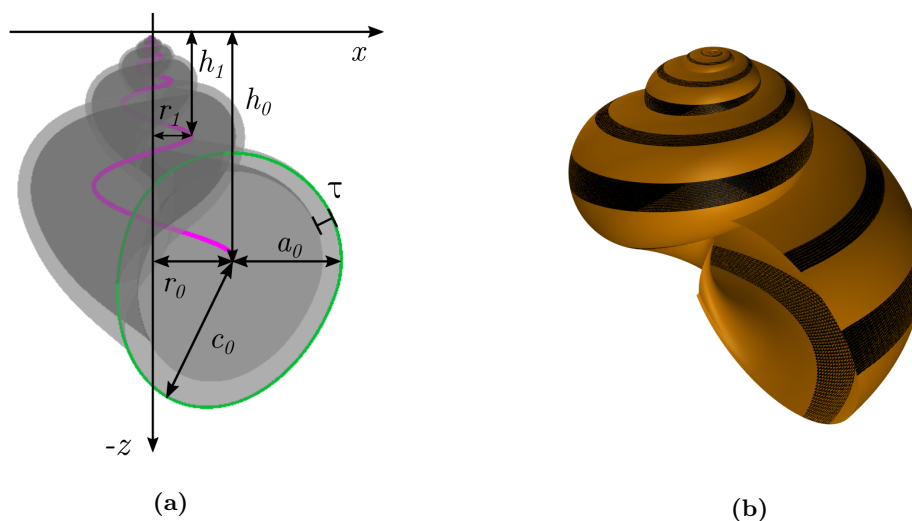


**Figure 1.10:** (a) A schematic view of the shell shape quantification developed in this thesis. For full explanation, see chapter 2. (b) An example of a banding pattern on the surface of a shell. An analysis of the position and width of bands in *Cepaea* land snails can be found in chapter E.

summarising the largest variations using a PCA, and using the same set of landmarks for both methods. This comparison is done to showcase how much more informative a growth-based quantification is when it comes to understanding how the variability in shape relates to development in the case of gastropod shells.

### 1.7.2 Chapter 3 - Genetic architecture of Shell Shape

In chapter 3 I use the quantification method developed in chapter 2 to gain new insights into the genetic architecture of shell shape variability in *L. saxatilis*. I also compared these results to those obtained for the GM method using the same data set, and discuss the different abilities of the two methods. The main improvement of the new growth based method is how it allows us to investigate the genetic architecture of distinct components of shape, which relate to the shell's development. In particular, I found evidence of a genetic component to allometric variation in shape.

### 1.7.3 Chapter 4 - Hydrodynamical Effects of Shell Shape

To relate the large shape variation found in *L. saxatilis* to environmental factors, I performed an analysis of the fluid dynamical properties of the various shell shapes. I performed both a computational fluid dynamics simulation, as well as a flume experiment, to understand why the wave ecotype in *L. saxatilis* has the shape it does. The results suggest that shape affects the optimal orientation of the shell, suggesting that if flow direction can be predicted, shells will orient themselves with their spire in different directions depending on relative spire height. The main contributing factor to survival in wave swept shores is likely to be foot size, making shell shape more likely to be secondary. Shell shape will be constructed to maximise the possible foot size, and only be as hydrodynamically efficient as maximising foot size allows.

### 1.7.4 Chapter 5 - Discussion

The discussion chapter summarises the main findings of the analyses in this thesis, and puts them into the perspective of current scientific research. I also propose a few possible continuations of this research, which could give further context to my conclusions, and address some of the questions which my research has raised.

### 1.7.5 Appendix E

As an additional example of when a growth based method is useful for morphological analysis, I include, in appendix E, an analysis investigating if shell shape and banding patterns follow the expectations of a logarithmic spiral growth, also allowing for convex or concave growth. Band width and position could be inferred using the interactive program called ShellShaper that I created for this reason (figure 1.10b). ShellShaper is constructed to infer a set of growth based shape parameters similar to the method presented in chapter 2. However, instead of using the landmark points as used for GM analysis, a new set of points and geometric objects positioned on the shell images was specifically chosen to improve the accuracy of the growth based parameters. The program is currently implemented in MATLAB, which is proprietary software and requires a user license, but the user does not need to be proficient in MATLAB, or the mathematics involved in the method, as the interface has been created with this in mind. This work has been published in Jackson et al. (2021).

### 1.7.6 Appendix F

Lastly, appendix F consist of a paper which relates the shape dimorphism of the crab and wave ecotypes of *L. saxatilis* to the chromosomal inversions suggested to underlie much of the persistence of ecotypes despite ongoing gene flow, and its corresponding supplementary information. A large component of the *L. saxatilis* genome is suggested to consist of inversions, and a current question in population genetics is to find what role inversions play in the emergence and persistence of phenotypic variation as well as in speciation. This work has also been published in Koch et al. (2021).

## Chapter 2

# A developmentally descriptive method for quantifying shape in gastropod shells

Presented in its accepted form for publication.

Larsson, J., Westram, A. M., Bengmark, S., Lundh, T., and Butlin, R. K. (2020). A developmentally descriptive method for quantifying shape in gastropod shells. *Journal of the Royal Society Interface*, 17(163), doi: 10.1098/rsif.2019.0721.

J. Larsson<sup>1</sup>, A.M. Westram<sup>2</sup>, S. Bengmark<sup>3</sup>,  
T. Lundh<sup>3</sup>, R. K. Butlin<sup>1,4</sup>

<sup>1</sup>Department of Animal and Plant Sciences, University of Sheffield, Sheffield, UK

<sup>2</sup>IST Austria, Klosterneuburg, Austria

<sup>3</sup>Mathematical Sciences, Chalmers University of Technology  
and University of Gothenburg, Gothenburg, Sweden

<sup>4</sup>Department of Marine Sciences, University of Gothenburg, Strömstad, Sweden

**Contributions:** R.K.B. and T.L. conceived the project. J.L. developed the analytical method with S.B. and T.L. providing input. A.M.W. and R.K.B. collected the snails. J.L. drafted the manuscript and all authors provided input on subsequent versions.

## Abstract

The growth of snail shells can be described by simple mathematical rules. Variation in a few parameters can explain much of the diversity of shell shapes seen in nature. However, empirical studies of gastropod shell shape variation typically use geometric morphometric approaches, which do not capture this growth pattern. We have developed a way to infer a set of developmentally-descriptive shape parameters based on 3D logarithmic helicospiral growth and using landmarks from two-dimensional shell images as input. We demonstrate the utility of this approach, and compare it to the geometric morphometric approach, using a large set of *Littorina saxatilis* shells in which locally-adapted populations differ in shape. Our method can be modified easily to make it applicable to a wide range of shell forms, which would allow for investigations of the similarities and differences between and within many different species of gastropods.

**Keywords**— Growth, Morphometrics, Snail shells, Shape variation

## 2.1 Introduction

Snail shells are a beautiful example of how seemingly complex structures in nature can be described by simple mathematical rules. Logarithmic helicospirals, or conchospirals, are spirals which increase with a constant factor in height and radius for each revolution around a coiling axis, and they are well known to approximate the shell development of most gastropods (Moseley, 1838; Thompson, 1917; Illert, 1983; Cortie, 1992). Raup developed a method for describing self-similar shells by measuring a set of growth-related parameters and investigating the related shape space (Raup, 1961, 1966). Several extensions have been made to Raup's initial version (Illert, 1989; Løvtrup and Løvtrup, 1988; Cortie, 1989; Stone, 1995; Fowler et al., 1992; Savazzi, 1985), making it possible to model a more variable collection of shells and to give more accurate representations of features such as the aperture inclination. In addition to these fixed reference frame descriptions, there have also been efforts to describe the growth locally at the aperture, which describes the construction process from the viewpoint of the snail (Moulton et al., 2012; Noshita, 2014). This type of method has rarely been used for quantification because it is difficult to infer the parameter values directly from empirical data, such as 2D photographs, without first obtaining the parameters of a Raup-like description.

Despite the strong connection between these growth-related developmental parameters and the shell shape, population level studies of shape variation have often favoured the more general method of landmark based geometric morphometrics (GM) using the Procrustes method (Rohlf and Slice, 1990). This approach quantifies the variation of a set of homologous points, called landmarks, positioned on images. It is widely and successfully used for morphological analysis of many biological organisms and structures, including snail shells (Stankowski, 2011; Cruz et al., 2012; Westram et al., 2018). However, it has some drawbacks when considering gastropod shells due to their spiralling accretionary construction process, where the shell grows by new material being deposited at the aperture. One issue with this process is that there is only one truly homologous point on the shells, the apex. The other points used are often semilandmarks, points at arbitrary positions on curves where there is a lack

of corresponding anatomical features. Another limitation is that the GM method does not provide a description directly relating to the shell's development in the same way that a growth-based method does, making it harder to interpret the shape variation in biologically meaningful terms. Also, in GM analyses allometric changes can be hard to separate from other size-related variability.

There are examples of inferring growth parameters from 3D  $\mu$ -CT data (Monnet et al., 2009). However, this is both expensive and time consuming, and thus not currently realistic for large sample sizes. None of the growth-based methods mentioned above have so far been implemented to quantify shape variation of large empirical data sets that includes variable aperture shapes. This is one of the reasons why GM is the current standard method despite lacking the direct connection to development. Therefore, we have developed a high-throughput method for quantification of shape variation in shells with variable aperture shapes using commonly-available 2D data, which is built on the original ideas of Raup. This gives an intrinsic shape description of each shell in 3D, with developmentally-descriptive parameters, i.e. parameters that can be clearly related to the accretionary growth of the snail shell. This will make it possible to relate the different aspects of shape to environmental and functional factors, and developmental processes. Additionally, since the parameters describe the shells intrinsically, we can extend the analysis by including more shells, e.g. from different sample sites or different species, and directly compare the distributions in the shape space. By contrast, GM analyses are specific to their data sets.

We have used the marine snail *Littorina saxatilis* to test our method because of its high shape variability, see Johannesson (2016) for a review of this species. In particular, we focused on the differences between two ecotypes, one adapted to resist crab predation by having a large, thick shell with a narrow aperture (Johannesson, 1986), and the other adapted to endure wave action and characterised by having a small shell with a round and relatively large aperture (Le Pennec et al., 2017). This ecotype dimorphism can be found on rocky shores throughout the north Atlantic coasts, and is especially well studied from the viewpoint of local adaptation, speciation, and parallel evolution in parts of Spain, Sweden and the UK (Westram et al., 2014; Rolán-Alvarez, 2007; Butlin et al., 2014; Johannesson et al., 2010). In this analysis we investigated the Swedish system, and we have focused specifically on shape, which is one of the adaptive traits that differ between the ecotypes, and which has been shown to have a high heritability (Conde-Padín et al., 2009; Carballo et al., 2001; Hollander et al., 2006b). Some genetic differences between similar environments on geographically close islands (< 10km), have been observed in the Swedish system (Ravinet et al., 2016), thus it is possible that there are also phenotypic differences between sites at this scale. Therefore, we investigated how shell shape varies across boundaries between adjacent crab-type and a wave-type environments, and compared this pattern between separate sites.

Recent research on *L. saxatilis* has mainly used GM for quantifying shape (Ravinet et al., 2016; Westram et al., 2018), but other methods have also been used, including linear measurements (Grahame and Mill, 1989), outline analysis (Dytham et al., 1992), and a version of Raup's original growth parameters (Walker and Grahame, 2011). Since all these methods can quantify shape variability, the way to choose which method to use should be decided by which type of description we are interested in (Stone, 1998). GM makes it possible to quantify the ecotype variation, and to correlate this with changes in different parts of the environment and the genome (Westram et al., 2018). However, with a more developmentally-descriptive shape characterisation it could be possible to get a clearer picture of which aspects of shape

and growth are related to which biological and environmental factors, and to improve the understanding of which genomic regions underlie these differences. Similar advances could be made by applying this approach to other gastropods, other mollusc shells, or to other structures with similar growth patterns such as beaks or claws.

## 2.2 The model

The model used in this analysis is based on an internal logarithmic helicospiral coiling around the vertical  $z$ -axis in 3D with apex at the origin (Fowler et al., 1992; Cortie, 1989). We use separate growth parameters for the increase in width,  $g_w$ , and height,  $g_h$ , which relate directly to how much taller and wider the spiral becomes for each revolution around the coiling axis (figure 2.1). This internal spiral can be described in vector form by the equation

$$L(t) = (r_0 e^{g_w t} \cos(t), -r_0 e^{g_w t} \sin(t), -h_0 e^{g_h t}), \quad t \in [-2\pi n, 0], \quad (2.1)$$

where  $n$  is the number of revolutions around the coiling axis to be included in the visualisation, which can be chosen as a constant and should relate to the number of whorls visible for the species of interest. It is convenient to use start values  $r_0$  and  $h_0$  that are the radial and vertical distances from the origin to the spiral at the current aperture position, where  $t = 0$ . Since we are interested in spirals which are expanding downwards, as  $t$  increases to zero, in accordance with the standard way of visualising snail shells, there is a minus sign in the vertical  $z$ -component. We only consider clockwise rotation downwards in this paper, it is however possible to change to counter-clockwise rotation by removing the minus sign in the  $y$ -component.

The growth parameters are assumed constant throughout the shell's development. However, whenever  $g_w \neq g_h$  there are allometric changes. If  $g_w = g_h$  we obtain a straight profile and therefore isometric growth, but if  $g_w > g_h$  then the shell will obtain a concave spire profile, and if  $g_w < g_h$  we get a convex profile (figure 2.1).

In order to include the variable aperture forms found in *L. saxatilis*, we introduce a one-parameter family of egg-like shapes that we have named "circlipses", which smoothly combine a half-circle with a half-ellipse (figure 2.1).

**Definition.** A circlipse of size  $a_0$  with extension length  $c_0$ , is defined by the radial function

$$C(s) = \begin{cases} \frac{a_0 c_0}{\sqrt{c_0^2 \cos^2(s) + a_0^2 \sin^2(s)}}, & s \in [0, \pi) \\ a_0, & s \in [\pi, 2\pi), \end{cases} \quad (2.2)$$

around its reference point, i.e. the centre of the semicircle diameter.

The circlipse extreme point is at  $s = \pi/2$  and has the value  $C(\pi/2) = c_0$ . The extension parameter  $c$  is the factor defining how much longer (or shorter) the major (or minor) semiaxis  $c_0$  of the ellipse is compared to the circle radius  $a_0$ , where  $c = 1$  gives a circle. This describes the directional eccentricity of the half-ellipse, and the value of  $c$  uniquely determines the shape of the circlipse for a given size  $a_0$ . This generating curve is assumed to not change shape during growth, however, the amount of the circlipse that is visible, and hence the

resulting total aperture shape, might change over time, depending on the growth parameters  $g_w$  and  $g_h$ .

The size of the aperture also modelled to grow with a constant value for each revolution, hence we have an aperture growth function

$$A(t) = e^{g_w t}, \quad t \in [-2n\pi, 0], \quad (2.3)$$

where the aperture is assumed to increase the same value as the radial growth of the internal spiral  $g_w$ . By only considering equal growth of the aperture and spiral radius we restrict the shell shapes we can obtain to ones where the position of the aperture relative to the coiling axis does not change during growth, i.e. the radius of the spiral relative the total width of the aperture has the constant value  $r_0/(r_0 + a_0)$  as the shell grows. This is a simplification needed in order to have a robust parameter approximation method given the currently available data. However, with improved input data it is possible that this assumption could be relaxed.

Using a circlicptic aperture shape from equation (2.2) as a generating curve, sweeping out a surface as its reference point moves along the spiral defined in equation (2.1), we get the following surface function:

$$S(t, s) = L(t) + A(t)C(s - \theta)(\mathbf{N}(t) \cos(s) + \mathbf{B}(t) \sin(s)), \quad \begin{cases} s \in [0, 2\pi), \\ t \in [-2n\pi, 0], \end{cases} \quad (2.4)$$

where  $\mathbf{N}(t)$  and  $\mathbf{B}(t)$  are the unit normal and unit binormal for the internal spiral  $L(t)$ . This gives an aperture plane which is oriented perpendicular to the curve, and has been suggested as a reasonable approximation of the true orientation for many shells (Illert, 1989). We also allow the aperture circlicpt to be rotated in this plane by the angular parameter  $\theta$  around the reference point. Note that this angle has little to no effect on the shell shape if the aperture is close to circular, i.e.  $c \approx 1$ .

By including a relative shell thickness parameter  $\tau \in (0, 1)$  we can create an inner surface boundary which gives the model thickness without affecting the outside shape (figure 2.1). This is constructed by making a second surface with identical parameter values as the outside surface, except for the aperture size which will have the value  $a_0(1 - \tau)$ , e.g. if the relative thickness is  $\tau = 0.1$  of the aperture size  $a_0$ , then the internal surface will have aperture size  $0.9a_0$ .

The shell shape model presented above contains eight intrinsic parameters,  $g_w$ ,  $g_h$ ,  $r_0$ ,  $h_0$ ,  $a_0$ ,  $c$ ,  $\theta$ , and  $\tau$ , which is enough to create a large set of realistic shell shapes. Since they describe the accretionary construction process of the shells in nature, these parameters are straightforward to interpret in biological terms. The parameters are algebraically independent in the description above, but this is not the case after rescaling all shells to unit length, since for example spiral height  $h_0$  together with the elliptic extension length  $c_0 = a_0c$  are tightly linked with the total height. Shell size differs greatly between the analysed ecotypes, with crab type shells generally being much larger than wave types. Normalisation removes the part of the variation related to size. Rescaling therefore reduces the measured ecotype variability, and allows us to focus only on the shape variation. In addition to the parameters not all being algebraically independent, they are also unlikely to be biologically independent.

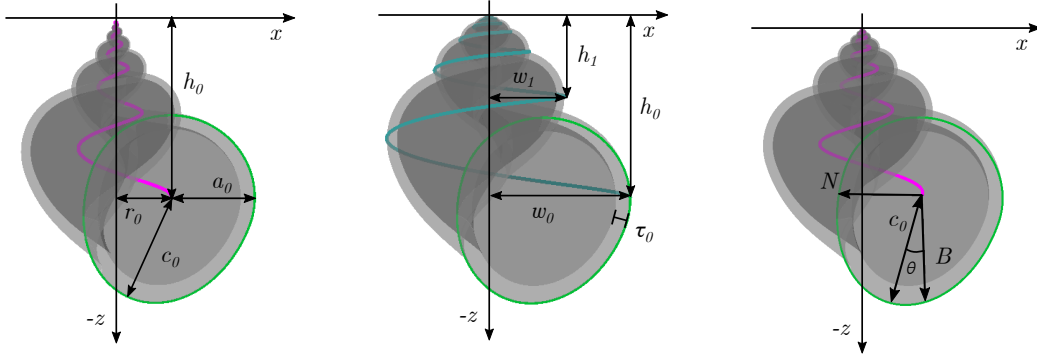


**Figure 2.1:** Two semi-transparent shell models, one concave ( $g_w > g_h$ ) on the left, one convex ( $g_w < g_h$ ) in the middle, and one straight ( $g_w = g_h$ ) on the right, while all other parameter values are unchanged between them. In the examples on the left and right the internal spiral  $L(t)$  are marked in pink, and on the middle one the external width spiral is displayed in teal. The growth parameters can be calculated as  $g_w = \ln(w_0/w_1)/(2\pi)$ , and  $g_h = \ln(h_0/h_1)/(2\pi)$ . The circliptic aperture is marked in green, it has the extension parameter  $c = c_0/a_0$ , and rotated by  $\theta$  relative to the internal spiral's normal plane defined by its normal  $\mathbf{N}$ , and binormal  $\mathbf{B}$ , here rescaled to reach the aperture curve. The relative thickness of the aperture is  $\tau = \tau_0/a_0$ . For the implementation in this paper all shells are normalised with respect to shell length, hence all linear measurement parameters are relative.

### 2.3 Sample collection and shell photography

We use snails collected from environmental contact zones on four islands within a few kilometres from each other on the Swedish west coast during 2013-2014: Ramsö ( $58^\circ 49' 27.8''\text{N}$   $11^\circ 03' 45.3''\text{E}$ ), Inre Arsklovet ( $58^\circ 50' 00.5''\text{N}$   $11^\circ 08' 19.6''\text{E}$ ), Ramsökälv ( $58^\circ 50' 04.0''\text{N}$   $11^\circ 02' 26.5''\text{E}$ ), and Yttre Arsklovet ( $58^\circ 49' 51.3''\text{N}$   $11^\circ 07' 59.0''\text{E}$ ), which are labelled CZA, CZB, CZC, and CZD, respectively. For sites CZA, CZB, and CZD, the snails are the same ones as in Westram et al. (2021). On each island, the snails were sampled across two environmental transitions in a transect going from an exposed cliff (wave) environment to a sheltered boulder field (crab) environment, and ending on another exposed cliff environment. This was done to include specimens from both ecotypes and intermediates from the environmental transition zones. The spatial position of each snail was recorded using a Total Station (Trimble M3), and simplified to a one dimensional relative position along the shoreline by calculating a least cost path where cost is proportional to the inverse of local population density (Westram et al., 2021).

Approximately 600 snails were collected from each site, and four environmental factors describing the immediate surroundings were recorded along the sampling transect (Westram et al., 2021). These factors were the type of substrate (bedrock vs. boulders), presence/absence of barnacles (indicating wave exposure), presence/absence of furoid seaweed (indicating a more sheltered environment), and local topography. They were combined into a single habitat score using a PCA, indicating the habitat type at each snail's position.

The shells were photographed in a standardised orientation using a digital camera, Canon EOS 1000D or 600D, mounted on a dissecting microscope and the positions of 15 points,  $L_1, \dots, L_{15}$  (figure 2.2), were recorded for each image. These points were chosen for GM

analysis and obtained according to a process similar to (Ravinet et al., 2016). We will refer to these points as landmarks, for simplicity, although the majority are, in fact, semilandmarks. The shell thickness was calculated as the mean value of three measurements taken with a thickness gauge (Neoteck DTI Digital Dial Indicator Probe, 0.001 mm resolution) close to the current aperture at its widest point. The sex was recorded as either male, female or juvenile during dissection (Reid, 1996). The juveniles were included in all analyses except for the comparisons between males and females. Specimens with missing data were excluded from the relevant analyses, making the total number at each stage at least 1923 shells.

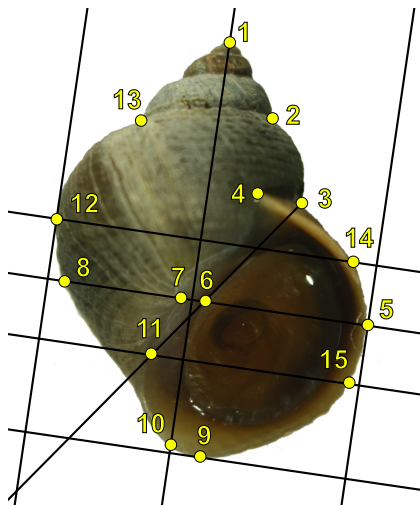


**Figure 2.2:** Landmarking procedure. The line from the apex, landmark 1, to the bottom of the shell, which is tangent to the empty part of the aperture defines the landmarking reference frame, we say that this line is "vertical", and lines perpendicular to it are "horizontal". The landmark point 10 is positioned at the lower extreme of the shell on this vertical line, and landmark 9 is at the lower extreme point of the whole shell. Landmarks 3, 13 and 2 are the three suture points on the outline where the most recently constructed consecutive whorls intersect, and landmark 4 is the end point of the suture at the current aperture. Landmarks 5 and 12 are the right and left extreme points of the shell in this reference frame, and using horizontal lines from these we define landmarks 8 and 14 as points on the opposite sides at the shell outline. On the vertical line through points 5 and 8, we position point 6 and 7 as the right and left points of the lip. A line from landmark 3 which is tangent to the empty part of the aperture is constructed, and Landmark 11 is positioned where this line touches the outer edge of the lip, and landmark 15 is then positioned on the outer edge of the aperture using a horizontal line from landmark 11.

## 2.4 Parameter Approximation Method

This method for estimating the parameter values for the shell shape model described in figure 2.1 has been implemented in MATLAB, and is visually summarised in figure 2.3.

## Reorientation

In order to be consistent with the 3D coordinate description, we let the 2D image coordinates be  $x$  and  $z$ , and translate the coordinate system to have its origin at the apex point, i.e.  $L_1 = (0, 0)$ . We assume that the photo was taken such that the columnella is parallel with the viewing plane.

The landmarks  $L_3$ ,  $L_5$ , and  $L_{12}$  are assumed to be placed at homologous positions on the last three half whorls, which allows us to find an approximation of the coiling axis by using properties of logarithmic helicospirals described in (Van Osselaer and Grosjean, 2000). Applied to our set of known points, we use the following equations to approximate the orientation of the coiling axis:

$$\begin{cases} X = L_{12} + \alpha(L_3 - L_{12}), \\ Y = L_5 + \alpha(L_{12} - L_5), \\ Y = \beta X, \end{cases} \quad (2.5)$$

where  $X, Y$  are the two unknown points where the the coiling axis intersects the straight lines between the points on consecutive half whorls (figure 2.3a). We can use these equations since the widths of consecutive half-whorls are assumed to be proportional to each other, and since  $X$  and  $Y$  are on a straight line through the origin. We calculate the coordinates of  $X$  and  $Y$  by doing coordinate-wise algebraic manipulation of the above equations, resulting in a second degree polynomial in  $\alpha$ . We solve this equation and choose the solution where  $\alpha \in (0, 1)$ , meaning that  $X$  and  $Y$  are restricted to being between their respective whorl points. The disregarded solution describes where  $X$  and  $Y$  lie on the extended lines through their whorl points, with the origin on the straight line between them. Using this we can find the angle  $v$  needed to align the negative  $z$ -axis with the inferred coiling axis through  $L_1$ ,  $X$ , and  $Y$ . After reorienting the landmarks to the desired coordinate system, we can proceed to approximate the values of the shape parameters.

## Estimating the values

To approximate the aperture size and position in the above-defined coordinate system, we start by least square fitting a circle to the upper part of the aperture using  $L_7, L_4, L_3, L_{14}, L_5, L_{15}$ , and  $L_{11}$ . This gives us the circlipse reference point and its size, i.e. the parameters  $r_0, h_0$  and  $a_0$  (figure 2.3b).

To find approximations for the growth parameters,  $g_w$  and  $g_h$ , we use the four landmarks  $L_2, L_3, L_{12}, L_{13}$ , together with the widest point of the fitted circle,  $W = (r_0 + a_0, h_0)$ . We use  $W$  rather than  $L_5$  as the widest point of the whorl since it relates to the reoriented coordinate system. However, these points are usually close together and so this choice is unlikely to make a large difference. The values are estimated by fitting exponential functions to the  $x$  and  $z$  coordinate values, respectively, as functions of  $t$ , and being a rotation of  $\pi$  apart. To make this approximation more robust we only consider functions close to the respective coordinate values of  $W$ , deviating with at most a factor of 0.01, since this point best satisfies our assumptions of being at the widest point of the whorl.

We also need to approximate the extreme point of the circlipse and its orientation, where we will take into account that the image is a projection of a 3D shape, and that the extreme

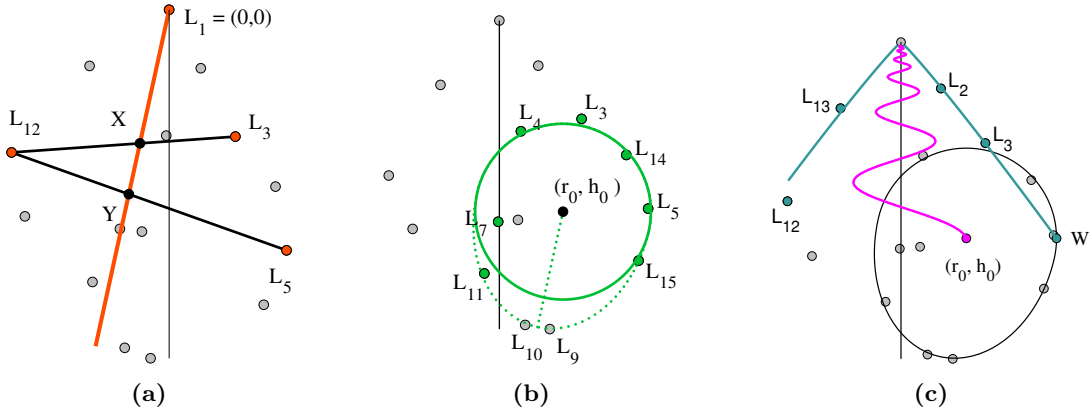


**Figure 2.3:** Procedure for approximation of parameter values. (a): Approximation of the coiling axis (orange) from the photograph, which is used for reorientation equation (2.5). (b): Position and size of the circular part of the aperture (green). The projection of the circliptic extension, and its orientation (dashed green). (c): Growth parameters generating the internal spiral, in pink, with the outer spiral profile in blue.

point of the circlipse does not correspond to a specific landmark. We use both  $L_9$  and  $L_{10}$  to define the 2D projection of the circliptic extension and orientation; their mean length from the midpoint  $(r_0, h_0)$ ,  $\hat{c} = (|L_9 - (r_0, h_0)| + |L_{10} - (r_0, h_0)|)/2$ , and mean angle relative to the  $z$ -axis,  $\hat{\theta} = (\theta_9 + \theta_{10})/2$  (dotted line in figure 2.3b).

We note that the aperture of the model is not parallel to the image  $xz$ -plane, as it lies in the normal plane of the spiral  $L(t)$  at  $t = 0$ , which can be found using the parameters previously obtained. To simplify the calculations, we rotate the curve  $L(t)$  around the vertical  $z$ -axis to make the aperture plane parallel to the  $x$ -axis, note however that the normal plane is still both tilted and rotated relative to the  $xz$ -plane. The angle between the spiral's normal vector at the aperture,  $\mathbf{N}(0)$ , and the  $x$ -axis is therefore subtracted from the angle  $\hat{\theta}$ , giving us the desired approximation of the circlipse rotation angle  $\theta$ .

We can now calculate what value of the circlipse extension parameter  $c$  is needed in order to have length  $\hat{c}$  after projection. We calculate the length of the projected aperture unit vector in the direction of the extreme point, and use the fact that this vector has the same length relation before and after projection as the length  $c_0$  to the length  $\hat{c}$  of its projection.

In addition to the seven parameters obtained from the landmark data, we have the thickness parameter obtained from separate measurements. Since we are interested in the relative thickness, we divide the measured thickness value for each shell with the approximated aperture size value  $a_0$ , giving us the parameter  $\tau = \tau_0/a_0$ . To further remove size from this analysis, we normalise each shell to have unit length, defined as the distance between the apex and landmark  $L_9$ . This only affects the value of the linear measurements in the model,  $r_0$ ,  $h_0$ , and  $a_0$ , while the rest of the parameters are relative, and hence invariant under scaling.

### Assessing the approximation method

To be able to tell if the parameter approximation method gives us reasonable shell models, we position points  $M_i$  on the models to mimic the original landmarks  $L_i$  on the photo. These points are then projected to the  $xz$ -plane to be compared with their respective original

landmark points. However, only 10 of the original 15 points can be positioned on the models, and the apex is not included in the comparison since it by definition has the same coordinates for both sets of landmarks. Hence, only nine points are compared (figure 2.4).

To reorient the shell, we start by rotating it around its coiling axis to get the aperture parallel with the  $x$ -axis, using the same angle as in the aperture parameter approximation. For the next step we need to rotate the shell around the  $y$ -axis, i.e. in the 2D image plane, to get the same reference frame as when the original landmarking was done. We need to take into account both the reorientation angle  $\nu$  of the inferred coiling axis relative to the image, and the reference frame used in the original landmarking procedure, defined by the line between  $L_1$  and  $L_{10}$ . Note that the apex stays fixed in the same position during the rotations since it is at the origin. After these rotations we position  $M_{10}$  as the lowest point on the shell for which  $x = 0$ .

The points  $M_5$  and  $M_{12}$  are positioned at the widest points of the shell, i.e. maximum and minimum  $x$ -value of the shell's the outline, and the points  $M_8$  and  $M_{14}$  are placed to have the same  $z$ -values but positioned on the outline on their respective opposite sides. The points  $M_2$ ,  $M_3$  and  $M_{13}$  can be found where the outlines of consecutive whorls have equal  $x$ - and  $z$ -values. Lastly, we put  $M_9$  as the extreme point in  $z$  value.

We make an orthogonal projection to the  $xz$ -plane which gives the 2D coordinates to compare with the original landmark points. The difference score is defined as the mean distance between the nine pairs of corresponding points (figure 2.4). We use the score obtained for the shells in this analysis to quantify the performance of the parameter approximation method. This is only a rough estimate of their likeness since the comparison relies on only nine points of the shells outline. Note also that this does not directly measure how accurate the parameter values are, but how well the model and original landmarks match.

## 2.5 Statistical analysis

### Parameter analysis for the growth-based method

The growth parameters,  $g_w$  and  $g_h$ , and the circlipse extension parameter,  $c$ , were log-transformed before the statistical analyses.

To investigate how strongly the parameters were related to the habitat difference, we computed the Pearson correlation coefficient between each of them and the habitat score. This was done for each of the four sites separately and compared to see if the correlations were consistent or differed between them.

To visualise how and where the parameter values changed in transects across the environmental transitions, we rescaled the values of the parameters between  $[0, 1]$  at each site, and reoriented them such that greater values were associated with the wave habitat. Then we calculated a moving average using 10% of the total number of snails as a function of their position on the shoreline. This smoothed function was then viewed together with the habitat score. One growth parameter value outlier was removed for this analysis to make the rescaling consistent.

To investigate the presence of sexual dimorphism, we computed the canonical variable maximising the differences between the sexes, a linear combination of the parameters, and compared the difference in distributions for males and females. We also calculated the correlation coefficients for each shape parameter with sex. The parameter with the strongest

correlation was further investigated and viewed as a function of shore position, including the moving averages using 15% of the snails for each sex. This was done to examine whether the sex difference varied between the environments.

## Geometric morphometrics

Using the same set of 15 landmarks as for the growth-based method, we investigated the shape variation using the traditional GM method implemented in the R package geomorph (Adams et al., 2019). We conducted a PCA of the full set of shells to verify that we obtain results consistent with previous analyses, i.e. that the largest component of shape variation, PC1, relates to the difference in habitat (Ravinet et al., 2016; Johannesson and Johannesson, 1996). We also did a PCA of the parameters from the growth based method, and calculated the correlation coefficient between the first PC of each method, together with visualisations of their associated shape variations, and used that as an indication of how well these two shape scoring systems coincide.

## 2.6 Results

### Method assessment

The difference in landmark position between the original image and the model suggests that our method achieved a reasonable model approximation for most shells. All shells obtained a mean distance between landmarks on the original image and model of less than 0.076, i.e. 7.6% of shell length, and 96% of shells had a mean distance of less than 0.05 (figure 2.4). The most common mismatches between landmarks were in the vertical position of the two leftmost and two rightmost points (figure 2.4h), this can usually be attributed to an underestimation of the aperture size  $a_0$  when landmarks  $L_{15}$  and  $L_{11}$  are high up and close to landmarks  $L_5$  and  $L_7$  respectively. This is a result of the variability in landmark  $L_{11}$  when placed according to the landmarking procedure. The method was in general slightly more stable for crab type shells (figure 2.4a), this could be because some wave type shells did not have much spire visible, which can introduce some uncertainty of the position of the apex landmark, and this also causes the suture landmarks  $L_2$ ,  $L_3$ , and  $L_{13}$  to conform less well to the assumptions of the new method. Since these are problems relating to the landmarking process in itself, it is also an issue for the GM method, and emphasises the problems of not having true homologous points to work with on snail shells.

### Comparison with Geometric Morphometrics

The PC1 scores from GM and the growth based method had a high correlation with each other. The calculated Pearson's correlation coefficient was  $r = 0.94$ . Visually, the two methods showed the same type of general shape changes when comparing the deformation grids of GM to the models of the growth based method (figure 2.5). This variation is also consistent with the previously described shape differences between the habitats: small, narrow apertures and tall spires in the crab habitat, and large, round apertures with short spires in the wave habitat. For our new growth-based method, the habitat-related PC1 explained 53% of the total variation of the eight parameters.

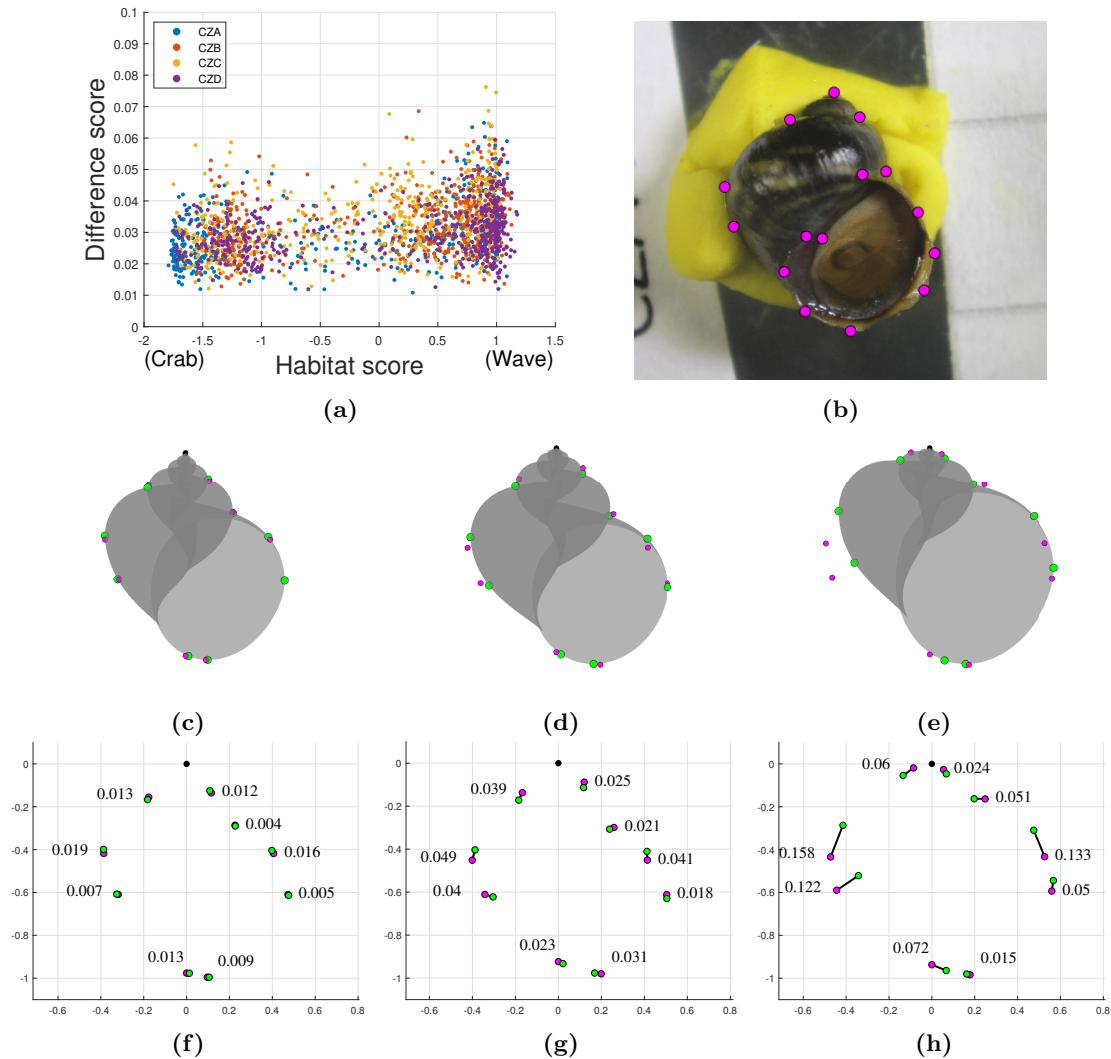


**Figure 2.4:** Success of the method. (a) The difference score for each model plotted against the habitat score, and coloured by site. (b) The original photo with superimposed landmarks of a typical example with a difference score of 0.032. We show the model with the best fit (c) with a difference of 0.011, the fit (d) of the typical shell in (b), and the worst fit (h) with a difference of 0.076. In the bottom row we have the comparison between respective landmarks of the models above, numbers indicating the pairwise distance relative the shell height. Original landmarks are visualised in pink, and model landmarks are green.

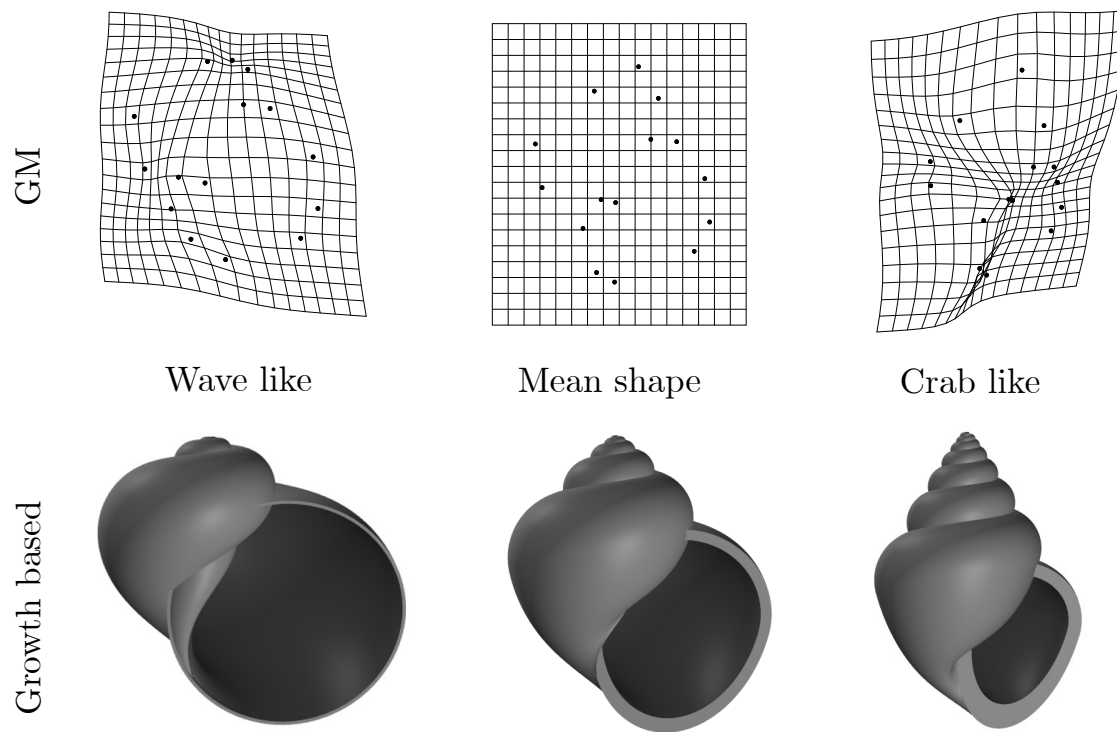


**Figure 2.5:** Visualisations of the means and extremes of PC1 for the geometric morphometrics method and growth-based method.

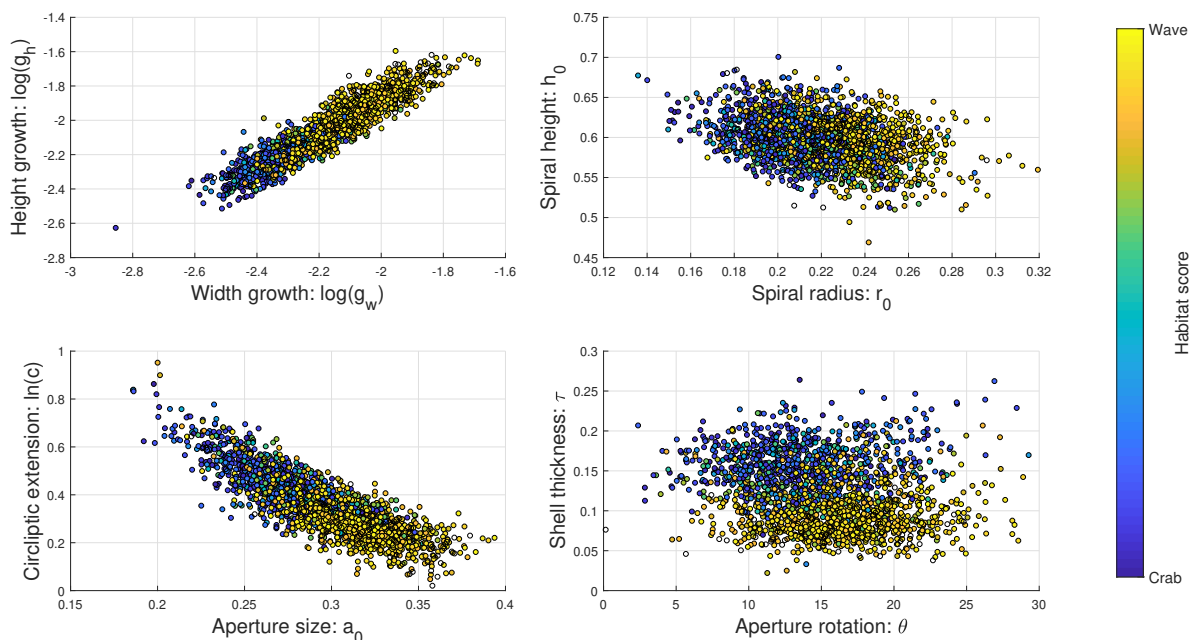


**Figure 2.6:** Distribution in the parameter space of the analysed shells, coloured by the habitat score.

|     | $g_w$ | $g_h$ | $r_0$ | $h_0$   | $a_0$ | $c$    | $\theta$ | $\tau$ |
|-----|-------|-------|-------|---------|-------|--------|----------|--------|
| CZA | 0.763 | 0.758 | 0.485 | -0.108  | 0.742 | -0.65  | 0.419    | -0.761 |
| CZB | 0.635 | 0.633 | 0.451 | -0.19   | 0.582 | -0.458 | 0.232    | -0.714 |
| CZC | 0.717 | 0.69  | 0.515 | -0.0341 | 0.619 | -0.537 | 0.405    | -0.689 |
| CZD | 0.735 | 0.711 | 0.477 | -0.222  | 0.668 | -0.523 | 0.0562   | -0.641 |

**Table 2.1:** The correlation coefficients for each parameter with the habitat score, separated by site. Positive correlation values indicate that larger values of that parameter were associated with the wave habitat, negative values indicate larger values were associated with the crab habitat.

## Growth-based method

In terms of ecotype difference, six of the eight parameters co-varied with habitat at all four sites, having moderate or high correlation coefficients ( $|r| > 0.45$ ) at each site (table 2.1). The parameters that did not show a consistent correlation with habitat were the relative height of the spiral,  $h_0$ , and the aperture angle,  $\theta$ . The values of the six environmentally correlated parameters varied continuously between the habitats rather than splitting the snails into two separate clusters (figure 2.6), indicating that no intermediate shapes were missing. There was also substantial variation within the different environments, but this was smaller than between the habitats.

The six consistently habitat-correlated parameters covaried as the environment changed, and the main shifts in values were close to the environmental transitions (figure 2.7). Small areas of wave-type environment in the crab habitat, as in site CZA, did not have a great influence on the parameter values, while small crab-type environmental patches in the wave

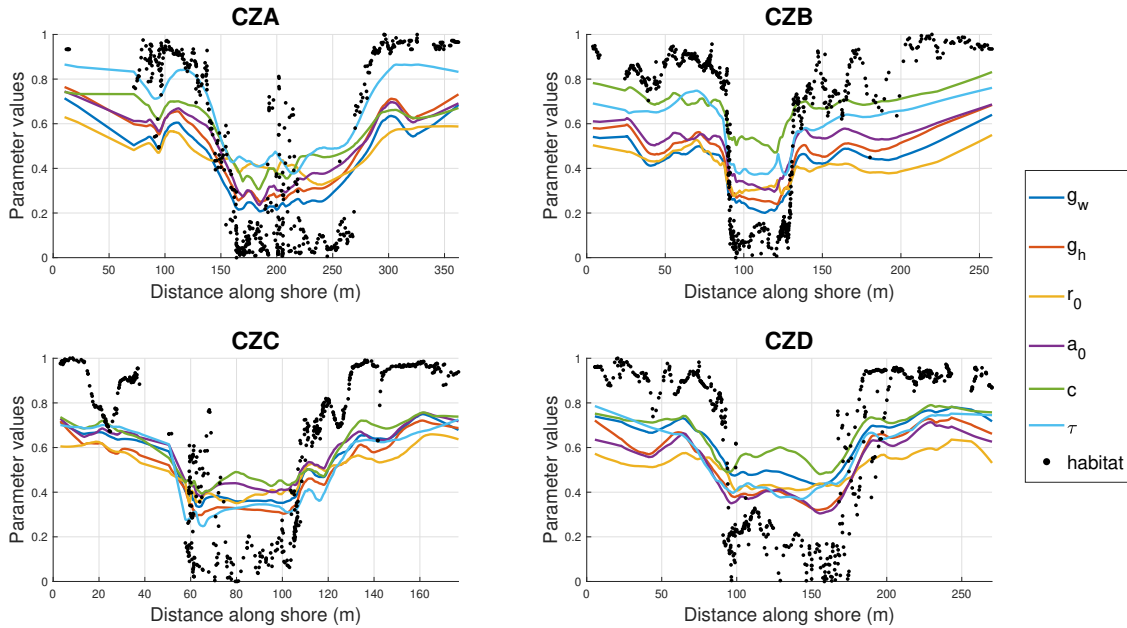


**Figure 2.7:** The relative variation of the parameters as a function of shore position, separated by site. Each line represents the moving average of one parameter, and the dots represent the habitat score at the position of each snail. Oriented such that the higher values are associated with the wave habitat. The two parameters  $h_0$  and  $\theta$  were excluded from this figure since they had no clear correlation with habitat.

habitat showed a stronger effect on shape, as in site CZB. This has been observed before, and has been suggested to be an effect of crab predation being a stronger selective pressure than wave exposure (Westram et al., 2018). In addition to the parameters covarying across the largest environmental transitions, we can also see that they covary to a large extent even within the separate environments. Note also that the independently measured thickness parameter shows a similar pattern to the other habitat-related parameters.

At site CZD we obtained a difference in some parameter values compared with the other sites. The parameters mainly showed the same type of variation relating to habitat (table 2.1), but located around a different mean value. This can be seen, for example, in the parameter with the lowest habitat correlation, the spiral height  $h_0$ , as well as in a parameter with much stronger habitat correlation, the aperture size  $a_0$  (figure 2.8). The aperture rotation angle  $\theta$  on the other hand, did not show this pattern, instead it changed to having a even weaker correlation with habitat at CZD compared with the other three sites (table 2.1).

There was also a difference in parameter values between males and females, independently of sites and habitat. Viewed along the canonical vector maximising the distance between males and females from all sites combined, there was a clear difference between their means (1.4 standard deviations), but the distributions were still mostly overlapping (figure 2.9). The parameter most strongly correlated with sex was the aperture size,  $a_0$ , with males having larger apertures for their height than females (table 2.2). This, together with larger growth parameter  $g_w$  and  $g_h$ , and smaller height,  $h_0$ , and radius,  $r_0$ , of the internal spiral, and smaller circlipse extensions,  $c$ , suggests a larger and rounder aperture, without changing the total width much. However, the difference between males and females was small compared with

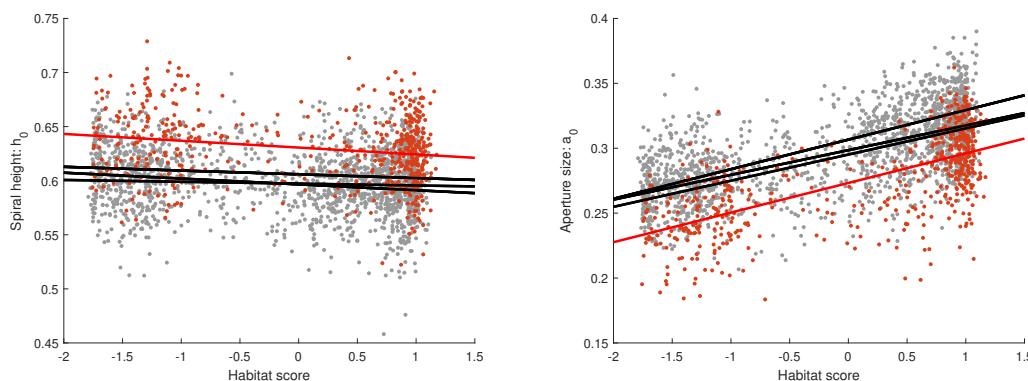


**Figure 2.8:** The difference in values of the spiral height  $h_0$  and aperture size  $a_0$  between sites. Site CZD in red, other sites in grey. Lines show the least square fits relative to the habitat score, one for each site with CZD in red.

|     | $g_w$ | $g_h$  | $r_0$  | $h_0$   | $a_0$ | $c$    | $\theta$ | $\tau$ |
|-----|-------|--------|--------|---------|-------|--------|----------|--------|
| CZA | 0.101 | 0.0754 | -0.204 | -0.292  | 0.146 | 0.0622 | -0.0481  | 0.078  |
| CZB | 0.274 | 0.197  | -0.107 | -0.294  | 0.288 | -0.147 | -0.223   | 0.125  |
| CZC | 0.143 | 0.147  | -0.21  | -0.0964 | 0.183 | -0.107 | -0.173   | 0.137  |
| CZD | 0.183 | 0.144  | -0.127 | -0.207  | 0.24  | -0.126 | -0.147   | 0.072  |

**Table 2.2:** Correlation coefficients for each of the parameters and sex, at each site. Positive correlation coefficient indicate that larger parameter values are associated with males, while negative correlations indicate larger parameter values are associated with females.

the total variation, and therefore the correlation was not very strong for any of the parameters, although it was fairly consistent in both types of habitats and at all sites (figure 2.9).

## 2.7 Discussion

This new method for quantification and description of gastropod shell shape variation achieves reasonably accurate approximations despite using only 2D data designed for GM analysis. Note however that the accuracy is not measured for the individual parameters, but for how well the landmarks on the shell model that they generate coincide with the landmarks from the original image. The two main advantages to using a growth-based method over GM are that it describes the developmental process underlying formation of the shell structure, and that this description is intrinsic and not relative, meaning that different samples or species can be added to, and compared directly in the resulting parameter space. Having a growth-based description should give new insights into the environmental and genetic factors underlying variation in different aspects of shell shape. Additionally, the method generates shell models that can be used for further analyses, e.g. fluid dynamic studies of shells in water flows or structural analysis of shell strength, which relate back to the contrasting natural selection pressures for the ecotypes of *L. saxatilis* discussed here. It should be noted, however, that the

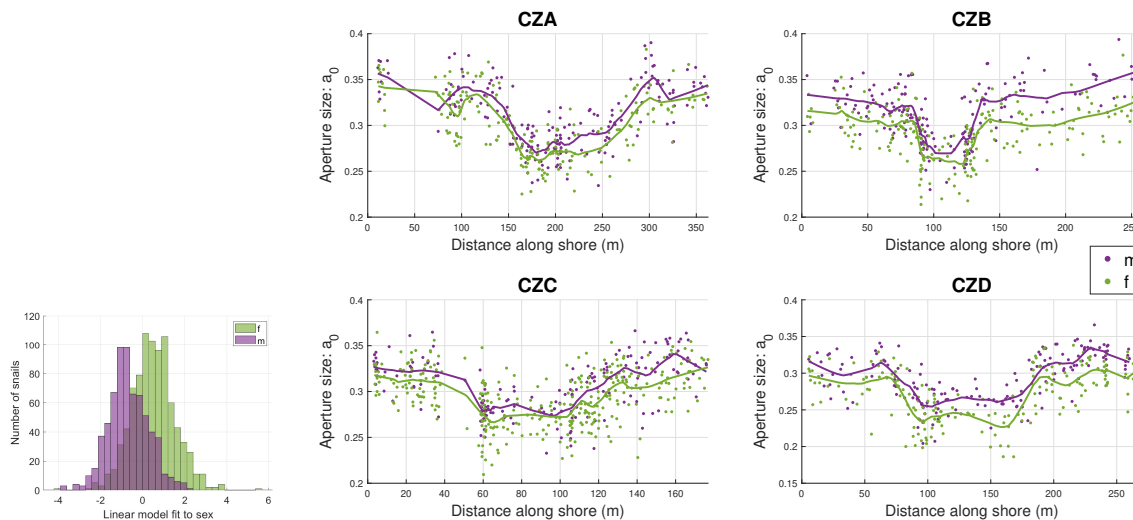


**Figure 2.9:** Left: Distribution of the sexes along the canonical variable maximising their difference in means when combining the data from all sites. Right: The aperture size values  $a_0$  plotted as points along the shoreline with males in purple and females in green, juveniles not shown. Moving averages are plotted as curves of their respective colour.

models do not include any surface roughness or information on material strength or thickness variation. This needs to be taken into account in any further analysis.

This method provides an intuitive way of describing the shell shape variation of many gastropods. It is possible to apply this method to any structure which can be approximated as a tube with a circliptic cross section and which is increasing in size proportionally to, and along a, logarithmic helicospiral. This regular growth pattern is commonly, but not exclusively, found in snail shells, and is what allows us to go from a single 2D image to a 3D representation, which is not possible to do in general. Further, the stability of finding the reference point of the aperture circlipse from its circular part, together with the flexibility of extending parts of it without affecting this reference point, is a feature which lets us apply this method to a large range of snail species (appendix B). This idea could also be built upon, to account for an even more diverse range of shell shapes, by incorporating more complex aperture shapes as long as we can consistently fit a circle to part of the aperture. From this description it should also be possible to convert the parameters to those of a growing tube model (Noshita, 2014), giving us two different characterisations describing the same growth. This could further improve the understanding of shape variation from the perspective of the local accretion process at the aperture.

Using this method we can account for certain types of variation in shape during growth. If the growth parameters are equal for a shell,  $g_h = g_w$ , then it has isometric growth, i.e. the shape does not change over time. However, for this sample we mainly obtained larger growth values for height than for width,  $g_h > g_w$ , although still close to equal, suggesting a slightly convex spire profile (figure 2.1). Previous work has already shown some evidence of shape variation of *L. saxatilis* during growth using other methods (Carvajal-Rodríguez et al., 2005; Hollander et al., 2006a; Johannesson and Johannesson, 1996), but using GM it can be hard to separate ontogenetic changes from other size-related variation (Klingenberg, 2016). To

investigate how much size-related variation can be accounted for by the convexity described above, rather than, for example, changes in the growth parameters, further growth-based analysis of shells at different stages of development will be needed. For shells where allometry can be attributed to unequal but constant growth parameters, it is possible to use this method to visualise the ontogeny of a given shell, and to predict the future shape of a shell that will continue growing. For isometrically growing shells, this is trivial since their shape does not change over time.

In our analysis of *L. saxatilis* shells, we could quantify the same major differences between ecotypes which has been described in previous studies using other methods (Le Penneec et al., 2017; Ravinet et al., 2016). However, the variation described when using GM is interpreted by visual inspection of the point variation in thin plate splines obtained after a PCA, which therefore depends on the samples used. By contrast, in the growth-based analysis variation is described by a set of intrinsic values which are directly comparable between studies and gives a quantification of parameters such as growth rates. In addition, the description presented in this paper allows us to relate the current shape of the shell to how it developed over time. We obtained larger growth values in snails of the wave ecotype, meaning that their shells increase in height and width more per revolution than in the crab ecotype, and therefore the aperture and most recent whorl make up a larger proportion of the whole shell. The apertures were smaller in the crab ecotype but also more elongated. The reason for the relative spiral height  $h_0$  not varying much between habitats is that the elongation of apertures in the crab ecotype covaries with taller shell spires. The aperture rotation angle  $\theta$  does not affect the shape of circular apertures and is therefore not informative in the wave habitat. To further understand how the correlation between parameters relates to constructional, environmental and genetic factors, more analysis is needed.

In addition to the large ecotype-related variation, we also found a consistent difference between the two sexes at all four sites, though the total effect this has on shape is very small. Some shape differences between the sexes have been detected in previous studies, although they were only described separately in terms of allometry at different growth stages for different habitats (Hollander et al., 2006b). The differences found in this analysis mainly suggest that males have a slightly larger and rounder aperture relative to their size than females. This difference could be due to the position of their reproductive organs. Since the distributions are mostly overlapping, it is unlikely to be directly useful as a method for sexing individuals. However, the ability to pick up such a small difference and describe it in terms of growth could still be useful in future analyses and the model could be extended to consider the impact on internal volume.

We also found that the shape of snails at site CZD was consistently different from the other sites. This was mainly due to a difference in the position of the landmark  $L_4$ , which is therefore also detectable as a difference when using GM. There are two possible explanations for this deviation: either the shells were consistently positioned differently for the photographs at this site, or there is a true difference in shape at that site. The shells were destroyed during dissection, and therefore cannot be examined further. Either way, there is a difference in landmark position on the photographs. If this is not a true shape difference, it suggests that changing to a more stable method of positioning shells and extracting data than the current method would be desirable. This highlights the problems of consistency in positioning and selection of homologous points on a structure that grows by accretion, a problem common to GM and our approach. However, the combined effect of variability in shell orientation

and landmark position was small enough that it did not obscure the main shape variation of biological interest, the difference between ecotypes.

The method could be improved further. As noted before we could improve the input data, selecting different points and other geometric structures (e.g. manually placing the circlipse) in the images, and making use of outline data, as well as standardising the shell position differently to be more optimal for finding growth parameters, for example following the procedure found in (Callomon, 2019). This could improve both the accuracy itself, and the ability to measure the accuracy, and possibly lead to an automatisation of the process. In addition, this could make it possible to compare a larger range of shell types, for example by allowing relaxation of the assumption that the spiral radius and aperture growth rates are equal. A slightly modified version of the parameter approximation method was applied to shells from other species of snails to illustrate its potential range of applicability (see supplementary material). Future effort will include making this method accessible to conchologists, without requiring full mathematical understanding of the procedure.

## 2.8 Acknowledgements

We thank Kerstin Johannesson for her input at all stages of the project. Irena Sencic, Laura Brettel, Anne-Lise Liabot, Juan Galindo and Mark Ravinet helped in the collection and landmarking of snails, and Sean Stankowski provided feedback on the manuscript. JL was funded by a studentship from the Leverhulme Centre for Advanced Biological Modelling. We are also grateful for support from the European Research Council, Natural Environment Research Council (UK), Swedish Research Council (VR), the University of Gothenburg and the Centre for Marine Evolutionary Biology. We also thank Martha Gibson for help with naming the circlipse.

## Chapter 3

# Investigating the genetic architecture of shell shape

J. Larsson<sup>1</sup>, E. Koch<sup>1</sup>, T. Lundh<sup>2</sup>, R. K. Butlin<sup>1,3</sup>

<sup>1</sup>Department of Animal and Plant Sciences, University of Sheffield, Sheffield, UK

<sup>2</sup>Mathematical Sciences, Chalmers University of Technology  
and University of Gothenburg, Gothenburg, Sweden

<sup>3</sup>Department of Marine Sciences, University of Gothenburg, Strömstad, Sweden

**Contributions** R.K.B. conceived the project. J.L. did the analysis and interpretation of the shape variation. E.K. contributed with the QTL and variance partitioning analyses. J.L. drafted the manuscript and all authors provided input on subsequent versions.

## Abstract

When relating complex biological traits, such as shape, to their genetic basis, choosing an appropriate quantification method is crucial. We therefore implemented two types of shape quantification, the standard geometric morphometrics (GM) method and a new growth based method, to better understand how they differ in their ability to identify genomic regions responsible for variation in different aspects of shape in gastropod shells. For the intertidal snail *Littorina saxatilis*, shell shape variation has been shown to be largely heritable and is an important adaptive trait for survival in contrasting environments. We implemented both quantitative trait loci (QTL) and variance partitioning analyses to associate parts of the genome to different aspects of shape, providing new insights into the genetic architecture of these traits. The growth based quantification is more informative in describing genetic effects on different biologically relevant traits as its parameters relate to the shell construction process, while the geometric morphometrics method employs a principal component analysis which combines aspects of shape to explain the greatest amount of variation with a small number of components, making these results more difficult to interpret in terms of distinct biological features. We found evidence both for specific loci responsible for determining significant amounts of variation in different shape traits, and traits more likely to be determined by genomic regions containing several loci of small effect. The growth based method also indicated the existence of a genetic component associated with variation in allometric growth.

**Keywords**— Growth, Morphometrics, Snail shells, Shape variation, Gastropod

## 3.1 Introduction

To improve our understanding of the connection between long-term evolution, environmental adaptations, and the developmental processes of organisms, it is important to have useful quantification methods (Klingenberg, 2010; Liew and Schilthuizen, 2016). Different methods are able to describe different types of variation, and are therefore expected to be able to answer different types of biological questions (Bo et al., 2014). The type of method used to quantify such complex traits as shape will affect the ability to describe variation in terms of development and functional properties, and also how effectively genetic analyses can attribute different aspects of variation to specific genetic regions. To this end, snail shells are an ideal structure to study, as it is possible to see their growth process from the final shape due to the accretionary construction process (Hammer and Bucher, 2005), and to follow how the shape evolves over time in response to natural selection in different environments (Giokas et al., 2014).

Geometric morphometrics (GM) using Procrustes superimposition is commonly used for shell shape quantification in many species of snails, for example to investigate morphological adaptations to different environments (Guerra-Varela et al., 2009; Cazenave and Zanatta, 2016; Dowle et al., 2015), effects of pollution (Márquez et al., 2017; Abdelhady, 2016), and to explore the genetics and heritability of shape (Westram et al., 2018; Dillon and Jacquemin, 2015; Pascoal et al., 2012). Due to the accretionary growth of snail shells, there are very few truly homologous points throughout growth and between specimens, which is a key issue when implementing a GM approach. Despite the lack of homologous points, the GM method has

been successfully used to quantify the main shape differences using sets of landmarks including non-homologous points as if they were homologous (Carvajal-Rodríguez et al., 2005; Ravinet et al., 2016). The GM method generally describes the shape differences using principal component analysis (PCA) to summarise the variation into its main correlated components, which often describing covariation in several traits at once. This is very useful for distinguishing between groups of specimens and describing their overall differences, but can be hard to interpret in functional terms (Cooke and Terhune, 2015; Bookstein, 2015), and when relating to development and genetics, especially in the case of the rigid accretionary construction method of gastropod shells.

A shape description based on Raup's parameters is suggested to give additional information about growth and form (Hammer and Bucher, 2005), as it uses parameters that describe the shell's development (Raup, 1961). Additionally, as it is an intrinsic shape description, not dependent on the data set it is obtained from, the set of parameter values obtained can be compared directly between samples and species. We are therefore testing the potential of a recent addition to the growth based quantification methods of snail shells (Larsson et al., 2020), which was developed to be able to handle large data sets of shells with variable aperture shapes of the type found in many taxa, including our study species *Littorina saxatilis*. This quantification can also account for certain types of allometry, by having separate growth parameters for the increase in height and width per revolution. Despite the two growth parameters each being assumed constant throughout growth, we can account for two growth types in addition to isometric growth, namely convex and concave spire profiles. A convex shell is generated when, for each whorl constructed, the height of the shell increases more than its width, while for a concave shell the opposite holds (section 3.3.2).

The intertidal snail *Littorina saxatilis* is a well studied example of how local adaptation can produce ecotypes of high morphological differentiation in response to contrasting environments (Johannesson et al., 2010; Butlin et al., 2014). The differentiation of interest in this analysis is between the ecotypes known as 'crab' and 'wave', named after the main selective pressure in their respective habitats. Snails from wave exposed environments are small, have a thin shell, a round aperture which is large relative to shell size, and they are adapted to withstand the strong forces from crashing waves (Le Pennec et al., 2017). In contrast, snails from more sheltered parts of the shore are larger, have a thicker shell with a narrower aperture, which are adaptations to resist crab predation (Johannesson, 1986; Boulding et al., 2017). In analyses using growth-based parameters, ecotypes show a clear difference in growth per whorl, with the wave ecotype shells having a larger increase in size per revolution of shell (Walker and Grahame, 2011; Clarke et al., 1999; Larsson et al., 2020). The consistent formation of crab and wave adapted ecotypes can be found on rocky shores in much of the North Atlantic, and has been suggested as an example of parallel speciation with ongoing gene flow (Butlin et al., 2014). Current research into the *Littorina* system is aiming to better understand the process of speciation, and the emergence and persistence of ecotypes despite ongoing gene flow, and it is therefore desirable to have a functionally relevant connection between genotype and phenotype of the ecotypic adaptations.

Previous analysis of *L. saxatilis* has found that the shell shape differences between the crab and wave ecotypes can largely be attributed to genetics (Carballo et al., 2001; Conde-Padín et al., 2007, 2009). Some phenotypic plasticity and allometric variability of shape have also been detected (Saura et al., 2012; Hollander et al., 2006a; Johannesson and Johannesson, 1996), although having a smaller effect on shape than the genetics (Hollander et al., 2006b;

Conde-Padín et al., 2009). Two recent analyses using GM in Swedish and Spanish snails respectively, suggested that the biggest effect on *L. saxatilis* shape variation could be attributed to specific subsets of linkage groups, with LG17 indicated in both samples (Westram et al., 2018; Kess et al., 2021). In the case of the Swedish snails it was also showed that there was a high heritability in this trait (Westram et al., 2018). In contrast, other phenotypic traits, such as shell thickness, have been shown to have greater plasticity in other *Littorina* species, *L. obtusata* and *L. littorea*, where the thickness is increased in response to presence of crabs (Trussell, 1997a, 1996; Kemp and Bertness, 1984).

The main aim of this study is to better understand how the choice of quantification scheme affects the ability to connect genotype with phenotype. To this end we have investigated whether a developmentally descriptive method can give a clearer picture of the genetic architecture of different aspects of shell shape than the previously used GM approach, since it relates more directly to the shell’s construction process. This gives insight into which type of traits are useful for quantitative genetic analysis, as this can be different from traits which are good for quantitatively distinguishing the main morphological differences between groups, and therefore improves the ability to relate the genetic basis of shell shape with functionality and environmental adaptations.

## 3.2 Methods

### 3.2.1 The F2 setup and genetic analysis

Four field collected snails, two from the crab environment and two from the wave environment, were obtained from Ängklåvebukten ( $58.8697^\circ$ ,  $11.1197^\circ$ ), which is the same site as investigated in (Westram et al., 2018; Faria et al., 2019a). Tissue for genotyping was obtained from the foot of the second generation offspring, F2, of lab reared hybrid crosses generated from the four field collected snails, to provide genetic data for a set of related individuals with varying morphologies expected to be spanning the range of phenotypes between those of the four grandparents. DNA extraction was performed using a CTAB protocol Panova et al. (2016), and were sequenced using a targeted re-sequencing approach as described in Faria et al. (2019a) and Westram et al. (2018). In total 25 000 (120 base pair) enrichment probes were used, most of which were chosen due to being informative in Westram et al. (2018). The processing of raw genetic data was implemented as in Faria et al. (2019a), including trimming with Trimmomatic v. 0.36 Bolger et al. (2014), quality control with FastQC v0.11.5 Andrews (2010), mapping with BWA v0.7.15 Li and Durbin (2009), duplicate removal and InDel realignment with Picard v. 1.138 (<http://broadinstitute.github.io/picard/>), and SNP calling with GATK UnifiedGenotyper v3.7-0 Depristo et al. (2011). After processing and further aggressive filtering to only include high confidence results using with vcftools Danecek et al. (2011) and vcflib (<https://github.com/vcflib/vcflib>), a final set of 22 759 sites remained.

Despite efforts to control each mating pair by separating them into tanks before the snails reached maturity, this was not completely successful. To compensate for the incomplete pedigree, the relationship between the F2 offspring was evaluated similar to VanRaden (2008) using genomic data and the R-package AGHmatrix (Amadeu et al., 2016). Further details can be found in Koch et al. (2021) (appendix F). The genetic data of 386 F2 snails were ordered into a linear linkage map using LepMap3 (Rastas, 2017), which does not require the

samples to come from inbred lines, and using the module ParentCall2 to estimate the missing parental data. The generated linkage map consists of 17 putative chromosomes referred to as linkage groups (LG), with a good correspondence to the previous map in Westram et al. (2018). After construction of the genetic linkage map, quantitative trait loci (QTL) mappings were implemented for univariate traits using the R/qtl2 software (Broman et al., 2019), to infer the positions of genomic regions associated with the shape traits described below on each LG, which expands the R/qtl software (Arends et al., 2010) by allowing samples from multiple parents and non-inbred lines. These associations suggest the presence of loci that influence the relevant traits. Trait associations were evaluated using the logarithm of odds (LOD) score as a measure of the likelihood of a locus contributing to the quantitative trait, where we discuss any peak with a LOD score above the significance threshold (LOD  $\approx$  4, but the exact value specific to each trait and obtained by permutation), as well as suggestive peaks (LOD  $>$  3).

A variance partitioning analysis was also implemented to estimate if a significant part of the variation of any trait could be explained by each separate LG, and if this variation was greater than expected from the length of the LG (Yang et al., 2010; Robinson et al., 2013). Variance partitioning uses the genetic relatedness matrices of the markers to estimate the trait variability attributed to separate genomic regions, such as LG, and thus complements the QTL analysis by indicating which LG contribute most to the variation, taking both single large effect loci and multiple small effect loci into account. Therefore, it gives additional insight into the genetic architecture of different traits as these loci in themselves might not have large enough effects on shape to be individually detectable in a QTL analysis (Rockman, 2012). In the extreme of many genes of small effect, each LG is expected to contribute to trait variation in proportion to its length. Since the variance partitioning estimates how much of each trait can be attributed to each LG, it provides heritability estimates for each trait, both per LG as well as overall.

A total of 373 genotyped lab reared F2 snails were included in the analysis, after removing snails which did not have complete morphometric data.

### 3.2.2 Geometric Morphometrics

Landmarks were positioned on the shell images (figure 3.1a) using the procedure described in (Ravinet et al., 2016; Larsson et al., 2020). The landmark positions were then processed using the GM software MorphoJ (Klingenberg, 2011), which implements a Procrustes alignment and a PCA. The output from the GM method describes how the set of landmark points varies in the 2D image plane (section 3.3.1), and is quantified by a set of principal components ordered by the amount of variation they account for (figure 3.1b). Sources of noise in the landmark positions include those introduced from inconsistencies in the positioning of the shells for the photographs, and variation in the placement of the landmarks. One should note that the landmarks are not truly homologous, due to the lack of biologically equivalent points on the shells, but are still used as such since they still provide information for quantitatively measuring shape variation. The threshold for inclusion in the downstream analyses was set to when the PCs cumulatively explain more than 90% of the total variation, which in this case included the first seven PCs, where PC7 explained 2.9% of the total variation. Normally only one or two PCs are used to quantify shape variation using GM, as this is usually enough when the main aim is to distinguish the differences between groups. However, as we were

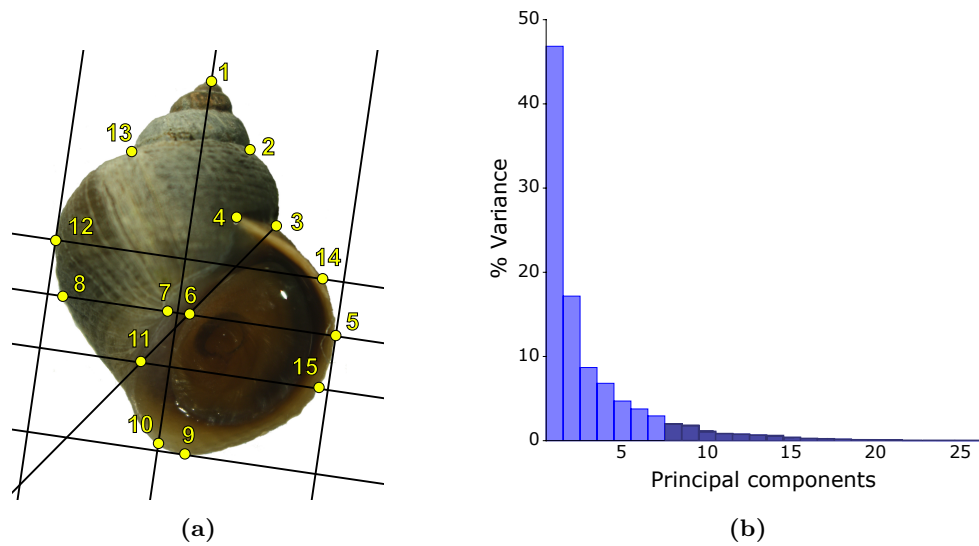


**Figure 3.1:** (a) Visualisation of the landmark positions used as the morphometric data in both the GM and growth based analysis. Due to the accretionary and spiralling growth of shells, only landmark 1 is truly homologous between specimens and throughout development. Landmarks 2, 3, 4, and 13 can be defined independently by local geometry, while the remaining ten are semi-landmarks defined using Landmarks 1 and 3 together with the construction of lines tangential to different morphological features, e.g. the aperture. (b) A scree plot of variance explained by the principal components. The first seven PCs (light blue) are included in the analysis as these combined explain over 90% of the total variation.

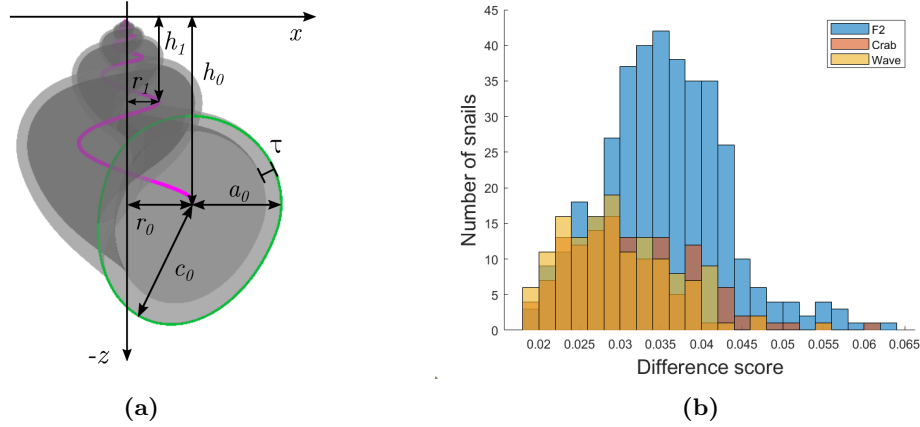


**Figure 3.2:** (a) Description of the growth based shape parameters, all shells are normalised by unit height to remove the size component. The growth parameters describes the rate of growth per whorl of the theoretical internal spiral (pink), i.e.  $g_w = \log(r_0/r_1)/2\pi$ , and  $g_h = \log(h_0/h_1)/2\pi$ , where  $\log$  is the natural logarithm. Aperture position consists of a radial,  $r_0$ , and a vertical,  $h_0$ , component of the internal spiral reference point. Aperture size is defined as  $a_0$  and aperture shape as  $c = c_0/a_0$ . The aperture rotation  $\theta$  is the relative angle of  $c_0$ , and the relative shell thickness  $\tau$  is measured as a fraction of the aperture size  $a_0$ . (b) The difference score of the growth based method for the F2 hybrids, and the pure crab and wave ecotypes. This is a rough accuracy measure of how well the shell models, and thus the shape parameters, represents the real shell. All lab reared shells received values of less than 0.065, which is no worse than the difference scores accepted for the wild snails published in (Larsson et al., 2020).

interested in examining if we could attribute different aspects of shape to different parts of the genome, we included more PCs than is normally warranted by the amount of variation they describe, despite later PCs having an increased risk of falsely attributing morphological variation or noise to genomic positions.

### 3.2.3 Growth based method

The shape parameters used in this analysis were inferred from the same set of landmarks used in the GM setup, using the parameter inference method developed in (Larsson et al., 2020). The parameters describe shell models constructed using the current aperture's shape  $c$ , orientation  $\theta$ , size  $a_0$ , and position  $r_0$ ,  $h_0$ , together with the parameters describing growth in height  $g_h$  and width  $g_w$  (figure 3.2a). The shell surface can be defined by the following function

$$S(t, s) = (r_0 e^{g_w t} \cos(t), -r_0 e^{g_w t} \sin(t), -h_0 e^{g_h t}) + e^{g_w t} C(s - \theta) (\mathbf{N}(t) \cos(s) + \mathbf{B}(t) \sin(s)) \quad (3.1)$$

where  $s \in [0, 2\pi)$  and  $t \in [-2\pi n, 0]$  for some large enough  $n$  to account for the number of whorls visible for the species used. The plane which the aperture is contained within is defined by the normal,  $\mathbf{N}$ , and binormal,  $\mathbf{B}$ , of the growth trajectory which is visualised as the internal spiral in figure 3.2a. Shells with various aperture shapes  $C(s)$  could be modelled using the above surface description. However, we currently use only the circliptic aperture

shapes introduced in (Larsson et al., 2020), i.e. those consisting of half a circle and half an ellipse of variable eccentricity described by the parameter  $c$ . More in-depth descriptions of the shell models and parameter inference method are provided in (Larsson et al., 2020).

The shape parameter values of the 373 F2 hybrids were compared to those of 277 lab reared pure ecotype snails (134 whose mothers were collected in the crab habitat and 143 whose mothers were from the wave habitat) as a control for plastic effects due to being reared in the lab. They were also compared to a set of previously published data for 2328 snails from a wild population (Larsson et al., 2020) (one extreme crab outlier was removed). The snails from the wild populations were collected from four nearby crab-wave environmental contact zone sites (CZA at 58°49'27.8"N 11°03'45.3"E, CZB at 58°50'00.5"N 11°08'19.6"E, CZC at 58° 50' 04.0" N 11° 02' 26.5" E, and CZD at 58°49'51.3"N 11°07'59.0"E), and the parents of the lab-reared snails were collected from within the crab and wave environments, away from the contact zone, at two of these sites (CZA and CZD).

The shell thickness was measured for all 373 F2 snails, 110 pure crab, 143 pure wave ecotype snails, and 1983 shells from the previously published analysis of field collected snails in Larsson et al. (2020). The relative shell thickness  $\tau$  is determined by using the absolute thickness value, measured with a thickness gauge, but as a fraction of the current external aperture radius,  $a_0$ , to remove the shell size effect, as in Larsson et al. (2020). This thickness value cannot be inferred from the current set of landmarks alone, but combines the parameters obtained from the landmarks with additional data.

The difference score between original landmark position on the shell images and estimated landmark position of the shell models were computed as a rough accuracy check of the inferred parameters, to detect any problematic specimens for the parameter inference procedure. The shell models all obtained difference scores no worse than the maximum values used in Larsson et al. (2020) (figure 3.2b), hence the parameter values are assumed to represent the shell shape reasonably well, and no shells were removed from the analysis at this stage. Note also that the thickness parameter does not affect the external shape of the shells when defined as in this model, and therefore does not affect the difference score.

The two growth parameters were transformed by the natural logarithm,  $\log(g_h)$  and  $\log(g_w)$ , to obtain a linear correlation between parameter values, and this was also how they were used in the QTL analysis. In addition, we included two more values in the genetic analysis, namely the sum,  $\log(g_h) + \log(g_w)$ , and difference,  $\log(g_h) - \log(g_w)$ , of the two transformed growth parameters as measures of the overall growth and the allometric convexity/concavity, respectively. To investigate if convexity varies between ecotypes, we did linear regressions of convexity against overall growth, as overall growth had a strong correlation with ecotype (Larsson et al., 2020). The correlation between ecotype and convexity was investigated for the pure morphs and the hybrids as well as the field collected snails. We also included shell length, weight, and absolute shell thickness as traits in the QTL analysis, to investigate overlaps in the genetic architecture of shape variability and general size differences.

Note that these growth-based parameters have been rescaled geometrically, but not statistically, to remove the size component and obtain measures of shape at the individual level rather than compensating for size at the population level. This has been done in an effort to further decouple the ecotypic shape and size covariation, but might decrease the power of detecting relevant QTL since it means computing statistical LOD-scores from trait-values without statistically controlling for size. It should not have a very large effect on the analysis presented here, due to how large the variations in both size and shape are in *L. saxatilis*,

but might be worth investigating further if analysing sample sets where the morphological variations are more subtle, or have a more complex relationships.

### 3.2.4 Comparison of methods

The Pearson correlation coefficients between the PCs of the GM method and the shape parameters were compared, and related with previous results described in Larsson et al. (2020). The correlations were also used to further interpret what shape differences were represented by the PCs.

## 3.3 Results

### 3.3.1 Geometric morphometrics

For the GM method we obtained one peak of association ( $\text{LOD} > 5$ ) reaching the significance threshold in the QTL analysis at the end of LG 17 (figure 3.3), for PC1, with this peak explaining 6.1% of the variation of PC1 values (appendix figure C.1). PC1 described a combination of variation in the shape of the aperture and a difference in the size of the spire (figure 3.4), explaining 46.8% of the total shape variation, which is roughly consistent with the main crab-wave ecotypic difference previously described. Some suggestive peaks ( $\text{LOD} > 3$ ) were detected for other PCs. For PC3 there were several suggestive peaks, positioned in the middles of LG 2, 5, and 17 (each explaining just below 4% the total variation of PC3), and this PC explained 8.7% of the total variation in shape, mainly describing the overall height to width ratio of the shell (figure 3.4). For PC4 there was a suggestive peak on LG 2 (explaining 4.4% of the PC4 variation), and this PC explained 6.8% of the total variation, and mainly describing a small variation in positions of landmarks LM4 and LM12 (appendix figure C.2). Lastly, for PC7 (which explained 2.9% of the total variation) we obtained a suggestive peak on LG 8, and this PC describes a very small interaction between the positions of LM2, LM4, LM12, and LM13 (appendix figure C.2). Neither PC2, PC5 or PC6 (appendix figure C.2) obtained and peak with  $\text{LOD} > 3$ .

The variance partitioning showed the clearest contributions from LG17 for PC1, LG12 for PC3, as well as LG6 and LG9 for PC6, which all explained more variation than expected from the length of the LG (figure 3.5, and appendix figure C.3). In addition, LG17, LG12, and LG6 were indicated to account for significant variation in other PCs. Several other LG also showed significant contributions, but not more than expected from their size, to the different PCs, most notably LG2 and LG5. The overall heritability estimates were between 0.12, for PC2, and 0.39, for PC3, describing the fraction of variation in each trait which could be attributed to genetic effects.

### 3.3.2 Growth parameters

We found two LG with significant QTL peaks for the growth based shape parameters, on LG17 and LG6, and additional suggestive peaks on LG12 and LG2 (figure 3.6). The parameter height growth,  $g_h$ , obtained a peak in the middle of LG17, which reached just above the significance threshold, while the parameter width growth,  $g_w$ , shows two suggestive peaks, one at the end of LG17 and one near the peak of height growth. The sum of the two

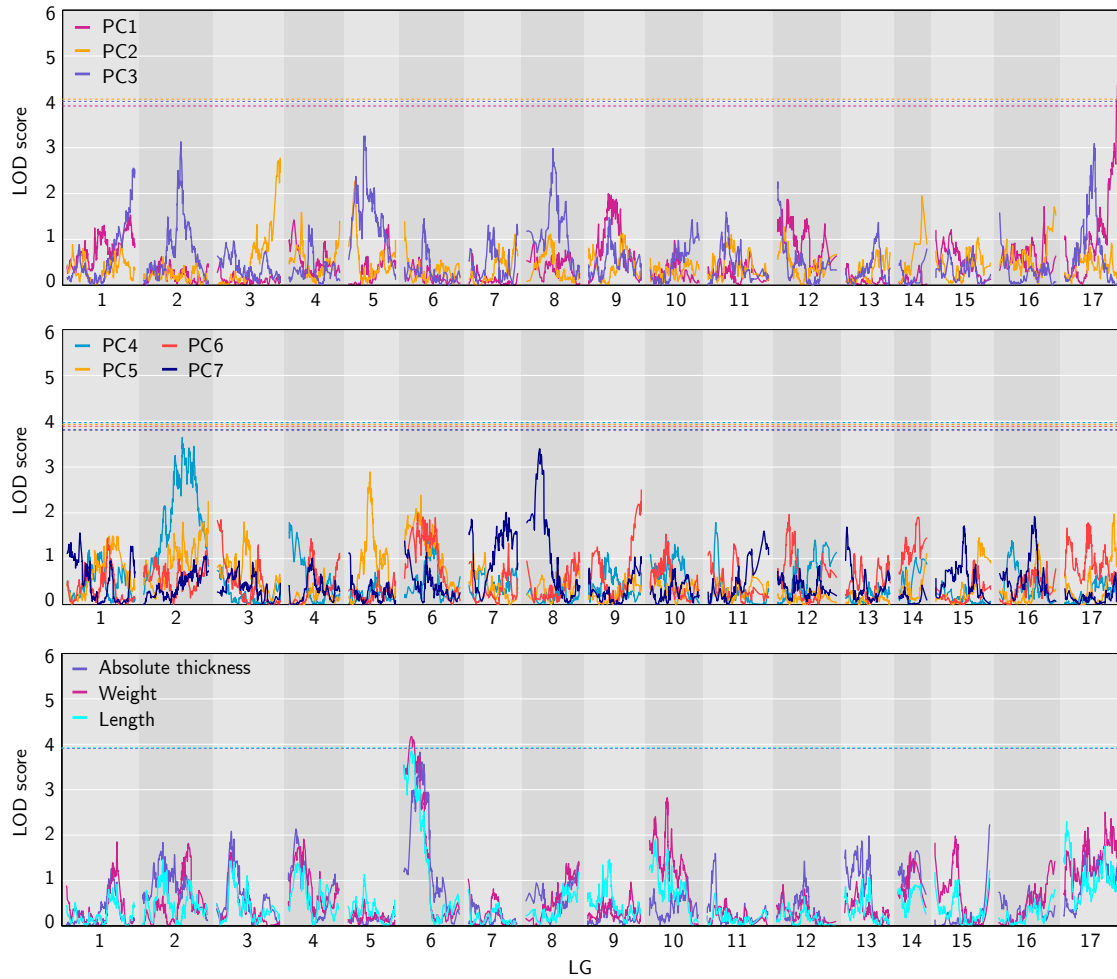


**Figure 3.3:** QTL plots for GM PCs and the size related traits, with significance thresholds visualised as dashed lines in respective colours. A score above the significance threshold indicates the positions likely contributing to the trait measured. Only one significant QTL was found, for the ecotype related PC1 at the end of LG 17, but several suggestive peaks were also detected. The shape variation described by each PC can be viewed in figure 3.4 and appendix figure C.2

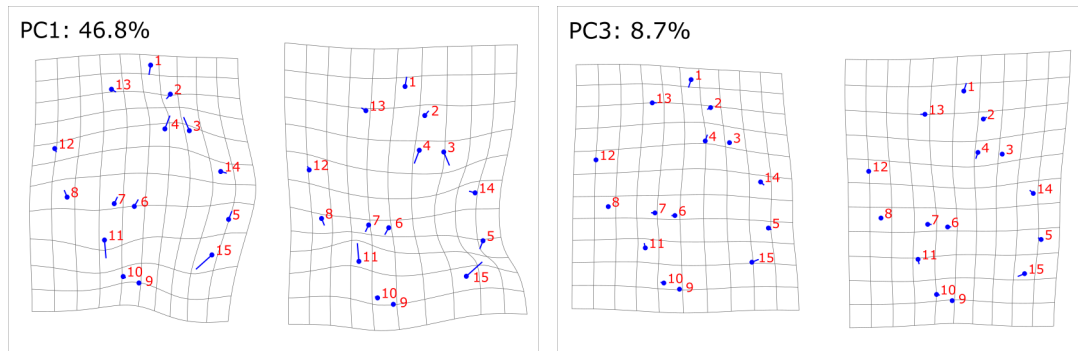


**Figure 3.4:** Landmark positions and transformation grids visualising the shape variation corresponding to the two principal components of the GM method indicated to be most likely affected by genetic components, both in the QTL and the variance partitioning analyses. Numbers indicate the amount of variation explained by the PC. PC1 describes a large variation correlating a decrease in aperture size with an increase in spire height, which is consistent with the large ecotypic differentiation described in previous analyses, while PC3 visually describes a much smaller variation of the overall height to width ratio of the shell. Remaining PCs analysed can be found in appendix figure C.2.

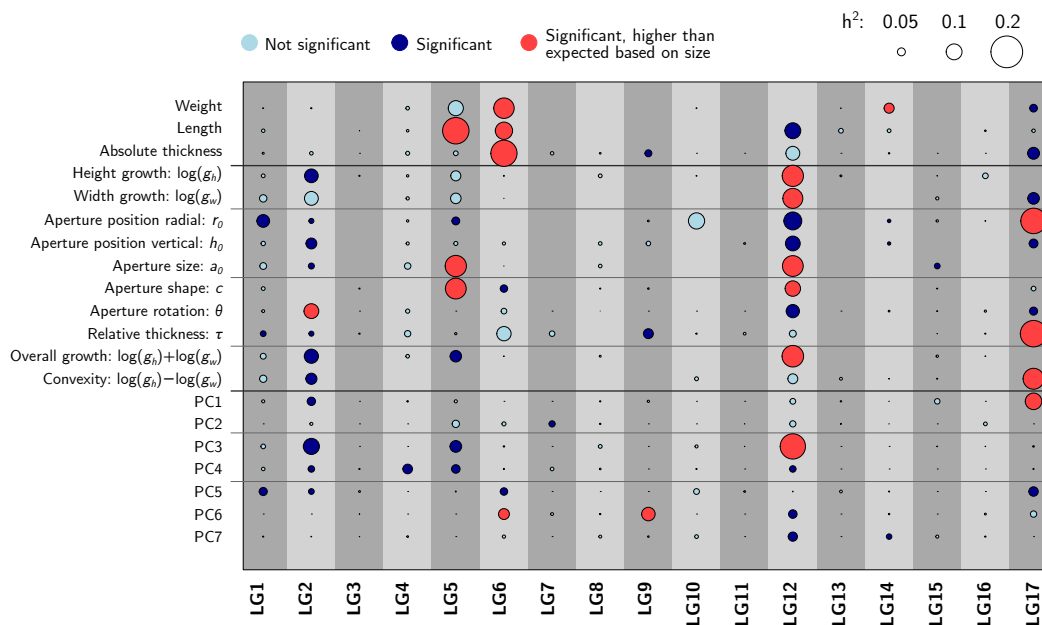


**Figure 3.5:** Summary of variance partitioning results. LG with a significant amount of variation explained are marked in dark blue, and those explaining more than expected by their size are marked in red, non significant LG are marked as light blue. Circle size indicates the estimated amount of heritability of the traits for each LG, as a fraction of the total variability of the trait in this set.

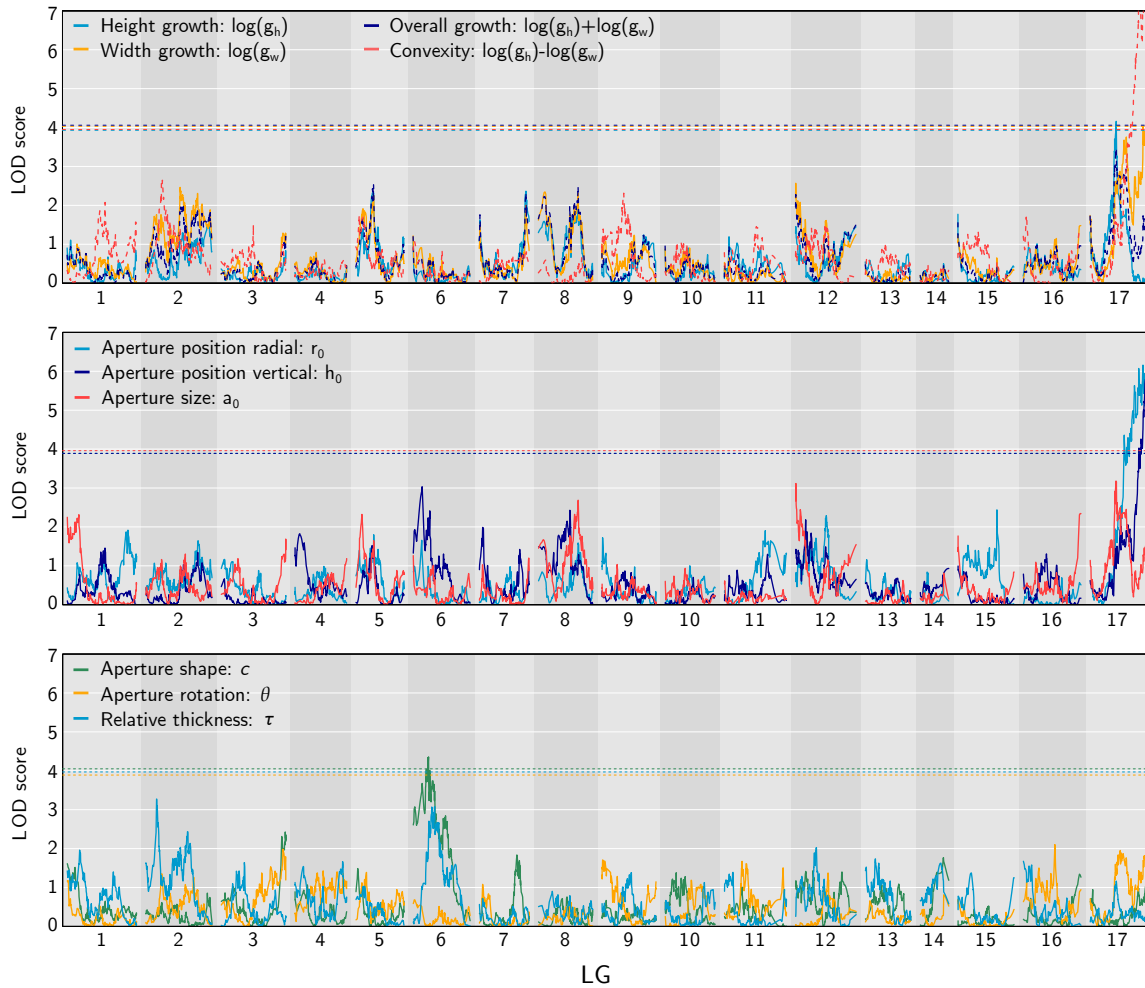


**Figure 3.6:** QTL plots for the growth based shape parameters, with significance threshold indicated by dashed lines in respective colours. Two separate positions on LG 17 reached the threshold value, related to growth as well as the aperture positions, a more detailed view of LG 17 can be found in figure C.4 in the appendix. In addition, the aperture shape reached the threshold on LG 6. Two other peaks, on LG 2, and 12, indicated suggestive QTL.

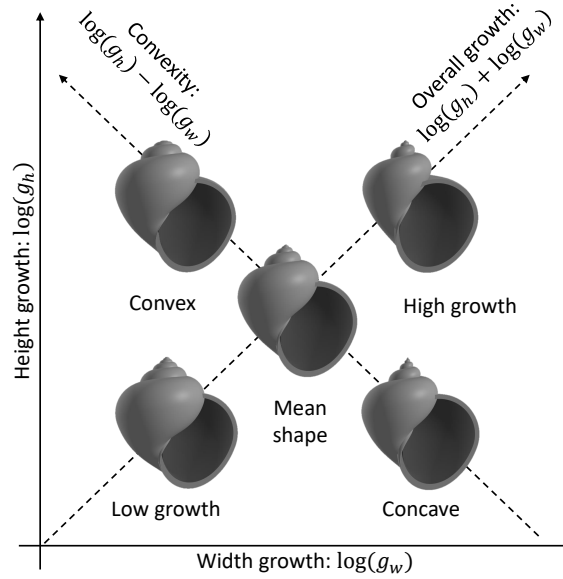


**Figure 3.7:** Visualisations of growth parameter variability while all other parameters are kept constant. A plot having the two growth parameters as axes can be viewed as a plot of convexity and overall growth by essentially rotating it by  $45^\circ$ . The real shells also co-vary in other parameters as the growth values change, e.g. high overall growth is correlated with large round aperture which also decreases the amount of spire visible, and the opposite for shells with low overall growth, hence this image is not representative of the observed shape variability in the data set.

growth parameters,  $\log(g_h) + \log(g_w)$ , did not show any additional peaks beyond those for the parameters separately, and none above the threshold value, while their difference,  $\log(g_h) - \log(g_w)$ , describing convexity, had a very high peak ( $\text{LOD} > 9$ ) at the end of LG17, explaining over 10% of its total variation. It has been suggested that there is an inversion on LG 17, which would include the peaks at the end of the LG, i.e. for width growth and convexity, but not the peaks in the middle of the LG, i.e. for height growth and the growth parameter sum (appendix figure C.4). The effect on overall shape, depending on which growth parameter has the larger value, is visualised in figure 3.7.

The aperture position parameters  $r_0$  and  $h_0$  (figure 3.2a) both had peaks at the very end of LG17, both within the suggested inversion (figure 3.6 and appendix figure C.4). The scores for aperture size,  $a_0$ , did not reach the significance threshold, however this trait did show two suggestive peaks, one on the start of LG12, and the other near the middle of LG17 together with the width growth parameter (appendix figure C.4). Aperture extension,  $c$ , showed a significant peak in the middle of LG6, which also had a suggestive peak for vertical aperture position,  $h_0$ , and these were positioned close to where most of the size-related QTL peaks have been found (figure 3.3), all of which are within a region suggested to be an inversion. The aperture rotation,  $\theta$ , did not show any QTL peaks of interest.

The variance partitioning found that the clearest contributions to the variability in the growth parameters separately, and their sum, could be attributed to LG12, while their difference was attributed to LG17, each explaining around 13% of the respective trait variability (figure 3.5). The aperture position parameters showed some significant contributions from

LG12, but the only LG which contributed more than expected for its size was LG17 for the radial position. The aperture size and shape had large contributions from LG5 and LG12. Aperture rotation also indicated significant variation attributed to LG2 and LG12, but only the effect of LG2 was more than expected due to LG size. The relative thickness showed a large contribution from LG17 in contrast with absolute thickness which was mainly attributed to LG6 together with size and weight. Overall, the heritability estimates for the growth based traits ranged from 0.24, for aperture rotation, to 0.60, for vertical aperture position.

A direct comparison of the shape parameter values obtained for the F2 hybrid crosses with those for a set of pure ecotype lab reared snails, as well as with field collected snails can be found in figure 3.8. The vast majority of shells were on the convex side in all three sets, i.e.  $\log(g_h) > \log(g_w)$ , with the amount of convexity showing significant but small trends correlated with overall growth, which differed in direction between lab reared and field collected snails. The wild snails tended to be more convex the larger the overall growth, i.e. wave shells were more convex than crab shells, while the lab reared shells showed the opposite trend, less convex when overall growth was larger.

In general, the F2 and pure ecotype parameter values were within the range found in the field collected snails, but not covering the full spectrum. The expected pattern was found in the aperture size parameter,  $a_0$ , where the pure wave ecotype snails in general had larger apertures than the pure crab ecotype snails, the F2 hybrids had intermediate values between them, and the field collected shells, while spanning a larger range, had similar mean value to the F2 shells. This pattern did not hold for the remaining parameters, however, as the F2 shells instead showed a more extreme mean value, larger for radial position,  $r_0$ , and shape,  $c$ , and smaller for vertical position,  $h_0$ , and aperture rotation,  $\theta$ , than either pure ecotype snails and wild shells. These parameters are neither geometrically nor biologically independent from one another, e.g.  $h_0 + c \cdot a_0 \approx 1$ , as we have normalised shells to unit length, hence they should not necessarily be interpreted as multiple separate differences as they could all be due to a single change in shape.

The thickness differs between the pure ecotype snails, with the crab ecotype in general having thicker shells than the wave ecotype. Contrary to expectations, however, the F2 hybrids did not show intermediate thickness to the pure morphs but instead had thicker shells than both. The thickness of the wild shells shows a possibly bimodal distribution containing thicker shells than any of the other groups.

### 3.3.3 Comparison of the shape descriptions

The correlation of PC1 with the shape parameters (figure 3.9, and appendix figure C.6), and the visual representation of its variation (figure 3.4), is largely consistent with PC1 describing the crab-wave shape differentiation. PC1 had a negative correlation with  $g_w$ ,  $g_h$ ,  $r_0$ , and  $a_0$ , consistent with the results in (Larsson et al., 2020), which suggests that high values for PC1 are indicative of a crab ecotype shape. Contrary to the previous analysis, we found a positive correlation between PC1 and  $h_0$  in this new data set, and a lack of correlation of PC1 with either the aperture extension parameter  $c$ , which instead correlated more with PC2, or the relative thickness,  $\tau$ , which correlated most with PC3 in the current analysis. There was a general trend of less strong correlation with the shape parameters the higher the PC number, which is expected as the PCs are ordered decreasingly by the amount of shape variation they account for.

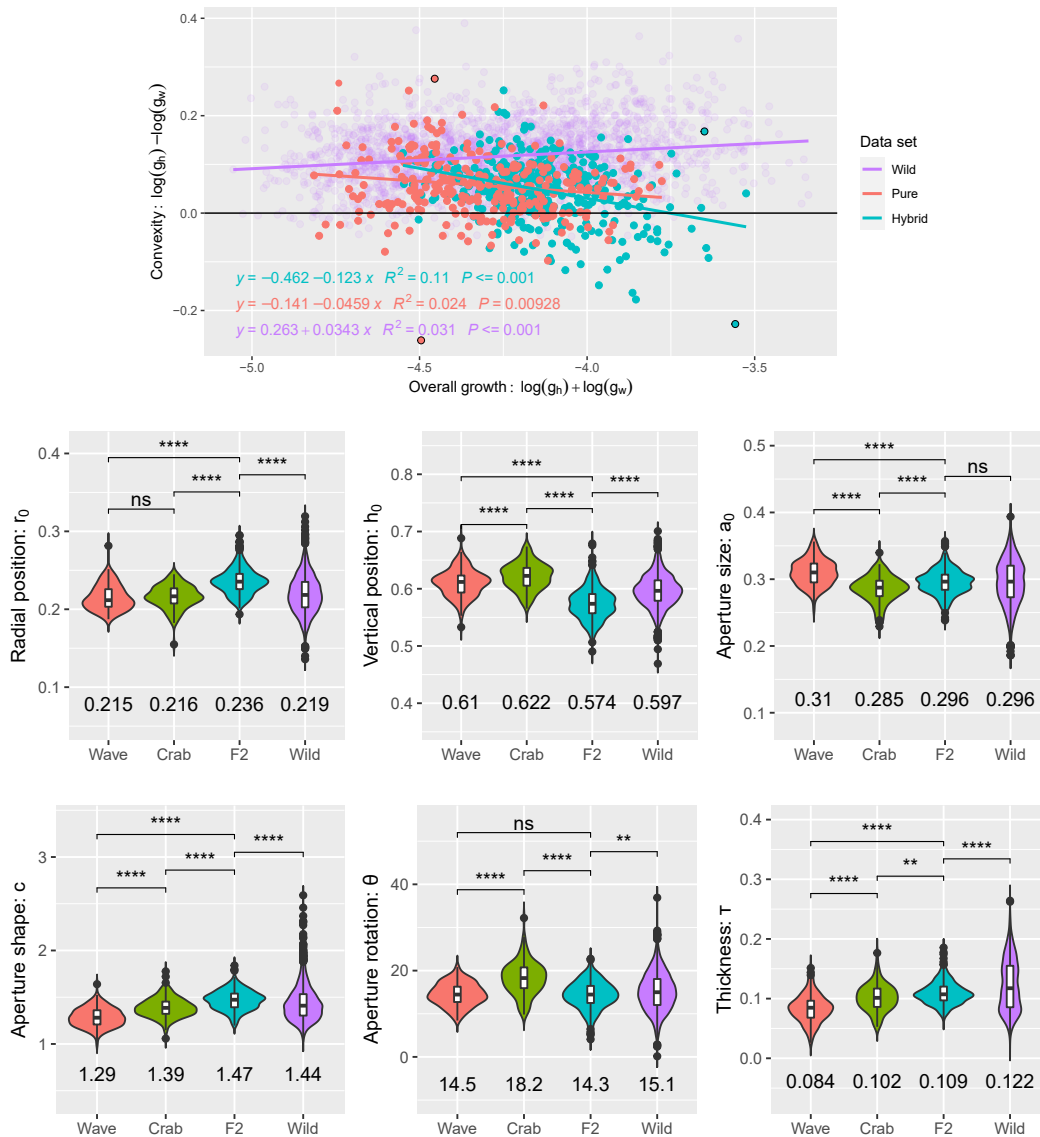


**Figure 3.8:** Top: Convexity plotted against overall growth. The lab reared snails, both F2 hybrids and pure ecotypes, showed a minor but statistically significant trend of less convexity with increased overall growth, while the wild snails showed a minor significant trend of the opposite. Four outliers are marked, and their shell images can be found in figure C.5 in the appendix. The horizontal black line indicates growth parameters of equal values, i.e. isometric growth. Bottom two rows: Comparison using Wilcoxon tests of the difference in parameter values between the F2 hybrids and each of the two lab reared pure ecotypes, and field collected shells, as well as between the two pure ecotypes, all mean values shown.

Correlation Coefficients

|                       | PC1    | PC2    | PC3    | PC4    | PC5    | PC6    | PC7    |
|-----------------------|--------|--------|--------|--------|--------|--------|--------|
| Height Growth         | -0.493 | -0.439 | -0.484 | -0.151 | -0.372 | 0.112  | -0.125 |
| Width Growth          | -0.767 | -0.370 | -0.324 | -0.198 | -0.104 | -0.012 | -0.067 |
| Ap. Position Radial   | -0.609 | 0.118  | -0.048 | -0.305 | -0.115 | 0.069  | 0.350  |
| Ap. Position Vertical | 0.774  | -0.045 | 0.416  | 0.073  | -0.126 | -0.214 | 0.096  |
| Aperture Size         | -0.602 | -0.512 | -0.505 | -0.139 | 0.030  | -0.072 | 0.161  |
| Aperture Shape        | 0.079  | -0.651 | -0.054 | -0.118 | -0.186 | -0.408 | 0.316  |
| Aperture Rotation     | 0.361  | 0.519  | -0.084 | 0.102  | 0.160  | 0.185  | 0.073  |
| Relative Thickness    | -0.053 | 0.032  | 0.166  | -0.043 | -0.002 | 0.004  | -0.125 |
| Overall Growth        | 0.169  | -0.039 | 0.457  | 0.216  | -0.175 | -0.023 | -0.235 |
| Convexity             | -0.684 | -0.425 | -0.419 | -0.188 | -0.237 | 0.046  | -0.098 |

P-values

|                       | PC1            | PC2            | PC3            | PC4            | PC5            | PC6            | PC7            |
|-----------------------|----------------|----------------|----------------|----------------|----------------|----------------|----------------|
| Height Growth         | <b>3.1E-24</b> | <b>5.1E-19</b> | <b>2.7E-23</b> | <b>3.4E-03</b> | <b>1.1E-13</b> | 0.030          | 0.016          |
| Width Growth          | <b>1.6E-73</b> | <b>1.5E-13</b> | <b>1.5E-10</b> | <b>1.2E-04</b> | 0.044          | 0.815          | 0.199          |
| Ap. Position Radial   | <b>3.4E-39</b> | 0.023          | 0.354          | <b>1.9E-09</b> | 0.027          | 0.186          | <b>3.6E-12</b> |
| Ap. Position Vertical | <b>9.1E-76</b> | 0.391          | <b>4.8E-17</b> | 0.160          | 0.015          | <b>3.2E-05</b> | 0.065          |
| Aperture Size         | <b>3.3E-38</b> | <b>2.8E-26</b> | <b>1.4E-25</b> | <b>7.3E-03</b> | 0.570          | 0.167          | <b>1.8E-03</b> |
| Aperture Shape        | 0.128          | <b>2.1E-46</b> | 0.301          | 0.022          | <b>2.9E-04</b> | <b>2.3E-16</b> | <b>4.5E-10</b> |
| Aperture Rotation     | <b>6.0E-13</b> | <b>4.4E-27</b> | 0.107          | 0.049          | <b>1.9E-03</b> | <b>3.2E-04</b> | 0.162          |
| Relative Thickness    | 0.312          | 0.539          | <b>1.3E-03</b> | 0.411          | 0.972          | 0.937          | 0.015          |
| Overall Growth        | <b>1.0E-03</b> | 0.455          | <b>1.1E-20</b> | <b>2.5E-05</b> | <b>6.6E-04</b> | 0.662          | <b>4.5E-06</b> |
| Convexity             | <b>1.0E-52</b> | <b>8.5E-18</b> | <b>2.8E-17</b> | <b>2.6E-04</b> | <b>3.7E-06</b> | 0.377          | 0.058          |

**Figure 3.9:** Top: Correlation matrix between GM PCs and growth based shape parameters, intensity of colour indicate strength of correlation, blue for positive and red for negative. Bottom: Matrix of p-values for the correlations above, values less than 0.05 are highlighted.

There was no single GM PC which fully represented the convexity measure, but it showed a moderately strong correlation with PC1, PC2, and PC5. As the effect of convexity on the landmarks is smaller than the general crab-wave difference, and we see a possible but small difference in convexity between the ecotypes (figure 3.8), it is likely that the convexity was mainly contained within PC1, as a morphologically undetectable component overpowered by ecotype related differences.

### 3.4 Discussion

In this paper we have compared the ability of two different shape quantification methods to assign genomic regions that relate to different shape traits of the marine snail *L. saxatilis* using both QTL analysis and variance partitioning analysis. Shape is one of several divergent

traits within the crab-wave ecotype differentiation of *L. saxatilis*, and has been previously attributed to regions suggested to be contained in genomic inversions (Westram et al., 2018; Faria et al., 2019a). However, shape is a complex trait, thus it should be expected that not all variability can be attributed to contrasting adaptations to the crab and wave environments. It should also include general adaptations to common environmental factors, and even non-adaptive variation. In general, we found the growth based method to be easier to interpret in biological terms and to give a clearer connection between genomic regions and the morphological differences that they influence.

We found that both quantification methods indicated an area at the end of LG17 as a genomic region responsible for a significant part of the shell shape variability in both the QTL analysis and variance partitioning, as has also been indicated by previous analysis (Westram et al., 2018; Kess et al., 2021). In addition, the growth based quantification showed two more genomic regions with scores above the threshold values in the QTL analysis, on LG6 relating to aperture shape, and in the middle of LG17 for height growth. The GM method did not reach the significance threshold for any additional QTL. However, the highest peaks below the threshold for both quantification methods indicate a few more sites of interest, which should all be investigated further.

The height growth and width growth parameters show very similar trends for the QTL analysis in general, but the most interesting is how they differ within LG17 (figure 3.6 and appendix figure C.4). At the end of LG17 we found a large peak for the difference in height and width growth, i.e. relating to convexity and thus allometric variation. This locus co-occurs with peaks for the aperture position parameters, which are expected to covary with a change in convexity, while the peak in the middle of LG17 is related to the sum of the growth parameters, i.e. describing the overall growth component of how much larger the shell becomes for each whorl. This suggests that there could be two different loci of significant effect related to the different aspects of growth on LG17, one controlling their positive interaction while the other controls their difference. Interestingly there is suggested to be an inversion on LG17 which would include the locus at the end but not the one in the middle (Faria et al., 2019a). A more in depth discussion on the connection between the ecotypic shape differentiation and inversions can be found in Koch et al. (2021) (appendix F). These two loci on LG17 were also indicated in the GM analysis, for PC1 and PC3 (figure 3.3), but such a clear relation to distinct functional properties could not have been inferred from the transformation grid representations (figure 3.4). Additionally, this suggests that introducing separate measures for growth in height and width allows us to quantify developmentally and genetically relevant variability, and that the sum and difference of the growth parameters could be more informative to investigate than the parameters separately. In biological terms this indicates that we have found one locus which affects the shell's overall growth per revolution, which has been found to differ between the habitats (Larsson et al., 2020), while another controls the allometric effect of how convex or concave the spire becomes, which does not differ much between the habitats (figure 3.8). Deviation from isometric growth is not known to relate to any functional adaptation in this species, but there are some indications that an increased availability of food could have a plastic effect making the shells having a taller spire and a larger aperture, particularly the wave shells (Saura et al., 2012), which is consistent with our comparison of decreased convexity in lab reared wave snails compared to wild (figure 3.8). However, the variance partitioning analysis indicated that the main contribution to overall growth comes from LG12, suggesting that there are likely multiple small effect loci which,

when combined, have a greater contribution to overall growth than the single locus found on LG17. It should be noted that LG12 has been shown to contain a sex determining locus (Koch et al., 2021) (appendix F, indicating that the small sex difference in shape detected in (Larsson et al., 2020) could have a genetic component. Furthermore, the two loci on LG17 should not be expected to be completely independent in their effects, as both are still on the same LG.

While a QTL analysis is biased to find single loci of large effect, the variance partitioning analysis is able to describe how the combined effect of several loci on each LG contributed to explaining variation in the analysed traits. For highly polygenic traits, the amount of variation explained by each LG is expected to be determined by the size of the LG. The results of the variance partitioning indicated that the LG contributing most to shape variation for both quantification methods were LG2, LG5, LG12, and LG17, while the size related traits were mainly attributed to LG6. There is evidence of LG12 including a sex-determining locus (Koch et al., in review), and several of the growth based parameters associated with LG12 in the variance partitioning analysis had previously been indicated to show some differences between sexes (Larsson et al., 2020), hence it is possible that there is some genetic component of the effect of sex on shape. The LG which were only indicated for one of the quantification methods were LG15 for the growth based method and LG4 and LG7 for the GM method. In general, the growth based parameters had a higher estimated heritability than the PCs, which could be due to them being closer representations of distinct, biologically- relevant shape components.

A likely explanation for the discrepancies in genomic areas of interest between the QTL and variance partitioning analyses is that different aspects of shape have different genetic architecture, some being determined by a few large effect loci, while others depend on several small effect loci, or any combination thereof. For example, convexity indicated contributions mainly from LG17 both for the QTL (this single locus explaining 11% of the variation in convexity, appendix figure C.1) and variance partitioning analysis (the whole of LG17 explaining 13%, appendix figure C.7), suggesting that the genetically determined variation in the shell convexity could be largely controlled by a single locus, or several tightly-linked loci within the inversion effectively acting like a single locus. Similarly, aperture shape was attributed mainly to LG6, showing both a significant QTL and significant contribution from variance partitioning (both explaining 5% of the variation). While the overall growth suggestive QTL peak was on LG17 (explaining 4% of the variation), the main contributing LG were LG2, LG5, and LG12 (explaining 9%, 7%, and 14% respectively), making several small effect loci more likely to explain the genetically determined variation in this trait. This shows that it is likely a combination of loci of small and large effects that are involved in the variation in shell shape of *L. saxatilis*, which has also been previously indicated in an analysis using only GM (Kess and Boulding, 2019). This further confirms that shape is a complex trait consisting of several components, and treating it as such will improve the ability to draw connections between genotype and phenotype.

Since the GM method used here combines variation into principal components, their effect on shape is highly variable, i.e. PC1 which is assumed to describe most of the crab-wave shape differentiation, as well as most of the convexity, explains almost half of the total GM variation by itself, while PC7 explains less than 3% and is thus more likely to contain a larger proportion of noise (figure 3.1b). The visual representations of the shape variation confirms this, as PCs 5-7 are describing very small differences (appendix figure C.2). Despite this large discrepancy in effect size, the PCs are treated in the same way in the genetic analysis, and

the results found for later PCs should therefore be taken as more uncertain than those from the earlier PCs. The shape variation described by the PCs also needs interpretation of the positions of points and gridlines (figure 3.4) which can be a somewhat subjective endeavour, in particular when dealing with the accretionary growth pattern of gastropod shells. For example, the variation in convexity found in this data set would not necessarily generate a large effect on the linear position of landmarks in 2D images, and could therefore easily be missed in a GM-only analysis. As the analysed ecotypes also differ a lot in size, this further confounds the abilities of a GM analysis to differentiate between ontogenetic and ecotypic shape variability. By using only a GM analysis the QTL peak found at the end of LG17 would likely be interpreted as a purely ecotypic difference, while the growth based analysis indicated this site to be involved in the convexity which has no large differentiation between ecotypes.

The PCs are in general not directly comparable between different data sets, as they are defined relative to the variation within each analysed sample set, and are statistical rather than functional scores in contrast to the growth based shape parameters. The PCs represent large components of combined variation, and can include biologically distinct components of small morphological effect which are not possible to detect in the transformation grids due to being included in a PC which also contains another variation of larger effect, such as the convexity in this analysis. Additionally, any allometry detected in GM analyses of shell shape should be interpreted with care, as even perfect logarithmic helicospiral growth could be interpreted as allometry (Urdu et al., 2010a). Improvements of the GM method for genetic analyses of this type could include replacing the PCA, as it mainly summarises the largest variations within a sample set into a few informative components. Replacements for the PCA would likely need additional data to disentangle the variability into more biologically relevant components, such as using functionally relevant predefined reference directions of the morphospace (Bookstein, 2015), or taking allometric growth trajectories into account (Outomuro and Johansson, 2017; Zhao et al., 2005; Hollander et al., 2006a; Gefaell et al., 2020). However, even with an improved description of the components of variation, it would likely still lack the direct connection with development, and with the non-linearity of shell construction, that a growth based method grants us.

The direct comparison of shape parameters between the shells in the F2 hybrid data set with lab reared shells from pure ecotypes and wild specimens showed that, in general, they obtain roughly similar values, and the crab-wave ecotype differentiation is still a large contributor to shape variation. However, there were some differences which could be due to the F2 and pure ecotype snails descending from a small set of respective grandparents which might not be representative of the full range found in nature, at least not for growth parameters, or that there could be a hybridisation effect making the offspring less extreme, or perhaps differences between collection sites. The aperture parameters of the F2 hybrids did not show intermediate values between the pure ecotypes, except for aperture size, suggesting that there could be some hybrid overdominance. In general, the F2 shells had the aperture position centred at a larger  $r_0$ , and a smaller  $h_0$ , and showed more elongated apertures, with the elongation directed more downwards rather than inwards, compared with the pure ecotype shells, while still being within the full range of shells found in the wild (figure 3.8). The aperture position, shape and rotation are not independent measures as we have normalised the shells to unit height, hence atypical grandparents or possible overdominance causing a difference in several traits might functionally be caused by as little as a single underlying

factor.

The lack of shells with high relative thickness in the lab reared snails is likely partly due to plasticity, which is in line with previous research showing shell thickness to be a highly plastic trait responding to the presence of crabs in closely related species (Trussell, 1997a, 1996; Kemp and Bertness, 1984). We did however still see some indications of shell thickness having a genetic, possibly overdominant, component with two suggestive QTL and a significant contribution to the variance partitioning (e.g. 17% of variation was attributed to LG17, figure 3.5), as well as a significant difference in thickness between the two pure ecotypes when reared under standard conditions (figure 3.8).

The main improvement of using the growth based shape quantification is not primarily about detecting the genomic regions contributing to the main phenotypic variation, but in its ability to more clearly describe this variation in terms of biological traits and processes, improving our knowledge of the connection between genotype, phenotype and environment. Despite using the same input data as the GM method, the shape parameter method has been more informative in untangling some different components of shape and growth, inferring new information about their genetic architecture, and revealing a genomic region contributing to ontogenetic variation. We do not yet, however, know the exact positions of the genes, or what they do, or how polygenic the different traits are. It is possible that other combinations or transformations of the shape parameters not tested here could further improve the assignment of genomic positions to different traits, as these shape parameters are neither algebraically nor biologically independent. An ideal quantification is one which not only describes and isolates the different biologically important traits in the given ecological setting, such as, but not limited to, the traits under divergent selection, e.g. shell shape adaptations to crab rich or wave swept environments, but which also can be interpreted in terms of function and development.

We are still only at the beginning of understanding the genetics relating to shell construction and shape in gastropods, and how different choices of quantification methods can affect the ability to identify and understand this connection. It should be expected that different shape parameters or combinations thereof will be important for different species in various ecological niches, that their genetic architecture should differ, and that the amount of variability attributed to genetics or plasticity will vary. Further analysis is therefore needed to investigate how consistent these conclusions are within and across species, both when there is a similar adaptive shape differentiation and when there is not. An obvious goal for future work would be to identify the specific genes involved and their respective functions in determining shape variation, to further improve the understanding of the connection between environment, genetics, and development. Particularly interesting would also be to investigate if the convexity is a functional adaptation to any specific environmental factors, e.g. by analysing the hydrodynamic properties of shells for different levels of convexity and concavity, or whether it might allow a more general optimisation relating to, for example, the the internal volume available relative to the amount of shell material needed throughout development.

## Chapter 4

# Hydrodynamical effects of shell shape for snails in flow with variable directionality

J. Larsson<sup>1</sup>, P. Jonsson<sup>2</sup>, A. Larsson<sup>2</sup>, R. K. Butlin<sup>1,2</sup>, T. Lundh<sup>3</sup>

<sup>1</sup>Department of Animal and Plant Sciences, University of Sheffield, Sheffield, UK

<sup>2</sup>Department of Marine Sciences, University of Gothenburg, Strömstad, Sweden

<sup>3</sup>Mathematical Sciences, Chalmers University of Technology  
and University of Gothenburg, Gothenburg, Sweden

**Contributions** T.L., J.L. and R.K.B. conceived the project. P.J. and A.L. developed the experimental setup. J.L. developed and implemented the simulation, and performed the experiment. J.L. drafted the manuscript and all authors provided input on subsequent versions.

## Abstract

In order to understand why organisms have certain shapes, it is important to investigate whether and how they affect survival in different environments. Snail shells are a prime example of a biological structure that has evolved into various shapes depending on the selection pressures found in different types of habitat. The intertidal marine snail *Littorina saxatilis* is a useful study species for investigating morphological adaptations to water flows, as this species includes both one ecotype adapted to intense wave action, and one adapted to a contrasting sheltered and crab-rich environment. In this analysis we have used both flume experiments and computational fluid dynamics (CFD) simulations with the aim of understanding how and why shell shape matters in the context of hydrodynamics, and how it relates to other adaptive traits such as foot size. We analysed variation in the forces experienced by different shell shapes, at several different sizes, orientations, and flow speeds.

Our results indicate that while the typical wave shape experiences lower drag forces on average, the difference is not very large unless one accounts for foot size. Since the wave ecotype snails have a relatively larger foot, both the lift and the drag forces are spread out over a larger attachment area, which allows the snail to more easily stay attached despite strong flows. As foot size is indicated to have a larger effect on ability to resist flow forces than shape and orientation, we suggest that the main adaptive reason for the shape variation found in *L. saxatilis* could be to accommodate a larger foot in the wave-swept habitat, while the shells hydrodynamical properties become a secondary factor. In addition, we found that shape has a direct effect on the optimal orientation, as the minimal area against the flow will correspond to different orientations for the different shapes. The suggested optimal orientations of shells with taller spires were with their apex closer to straight back along the flow, compared to those with shorter spires that were preferentially aligned with their apex more to the side.

**Keywords**— Snail shells, Fluid Dynamics, *Littorina saxatilis*

## 4.1 Introduction

The shells of gastropods evolve over time to be better adapted to survive the selective pressures present in different environments. There are many types of ecological and biological factors that will affect which shell shapes are more or less optimal for a specific species of snail in a specific ecological niche. One of the environmental factors that has a large impact on intertidal snails is wave action, as snails which are not well adapted risk being detached from the substrate and swept away (Trussell, 1997a). With the very high impact of waves on rocky shores, with measured water speeds of up to 25 m/s (Denny et al., 2003), and intense accelerations of up to 400 m/s<sup>2</sup> (Denny et al., 1985; Denny, 1985), being able to resist the hydrodynamical forces is crucial. In addition to the high velocities, crashing waves are highly turbulent and the direction of flow is unpredictable (Jensen and Denny, 2015; Nowell and Jumars, 1984; Koehl, 1984; Gaylord, 1999).

The fluid dynamics of waves turbulently breaking on rocky shores becomes even more complex due to the rough topography (Carrington Bell et al., 1994; Helmuth and Denny, 2003). Simplifications are therefore necessary to disentangle how different morphological factors affect the fitness of organisms in this setting. We can divide the forces acting on an organism into the drag component,  $F_d$ , acting in the direction of the flow, the lift,  $F_l$ ,

component acting vertically, and the lateral component,  $F_{lat}$ , acting sideways. The reasons for separating the total force into these three perpendicular components are to be able to differentiate between lift forces up or down, since this affects the risk of dislodgement, and because drag is the easiest and most commonly measured component in experiments. The relative importance of the three components varies in different settings, but they are all expected to scale roughly proportional to both the front-facing area and the square of flow speed (Denny et al., 1985). We are mainly interested in the drag and lift components as these are the most likely forces to peel the snail off from the substrate, and the lateral forces are expected to be small in comparison, in particular if the flow is unidirectional.

The intertidal marine snail *Littorina saxatilis* is a good example for studying adaptation to wave exposure because of extreme morphological differences found in contrasting environments over short geographical distances. Wave action on exposed rocky shores has been indicated as one of the main environmental factors for formation of locally-adapted ecotypes (Johannesson, 2003; Rolán-Alvarez et al., 1997; Trussell, 1997b; Grahame and Mill, 1986), and the wave adapted ecotype have been shown to be better at resisting water flow in a flume experiment (Le Pennec et al., 2017). The shells of *L. saxatilis* in wave-swept environments are in general smaller, thinner and have rounder apertures that are larger relative their total size, compared with shells in more protected environments. The relatively large aperture of the wave-adapted ecotype in *L. saxatilis* has been assumed to help mainly by accommodating a larger foot, as foot area has been found to scale proportionally to the ability to stay attached (Hohenlohe, 2003; Etter, 1988; Trussell, 1997a; Grahame and Mill, 1986). Foot area has also been shown to vary as a plastic response to wave forces in some species, e.g. in *L. obtusata* (Trussell, 1997a) and in the whelk *Nucella lapillus* (Etter, 1988), where both species have an asymmetric response, meaning that foot sizes increased when snails from sheltered environments are subjected to stronger forces, but did not decrease for snails from exposed environments reared in low-speed environments.

The smaller sizes found in *L. saxatilis* from the wave exposed environments might not be having a direct effect on flow resistance (Le Pennec et al., 2017; Gaylord, 2000), but a smaller size gives the snail access to more and smaller crevices, where snails are known to take refuge (Raffaelli and Hughes, 1978; Janson, 1983; Johannesson and Johannesson, 1996; Johannesson et al., 1997). The crevices should not be assumed to reduce flow speed, but could help by allowing the shell to wedge itself into cracks and thus transfer the forces through to the rock (O'Donnell and Denny, 2008).

Fluid forces are also of major importance for snails in streams and rivers, although they take a different form. While intertidal snails subjected to wave action experience highly variable, intermittent, and turbulent forces from all directions (Denny, 1985; Helmuth and Denny, 2003; Gaylord, 1999), the snails in rivers usually experience a slower, constant, and unidirectional flow as they tend to be aligned with, and move against, the flow (Huryn and Denny, 1997). The morphological adaptations to the different types of flow will likely vary, as it is only useful to be streamlined if the direction of the flow is predictable (Koehl, 1977). Despite this, the shell shapes found in the faster parts of rivers and streams tend to be larger and more globular than those found in stagnant waters, which was hypothesised to be caused by having a larger foot and thus needing a larger aperture (Verhaegen et al., 2019; Lam and Calow, 1988), again indicating that the foot size has a very large role in the ability to resist water flow.

In this analysis we compare computational fluid dynamics (CFD) simulations to measure-

ments in a flume experiment to investigate how hydrodynamical forces act on *L. saxatilis* shells, and how closely the results coincide. The simulations allowed us a highly controlled way of measuring variations in drag and lift forces since we could define all parameters to a high precision, giving us the ability to compare factors separately and in specific combinations. The morphology of snail shells is likely a trade-off between adaptations to several different environmental and biological factors and constraints, and this analysis attempted to isolate the effects of shape in terms of its hydrodynamic efficiency, and thus its contribution to fitness in a wave-swept environment.

## 4.2 Methods

### 4.2.1 Data

The data used to construct the shell models were the same data investigated in chapter 2 (Larsson et al., 2020), consisting of snails collected across several hybrid transition zones between crab- and wave-type habitats in Sweden. The shape parameters obtained from this analysis represent a logarithmic spiral type growth, and can thus be used to generate 3D computer models of shells (figure 4.1). We used the results from a PCA of the seven shape parameters (excluding one outlier), where the first principal component was used to obtain typical crab and wave models,  $\pm 0.6 \cdot \text{PC1}$ , extremes of both types,  $\pm 1.2 \cdot \text{PC1}$ , and the mean shape of the data set was used as an intermediate hybrid type. These five shell models can be found in figure 4.2, and will be ordered throughout the chapter as follows: Extreme crab, typical crab, intermediate, typical wave, and extreme wave. The shell models were constructed in MATLAB using the shell visualisation presented in Larsson et al. (2020). The apertures of these models were filled in with a flat surface and exported as .stl-files. The models were then re-meshed using the program Meshmixer (Autodesk) to improve mesh quality and make them compatible with the CFD software of COMSOL Multiphysics (version 5.3.1), and the apex and columella areas were smoothed out to simplify complex components in the geometry and to make these parts more similar to real shells. The shell models were also tilted manually in Meshmixer to obtain realistic orientations against the substrate (figure 4.3), and we repeated the simulations for two sets of slightly different tilts of the shells (figure 4.2).

We compared foot size with aperture size and shell length data from one of the sites (CZA,  $n = 499$ ) in the above mentioned data set to infer whether and how foot size varies with aperture area. Foot area was measured from photographs of snails crawling on a transparent surface (figure 4.4) while the aperture areas were obtained from photographs oriented with the aperture parallel with the photographic plane (figure 4.1), using the polygon tool in the software ImageJ (Schneider et al., 2012) similar to Le Pennec et al. (2017). Since the foot size varies as the snail crawls, it was photographed and measured twice, and the larger of the two value was used. No compensation was made for the curvature of the tube in which the snail were photographed, since this is assumed to be of negligible effect relative the ecotype difference and the variation during crawling. A linear least square function was fitted to the relative linear foot size as a function of relative linear aperture size, i.e. square root of the respective area divided by the shell length. The fit was used to estimate the relative foot size of the different computer-generated shells, as we can calculate the aperture sizes of the shell models from the parameters used to generate them (appendix figure D.1). The estimated foot areas  $A_{\text{foot}}$  (table 4.1) were then used to determine the detachment stresses to which the

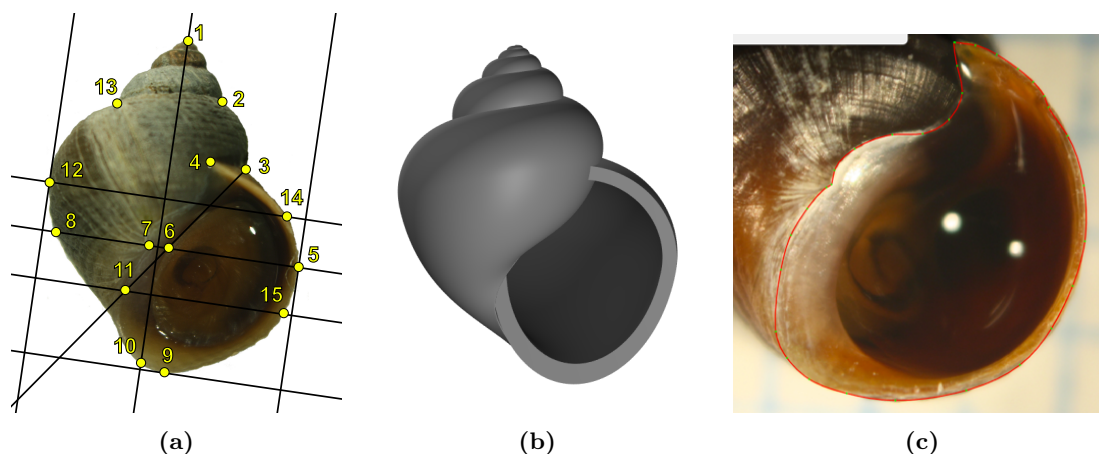


**Figure 4.1:** The shell measurements. (a) The placement of landmarks used to construct 3D shell models, see chapter 2. (b) An example of a 3D shell model constructed using the method in chapter 2. (c) Example of aperture area outline.

animal would be subjected.

#### 4.2.2 Simulations

We are mainly interested in the effects of shape on the hydrodynamical properties, and to separate them from the effects of the ecotypic difference in size. Therefore we used four sizes of each shell shape, having total volumes of  $V = 12 \text{ mm}^3$ ,  $96 \text{ mm}^3$ ,  $768 \text{ mm}^3$ , and  $6144 \text{ mm}^3$  respectively. In figure 4.2 the shells are shown having equal volume. These sizes were chosen as the length scale is doubling, making the area increase four-fold, and volume increase eight-fold between consecutive sizes. The smallest three sizes are representative of normal sized adult specimens in the wild, while the largest size represents the 3D printed shell models used in the experimental setup. The area size factor,  $A_{\text{size}} = V^{2/3}$ , where  $V$  is the volume of the shell (in  $\text{m}^3$ ), was used to rescale the force values to be comparable between shells of the same external volume, as an addition to the standard drag and lift coefficients which normalise forces by front-facing area (equation (4.1)).

The simulation was set up as a water flow in a rectangular duct, 10 cm wide 5 cm tall, and 14 cm long, (figure 4.3), with flow in from one of the short sides at velocities of 0.1, 0.3, 0.5, 1, 2, and 4 m/s, representing common velocities in the field (Denny, 1985; Denny et al., 2003). The dimensions of the duct together with the flow speeds gives a high estimation of the Reynold's number ( $\text{Re} = \rho u D_H \mu^{-1} \geq 6.6 \cdot 10^5$ , where  $\rho = 998 \text{ kg/m}^3$  is the fluid density,  $u \geq 0.1 \text{ m/s}$  is the fluid velocity,  $D_H = 0.067 \text{ m}$  is the hydraulic diameter of the duct, and  $\mu = 1 \text{ mPa}\cdot\text{s}$  is the dynamic viscosity of the fluid), and thus suggests a turbulent flow in the duct. Similar experimental flume setups have also been measured to have turbulent flow (Denny, 1994; Jensen and Denny, 2015). The simulations were carried out in the COMSOL Multiphysics (version 5.3.1) CFD module, as a stationary analysis with the k- $\epsilon$  turbulent flow interface, which solves the Reynolds-averaged Navier-Stokes equations with wall functions (COMSOL Multiphysics, 2016), where we were using the properties of fresh water at a temperature of 20 °C, which was similar to the experimental setup. The walls of the duct, and the surface of the shell all had no-slip boundary conditions with no surface roughness, and the short end

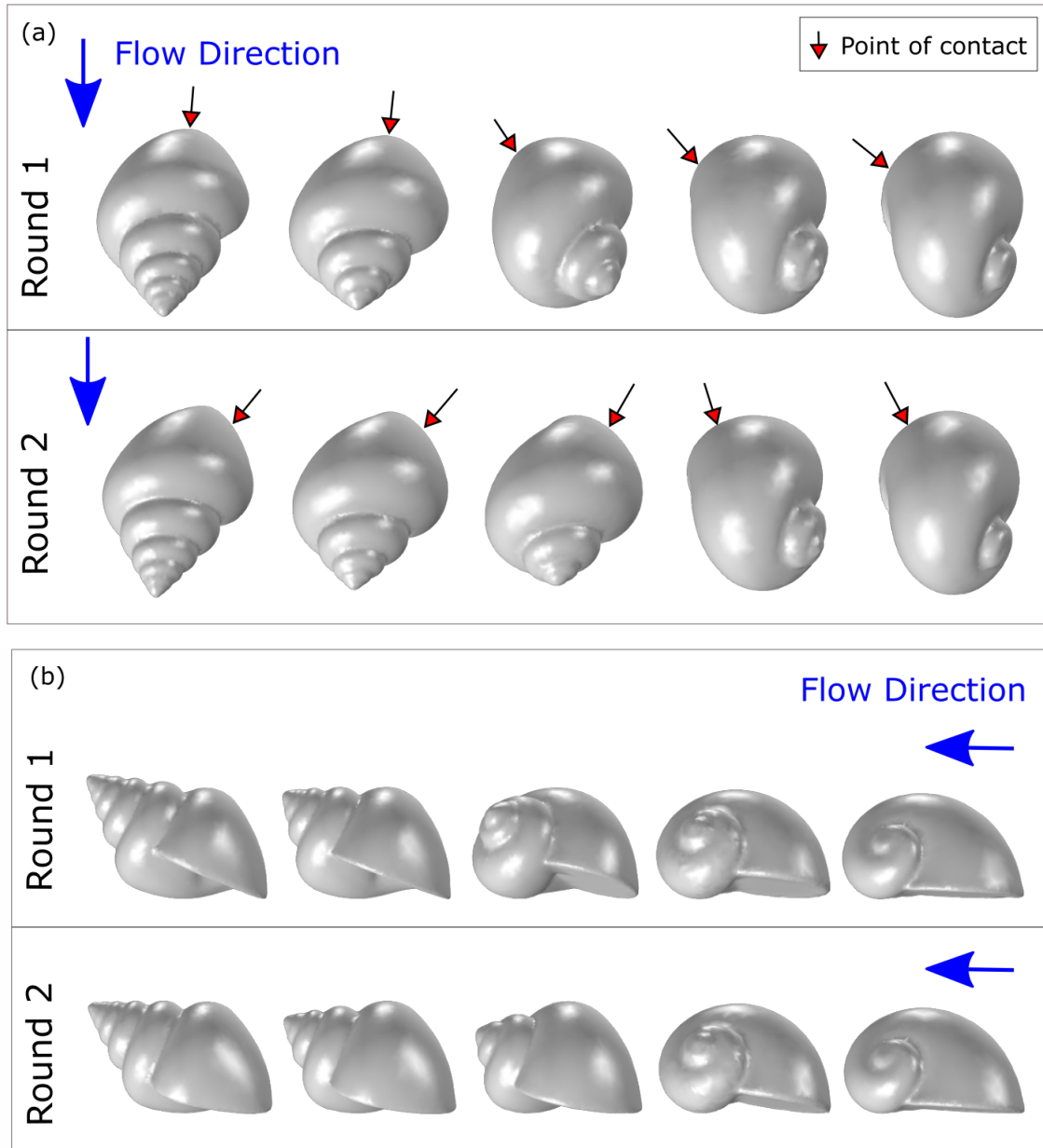


**Figure 4.2:** Orientations of the different shell models against the flow in the flow chamber, as seen from (a) above, and (b) the right hand side. All rows from left: Shell models of an extreme crab shape, a typical crab shape, the intermediate hybrid shape, the typical wave shape and an extreme wave shape. They are oriented in the direction found to give the least drag, as flow comes from the top or from the right as indicated. This was used as the standard orientation denoted as  $0^\circ$ , and the other orientations were counter-clockwise rotations of  $90^\circ$ ,  $180^\circ$  and  $270^\circ$  as viewed from above, respectively. Note that the two rounds represent different tilts against the substrate, with the point of contact shown with arrows. The intermediate shape was optimally aligned once in the "crab alignment" and once in the "wave alignment".

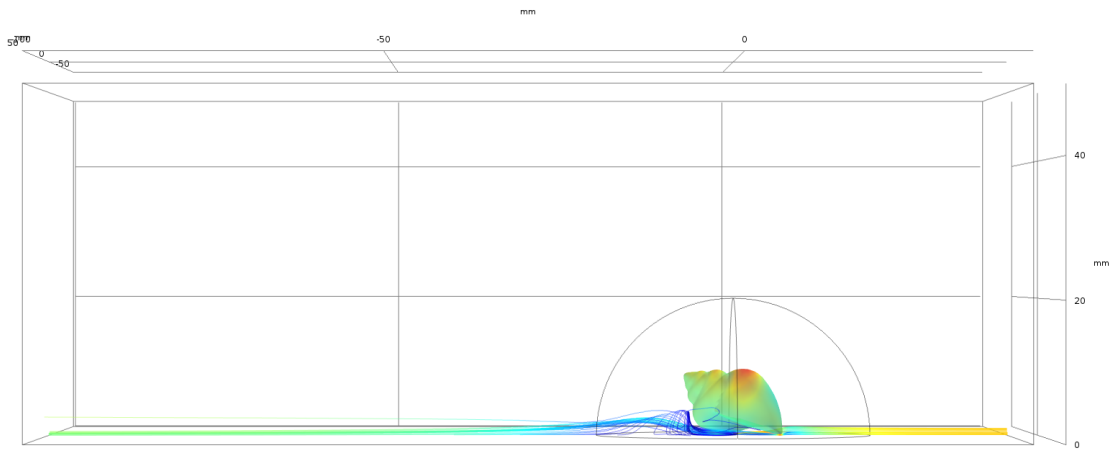


**Figure 4.3:** Visualisation of the CFD setup in COMSOL. Flow lines coloured by flow speed with blue representing a slow flow while red represents a faster flow. The shell surface is coloured by the local vertical pressure, with red indicating pressure upwards, while blue indicates pressure downwards. This is the large-sized model of a crab shape in its front-facing orientation, where the inflow is from the right of this image.

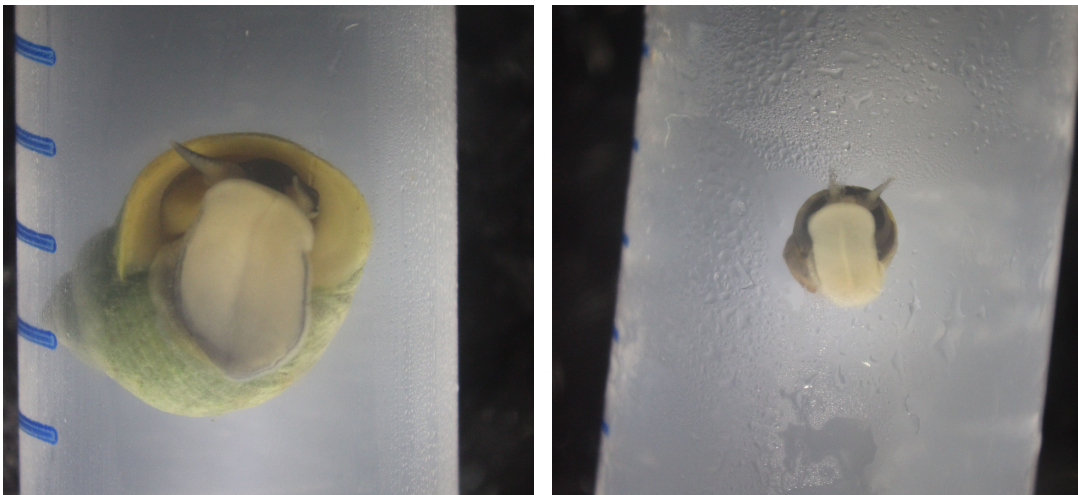


**Figure 4.4:** Example of foot sizes for the crab (left) and the wave (right) ecotypes. The distance between blue lines on the tubes is 3.2 mm.

opposite to the inflow had free outflow. Simulations were run on the Chalmers Centre of Computational Science and Engineering (C3SE) high performance computing cluster, which is part of the Swedish National Infrastructure for Computing (SNIC).

The shell models were placed early in the duct, 4 cm from the inflow, to minimise the effects of boundary layer formation, and there was a small gap between the shells and the substrate which increased proportionally with the shell size.

### Alignment

Snails tend to orient themselves against the flow (Boulding and Van Alstyne, 1993; Huryn and Denny, 1997; Le Pennec et al., 2017), a process known as rheotaxis. Therefore, we did an initial analysis to find out how they would likely be oriented in this setup. The models were first manually aligned by eye to a reference orientation of having the apex backwards, away from the inflow, and the orientation measures in the alignment analysis are relative this reference direction. An investigation of the drag using  $1^\circ$  increments was performed for a  $120^\circ$  sector, including both the alignment with spire straight backwards, and more to the right hand side, i.e. a counter-clockwise rotation, which has been suggested to minimise front-facing area of some short-spined shells (Trussell et al., 1993). A separate alignment test was done for each shape, and for the two different tilts against the substrate, at a flow speed of 1 m/s for the intermediate-sized shells of volume  $96 \text{ mm}^3$ . The orientations minimising drag forces are referred to as the front-facing orientation (figure 4.2), and from this we rotated the shells by  $90^\circ$ ,  $180^\circ$ , and  $270^\circ$  counter-clockwise relative to the substrate, which will be called the right-, back-, and left-facing orientations, respectively.

The drag,  $F_d$ , and lift,  $F_l$ , forces for each parameter combination were outputs from the simulations. The drag and lift coefficients, are a way to get a shape-specific, dimensionless measure of drag which largely controls for size and flow speed,

$$c_d = \frac{2F_d}{\rho u^2 A_{\text{front}}}, \quad c_l = \frac{2F_l}{\rho u^2 A_{\text{front}}}, \quad (4.1)$$

calculated from the above forces,  $F_d$  and  $F_l$ , the water density  $\rho$ , flow velocities  $u$ , and the projected front facing area of the shells  $A_{\text{front}}$ . To further estimate the biologically-relevant stresses the animal would be subjected to, we calculated two more dimensionless relative drag and lift measures, namely drag force per volumetric size,  $c_d^{\text{size}}$ , and drag force per foot area,  $c_d^{\text{foot}}$ , using variations of the formula above (equation (4.1)), with the size factor,  $A_{\text{size}}$ , and estimated foot area,  $A_{\text{foot}}$ , respectively, replacing the front facing area,  $A_{\text{front}}$ . This gave us three different ways of looking at the effect of the forces the snail would be subjected to: Forces scaled by either front facing area as a measure of direction-specific streamlining, by a volume-related size factor as a biological size measure, or by foot area to relate with tenacity.

### 4.2.3 Experimental setup

The real shells selected for this analysis were chosen to represent both the crab-wave dimorphism and include various intermediate shapes (figure 4.5). We used the relative tallness of the spire to represent the crab-wave shape gradient.

Real shells and 3D printed (polylactide) shell models were connected to a force gauge measuring the effects of only drag, and positioned in a large flume (figure 4.6a), which contained



**Figure 4.5:** The real shells used in the experiment, ordered by relative spire height, tallest spires on the left, shortest on the right, and oriented in the "wave" alignment when the inflow is from the right hand side of the image.

fresh water of temperatures of 18 °C–20 °C. The force transducers were measuring forces acting in one direction, in our case the drag, with very little contribution from orthogonal components, i.e. lift and lateral forces. The type of transducer used for the real snails was FORT10g (range 10 g, resolution <1 mg), while the force gauge used for the larger shell models was FORT100g (range 100 g, resolution < 0.1 g), both by World Precision Instruments. The orientations of the shells were recorded by photographs while in the flume (figure 4.6b). Frontal area was measured from additional photographs in the case of the real snails, while for the 3D printed models the values were obtained from the simulations. The 3D printed shells were constructed to represent the largest shells in the simulations, scaled by a length factor of 8, which is larger than any *L. saxatilis* snails found in nature. The drag force was measured for flow speeds of 0.2, 0.3, 0.4, and 0.5 m/s.

The alignment was set as the orientation with the least measured forces of the spire backwards (crab) alignment, and spire shifted towards the side (wave) alignment for the real shells (figures 4.2 and 4.5), while an additional three alignments were recorded for the 3D printed shells. This sideways shift for the wave alignment was not a set angle of the spire, but was described as how rotated the shell can be without having the spire visible from the direction of flow, and thus depended on the spire length. The recorded orientation of the spire relative to the flow direction was inferred from photographs of the shells' positions in the flume.

#### 4.2.4 Statistics

Both simulation and experimental results were compared between their respective shapes using multifactorial ANOVA's investigating shape, orientation, size, and all of their interactions. As we are specifically interested in the effects of shell shape, and since the variation between orientations is a result of having different shapes, we also directly compared their overall means using a simple ANOVA to find differences in the average forces the shells would be subjected to over longer timescales with variable flow directions. The drag coefficients were compared after linear regressions with respect to the logarithm of flow speed within each of the setups, i.e. for the simulations, experiment using 3D-printed models, and experiment using real shells respectively. The same linear regression was implemented for the drag scaled by volume measurements in the simulations, and for the (log transformed) drag scaled by foot area. The lift coefficient, lift per foot area, and drag to lift ratio were compared without any

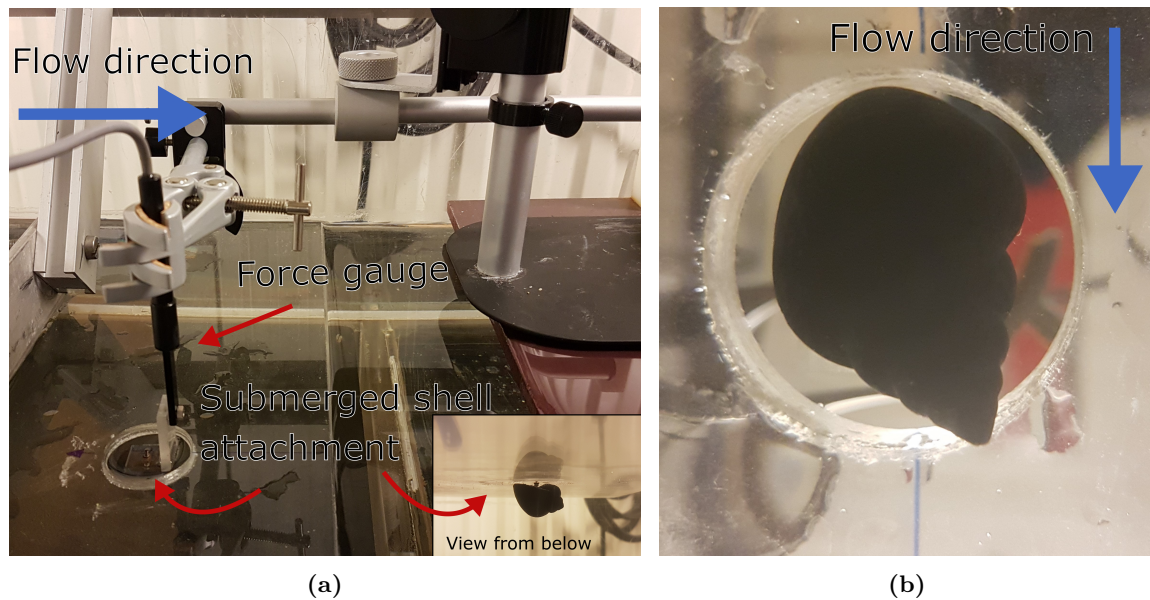


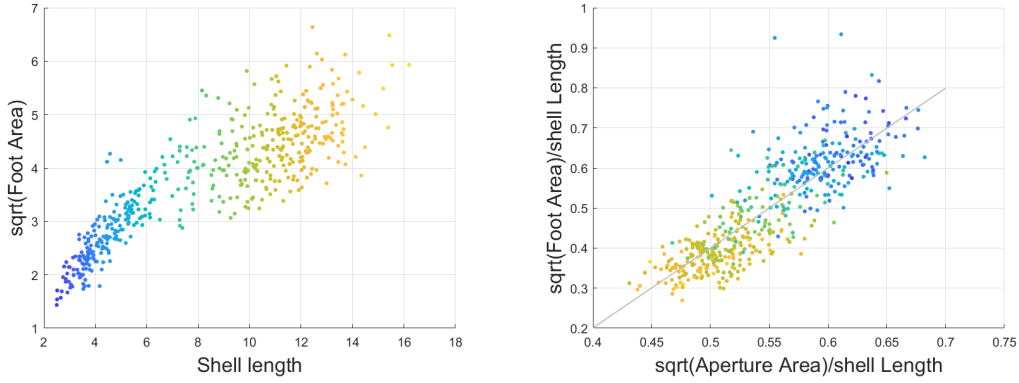
**Figure 4.6:** Flume experiment setup. (a) The shell is attached to a platform which in turn is attached to a force gauge. (b) Image from below, used for estimating the orientation of the spire relative the direction of the flow. Shell model shown in the "wave orientation", i.e. the spire is rotated counter-clockwise from aligning with the flow, but not extending beyond the largest whorl. Flow direction indicated by a blue line.

transformations of values. One should note that this analysis is more concerned with relative effect sizes attributed to the different factors than the level of statistical significance between them.

## 4.3 Results

### 4.3.1 Foot size

Foot size increases with increasing shell size in *L. saxatilis*, however, we were mainly interested in how it varies with shape. When normalised by shell length both the aperture size and foot size were relatively larger for the smaller shells, i.e. the wave ecotype has a larger foot per shell size (figure 4.7). The relative foot and aperture sizes showed a correlation of  $R^2 = 0.61$ , hence a bigger relative aperture is suggestive of a bigger relative foot size. The linear fit for relative foot size as a function of the relative aperture size had a slope of 2.0 and an intercept of  $-0.60$ . Since the slope was greater than 1, we saw a compound effect of having both relatively larger apertures in the wave ecotype, and larger feet relative to their aperture size, than for the crab ecotype. The estimated relative foot size for each of the models used in the simulations can be found in table 4.1, these values were then rescaled to match the shell length of their respective shell models.



(a) Linear foot size plotted over shell length, sample size is 499.

(b) Relative foot and aperture size. Least square linear fit giving slope 2.0, intercept  $-0.60$ , and  $R^2 = 0.61$ .

**Figure 4.7:** Absolute and relative foot size. Coloured by log of shell length, with blue being small, wave type, and yellow being large, crab type.

|               | Extreme Crab | Crab | Intermediate | Wave | Extreme Wave |
|---------------|--------------|------|--------------|------|--------------|
| Aperture area | 0.16         | 0.24 | 0.33         | 0.43 | 0.54         |
| Foot area     | 0.04         | 0.15 | 0.31         | 0.51 | 0.74         |

**Table 4.1:** Estimated aperture area and relative foot area of the shell models, using the linear equation obtained in figure 4.7.

### 4.3.2 Simulations

#### Alignment

We investigated the optimal alignment with respect to drag forces for each shape in an effort to find how the shells are likely to be oriented against the flow.

The minimum drag was found either at around  $0^\circ$ , the "crab alignment" with apex straight back, or around  $50^\circ$ – $60^\circ$ , the "wave alignment" with the apex shifted more to the side (figure 4.2), and was mostly consistent with the orientation having the minimal area against the flow (figure 4.8). In addition to minimising the drag forces and front-facing areas, these orientations were close to the minima in lift forces, and showed close to zero lateral forces.

#### Drag

The drag coefficient,  $c_d$ , in the simulations varied between the values 0.30 and 0.69 (figure 4.9a), with a clear decreasing trend with increasing flow speed for all shapes and orientations. Note that the  $c_d$  value is normalised by the square of the flow speed (equation (4.1)), but can still include secondary effects due to e.g. the relative viscosity at different speeds. There was also a small effect on the drag coefficient from size, which differed between the shapes (appendix figure D.3a). The extreme crab and wave shapes had their lowest mean drag coefficient for the size corresponding to the adult size of their respective ecotype in the wild, i.e. the small (size factor 1) extreme wave shape and large (size factor 4) extreme crab

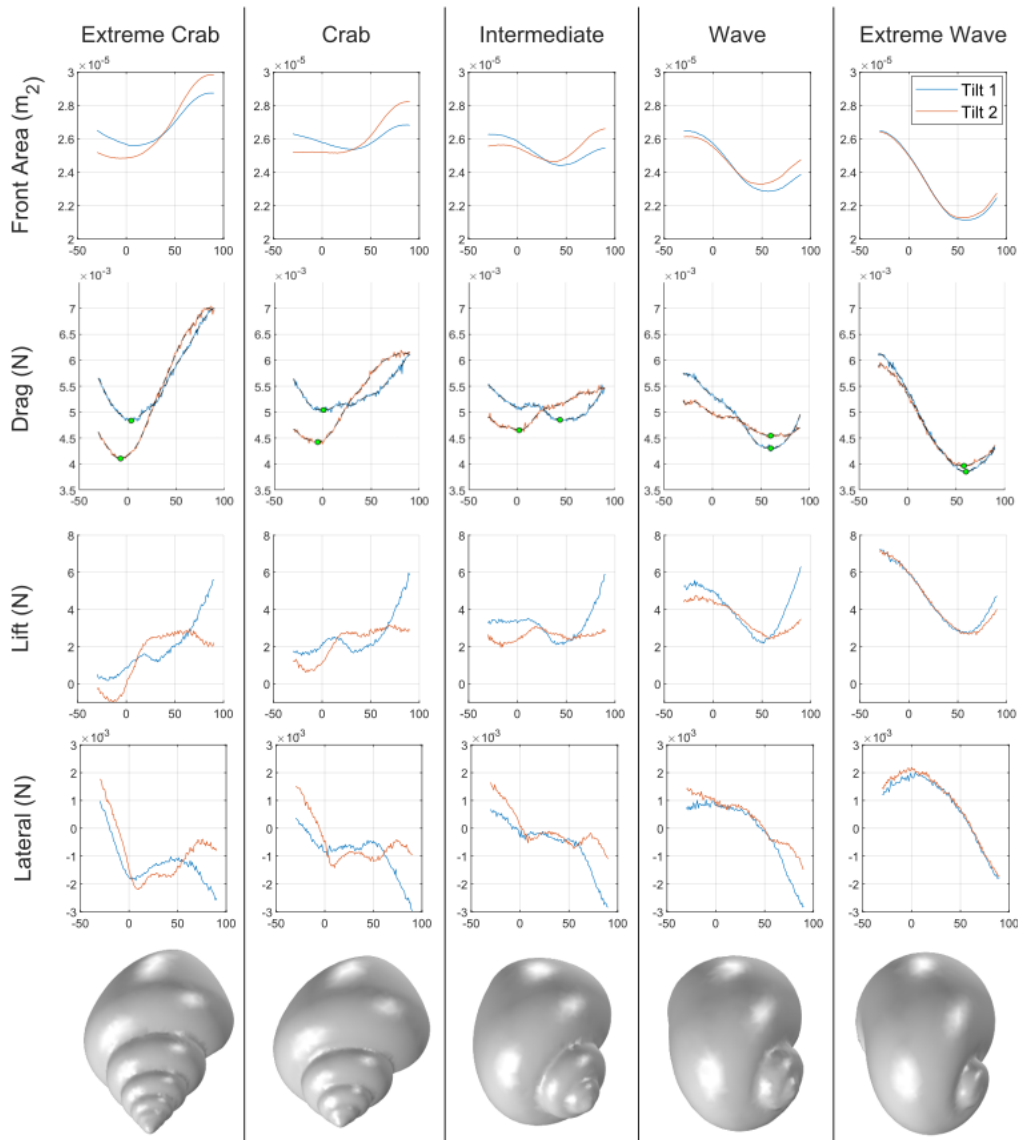


**Figure 4.8:** Alignment of shells to minimise drag for each shape, for medium-sized shell in flow speed of 1 m/s. Alignment with spire backwards corresponds roughly to an angle of 0°. Top row: The front-facing areas against the flow. Second row: The calculated drag force for the different shell models in simulations of different orientations against the flow, estimated minima marked in green. Colour indicates the two rounds of simulations that were performed, with slight variations of which point of the aperture were positioned to touch the substrate (figure 4.2). Third row: Lift forces. Fourth row: Lateral forces. Drag and lift coefficient plots can be found in appendix figure D.2.

shape were the optimal sizes, while increasing even further in size (to size factor 8) seemed worse for all shells. Since this variation was very small compared to the overall variability it is not clear that this would have a noticeable effect on snail survival, but is something that could be investigated further.

The extreme crab and wave shape showed the clearest differences in drag values between the alignments with short-side and broad-side against the flow, while this difference was present but less pronounced for the three intermediate shapes. The mean values for the residual of the drag coefficient,  $c_d$ , after a linear regression for the logarithm of flow speed showed a tendency toward lower values for wave-type shapes than for crab-type shapes (figure 4.9b). The trend toward lower values for wave type shells was even clearer for the residual drag forces scaled by volumetric size,  $c_d^{\text{size}}$ , after a linear regression for the logarithm of flow speed (figure 4.9c).

When comparing the drag force per foot area,  $c_d^{\text{foot}}$ , which should correspond to snail tenacity to stay attached to the substrate, it was clear that the foot area would have a very large effect, overpowering both the variation related to flow speed and shell orientation, and indicating a clear advantage for the larger foot size found in the wave type (figure 4.9d).

## Lift

The lift coefficient,  $c_l$ , in these simulations obtained values between  $-0.43$  and  $0.72$  (figure 4.10a). Negative values indicate that the shell experiences a force down against the substrate, while positive values indicate forces up and away from the substrate. The mean lift in these simulations was always positive, indicating that overall, snails experience a force upwards which would contribute to the dislodgement risk. The smallest lift upwards was for each shape obtained for the front-facing orientation, and the general trend was that less lift away from the substrate was experienced by the crab type shells. Both the lift coefficient (figure 4.10a) and the lift by size factor (figure 4.10b) showed very similar trends. The lift force per foot area,  $c_l^{\text{foot}}$  (figure 4.10c), showed that the foot area would have a large effect, where both the mean value and variability were much larger for the shells with a smaller foot.

The lift to drag ratio increased from the extreme crab to the extreme wave shape, similarly to the lift coefficient itself (figure 4.10d). This indicates that the relative importance of lift and drag varies between the different shapes, with lift playing a larger role for the wave-type shells than for the crab type, and drag playing a larger role for the crab type than the wave type. When oriented in the front-facing direction, the lift to drag ratio was smaller than for other orientations.

### 4.3.3 Experiment

#### Alignment

The alignment with the lowest mean in drag forces, after normalisation by the square of the flow speed, in both the experiment using 3D-printed shell models and the experiment using real shells corresponded to the "wave" alignment (figure 4.11a) and figure 4.11b). This means that none of the shells experienced lower drag forces when oriented with their spire straight back, compared to having the spire rotated as much as possible counter-clockwise without it being visible from the direction of flow.

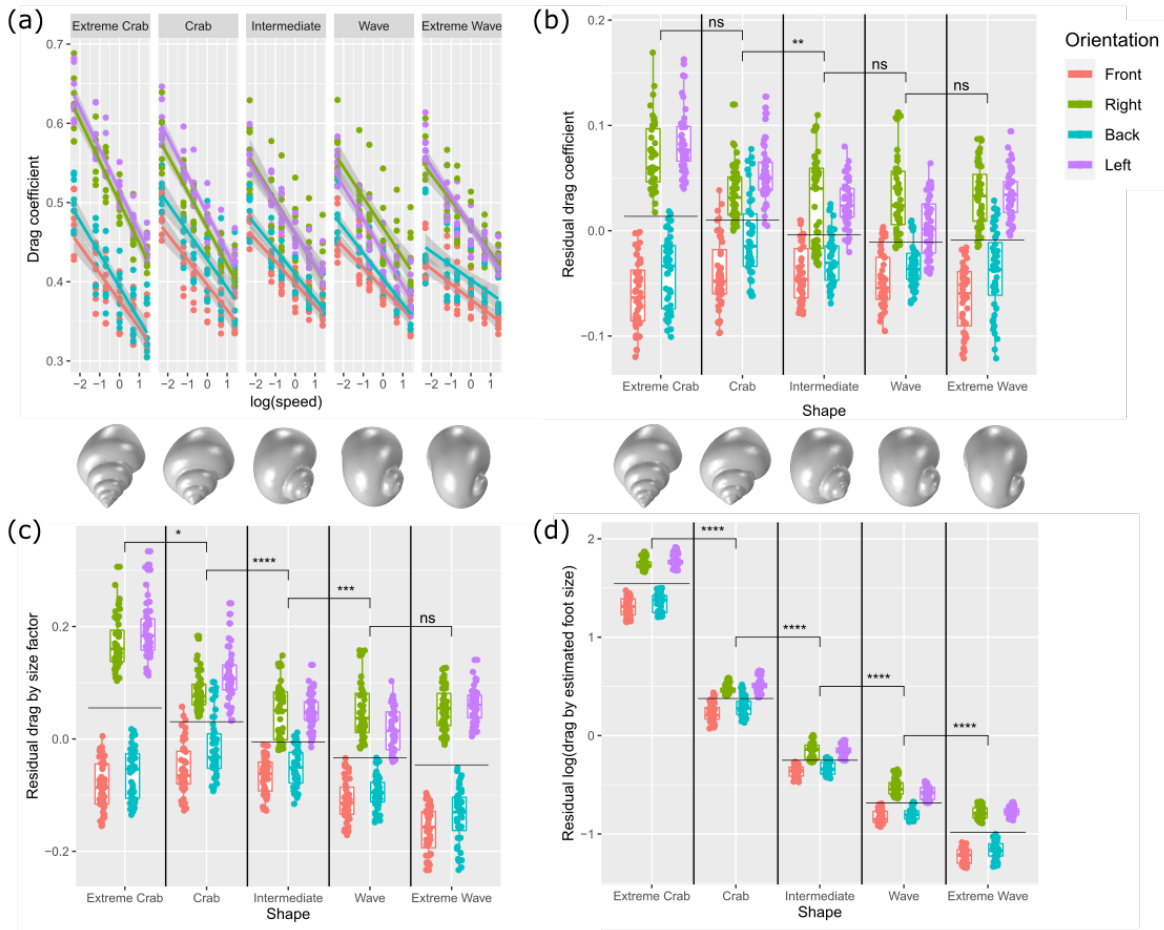


**Figure 4.9:** Results for different drag measurements in the simulations, corresponding ANOVA tables can be found in appendix figure D.4. Colour indicating the four orientations for each shape. Horizontal lines indicate the mean values for each shape, and significance levels of the difference between consecutive shapes are shown. (a) Drag coefficient  $c_d$  as it varied with the logarithm of flow speed, and linear regressions showing a decreasing trend for higher speeds for all shapes and orientations. (b) Drag coefficient residual for the overall linear regression for all simulations, to get a clearer picture of the difference between shapes and orientations. (c) Drag by size factor residual for an overall linear regression of all simulations with respect to flow speed. (d) Log-transformed drag per estimated foot area residual for an overall linear regression of all simulations with respect to flow speed.

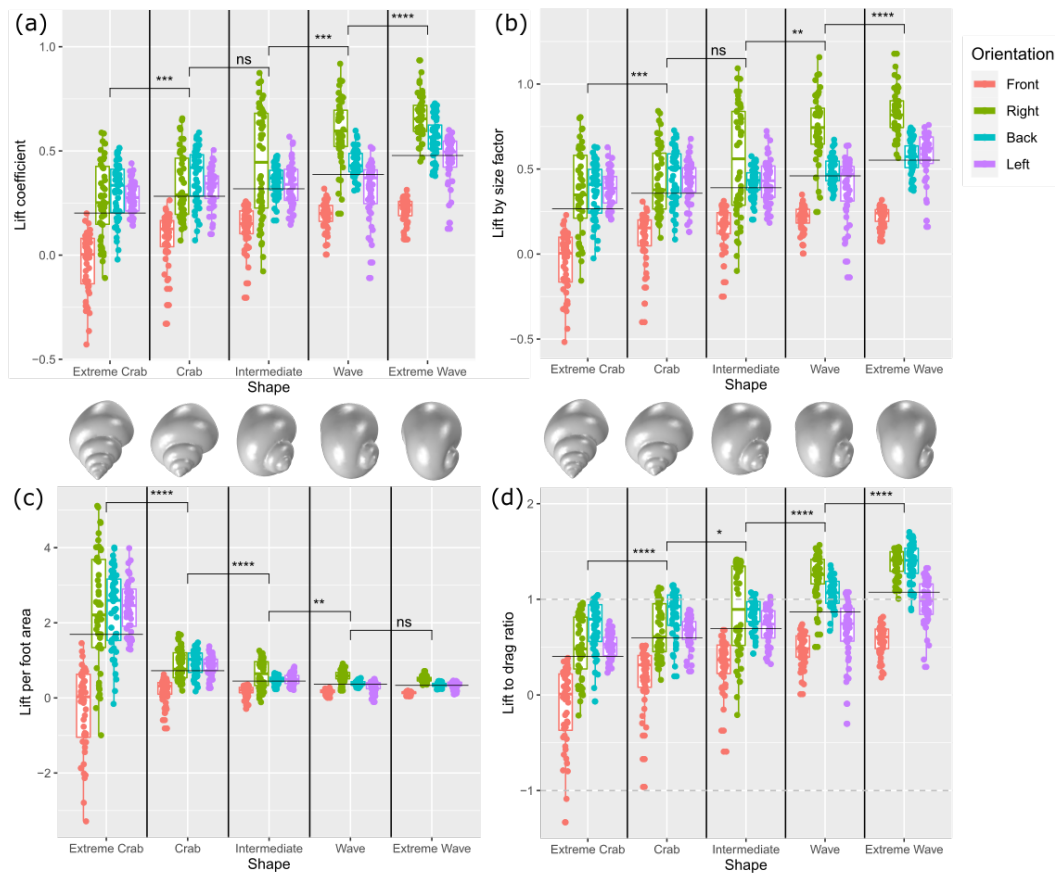


**Figure 4.10:** Results for lift in the simulations, with mean values for each shape indicated by black horizontal lines. Positive values indicate forces up and away from the substrate, while negative values indicate forces down against the substrate. Corresponding ANOVA tables can be found in appendix figures D.5 and D.6 (a) Lift coefficient,  $c_l$ , for the different shell shapes. (b) Lift force scaled by volumetric size factor. (c) Lift forces scaled by foot area. (d) Lift to drag ratio, values of magnitude larger than one indicate that lift forces were larger than drag forces, while values of magnitude less than one indicate the opposite.

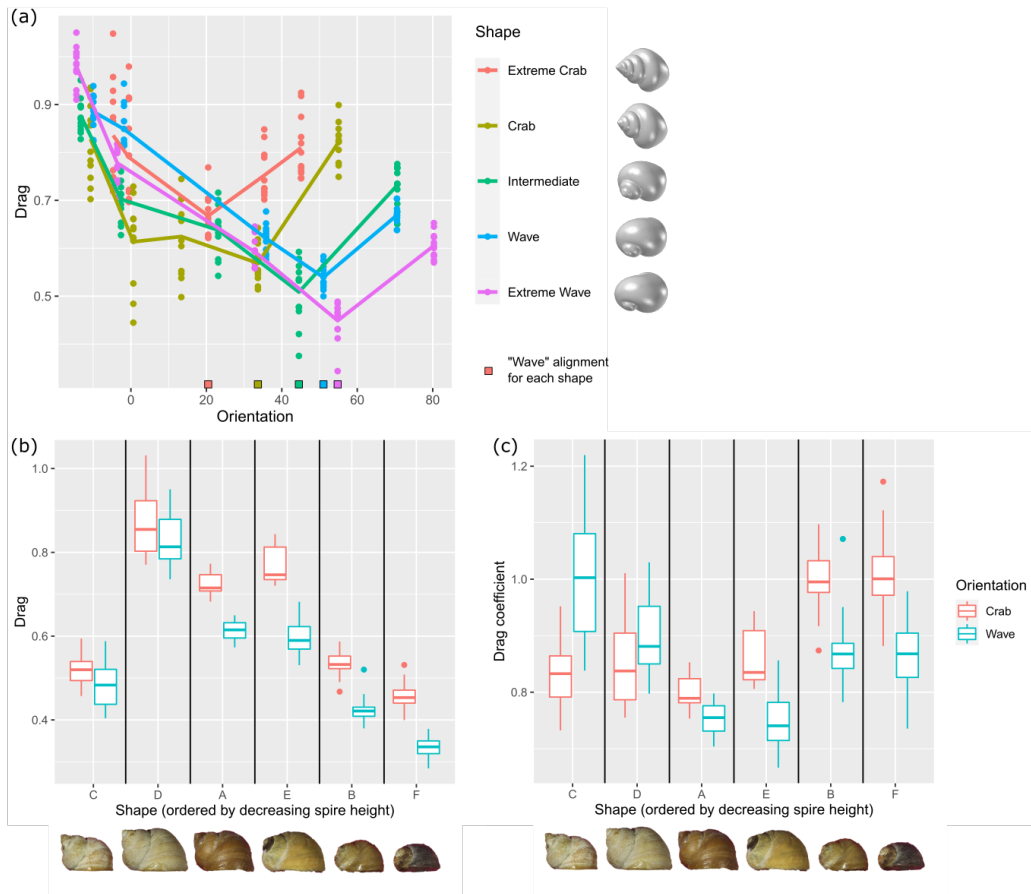


**Figure 4.11:** Alignment of shells in the experiment. (a) 3D printed shell models, using five orientations for each shape. (b) Real shells, comparing the "crab" and "wave" alignments, drag force scaled by area and flow speed. (c) Real shells, comparing the "crab" and "wave" alignments, drag coefficient.

On the other hand, when comparing the drag coefficients, i.e. taking the front-facing area into account, between the two orientations of the real shells, we observed lower values when aligned with the spire straight back for the two shells with the tallest spires (figure 4.11c).

## Drag

Drag coefficients in the experiment using 3D-printed shell models obtained values between 0.32 and 1.07, extending above the values in the simulations (figure 4.12a). Similar to the simulations, a general trend in the experiment using 3D-printed models was higher drag coefficient values when aligned with the broad-side against the flow, and lower values when aligned with the short-side against the flow. The trend toward lower mean drag coefficient values for the two wave-type shells than for the two crab-type shells could still be found, but the intermediate shape had the lowest mean value of all (figure 4.12c). Also here, the difference in mean between the shapes was smaller than the variability relating to orientation within each shape.

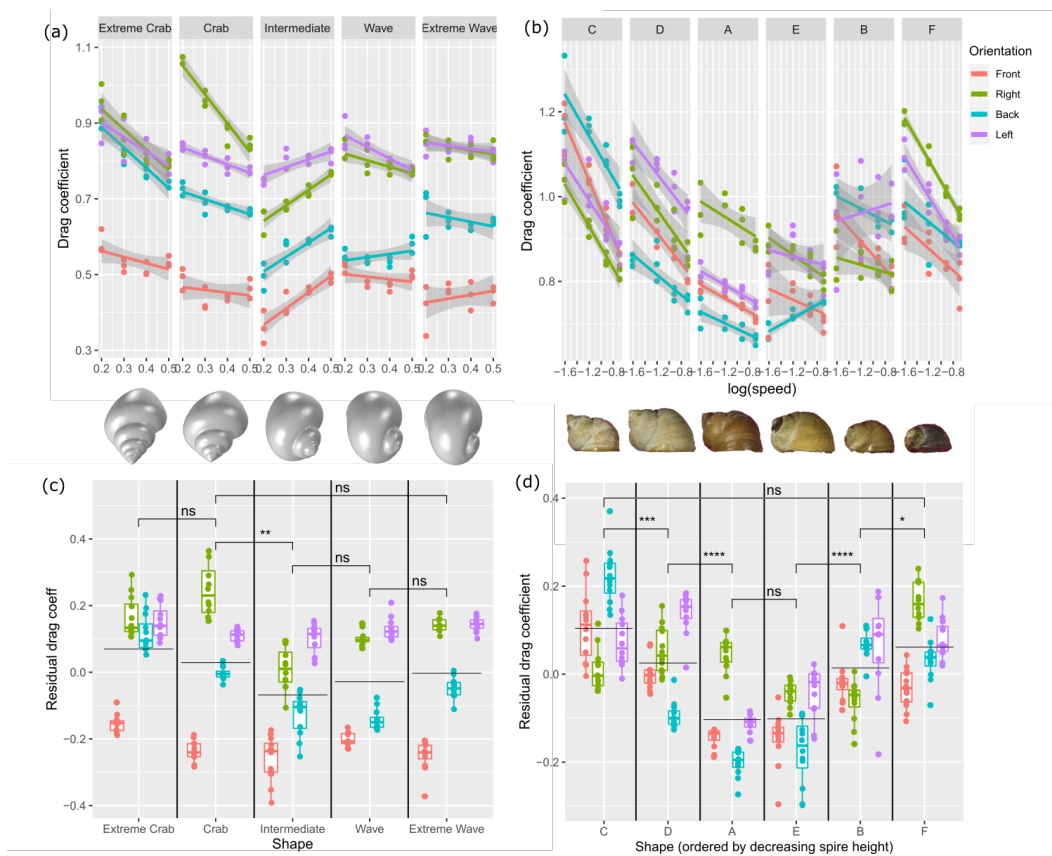


**Figure 4.12:** Top row: Drag coefficients measured from the flow experiment for the (a) 3D printed shell models and (b) real shells. Bottom row: Drag coefficient residual for the linear regression against flow speed for the whole data set in the respective flume experiments. The respective mean values for each shell are indicated by a horizontal line for the (c) 3D printed shell models and (d) real shells. ANOVA table can be found in appendix figure D.7.

For the real shells we obtained drag coefficient values between 0.65 and 1.33, which was noticeably higher than both the simulations and the 3D-model experiment (figure 4.12b). Similar to the 3D-model experiment, the intermediate shapes showed the smallest drag coefficient values, but in this case there was no difference between the most extreme crab and wave shells (figure 4.12d). The difference in drag between broad-side and short-side alignment, which was found in the simulations and 3D-model experiment, was not consistently found for the real shells.

## 4.4 Discussion

In general, shells of the intertidal snail *L. saxatilis* on exposed shores are smaller, more globular, and have relatively large apertures compared to snails in more protected areas (Heller, 1976; Trussell, 1997a), and they have been shown to be better at resisting high water flow (Le Pennec et al., 2017). In this investigation, we analysed different ways of measuring

how the shape of the shell affects the forces that the snails are subjected to, which relates to different biological traits. We found that increasing foot size could be the most important factor in resisting flow forces as this would spread out the pressure over a larger area of attachment, and we therefore suggest that the shape is mainly adapted to maximise the size of the foot, while minimising the hydrodynamical forces is of secondary importance. We also found an interesting interaction between shell shape and orientation, which suggests that the optimal orientation against the flow depends both on the area against the flow and the relative size of the spire (figures 4.2, 4.8, and 4.11). Shells in non-predictable flow directions would however need to optimise their shell shape to be able to withstand wave forces from any angle, and it is likely to be biologically crucial to be able to resist a combination of the average forces, the maximum forces, and the force variability, to avoid being dislodged (Denny, 1994; Denny et al., 2004). We mainly focused on comparing the mean values of the forces in this analysis, which in itself cannot tell the full story of the effect shape has on survival, but suggest variability should also be quantified in future research to identify how much of an effect it has on the risk of dislodgement.

To understand if and how the wave shells are better adapted to resist wave action, we investigated three different dimensionless characterisations of drag for the simulations, each representing different adaptations to the effects of flow. All of the three measures represent the dimensionless hydrodynamical efficiency of the particular shape in a specific orientation scaled by flow speed and density, but they differ in their way of accounting for size. The standard measure known as the drag coefficient,  $c_d$ , measures drag force per front-facing area and will be low for streamlined shapes, while  $c_d^{\text{size}}$  is a measure of drag scaled by volumetric size, and  $c_d^{\text{foot}}$  is the drag per foot area. We suggest that measuring forces per volume is more likely to reflect the biological size constraints compared to the standard drag coefficient, since the front-facing area does not relate as closely to a specific biological factor. The forces relative to foot size could however be the best measurement to estimate the snail's ability to survive by not getting dislodged from the substrate (figure 4.9d), which is consistent with previous experimental results where tenacity has been shown to scale linearly with foot area in different gastropods (Hohenlohe, 2003; Etter, 1988; Trussell, 1997a; Le Penneec et al., 2017). We confirmed that in *L. saxatilis* the wave ecotype has both a larger relative foot size as well as a larger relative aperture size than the crab shells (Grahame and Mill, 1986; Heller, 1976), and in addition we found that the difference in relative foot size is larger than the difference in relative aperture size.

It should also be noted that the crab-type shells of *L. saxatilis* in their natural habitat are much thicker, and have more tightly wound spiral patterns, and thus more internal walls which reinforces their shells and protects them from being preyed on by crabs. Therefore, the internal volume, and thus the living space available to the animal, is not directly determined by the external volume. Taking this into account by normalising the forces with respect to internal rather than external volume would affect the results (figure 4.9c) in favour of the wave shells compared to the crab shells, as the wave shells would be subjected to even lower forces for the same amount of internal shell volume, i.e. soft body size. There will also be a trade-off between the relative size of the foot and the rest of the animal, particularly for species such as *L. saxatilis* which can retract fully into their shell. Investigating this trade-off, where increasing the foot size leads to less space available for other body parts, could give insights into the biological limits of adaptation to strong flows.

In this study we obtained drag coefficient,  $c_d$ , values ranging between 0.30 and 1.33, which

partially overlap with previously measured values for different species of snails which range between 0.195 and 0.796 (Dussart, 2002; Dussart and Pontier, 1999; Denny, 1985; Jobin and Ippen, 1964). The simulations indicated that an increase in foot size would be the single most important factor to resist flow forces, as this would decrease the experienced force per attachment area with the substrate more than a change in shell shape would (figure 4.9). In both the simulations and 3D-printed shell model experiment there was a consistent pattern of lower drag coefficients when shells were aligned with their short-side against the flow than when aligned with their broad-side against the flow. This was, however, not the case for the experiment using real shells. In general, we obtained smaller values in the simulations compared to the experiment, in particular for the experiment using real shells. This inconsistency between experiments might be partially due to larger sensitivity to noise for the real shells, as they were smaller and we therefore needed to use a more sensitive force gauge. Another possible factor in this inconsistency could be if the force gauges are more sensitive to forces perpendicular to the drag than an initial analysis indicated. If the drag measurements in this experiment include lift forces to some extent, we expect this to have increased the measured values for the wave shapes more than the crab shapes in the experiment using the 3D printed shells (figure 4.10a), which in that case could explain why the wave shapes did not have lower  $c_d$  values than the intermediate and crab shapes in this experiment.

The lift coefficients in the simulations ranged between  $-0.4$  and  $1$ , with a trend of increasing values from the extreme crab to the extreme wave shape, suggesting that the wave type experiences larger forces away from the substrate (figure 4.10a). A negative value would indicate a vertical force pressing the shell down against the substrate, which would be preferable as it should reduce the risk of dislodgement and was more common for the crab shapes. However, the mean lift coefficient values were positive for all shapes suggesting that lift contributes to dislodgement. It was also clear that the front-facing orientation generated lower values than the remaining three, within each of the shapes, suggesting that this orientation, which minimised the drag forces, is also preferable in terms of lift. The lift scaled by the volumetric size factor showed very similar results to the standard lift coefficient, and thus might not provide any additional understanding into the effect of shell shape on snail survival in nature, unlike in the case of drag as discussed above. When scaling the lift forces relative to the estimated foot size,  $c_l^{foot}$ , there is a different story compared to the standard lift coefficient,  $c_l$ . The lift per foot area showed a much larger variability and a higher average for the crab shapes and less for the wave shapes (figure 4.10c), again suggesting that foot area has a very large impact on the attachment abilities for gastropods, much larger than the hydrodynamical effects of shell shape itself. The effect of shell size on lift showed an interesting interaction with flow speed, where there was a decrease in lift for higher speeds except for the smallest size (figure D.3b). The flow around, and particularly under, the shells will be affected by the flow boundary layer, and since the smallest shells have the highest proportion contained within it, this could be the reason for the differences due to shell size. We were not able to measure lift in our experimental setup, so we could not confirm or dispute the conclusions about lift from the simulations, but we expect that the effects of foot size would still exceed the direct effects of shape, and this should be analysed in future research.

Since shape and orientation interact in their effect on drag and lift, it is unlikely enough to look only at a few orientations to understand the effects of the chaotic wave action on rocky shores. While a behaviour of aligning their shells with the flow was observed for *L. saxatilis* in flume experiments (Boulding and Van Alstyne, 1993), it has not been investigated in detail.

We therefore analysed which orientation of the shells minimised the measured drag forces. We found that the optimal alignments for the shells in the simulation could be categorised as two different types, either aligned with the apex straight back when the spire was long, or rotated counter-clockwise, as much as possible without the spire showing when viewed from the direction of the inflow, when the spire was short. We also found that this alignment could be affected by varying the tilt of the shell, altering the space between shell and substrate in the simulations. In general, the optimal orientation coincided well for minimising the front-facing area, drag, and lift, as well as obtaining a near-zero value for lateral forces.

In the experiment we found that shells in the wave alignment were subjected to lower forces than when in the crab alignment (figure 4.11). However, the wave alignment is defined in a way that depends on the spire height. This means that the direction of the spire in the wave alignment is more straight back the taller the spire is (figure 4.11a), since it requires less of a rotation to be visible and sticking out on the side, and for shells with very long spires the two alignments could even be functionally indistinguishable. To fully understand the preferred orientation, one would also need to take lift and lateral forces into account, but if the results from the simulations give a correct indication, then we would expect the optimal alignment for drag to be close to optimal also for lift and lateral forces.

The aperture orientation used for the shell models in this analysis is not completely realistic, it should ideally be flat against the substrate (compare figure 4.2 with figure 4.5) (Noshita et al., 2012; Linsley, 1977). The reason for using the models despite this inaccuracy is that the modelling procedure used currently has no better way of defining the aperture orientation than using the Frenet frame, i.e. perpendicular to the direction of growth. The empty space this problematic aperture orientation generates, between shell model and substrate, affects the flow pattern underneath the shell, which is especially likely to affect the lift forces. It would therefore be useful to improve the shell model construction method to be able to take this into account. The soft bodies of the snails have not been included in this analysis either, as we mainly wanted to test the effect of shell shape alone. However, since the soft body would fill out the space between shell and substrate, it would affect the forces measured, and possibly alter the optimal alignment. We have also excluded any surface roughness of the shells in this analysis, which can impact the magnitude of the forces due to its effect on turbulence in the boundary layer near the shell surface (Chamberlain and Westermann, 1976). More simulations with this in mind could give us a fuller picture of the hydrodynamical effects of surface roughness, as well as be extended to analysis of the effects of ridges and spines on shells.

We did not investigate the effects of acceleration as this has been suggested not to be an important factor for survival on wave-swept shores (Denny, 1995), despite having been measured at very high values (Denny, 1985). Acceleration forces scale with volume, which would suggest larger effects for the larger snails (Denny et al., 1985). However, the accelerations are confined to very short intervals in the case of crashing waves on rocky shores, short enough that the forces generated from acceleration should not be able to act on the whole shell simultaneously for those shells which are large enough for the accelerational forces to become meaningful. Hence, the stresses from acceleration in the field would not be crucial for wave resistance (Gaylord, 2000). There are, however, still some questions around whether and how wave accelerations might affect animals on the shoreline, e.g. large accelerations has been suggested to change the drag to lift ratio (Weissenberger et al., 1991), which could affect the optimal morphology in different settings. To better understand the forces relating

to acceleration, when they could be of importance, and how they interact with shape, size and flow speed, we suggest further CFD analyses and comparing the effects of the magnitudes of acceleration observed both on rocky shores and in rivers.

We have constructed this analysis to compare computer simulations to flume experiments in the lab, rather than to the much more diverse conditions found in the wild, in order to simplify comparisons between empirical measurements and simulations (Yamazaki and Goshima, 2012; Dussart, 1987; Verhaegen et al., 2019). As we found some inconsistencies between the simulations and the experiments, more analysis is needed in order to draw consistent conclusions. However, we are confident that more CFD simulations together with experimental verification would further improve our understanding of the specific effects of foot size, speed, orientation, acceleration, surface roughness and boundary layer effects, for a more diverse set of shell shapes, both realistic ones and ones not found in nature, in order to understand what makes a shell well adapted to different types of flow. To improve the comparison between simulations and empirical data, in addition to using an improved method to generate shell models, there is a possibility of using 3D models of scanned specimens, possibly including the soft body, which would be informative and improve the biological relevance of future simulations. There is also a need to understand the trade-offs between the biological factors when subjected to more than one selection pressure, e.g. evolutionary simulations of fitness in environments where both dislodgement and predation affect survival in varying degrees.

## Acknowledgements

We would like to thank Susanna Strömberg for printing the 3D shell models. The Leverhulme Centre for Advanced Biological Modelling provided funding the experiment, and the simulations were performed on the Chalmers Centre for Computational Science and Engineering (C3SE) computational cluster, which is part of the Swedish National Infrastructure for Computing (SNIC).

# Chapter 5

## Discussion

### 5.1 Summary of findings

The main task of any quantification method is to provide an accurate description of the specific properties of an object in a useful way, and to help in linking different fields and perspectives together. In our case, this means a shape quantification method that improves our understanding of the connections between morphology, function, developmental processes, environmental factors, and genetics. The accretionary growth of gastropod shells gives a unique possibility in making these connections, as the adult shells contains a full ontogenetic record, describing the incremental growth of the shell throughout its development. Therefore, the main aim of this thesis is to find a good description of shell shape in order to better understand the factors causing the ecotypic variation within the marine snail species *Littorina saxatilis*, both in terms of genetics, plasticity, and functionality at the individual level, as well as the effects of environmental factors, and to link this to natural selection over evolutionary timescales.

#### 5.1.1 Chapter 2 - Quantifying Shape in Shells

In chapter 2 I developed a high-throughput method for quantitatively inferring shape and growth parameters for gastropod shells with variable aperture shapes from a set of points on 2D images. This allowed me to analyse the variability found in the crab-wave ecotype dimorphism found in the marine snail *Littorina saxatilis*, and to construct representations of the shells as 3D computer models to visualise this diversity. We found that the most obvious difference between the ecotypes was in the growth parameter values, describing how much taller and wider the shell becomes for each whorl, i.e. for each full revolution of growth. I also found that both types showed a slightly convex spire profile, indicating allometric rather than isometric growth, and a small but consistent sex difference in shape was found in both ecotypes. This method for describing shape in gastropod shape thus shows potential for use as a quantification method in large data sets, to find and interpret both large and small differences.

### 5.1.2 Chapter 3 - Genetic architecture of Shell Shape

In chapter 3 we implemented the quantification method developed in chapter 2 to investigate if we could improve the identification of genomic regions involved in shape and growth of shells compared to a GM analysis. This analysis allowed us to gain new insights into the genetic architecture for different aspects of shape, and suggested that the growth based quantification gives a more direct connection between the genetics and the biologically relevant shape components. The results suggested that some of the ecotype-specific variation as well as the allometric convexity had a genetic component, and that the overall shape of the shells likely has a complex genetic architecture with several genomic regions of various effect sizes being involved in the variability.

### 5.1.3 Chapter 4 - Hydrodynamical Effects of Shell Shape

To investigate how shape affects the fitness in wave-swept environments, I implemented a computational fluid dynamics simulation and conducted a flume experiment in chapter 4. We found some general differences between the crab and wave type shells, possibly indicating that the wave type's shell shape is reducing the strength of forces relative the snail's body size, but the most important factor for survival is more likely foot size. This suggested that the primary factor in shell shape adaptation to extreme flow environments could be to accommodate a large foot and, thus, minimising hydrodynamical forces would be a secondary factor.

The shell shape was indicated to affect both the optimal orientation against the direction of the flow, and the extent of the force variability as the flow direction varied, thus shape could still affect survival. The optimal shape will likely differ between different flow types, e.g. steady unidirectional flow in rivers, or chaotic omnidirectional flow on wave-swept shores, but it could also be influenced by other environmental factors, such as predators.

## 5.2 Future work

### 5.2.1 Shell quantification

One of the main contributions to shape parameter inference in this thesis is the use of the "circlipse" to get a consistent point of reference for the aperture position despite the variable aperture shapes of *L. saxatilis*. The idea of obtaining a more stable aperture reference point by fitting a circle to only a specific section of the aperture, and then describing the full aperture shape in relation to this point, gives a consistent set of parameters, and can easily be extended to account for more complex and variable aperture curves, allowing a wider range of shell shapes to be quantified and modelled consistently. In its current version, this method can account for isometric, convex, and concave shell growth, but not e.g. the tri-phasic allometry found in *Cerion* (Gould, 1989), which would require growth parameters which vary throughout growth. These types of growth pattern are also possible to include in future versions of shell modelling, as stepwise constant values which change, e.g. at maturity, or even as continuous functions of time if the shell data has high enough resolution.

Quantifying more specimens at higher resolution from more species, both fossil and contemporary, using the ShellShaper program presented in chapter A and chapter E would generate a reference data base of shape parameters. Such a data base could be used to connect different fields of biology, since it could be analysed through the perspectives of both the

developmental process and across evolutionary timescales. This could also be connected to the increasing understanding of the genetics involved in shell construction and functionality of various traits in term of biological or environmental factors.

I have also started an investigation into the possibilities of having a mapping between the fixed reference frame model presented in this thesis and the moving reference frame description which defines the shell growth locally at the current aperture (Moulton and Goriely, 2014; Moulton et al., 2012), similar to the map developed in Noshita (2014). The moving reference frame description is expected to be a closer representation of growth from the perspective of the snail, and will provide yet another viewpoint of the shell construction process. This would yield a way of using both growth descriptions interchangeably, choosing the one most informative to the specific problem at hand.

### 5.2.2 The 3D shell models

When it comes to the future analysis into the fluid dynamics of shell shape, there are several possible directions. In the case of flow simulations, the main thing to improve from the analysis in this thesis would be to fix the shell models to have more realistic aperture orientations, and possibly to include the soft tissue, and then to do a comparison of a wider range of shape parameter combinations for the shell models, comparing realistic and unrealistic shapes. This should be combined with experiments measuring the drag and lift of a larger range of snail species of various shapes, as well as 3D printed versions of the computer generated shells, to better understand the inconsistencies found in the comparisons in chapter 4.

In addition to 3D computer models being used for fluid dynamics analysis, they can also be used for analyses of e.g. structural strength, internal volume, and shell thickness, or investigating the functional trade-off between them. With the possibility of such a wide variety of analyses, the optimisation of shell shape in various environments could be investigated simultaneously from different viewpoints where different selection pressures have different levels of importance.

As has been shown in chapter E, using the ShellShaper program to analyse the position and size of coloured bands can provide further insight into the process of shell construction. Similar analyses could be applied to a wider range of species, to quantify the position and size of bands or other shell features such as ridging or spines, and relate these features to genetics or functional properties.

### 5.2.3 Future implications for *Littorina* research

In the specific case of *Littorina* research, there are many research questions where a growth-based quantification of shape would provide additional insights. Possibly the most obvious continuation to the work in this thesis is to measure shells at multiple points throughout growth, to analyse developmental variation. I have started an analysis of a set of *L. saxatilis* shells originally collected from a crab, wave, or intermediate habitat, and then transplanted into the same or a different habitat to investigate if there are any plastic environmental effects on shape. This developmental analysis could also lead to additional understanding of the convex allometric growth found in both chapter 2 and chapter 3. An even more thorough investigation at several time points for each snail could further improve our ability to link the speed of growth in real time, as it is currently only described as growth per constructed whorl,

and not growth per time unit. This will be informative for understanding of how growth in overall size of the shell and the soft body relates to the shell thickness and total amount of shell constructed.

When it comes to large scale evolutionary biology, *L. saxatilis* and its sister species are famously used to study the processes of local adaptation and speciation using population level studies, which need useful quantifications of the traits under selection. Similarly to the results in chapter 3, I suggest that applying the method introduced in chapter 2 could improve both the accuracy and interpretation of quantitative morphological analyses of evolutionary processes in terms of biologically relevant traits and their functions, compared to when GM is used. A continued investigation into the genetics of shell shape and growth in *L. saxatilis* will provide more specific information about the genomic regions and specific genes responsible for the ecotype variation. For example, a growth-based perspective on morphology could be used to better understand how the crab and wave ecotypes can maintain their distinct shapes despite ongoing gene flow, and how the genetic architecture influences divergent adaptations.

#### 5.2.4 Wider implications

The causes of morphological variation throughout growth is one of the big questions in developmental biology, and gastropod shells provide a very interesting perspective on this. Even though the quantification method presented in this thesis only works for logarithmic spiral type of growth, such as shells and horns, it could still provide insights into the general processes of morphogenesis, as a reference to compare to and contrast with in e.g. genetics and developmental biology. More specifically, to investigate which genes and which processes of morphogenesis and allometry are preserved across large parts of the tree of life, which are only present in organisms with spiral growth, or which are even further restricted to a few closely related species. Different adaptations could be necessary at different life stages, and thus allometry in itself can be adaptive by improving different biological functions at different growth stages, which could differ between environments.

### 5.3 Conclusion

To summarise, in this thesis I have shown how the choice of quantification method can improve the ability to describe and investigate shape variability in gastropod shells. Using the method I developed in this thesis, which describes the shells in terms of the construction process, I uncovered new insights into the genetic architecture and environmental factors related to shape and growth in the marine snail *L. saxatilis*.

# Bibliography

- Abdelhady, A. A. (2016). Phenotypic differentiation of the Red Sea gastropods in response to the environmental deterioration: Geometric morphometric approach. *Journal of African Earth Sciences*, 115:191–202. doi:10.1016/j.jafrearsci.2015.12.001.
- Abe, M. and Kuroda, R. (2019). The development of CRISPR for a mollusc establishes the formin *Lsdia1* as the long-sought gene for snail dextral/sinistral coiling. *Development (Cambridge)*, 146(9):1–7. doi:10.1242/dev.175976.
- Ackerly, S. C. (1989). Kinematics of accretionary shell growth, with examples from brachiopods and molluscs. *Paleobiology*, 15(2):147–164. doi:10.1017/S0094837300009337.
- Adams, D., Collyer, M., and Kaliontzopoulou, A. (2019). Geomorph: Software for geometric morphometric analyses. R package version 3.1.0. Available from <https://cran.r-project.org/package=geomorph>.
- Allmon, W. D. (1994). Patterns and processes of heterochrony in lower Tertiary turritelline gastropods, U.S. Gulf and Atlantic Coastal Plains. *Journal of Paleontology*, 68(1):80–95. doi:10.1017/S0022336000025610.
- Allmon, W. D. and Smith, U. E. (2011). What, if anything, can we learn from the fossil record about speciation in marine gastropods? Biological and geological considerations. *American Malacological Bulletin*, 29(1-2):247–276. doi:10.4003/006.029.0214.
- Amadeu, R. R., Cellon, C., Olmstead, J. W., Garcia, A. A. F., Resende, M. F. R., and Muñoz, P. R. (2016). AGHmatrix: R Package to Construct Relationship Matrices for Autotetraploid and Diploid Species: A Blueberry Example. *The Plant Genome*, 9(3):1–10. doi:10.3835/plantgenome2016.01.0009.
- Andrews, S. (2010). FastQC: A Quality Control tool for High Throughput Sequence Data. Available from <https://www.bioinformatics.babraham.ac.uk/projects/fastqc/>.
- Arends, D., Prins, P., Jansen, R. C., and Broman, K. W. (2010). R/qtl: High-throughput multiple QTL mapping. *Bioinformatics*, 26(23):2990–2992. doi:10.1093/bioinformatics/btq565.
- Ashline, G. L., Ellis-Monaghan, J. A., Kadas, Z. M., and McCabe, D. J. (2009). Modeling Seashell Morphology. *UMAP/ILAP Modules: Tools for Teaching*, pages 101–139.
- Atkinson, W. D. and Newbury, S. F. (1984). The Adaptations of the Rough Winkle, *Littorina rudis*, to Desiccation and to Dislodgement by Wind and Waves. *Journal of Animal Ecology*, 53(1):93–105. doi:10.2307/4344.

- Bertness, M. D. and Cunningham, C. (1981). Crab shell-crushing predation and gastropod architectural defense. *Journal of Experimental Marine Biology and Ecology*, 50(2-3):213–230. doi:10.1016/0022-0981(81)90051-4.
- Bo, W., Wang, Z., Xu, F., Fu, G., Sui, Y., Wu, W., Zhu, X., Yin, D., Yan, Q., and Wu, R. (2014). Shape mapping: Genetic mapping meets geometric morphometrics. *Briefings in Bioinformatics*, 15(4):571–581. doi:10.1093/bib/bbt008.
- Boettiger, A., Ermentrout, B., and Oster, G. (2009). The neural origins of shell structure and pattern in aquatic mollusks. *Proceedings of the National Academy of Sciences*, 106(16):6837–6842. doi:10.1073/pnas.0810311106.
- Bolger, A. M., Lohse, M., and Usadel, B. (2014). Trimmomatic: A flexible trimmer for Illumina sequence data. *Bioinformatics*, 30(15):2114–2120. doi:10.1093/bioinformatics/btu170.
- Bookstein, F. L. (1992). *Morphometric Tools for Landmark Data*. Cambridge University Press. doi:10.1017/cbo9780511573064.
- Bookstein, F. L. (2015). The Relation Between Geometric Morphometrics and Functional Morphology, as Explored by Procrustes Interpretation of Individual Shape Measures Pertinent to Function. *Anatomical Record*, 298(1):314–327. doi:10.1002/ar.23063.
- Boulding, E. G. and Hay, T. K. (1993). Quantitative Genetics of Shell Form of an Intertidal Snail: Constraints on Short-Term Response to Selection. *Evolution*, 47(2):576. doi:10.2307/2410072.
- Boulding, E. G., Holst, M., and Pilon, V. (1999). Changes in selection on gastropod shell size and thickness with wave- exposure on northeastern pacific shores. *Journal of Experimental Marine Biology and Ecology*, 232(2):217–239. doi:10.1016/S0022-0981(98)00117-8.
- Boulding, E. G., Rivas, M. J., González-Lavín, N., Rolán-Alvarez, E., and Galindo, J. (2017). Size selection by a gape-limited predator of a marine snail: Insights into magic traits for speciation. *Ecology and Evolution*, 7(2):674–688. doi:10.1002/ece3.2659.
- Boulding, E. G. and Van Alstyne, K. L. (1993). Mechanisms of differential survival and growth of two species of *Littorina* on wave-exposed and on protected shores. *Journal of Experimental Marine Biology and Ecology*, 169(2):139–166. doi:10.1016/0022-0981(93)90191-P.
- Bourdeau, P. E. and Padilla, D. K. (2019). Cue specificity of predator-induced phenotype in a marine snail: is a crab just a crab? *Marine Biology*, 166(7):1–10. doi:10.1007/s00227-019-3526-0.
- Bourdeau, P. E. P. E., Butlin, R. K. R. K., Brönmark, C., Edgell, T. C. T. C., Hoverman, J. T. J. T. J. T., and Hollander, J. (2015). What can aquatic gastropods tell us about phenotypic plasticity? A review and meta-analysis. *Heredity*, 115(4):312–321. doi:10.1038/hdy.2015.58.
- Broman, K. W., Gatti, D. M., Simecek, P., Furlotte, N. A., Prins, P., Sen, S., Yandell, B. S., and Churchill, G. A. (2019). R/qt12: Software for mapping quantitative trait loci with high-dimensional data and multiparent populations. *Genetics*, 211(2):495–502. doi:10.1534/genetics.118.301595.

- Butlin, R. K., Saura, M., Charrier, G., Jackson, B., André, C., Caballero, A., Coyne, J. A., Galindo, J., Grahame, J. W., Hollander, J., Kemppainen, P., Martínez-Fernández, M., Panova, M., Quesada, H., Johannesson, K., and Rolán-Alvarez, E. (2014). Parallel evolution of local adaptation and reproductive isolation in the face of gene flow. *Evolution*, 68(4):935–949. doi:10.1111/evo.12329.
- Callomon, P. (2019). Standard views for imaging mollusk shells. American Malacological Society. Available from <https://ams.wildapricot.org/resources/Documents/Standardviewsforimagingmolluskshellsforweb2019.pdf>.
- Carballo, M., García, C., and Rolán-Alvarez, E. (2001). Heritability of shell traits in wild *Littorina saxatilis* populations: Results across a hybrid zone. *Journal of Shellfish Research*.
- Cardini, A. (2014). Missing the third dimension in geometric morphometrics: How to assess if 2D images really are a good proxy for 3D structures? *Hystrix*. doi:10.4404/hystrix-25.2-10993.
- Carrington Bell, E., Denny, M. W., Bell, E. C., and Denny, M. W. (1994). Quantifying "wave exposure": a simple device for recording maximum velocity and results of its use at several field sites. *Journal of Experimental Marine Biology and Ecology*, 181(1):9–29. doi:10.1016/0022-0981(94)90101-5.
- Carvajal-Rodríguez, A., Conde-Padín, P., and Rolán-Alvarez, E. (2005). Decomposing shell form into size and shape by geometric morphometric methods in two sympatric ecotypes of *Littorina saxatilis*. *Journal of Molluscan Studies*, 71(4):313–318. doi:10.1093/mollus/eyi037.
- Cazenave, K. R. and Zanatta, D. T. (2016). Environmental drivers of shell shape in a freshwater gastropod from small and large lakes. *Freshwater Science*, 35(3):948–957. doi:10.1086/686912.
- Chamberlain, J. A. and Westermann, G. E. G. (1976). Hydrodynamic Properties of Cephalopod Shell Ornament. *Paleobiology*, 2(4):316–331. doi:10.1017/S0094837300004954.
- Chapperon, C., Studerus, K., and Clavier, J. (2017). Mitigating thermal effect of behaviour and microhabitat on the intertidal snail *Littorina saxatilis* (Olivi) over summer. *Journal of Thermal Biology*, 67(March):40–48. doi:10.1016/j.jtherbio.2017.03.017.
- Checa, A. G., Jiménez-Jiménez, A. P., and Rivas, P. (1998). Regulation of spiral coiling in the terrestrial gastropod *Sphincterochila*: An experimental test of the road-holding model. *Journal of Morphology*, 235(3):249–257. doi:10.1002/(SICI)1097-4687(199803)235:3<249::AID-JMOR4>3.0.CO;2-1.
- Chirat, R., Moulton, D. E., and Goriely, A. (2013). Mechanical basis of morphogenesis and convergent evolution of spiny seashells. *Proceedings of the National Academy of Sciences of the United States of America*, 110(15):6015–6020. doi:10.1073/pnas.1220443110.
- Clarke, R. K., Grahame, J., and Mill, P. J. (1999). Variation and constraint in the shells of two sibling species of intertidal rough periwinkles (Gastropoda: *Littorina* spp.). *Journal of Zoology*, 247(2):145–154. doi:10.1017/S0952836999002022.

- COMSOL Multiphysics (2016). CFD Module User's Guide. Available from <https://doc.comsol.com/5.4/doc/com.comsol.help.cfd/CFDModuleUsersGuide.pdf>.
- Conde-Padín, P., Caballero, A., and Rolán-Alvarez, E. (2009). Relative role of genetic determination and plastic response during ontogeny for shell-shape traits subjected to diversifying selection. *Evolution*, 63(5):1356–1363. doi:10.1111/j.1558-5646.2009.00636.x.
- Conde-Padín, P., Carvajal-Rodríguez, A., Carballo, M., Caballero, A., and Rolán-Alvarez, E. (2007). Genetic variation for shell traits in a direct-developing marine snail involved in a putative sympatric ecological speciation process. *Evolutionary Ecology*, 21(5):635–650. doi:10.1007/s10682-006-9142-8.
- Cooke, S. B. and Terhune, C. E. (2015). Form, Function, and Geometric Morphometrics. *Anatomical Record*, 298(1):5–28. doi:10.1002/ar.23065.
- Cortie, M. (1992). The form, function, and synthesis of the molluscan shell. In Hargittai, I. and Pickover, C. A., editors, *Spiral Symmetry*, pages 369–387. World Scientific. doi:[https://doi.org/10.1142/9789814343084\\_0019](https://doi.org/10.1142/9789814343084_0019).
- Cortie, M. B. (1989). Model for mollusc shell shape. *South African Journal of Science*, 85:454–460.
- Cowie, R. H. and Jones, J. S. (1985). Climatic selection on body colour in cepaea. *Heredity*, 55(2):261–267. doi:10.1038/hdy.1985.100.
- Cross, E. L., Harper, E. M., and Peck, L. S. (2019). Thicker Shells Compensate Extensive Dissolution in Brachiopods under Future Ocean Acidification. *Environmental Science and Technology*, 53(9):5016–5026. doi:10.1021/acs.est.9b00714.
- Crothers, J. H. (1983). Variation in dog-whelk shells in relation to wave action and crab predation. *Biological Journal of the Linnean Society*, 20(1):85–102. doi:10.1111/j.1095-8312.1983.tb01591.x.
- Cruz, R. A. L., Pante, M. J. R., and Rohlf, F. J. (2012). Geometric morphometric analysis of shell shape variation in *Conus* (Gastropoda: Conidae). *Zoological Journal of the Linnean Society*, 165(2):296–310. doi:10.1111/j.1096-3642.2011.00806.x.
- Cuña, V., Saura, M., Quesada, H., and Rolán-Alvarez, E. (2011). Extensive microgeographical shell polymorphism in a planktotrophic marine intertidal snail. *Marine Ecology Progress Series*, 427(April):133–143. doi:10.3354/meps09033.
- Danecek, P., Auton, A., Abecasis, G., Albers, C. A., Banks, E., DePristo, M. A., Handsaker, R. E., Lunter, G., Marth, G. T., Sherry, S. T., McVean, G., and Durbin, R. (2011). The variant call format and VCFtools. *Bioinformatics*, 27(15):2156–2158. doi:10.1093/bioinformatics/btr330.
- Davison, A., Chiba, S., Barton, N. H., and Clarke, B. (2005). Speciation and gene flow between snails of opposite chirality. *PLoS Biology*, 3(9):1559–1571. doi:10.1371/journal.pbio.0030282.

- Davison, A., McDowell, G. S., Holden, J. M., Johnson, H. F., Koutsovoulos, G. D., Liu, M. M., Hulpiau, P., Van Roy, F., Wade, C. M., Banerjee, R., Yang, F., Chiba, S., Davey, J. W., Jackson, D. J., Levin, M., and Blaxter, M. L. (2016). Formin is Associated with Left-Right Asymmetry in the Pond Snail and the Frog. *Current Biology*, 26(5):654–660. doi:10.1016/j.cub.2015.12.071.
- De Wolf, H., Brito, C., Van Dongen, S., and Backeljau, T. (1999). Did a heavy storm affect the aperture area of wave-exposed and sheltered *Littorina striata*? *Journal of the Marine Biological Association of the United Kingdom*, 79(6):1129–1130. doi:10.1017/S0025315499001411.
- Denny, M. (1995). Predicting Physical Disturbance : Mechanistic Approaches to the Study of Survivorship on Wave-Swept Shores. *Ecological Monographs*, 65(4):371–418. doi:10.2307/2963496.
- Denny, M. W. (1985). Wave Forces on Intertidal Organisms: A Case Study. *Limnology and Oceanography*, 30(6):1171–1187. doi:10.4319/lo.1985.30.6.1171.
- Denny, M. W. (1994). Extreme drag forces and the survival of wind- and water-swept organisms. *Journal of Experimental Biology*, 194:97–115.
- Denny, M. W., Daniel, T. L., and Koehl, M. A. R. (1985). Mechanical Limits to Size in Wave-Swept Organisms. *Ecological Monographs*, 55(1):69–102. doi:10.2307/1942526.
- Denny, M. W., Helmuth, B., Leonard, G. H., Harley, C. D., Hunt, L. J., and Nelson, E. K. (2004). Quantifying scale in ecology: Lessons from a wave-swept shore. *Ecological Monographs*, 74(3):513–532. doi:10.1890/03-4043.
- Denny, M. W., Miller, L. P., Stokes, M. D., Hunt, L. J., and Helmuth, B. S. (2003). Extreme water velocities: Topographical amplification of wave-induced flow in the surf zone of rocky shores. *Limnology and Oceanography*, 48(1 I):1–8. doi:10.4319/lo.2003.48.1.0001.
- Denny, M. W. M. W. and Blanchette, C. A. C. A. (2000). Hydrodynamics, shell shape, behavior and survivorship in the owl limpet *Lottia gigantea*. *Journal of Experimental Biology*, 203(17):2623–2639.
- Depristo, M. A., Banks, E., Poplin, R., Garimella, K. V., Maguire, J. R., Hartl, C., Philipakis, A. A., Del Angel, G., Rivas, M. A., Hanna, M., McKenna, A., Fennell, T. J., Kernyt-sky, A. M., Sivachenko, A. Y., Cibulskis, K., Gabriel, S. B., Altshuler, D., and Daly, M. J. (2011). A framework for variation discovery and genotyping using next-generation DNA sequencing data. *Nature Genetics*, 43(5):491–501. doi:10.1038/ng.806.
- Dera, G., Eble, G. J., Neige, P., and David, B. (2008). The flourishing diversity of models in theoretical morphology: from current practices to future macroevolutionary and bio-environmental challenges. *Paleobiology*, 34(3):301–317. doi:10.1666/07070.1.
- DeWitt, T. J., Robinson, B. W., and Wilson, D. S. (2000). Functional diversity among predators of a freshwater snail imposes an adaptive trade-off for shell morphology. *Evolutionary Ecology Research*, 2(2):129–148.

- Dietl, G. P. and Hendricks, J. R. (2006). Crab scars reveal survival advantage of left-handed snails. *Biology Letters*, 2:439–442. doi:10.1098/rsbl.2006.0465.
- Dillon, R. T. and Jacquemin, S. J. (2015). The heritability of shell morphometrics in the freshwater pulmonate gastropod *Physa*. *PLoS ONE*, 10(4):1–13. doi:10.1371/journal.pone.0121962.
- Dommergues, E., Dommergues, J. L., Magniez, F., Neige, P., and Verrecchia, E. P. (2003). Geometric measurement analysis versus Fourier series analysis for shape characterization using the gastropod shell (*Trivia*) as an example. *Mathematical Geology*, 35(7):887–894. doi:10.1023/B:MATG.0000007785.96748.62.
- Dowle, E. J., Morgan-Richards, M., Brescia, F., and Trewick, S. A. (2015). Correlation between shell phenotype and local environment suggests a role for natural selection in the evolution of *Placostylus* snails. *Molecular Ecology*, 24(16):4205–4221. doi:10.1111/mec.13302.
- Dryden, I. L. and Mardia, K. V. (1998). *Statistical shape analysis*. Wiley, Chichester.
- Dussart, G. (1987). Effects of water flow on the detachment of some aquatic pulmonate gastropods. *American Malacological Bulletin*, 5(1):65–72.
- Dussart, G. (2002). Drag coefficients: a comparison of ten species of freshwater gastropod molluscs. *Halictis*, 31:63–70.
- Dussart, G. and Pontier, J.-P. (1999). A comparative study of the hydrodynamic performance of shells of *Thiara granifera* (Lamarck, 1822) and *Melanoides tuberculata* (Muller, 1774). *Freshwater Mollusca*, pages 19–29.
- Dytham, C., Mill, P., Grahame, J., and O’Higgins, P. (1992). Fourier analysis as a size-free descriptor of shape for rough periwinkle shells. *Proceedings of the Third International Symposium on Littorinid Biology*, pages 127–133.
- Edgell, T. C., Brazeau, C., Grahame, J. W., and Rochette, R. (2008). Simultaneous defense against shell entry and shell crushing in a snail faced with the predatory shore crab *Carcinus maenas*. *Marine Ecology Progress Series*, 371(1):191–198. doi:10.3354/meps07698.
- Ekaratne, S. U. and Crisp, D. J. (1983). A Geometric Analysis of Growth in Gastropod Shells, with Particular Reference to Turbinate Forms. *Journal of the Marine Biological Association of the United Kingdom*, 63(4):777–797. doi:10.1017/S0025315400071216.
- Ekendahl, A. and Johannesson, K. (1997). Shell colour variation in *Littorina saxatilis* Olivi (Prosobranchia: Littorinidae): A multi-factor approach. *Biological Journal of the Linnean Society*, 62(3):401–419. doi:10.1006/bijl.1997.0163.
- Emson, R. H. and Faller-Fritsch, R. J. (1976). An experimental investigation into the effect of crevice availability on abundance and size-structure in a population of *Littorina rudis* (Maton): Gastropoda: Prosobranchia. *Journal of Experimental Marine Biology and Ecology*, 23(3):285–297. doi:10.1016/0022-0981(76)90026-5.

- Escobar, J., Curtis, J. H., Brenner, M., Hodell, D. A., and Holmes, J. A. (2010). Isotope measurements of single ostracod valves and gastropod shells for climate reconstruction: Evaluation of within-sample variability and determination of optimum sample size. *Journal of Paleolimnology*, 43(4):921–938. doi:10.1007/s10933-009-9377-9.
- Etter, R. J. (1988). Asymmetrical Developmental Plasticity in an Intertidal Snail. *Evolution*, 42(2):322. doi:10.2307/2409236.
- Etter, R. J. (1989). Life History Variation in the Intertidal Snail *Nucella Lapillus* Across a Wave-Exposure. *Source: Ecology*, 70(6):1857–1876.
- Faria, R., Chaube, P., Morales, H. E., Larsson, T., Lemmon, A. R., Lemmon, E. M., Rafajlović, M., Panova, M., Ravinet, M., Johannesson, K., Westram, A. M., and Butlin, R. K. (2019a). Multiple chromosomal rearrangements in a hybrid zone between *Littorina saxatilis* ecotypes. *Molecular Ecology*, 28(6):1375–1393. doi:10.1111/mec.14972.
- Faria, R., Johannesson, K., Butlin, R. K., and Westram, A. M. (2019b). Evolving Inversions. *Trends in Ecology and Evolution*, 34(3):239–248. doi:10.1016/j.tree.2018.12.005.
- Ferreira, S., Ashby, R., Jeunen, G.-J., Rutherford, K., Collins, C., Todd, E. V., and Gemmill, N. J. (2020). DNA from mollusc shell: a valuable and underutilised substrate for genetic analyses. *PeerJ*, 8:1–20. doi:10.7717/peerj.9420.
- Forrester, G. E., Macfarlan, R. J., Holevoet, A. J., and Merolla, S. (2016). Dislodgement force and shell morphology vary according to wave exposure in a tropical gastropod (*Cittarium pica*). *Marine Biology Research*, 12(9):986–992. doi:10.1080/17451000.2016.1225956.
- Fowler, D. R., Meinhardt, H., and Prusinkiewicz, P. (1992). Modeling seashells. *Computer Graphics (ACM)*, 26(2):379–387. doi:10.1145/142920.134096.
- Fu, G., Huang, M., Bo, W., Hao, H., and Wu, R. (2018). Mapping morphological shape as a high-dimensional functional curve. *Briefings in Bioinformatics*, 19(3):461–471. doi:10.1093/bib/bbw111.
- Füllenbach, C. S., Schöne, B. R., and Branscheid, R. (2014). Microstructures in shells of the freshwater gastropod *Viviparus viviparus*: A potential sensor for temperature change? *Acta Biomaterialia*, 10(9):3911–3921. doi:10.1016/j.actbio.2014.03.030.
- Gaylord, B. (1999). Detailing agents of physical disturbance: Wave-induced velocities and accelerations on a rocky shore. *Journal of Experimental Marine Biology and Ecology*, 239(1):85–124. doi:10.1016/S0022-0981(99)00031-3.
- Gaylord, B. (2000). Biological implications of surf-zone flow complexity. *Limnology and Oceanography*, 45(1):174–188. doi:10.4319/lo.2000.45.1.0174.
- Gefaell, J., Varela, N., and Rolán-Alvarez, E. (2020). Comparing shape along growth trajectories in two marine snail ecotypes of *Littorina saxatilis*: a test of evolution by paedomorphosis. *Journal of Molluscan Studies*, pages 1–7. doi:10.1093/mollus/eyaa020.

- Gibbs, P. E. (1993). Phenotypic changes in the progeny of *Nucella lapillus* (gastropoda) transplanted from an exposed shore to sheltered inlets. *Journal of Molluscan Studies*, 59(2):187–194. doi:10.1093/mollus/59.2.187.
- Giokas, S., Páll-Gergely, B., and Mettouris, O. (2014). Nonrandom variation of morphological traits across environmental gradients in a land snail. *Evolutionary Ecology*, 28(2):323–340. doi:10.1007/s10682-013-9676-5.
- Goodwin, D. H., Schöne, B. R., and Dettman, D. L. (2003). Resolution and fidelity of oxygen isotopes as paleotemperature proxies in bivalve mollusk shells: Models and observations. *Palaeos*, 18(2):110–125. doi:10.1669/0883-1351(2003)18<110:RAFOOI>2.0.CO;2.
- Gould, S. J. (1989). A developmental constraint in *Cerion*, with comments on the definition and interpretation of constraint in evolution. *Evolution*, 43(3):516–539. doi:10.1111/j.1558-5646.1989.tb04249.x.
- Gouveia, N., Oliveira, C. R., Martins, C. P., Maranhão, L. A., Seabra Pereira, C. D., de Orte, M. R., Harayashiki, C. A., Almeida, S. M., and Castro, Í. B. (2019). Can shell alterations in limpets be used as alternative biomarkers of coastal contamination? *Chemosphere*, 224:9–19. doi:10.1016/j.chemosphere.2019.02.122.
- Grahame, J. and Mill, P. J. (1986). Relative size of the foot of two species of *Littorina* on a rocky shore in Wales. *Journal of Zoology*, 208(2):229–236. doi:10.1111/j.1469-7998.1986.tb01510.x.
- Grahame, J. and Mill, P. J. (1989). Shell shape variation in *Littorina saxatilis* and *L. arcana*: A case of character displacement? *Journal of the Marine Biological Association of the United Kingdom*, 69(4):837–855. doi:10.1017/S0025315400032203.
- Grahame, J. W., Wilding, C. S., and Butlin, R. K. (2006). Adaptation To a Steep Environmental Gradient and an Associated Barrier To Gene Exchange in *Littorina Saxatilis*. *Evolution*, 60(2):268. doi:10.1554/05-592.1.
- Guerra-Varela, J., Colson, I., Backeljau, T., Breugelmans, K., Hughes, R. N., and Rolán-Alvarez, E. (2009). The evolutionary mechanism maintaining shell shape and molecular differentiation between two ecotypes of the dogwhelk *Nucella lapillus*. *Evolutionary Ecology*, 23(2):261–280. doi:10.1007/s10682-007-9221-5.
- Haase, M. (2003). Clinal variation in shell morphology of the freshwater gastropod *Potamopyrgus antipodarum* along two hill-country streams in New Zealand. *Journal of the Royal Society of New Zealand*, 33(2):549–560. doi:10.1080/03014223.2003.9517743.
- Hammer, Ø. and Bucher, H. (2005). Models for the morphogenesis of the molluscan shell. *Lethaia*, 38(2):111–122. doi:10.1080/00241160510013222.
- Harayashiki, C. A. Y., Martins, C. P., Márquez, F., Bigatti, G., and Castro, Í. B. (2020). Historical shell form variation in *Lottia subrugosa* from southeast Brazilian coast: Possible responses to anthropogenic pressures. *Marine Pollution Bulletin*, 155(December 2019):111180. doi:10.1016/j.marpolbul.2020.111180.

- Heath, D. J. (1985). Whorl overlap and the economical construction of the gastropod shell. *Biological Journal of the Linnean Society*, 24(2):165–174. doi:10.1111/j.1095-8312.1985.tb00167.x.
- Hellberg, M. E., Balch, D. P., and Roy, K. (2001). Climate-driven range expansion and morphological evolution in a marine gastropod. *Science*, 292(5522):1707–1710. doi:10.1126/science.1060102.
- Heller, J. (1976). The Effects of exposure and predation on the shell of two British winkles. *Journal of Zoology*, 179:201–213. doi:10.1111/j.1469-7998.1976.tb02291.x.
- Helmuth, B. and Denny, M. W. (2003). Predicting wave exposure in the rocky intertidal zone: Do bigger waves always lead to larger forces? *Limnology and Oceanography*, 48(3):1338–1345. doi:10.4319/lo.2003.48.3.1338.
- Hohenlohe, P. A. (2003). Distribution of Sister Littorina species, I: Tenacity and the Wave-Exposure Gradient. *The Veliger*, 46(2):162–168.
- Hollander, J., Adams, D. C., and Johannesson, K. (2006a). Evolution of Adaptation Through Allometric Shifts in a Marine Snail. *Evolution*, 60(12):2490. doi:10.1554/06-071.1.
- Hollander, J. and Butlin, R. K. (2010). The adaptive value of phenotypic plasticity in two ecotypes of a marine gastropod. *BMC Evolutionary Biology*, 10(1). doi:10.1186/1471-2148-10-333.
- Hollander, J., Collyer, M. L., Adams, D. C., and Johannesson, K. (2006b). Phenotypic plasticity in two marine snails: Constraints superseding life history. *Journal of Evolutionary Biology*, 19(6):1861–1872. doi:10.1111/j.1420-9101.2006.01171.x.
- Hoso, M., Kameda, Y., Wu, S. P., Asami, T., Kato, M., and Hori, M. (2010). A speciation gene for left-right reversal in snails results in anti-predator adaptation. *Nature Communications*, 1(9):133–137. doi:10.1038/ncomms1133.
- Hughes, R. N. and Roberts, D. J. (1981). Comparative Demography of *Littorina rudis*, *L. Nigrolineata* and *L. Neritoides* on Three Contrasted Shores in North Wales. *The Journal of Animal Ecology*, 50(1):251. doi:10.2307/4043.
- Huryn, A. D. and Denny, M. W. (1997). A biomechanical hypothesis explaining up-stream movements by the freshwater snail *Elimia*. *Functional Ecology*, 11(4):472–483. doi:10.1046/j.1365-2435.1997.00116.x.
- Hutchinson, J. M. C. (1989). Control of gastropod shell shape; The role of the preceding whorl. *Journal of Theoretical Biology*, 140(4):431–444. doi:10.1016/S0022-5193(89)80107-9.
- Illert, C. (1983). The mathematics of gnomonic seashells. *Mathematical Biosciences*, 63(1):21–56. doi:10.1016/0025-5564(83)90049-4.
- Illert, C. (1989). Formulation and solution of the classical seashell problem. II - Tubular three-dimensional seashell surfaces. *Il Nuovo Cimento D*. doi:10.1007/BF02451562.

- Jackson, H. J., Larsson, J., and Davison, A. (2021). Quantitative measures and 3D shell models reveal interactions between bands and their position on growing snail shells. *Ecology and Evolution*, 11(11):6634–6648. doi:10.1002/ece3.7517.
- Janson, K. (1982). Phenotypic differentiation in *Littorina saxatilis olivi* (mollusca, prosobranchia) in a small area on the swedish west coast. *Journal of Molluscan Studies*, 48(2):167–173. doi:10.1093/oxfordjournals.mollus.a065633.
- Janson, K. (1983). Selection and migration in two distinct phenotypes of *Littorina saxatilis* in Sweden. *Oecologia*, 59(1):58–61. doi:10.1007/BF00388072.
- Jensen, M. M. and Denny, M. W. (2015). Experimental determination of the hydrodynamic forces responsible for wave impact events. *Journal of Experimental Marine Biology and Ecology*, 469:123–130. doi:10.1016/j.jembe.2015.04.013.
- Jobin, W. R. . and Ippen, A. T. . (1964). Ecological Design of Irrigation Canals for Snail Control. *Science*, 145(3638):1324–1326. doi:10.1126/science.145.3638.1324.
- Johannesson, B. (1986). Shell morphology of *Littorina saxatilis* Olivi: The relative importance of physical factors and predation. *Journal of Experimental Marine Biology and Ecology*, 102(2-3):183–195. doi:10.1016/0022-0981(86)90175-9.
- Johannesson, B. and Johannesson, K. (1996). Population differences in behaviour and morphology in the snail *Littorina saxatilis*: Phenotypic plasticity or genetic differentiation? *Journal of Zoology*, 240(3):475–493. doi:10.1111/j.1469-7998.1996.tb05299.x.
- Johannesson, K. (2003). Evolution in *Littorina*: Ecology matters. *Journal of Sea Research*, 49(2):107–117. doi:10.1016/S1385-1101(02)00218-6.
- Johannesson, K. (2016). What can be learnt from a snail? *Evolutionary Applications*, 9(1):153–165. doi:10.1111/eva.12277.
- Johannesson, K. and Butlin, R. K. (2017). What explains rare and conspicuous colours in a snail? A test of time-series data against models of drift, migration or selection. *Heredity*, 118(1):21–30. doi:10.1038/hdy.2016.77.
- Johannesson, K., Johannesson, B., and Rolán-Alvarez, E. (1993). Morphological Differentiation and Genetic Cohesiveness Over a Microenvironmental Gradient in the Marine Snail *Littorina saxatilis*. *Evolution*, 47(6):1770–1787. doi:10.1111/j.1558-5646.1993.tb01268.x.
- Johannesson, K., Panova, M., Kemppainen, P., André, C., Rolan-Alvarez, E., Butlin, R. K., Rolán-Alvarez, E., Butlin, R. K., Andre, C., Rolan-Alvarez, E., and Butlin, R. K. (2010). Repeated evolution of reproductive isolation in a marine snail: Unveiling mechanisms of speciation. *Philosophical Transactions of the Royal Society B: Biological Sciences*, 365(1547):1735–1747. doi:10.1098/rstb.2009.0256.
- Johannesson, K., Rolán-Alvarez, E., and Erlandsson, J. (1997). Growth rate differences between upper and lower shore ecotypes of the marine snail *Littorina saxatilis* (Olivi) (Gastropoda). *Biological Journal of the Linnean Society*, 61(2):267–279. doi:10.1006/bijl.1996.0122.

- Kemp, P. and Bertness, M. D. (1984). Snail shape and growth rates: Evidence for plastic shell allometry in *Littorina littorea*. *Proceedings of the National Academy of Sciences*, 81(3):811–813. doi:10.1073/pnas.81.3.811.
- Kess, T. and Boulding, E. G. (2019). Genome-wide association analyses reveal polygenic genomic architecture underlying divergent shell morphology in Spanish *Littorina saxatilis* ecotypes. *Ecology and Evolution*, 9(17):9427–9441. doi:10.1002/ece3.5378.
- Kess, T., Brachmann, M., and Boulding, E. G. (2021). Putative chromosomal rearrangements are associated primarily with ecotype divergence rather than geographic separation in an intertidal, poorly dispersing snail. *Journal of Evolutionary Biology*, 34(1):193–207. doi:10.1111/jeb.13724.
- Kistner, E. J. and Dybdahl, M. F. (2014). Parallel variation among populations in the shell morphology between sympatric native and invasive aquatic snails. *Biological Invasions*, 16(12):2615–2626. doi:10.1007/s10530-014-0691-4.
- Kitching, J. A. and Lockwood, J. (1974). Observations on shell form and its ecological significance in thaisid gastropods of the genus *Lepsiella* in New Zealand. *Marine Biology*, 28(2):131–144. doi:10.1007/BF00396304.
- Kitching, J. A., Muntz, L., and Ebling, F. J. (1966). The Ecology of Lough Ine. XV. The Ecological Significance of Shell and Body Forms in *Nucella*. *The Journal of Animal Ecology*, 35(1):113. doi:10.2307/2693.
- Klingenberg, C. P. (2010). Evolution and development of shape: integrating quantitative approaches. *Nature Reviews Genetics*, 11(9):623–635. doi:10.1038/nrg2829.
- Klingenberg, C. P. (2011). MorphoJ: an integrated software package for geometric morphometrics. *Molecular Ecology Resources*, 11(2):353–357. doi:10.1111/j.1755-0998.2010.02924.x.
- Klingenberg, C. P. (2016). Size, shape, and form: concepts of allometry in geometric morphometrics. *Development Genes and Evolution*, 226(3):113–137. doi:10.1007/s00427-016-0539-2.
- Koch, E. L., Morales, H. E., Larsson, J., Westram, A. M., Faria, R., Lemmon, A. R., Lemmon, E. M., Johannesson, K., and Butlin, R. K. (2021). Genetic variation for adaptive traits is associated with polymorphic inversions in *Littorina saxatilis*. *Evolution Letters*, 5(3):196–213. doi:10.1002/evl3.227.
- Koehl, M. A. (1984). How Do Benthic Organisms Withstand Moving Water? *Integrative and Comparative Biology*, 24(1):57–70. doi:10.1093/icb/24.1.57.
- Koehl, M. A. (1996). When does morphology matter? *Annual Review of Ecology and Systematics*, 27:501–542. doi:10.1146/annurev.ecolsys.27.1.501.
- Koehl, M. R. (1977). Effects of Sea Anemones on the Flow Forces They Encounter. *Journal of Experimental Biology*, 69(1):87–105. doi:10.1242/jeb.69.1.87.
- Kohn, A. J. and Riggs, A. C. (1975). Morphometry of the conus shell. *Systematic Biology*, 24(3):346–359. doi:10.1093/sysbio/24.3.346.

- Konuma, J. and Chiba, S. (2007). Trade-offs between force and fit: Extreme morphologies associated with feeding behavior in carabid beetles. *American Naturalist*, 170(1):90–100. doi:10.1086/518182.
- Kozminskii, E. V., Lezin, P. A., and Fokin, M. V. (2010). A study of inheritance of white spots on the shell of *Littorina obtusata* (Gastropoda, Prosobranchia). *Russian Journal of Genetics*, 46(12):1455–1461. doi:10.1134/S1022795410120082.
- Kozminsky, E. V. (2016). Inheritance of longitudinal white shell bands in the snail *Littorina obtusata* (Gastropoda, Prosobranchia). *Russian Journal of Genetics*, 52(8):882–886. doi:10.1134/s1022795416080068.
- Kuhl, F. P. and Giardina, C. R. (1982). Elliptic Fourier features of a closed contour. *Computer Graphics and Image Processing*, 18(3):236–258. doi:10.1016/0146-664X(82)90034-X.
- Lam, P. and Calow, P. (1988). Differences in the shell shape of *Lymnaea peregra* (Müller)(Gastropoda: Pulmonata) from lotic and lentic habitats; Environmental or genetic variance? *Journal of Molluscan Studies*, 54(2):197–207. doi:10.1093/mollus/54.2.197.
- Large, S. I. and Smee, D. L. (2013). Biogeographic variation in behavioral and morphological responses to predation risk. *Oecologia*, 171(4):961–969. doi:10.1007/s00442-012-2450-5.
- Larsson, J., Westram, A. M., Bengmark, S., Lundh, T., and Butlin, R. K. (2020). A developmentally descriptive method for quantifying shape in gastropod shells. *Journal of the Royal Society Interface*, 17(163). doi:10.1098/rsif.2019.0721.
- Le Pennec, G., Butlin, R. K., Jonsson, P. R., Larsson, A. I., Lindborg, J., Bergström, E., Westram, A. M., and Johannesson, K. (2017). Adaptation to dislodgement risk on waveswept rocky shores in the snail *Littorina saxatilis*. *PLoS ONE*, 12(10):1–15. doi:10.1371/journal.pone.0186901.
- Li, H. and Durbin, R. (2009). Fast and accurate short read alignment with Burrows-Wheeler transform. *Bioinformatics*, 25(14):1754–1760. doi:10.1093/bioinformatics/btp324.
- Liew, T. S. and Schilthuizen, M. (2016). A method for quantifying, visualising, and analysing gastropod shell form. *PLoS ONE*, 11(6):1–24. doi:10.1371/journal.pone.0157069.
- Linsley, R. M. (1977). Some “laws” of gastropod shell form. *Paleobiology*, 2:196–206. doi:10.1017/S0094837300005261.
- Løvtrup, S. and Løvtrup, M. (1988). The morphogenesis of molluscan shells: A mathematical account using biological parameters. *Journal of Morphology*, 197(1):53–62. doi:10.1002/jmor.1051970105.
- Lowell, R. B., Fletcher, C. R., Grahame, J., and Mill, P. J. (1994). Ontogeny of shell morphology and shell strength of the marine snails *Littorina obtusata* and *Littorina mariaae*: different defence strategies in a pair of sympatric, sibling species. *Journal of Zoology*, 234(1):149–164. doi:10.1111/j.1469-7998.1994.tb06062.x.

- Márquez, F., González-José, R., and Bigatti, G. (2011). Combined methods to detect pollution effects on shell shape and structure in Neogastropods. *Ecological Indicators*, 11(2):248–254. doi:10.1016/j.ecolind.2010.05.001.
- Márquez, F., Primost, M. A., and Bigatti, G. (2017). Shell shape as a biomarker of marine pollution historic increase. *Marine Pollution Bulletin*, 114(2):816–820. doi:10.1016/j.marpolbul.2016.11.018.
- Meinhardt, H. and Klingler, M. (1987). A model for pattern formation on the shells of molluscs. *Journal of Theoretical Biology*, 126(1):63–89. doi:10.1016/S0022-5193(87)80101-7.
- Minton, R., Hart, K. C., Fiorillo, R., and Brown, C. (2018). Correlates of snail shell variation along a unidirectional freshwater gradient in *Lithasia geniculata* (Haldeman, 1840) (Caenogastropoda: Pleuroceridae) from the Duck River, Tennessee, USA. *Folia Malacologica*, 26(2):95–102. doi:10.12657/folmal.026.007.
- Minton, R. L., Norwood, A. P., and Hayes, D. M. (2008). Quantifying phenotypic gradients in freshwater snails: A case study in *Lithasia* (Gastropoda: Pleuroceridae). *Hydrobiologia*, 605(1):173–182. doi:10.1007/s10750-008-9332-1.
- Monnet, C., Zollikofer, C., Bucher, H., and Goudemand, N. (2009). Three-dimensional morphometric ontogeny of mollusc shells by micro-computed tomography and geometric analysis. *Palaeontologia Electronica*, 12(12). doi:10.5167/uzh-23587.
- Morales, H. E., Faria, R., Johannesson, K., Larsson, T., Panova, M., Westram, A. M., and Butlin, R. K. (2019). Genomic architecture of parallel ecological divergence: Beyond a single environmental contrast. *Science Advances*, 5(12). doi:10.1126/sciadv.aav9963.
- Moseley, H. (1838). On the geometrical forms of turbinated and discoid shells. *Philosophical Transactions of the Royal Society of London*, 128(1):351–370.
- Moulton, D. E. and Goriely, A. (2014). Surface growth kinematics via local curve evolution. *Journal of Mathematical Biology*, 68(1-2):81–108. doi:10.1007/s00285-012-0625-7.
- Moulton, D. E., Goriely, A., and Chirat, R. (2012). Mechanical growth and morphogenesis of seashells. *Journal of Theoretical Biology*, 311:69–79. doi:10.1016/j.jtbi.2012.07.009.
- Newkirk, G. F. and Doyle, R. W. (1975). Genetic analysis of shell-shape variation in *Littorina saxatilis* on an environmental cline. *Marine Biology*, 30(3):227–237. doi:10.1007/BF00390745.
- Ng, T. P., Lau, S. L., Seuront, L., Davies, M. S., Stafford, R., Marshall, D. J., and Williams, G. A. (2017). Linking behaviour and climate change in intertidal ectotherms: insights from littorinid snails. *Journal of Experimental Marine Biology and Ecology*, 492:121–131. doi:10.1016/j.jembe.2017.01.023.
- Noshita, K. (2014). Quantification and geometric analysis of coiling patterns in gastropod shells based on 3D and 2D image data. *Journal of Theoretical Biology*, 363:93–104. doi:10.1016/j.jtbi.2014.08.010.

- Noshita, K., Asami, T., and Ubukata, T. (2012). Functional constraints on coiling geometry and aperture inclination in gastropods. *Paleobiology*, 38(02):322–334. doi:10.1666/10060.1.
- Noshita, K., Shimizu, K., and Sasaki, T. (2016). Geometric analysis and estimation of the growth rate gradient on gastropod shells. *Journal of Theoretical Biology*, 389:11–19. doi:10.1016/j.jtbi.2015.10.011.
- Nowell, A. R. and Jumars, P. A. (1984). Flow environments of aquatic benthos. *Annual review of ecology and systematics*, 15(98):303–328. doi:10.1146/annurev.es.15.110184.001511.
- Nuñez, J. D., Laitano, M. V., and Cledón, M. (2012). An intertidal limpet species as a bioindicator: Pollution effects reflected by shell characteristics. *Ecological Indicators*, 14(1):178–183. doi:10.1016/j.ecolind.2011.07.015.
- O'Donnell, M. J. and Denny, M. W. (2008). Hydrodynamic forces and surface topography: Centimeter-scale spatial variation in wave forces. *Limnology and Oceanography*, 53(2):579–588. doi:10.4319/lo.2008.53.2.0579.
- Okabe, T. and Yoshimura, J. (2017). Optimal designs of mollusk shells from bivalves to snails. *Scientific Reports*, 7(1):42445. doi:10.1038/srep42445.
- Okajima, R. and Chiba, S. (2009). Cause of bimodal distribution in the shape of a terrestrial gastropod. *Evolution*, 63(11):2877–2887. doi:10.1111/j.1558-5646.2009.00780.x.
- Okajima, R. and Chiba, S. (2013). Adaptation from restricted geometries: The shell inclination of terrestrial gastropods. *Evolution*, 67(2):429–437. doi:10.1111/j.1558-5646.2012.01772.x.
- Okamoto, T. (1988a). Analysis of heteromorph ammonoids by differential geometry. *Paleontology*, 31:35–52.
- Okamoto, T. (1988b). Developmental regulation and morphological saltation in the heteromorph ammonite *Nipponites*. *Paleobiology*, 14(3):272–286. doi:10.1017/S0094837300012008.
- Okamoto, T. (1996). Theoretical Modeling of Ammonoid Morphology. *Ammonoid Paleobiology*, 13:225–251. doi:10.1007/978-1-4757-9153-2.8.
- Oliveira, C. R. M., Mantovani de Castro, L., Alves da Cruz Nazareth, M., Harayashiki, C. A. Y., and Castro, Í. B. (2020). Shell structure and composition alterations in the limpet *Lottia subrugosa* along a contamination gradient in the Santos Estuary, Brazil. *Ecological Indicators*, 115:106417. doi:10.1016/j.ecolind.2020.106417.
- Outomuro, D. and Johansson, F. (2017). A potential pitfall in studies of biological shape: Does size matter? *Journal of Animal Ecology*, 86(6):1447–1457. doi:10.1111/1365-2656.12732.
- Palmer, A. R. (1977). Function of Shell Sculpture in Marine Gastropods: Hydrodynamic Destabilization in *Ceratostoma foliatum*. *Science*, 197(4310):1293–1295. doi:10.1126/science.197.4310.1293.

- Palmer, A. R. (1979). Fish predation and the evolution of gastropod shell sculpture: Experimental and geographical evidence. *Evolution*, 33(2):697–713. doi:10.1111/j.1558-5646.1979.tb04722.x.
- Panova, M., Aronsson, H., Cameron, R. A., Dahl, P., Godhe, A., Lind, U., Ortega-Martinez, O., Pereyra, R., Tesson, S. V., Wrangé, A. L., Blomberg, A., and Johannesson, K. (2016). DNA extraction protocols for whole-genome sequencing in marine organisms. In *Methods in Molecular Biology*, volume 1452, pages 13–44. Humana Press Inc. doi:10.1007/978-1-4939-3774-5\_2.
- Pascoal, S., Carvalho, G., Creer, S., Rock, J., Kawahii, K., Mendo, S., and Hughes, R. (2012). Plastic and heritable components of phenotypic variation in *nucella lapillus*: An assessment using reciprocal transplant and common garden experiments. *PLoS ONE*, 7(1). doi:10.1371/journal.pone.0030289.
- Phifer-Rixey, M., Heckman, M., Trussell, G. C., and Schmidt, P. S. (2008). Maintenance of clinal variation for shell colour phenotype in the flat periwinkle *Littorina obtusata*. *Journal of Evolutionary Biology*, 21(4):966–978. doi:10.1111/j.1420-9101.2008.01549.x.
- Prowse, T. A. A. and Pile, A. J. (2005). Phenotypic homogeneity of two intertidal snails across a wave exposure gradient in South Australia. *Marine Biology Research*, 1(3):176–185. doi:10.1080/17451000510018999.
- Raffaelli, D. (1982). Recent ecological research on some european species of littorina. *Journal of Molluscan Studies*, 48(3):342–354. doi:10.1093/oxfordjournals.mollus.a065656.
- Raffaelli, D. and Hughes, R. (1978). The Effects of Crevice Size and Availability on Populations of *Littorina rudis* and *Littorina neritoides*. *Journal of Animal Ecology*, 47(1):71–83.
- Rajabi, H., Darvizeh, A., Shafiei, A., Eshghi, S., and Khaeheshi, A. (2014). Experimental and numerical investigations of *Otala lactea*'s shell-I. Quasi-static analysis. *Journal of the Mechanical Behavior of Biomedical Materials*, 32:8–16. doi:10.1016/j.jmbbm.2013.12.008.
- Rastas, P. (2017). Lep-MAP3: Robust linkage mapping even for low-coverage whole genome sequencing data. *Bioinformatics*, 33(23):3726–3732. doi:10.1093/bioinformatics/btx494.
- Raup, D. M. (1961). The Geometry of Coiling in Gastropods. *Proceedings of the National Academy of Sciences*, 47(4):602–609. doi:10.1073/pnas.47.4.602.
- Raup, D. M. (1966). Geometric Analysis of Shell Coiling: General Problems. *Journal of Paleontology*, 40(5):1178–1190.
- Ravinet, M., Westram, A., Johannesson, K., Butlin, R., André, C., and Panova, M. (2016). Shared and nonshared genomic divergence in parallel ecotypes of *Littorina saxatilis* at a local scale. *Molecular Ecology*, 25(1):287–305. doi:10.1111/mec.13332.
- Reid, D. G. (1996). *Systematics and evolution of Littorina*. The Ray Society, London. doi:10.1017/S002531540004114X.
- Rice, S. H. (1998). The Bio-Geometry of Mollusc Shells. *Paleobiology*, 24(1):133–149.

- Robinson, M. R., Santure, A. W., Decauwer, I., Sheldon, B. C., and Slate, J. (2013). Partitioning of genetic variation across the genome using multimarker methods in a wild bird population. *Molecular Ecology*, 22(15):3963–3980. doi:10.1111/mec.12375.
- Rochette, R., Doyle, S. P., and Edgell, T. C. (2007). Interaction between an invasive decapod and a native gastropod: Predator foraging tactics and prey architectural defenses. *Marine Ecology Progress Series*. doi:10.3354/meps330179.
- Rockman, M. V. (2012). The QTN program and the alleles that matter for evolution: All that's gold does not glitter. *Evolution*, 66(1):1–17. doi:10.1111/j.1558-5646.2011.01486.x.
- Rohlf, F. J. (2015). The tps series of software. *Hystrix*, 26(1):1–4. doi:10.4404/hystrix-26.1-11264.
- Rohlf, F. J. and Slice, D. (1990). Extensions of the procrustes method for the optimal superimposition of landmarks. *Systematic Zoology*, 39(1):40–59. doi:10.2307/2992207.
- Rolán-Alvarez, E. (2007). Sympatric speciation as a by-product of ecological adaptation in the Galician *Littorina saxatilis* hybrid zone. *Journal of Molluscan Studies*, 73(1):1–10. doi:10.1093/mollus/eyl023.
- Rolán-Alvarez, E., Austin, C. J., and Boulding, E. G. (2015). The contribution of the genus *Littorina* to the field of evolutionary ecology. *Oceanography and Marine Biology: An Annual Review*, 53(September):157–214. doi:10.1201/b18733.
- Rolán-Alvarez, E., Johannesson, K., and Erlandsson, J. (1997). The Maintenance of a Cline in the Marine Snail *Littorina saxatilis*: The Role of Home Site Advantage and Hybrid Fitness. *Source: Evolution Evolution*, 51(516):1838–1847.
- Rosin, Z. M., Kobak, J., Lesicki, A., and Tryjanowski, P. (2013). Differential shell strength of *Cepaea nemoralis* colour morphs - Implications for their anti-predator defence. *Naturwissenschaften*, 100(9):843–851. doi:10.1007/s00114-013-1084-8.
- Saura, M., Rivas, M. J., Diz, A. P., Caballero, A., and Rolán-Alvarez, E. (2012). Dietary effects on shell growth and shape in an intertidal marine snail, *Littorina saxatilis*. *Journal of Molluscan Studies*, 78(2):213–216. doi:10.1093/mollus/eyl004.
- Savazzi, E. (1985). SHELLGEN: A BASIC program for the modeling of molluscan shell ontogeny and morphogenesis. *Computers and Geosciences*. doi:10.1016/0098-3004(85)90083-4.
- Savazzi, E. (1990). Biological aspects of theoretical shell morphology. *Lethaia*, 23(2):195–212. doi:10.1111/j.1502-3931.1990.tb01360.x.
- Schindel, D. E. (1990). Unoccupied morphospace and the coiled geometry of gastropods: architectural constraint or geometric covariation? *Causes of evolution: a paleontological perspective*, pages 270–304.
- Schneider, C. A., Rasband, W. S., and Eliceiri, K. W. (2012). NIH Image to ImageJ: 25 years of image analysis. Available from <https://www.nature.com/articles/nmeth.2089>. doi:10.1038/nmeth.2089.

- Seeley, R. H. (1986). Intense natural selection caused a rapid morphological transition in a living marine snail. *Proceedings of the National Academy of Sciences*, 83(18):6897–6901. doi:10.1073/pnas.83.18.6897.
- Shimizu, K., Iijima, M., Setiamarga, D. H., Sarashina, I., Kudoh, T., Asami, T., Gittenberger, E., and Endo, K. (2013). Left-right asymmetric expression of *dpp* in the mantle of gastropods correlates with asymmetric shell coiling. *EvoDevo*, 4(1):1–7. doi:10.1186/2041-9139-4-15.
- Shimizu, K., Sarashina, I., Kagi, H., and Endo, K. (2011). Possible functions of *Dpp* in gastropod shell formation and shell coiling. *Development Genes and Evolution*. doi:10.1007/s00427-011-0358-4.
- Shojaei, M. F., Mohammadi, V., Rajabi, H., and Darvizeh, A. (2012). Experimental analysis and numerical modeling of mollusk shells as a three dimensional integrated volume. *Journal of the Mechanical Behavior of Biomedical Materials*, 16(1):38–54. doi:10.1016/j.jmbbm.2012.08.006.
- Sousa, R., Vasconcelos, J., and Riera, R. (2020). Unravelling the effects of exploitation on the size–structure of the intertidal topshell *Phorcus sauciatus* in harvested and non-harvested Atlantic regions. *Regional Studies in Marine Science*, 38:101387. doi:10.1016/j.rsma.2020.101387.
- Stankowski, S. (2011). Extreme, continuous variation in an island snail: Local diversification and association of shell form with the current environment. *Biological Journal of the Linnean Society*, 104(4):756–769. doi:10.1111/j.1095-8312.2011.01748.x.
- Stone, J. R. (1995). CerioShell: A Computer Program Designed to Simulate Variation in Shell Form. *Paleobiology*, 21(4):509–519. doi:10.1017/S0094837300013518.
- Stone, J. R. (1996). The Evolution of Ideas: A Phylogeny of Shell Models. *The American Naturalist*, 148(5):904–929. doi:10.1086/285962.
- Stone, J. R. (1998). Landmark-Based Thin-Plate Spline Relative Warp Analysis of Gastropod Shells. *Syst . Biol*, 47(March):254–263. doi:10.1080/106351598260905.
- Tendler, A., Mayo, A., and Alon, U. (2015). Evolutionary tradeoffs, Pareto optimality and the morphology of ammonite shells. *BMC Systems Biology*, 9(1):1–12. doi:10.1186/s12918-015-0149-z.
- Thompson, D. W. (1917). *On Growth and Form*. Cambridge University Press, London.
- Trussell, G. C. (1996). Phenotypic plasticity in an intertidal snail: The role of a common predator. *Evolution*, 50(1):448–454. doi:10.1111/j.1558-5646.1996.tb04507.x.
- Trussell, G. C. (1997a). Phenotypic Plasticity in the Foot Size of an Intertidal Snail. *Ecology*, 78(4):1033–1048. doi:10.1890/0012-9658(1997)078[1033:PPITFS]2.0.CO;2.
- Trussell, G. C. (1997b). Phenotypic selection in an intertidal snail: Effects of a catastrophic storm. *Marine Ecology Progress Series*, 151(1-3):73–79. doi:10.3354/meps151073.

- Trussell, G. C. (2000). Predator-induced plasticity and morphological trade-offs in latitudinally separated populations of *Littorina obtusata*. *Evolutionary Ecology Research*, 2(6):803–822.
- Trussell, G. C., Johnson, A. S., Rudolph, S. G., and Gilfillan, E. S. (1993). Resistance to dislodgement: habitat and size-specific differences in morphology and tenacity in an intertidal snail. *Marine Ecology Progress Series*, 100(1-2):135–144. doi:10.3354/meps100135.
- Urabe, M. (1998). Contribution of genetic and environmental factors to shell shape variation in the lotic snail *Semisulcospira reiniana* (Prosobranchia: Pleuroceridae). *Journal of Molluscan Studies*, 64(3):329–343. doi:10.1093/mollus/64.3.329.
- Urdu, S., Goudemand, N., Bucher, H., and Chirat, R. (2010a). Allometries and the morphogenesis of the molluscan shell: A quantitative and theoretical model. *Journal of Experimental Zoology Part B: Molecular and Developmental Evolution*, 314 B(4):280–302. doi:10.1002/jez.b.21337.
- Urdu, S., Goudemand, N., Bucher, H., and Chirat, R. (2010b). Growth-dependent phenotypic variation of molluscan shells: implications for allometric data interpretation. *Journal of Experimental Zoology Part B: Molecular and Developmental Evolution*, 314B(4):303–326. doi:10.1002/jez.b.21338.
- Van Osselaer, C. and Grosjean, P. (2000). Suture and location of the coiling axis in gastropod shells. *Paleobiology*, 26(2):238–257. doi:10.1666/0094-8373(2000)026<0238:SALOTC>2.0.CO;2.
- VanRaden, P. M. (2008). Efficient methods to compute genomic predictions. *Journal of Dairy Science*, 91(11):4414–4423. doi:10.3168/jds.2007-0980.
- Verduin, A. (1982). How complete are diagnoses of coiled shells of regular build? A Mathematical Approach. *Basteria*, 45:127–142.
- Vergara, D., Fuentes, J. A., Stoy, K. S., and Lively, C. M. (2017). Evaluating shell variation across different populations of a freshwater snail. *Molluscan Research*, 37(2):120–132. doi:10.1080/13235818.2016.1253446.
- Verhaegen, G., Herzog, H., Korsch, K., Kerth, G., Brede, M., and Haase, M. (2019). Testing the adaptive value of gastropod shell morphology to flow: A multidisciplinary approach based on morphometrics, computational fluid dynamics and a flow tank experiment. *Zoological Letters*, 5(1):1–13. doi:10.1186/s40851-018-0119-6.
- Verhaegen, G., McElroy, K. E., Bankers, L., Neiman, M., and Haase, M. (2018a). Adaptive phenotypic plasticity in a clonal invader. *Ecology and Evolution*, 8(9):4465–4483. doi:10.1002/ece3.4009.
- Verhaegen, G., Neiman, M., and Haase, M. (2018b). Ecomorphology of a generalist freshwater gastropod: complex relations of shell morphology, habitat, and fecundity. *Organisms Diversity and Evolution*, 18(4):425–441. doi:10.1007/s13127-018-0377-3.
- Vermeij, G. J. (1971). Gastropod evolution and morphological diversity in relation to shell geometry. *Journal of Zoology*, 163(1):15–23. doi:10.1111/j.1469-7998.1971.tb04522.x.

- Vermeij, G. J. (1972). Intraspecific Shore-Level Size Gradients in Intertidal Molluscs. *Ecology*, 53(4):693–700. doi:10.2307/1934785.
- Wahl, M. (1996). Fouled snails in flow: potential of epibionts on *Littorina littorea* to increase drag and reduce snail growth rates. *Marine Ecology Progress Series*, 138:157–168. doi:10.3354/meps138157.
- Walker, T. N. and Grahame, J. W. (2011). Shell shape variation and fitness variables in the gastropod *Littorina saxatilis*. *Marine Ecology Progress Series*, 430:103–111. doi:10.3354/meps09122.
- Weissenberger, J., Spatz, H. C., Emanns, A., and Schwoerbel, J. (1991). Measurement of lift and drag forces in the mN range experienced by benthic arthropods at flow velocities below 1.2 m/s. *Freshwater Biology*, 25(1):21–31. doi:10.1111/j.1365-2427.1991.tb00469.x.
- Westram, A. M., Faria, R., Johannesson, K., and Butlin, R. (2021). Using replicate hybrid zones to understand the genomic basis of adaptive divergence. *Molecular Ecology*. doi:10.1111/mec.15861.
- Westram, A. M., Galindo, J., Alm Rosenblad, M., Grahame, J. W., Panova, M., and Butlin, R. K. (2014). Do the same genes underlie parallel phenotypic divergence in different *Littorina saxatilis* populations? *Molecular Ecology*, 23(18):4603–4616. doi:10.1111/mec.12883.
- Westram, A. M., Panova, M., Galindo, J., and Butlin, R. K. (2016). Targeted resequencing reveals geographical patterns of differentiation for loci implicated in parallel evolution. *Molecular Ecology*, 25(13):3169–3186. doi:10.1111/mec.13640.
- Westram, A. M., Rafajlović, M., Chaube, P., Faria, R., Larsson, T., Panova, M., Ravinet, M., Blomberg, A., Mehlig, B., Johannesson, K., and Butlin, R. (2018). Clines on the seashore: The genomic architecture underlying rapid divergence in the face of gene flow. *Evolution Letters*, 2(4):297–309. doi:10.1002/evl3.74.
- Williams, S. T. (2017). Molluscan Shell Colour. *Biological Reviews*, 92:1039–1058. doi:10.1111/brv.12268.
- WoRMS Editorial Board (2021). World Register of Marine Species (WoRMS). Available from <http://www.marinespecies.org>. doi:10.14284/170.
- Yamazaki, T. and Goshima, S. (2012). Adaptive Differences in Morphology of the Periwinkle *Littorina sitkana* between Two Habitats Separated by an Artificial Structure. *Venus (Journal of the Malacological Society of Japan)*, 70(1-4):1–10. doi:10.18941/venus.70.1-4.1.
- Yang, J., Benyamin, B., McEvoy, B. P., Gordon, S., Henders, A. K., Nyholt, D. R., Madden, P. A., Heath, A. C., Martin, N. G., Montgomery, G. W., Goddard, M. E., and Visscher, P. M. (2010). Common SNPs explain a large proportion of the heritability for human height. *Nature Genetics*, 42(7):565–569. doi:10.1038/ng.608.
- Yang, S.-Y., Lin, B.-S., and Chang, W.-L. (2007). The analysis and application of biological hydrodynamics on the freshwater snails *Sinotaia quadrata* and *Thiara granifera*. *Journal of Chinese Soil and Water Conservation*, 38(1):65–76.

- Zhao, W., Ma, C., Cheverud, J. M., and Wu, R. (2005). A unifying statistical model for QTL mapping of genotype x sex interaction for developmental trajectories. *Physiological Genomics*, 19:218–227. doi:10.1152/physiolgenomics.00129.2004.

# Appendices

# Appendix A

## ShellShaper

The ShellShaper program is a set of MATLAB scripts which provides a user interface and functionality for obtaining information about the shape of gastropod shells from 2D images. The program is currently separated into two versions which can be found at: <https://github.com/jslarsson/ShellShaper>. The main version which allows the user to infer the shape parameters presented in chapter 2 allowing variable aperture shapes, and the band version for inferring the position and size of coloured bands on the shell surface when apertures are circular. The github version of the program will be updated and improved over time, while the figshare version found below in appendix B will not. A user guide with visualisations of the user interface for the version of ShellShaper for inferring the position of coloured bands is also included in chapter E.

## Appendix B

# Chapter 2 supplementary material

By making two small modifications to the shell model presented above, we can apply it to a greater range of gastropod shell shapes. The first modification is adding the ability to remove a section from the aperture and only include the part that is actually constructed. Secondly, by calculating the aperture plane using the normal plane of a spiral tracing the widest part of the shell instead of the internal spiral, it is possible to reduce the variability of the aperture orientation that occurs when the internal spiral is very close to the coiling axis, i.e.  $r_0$  is very small. These modifications have been included in a package, ShellShaper, that allows interactive fitting of the growth model to a shell photograph without landmarks, which is freely available at <https://figshare.shef.ac.uk/articles/ShellShaper/9944591>. Examples of models obtained using ShellShaper are given in figure B.1. Note however that thickness is not measured from the images, and has been set to a standard value as it does not affect the outside shape. Further extensions could be to include more diverse aperture shapes, such as ridges, by modifying the generating curve rather than restricting it to a circlipse, or colour variation, such as the placement of bands.



**Figure B.1:** Examples of gastropod species which can be described using a slight variation of the model in section 2.2. Photographs obtained from the WoRMS database (WoRMS Editorial Board, 2021). From left: *Dicathais orbita*, *Ocenebra edwardsii*, *Naticarius manceli*, *Margarites rossicus derjugini*, *Glabella bellii*.

## Appendix C

### Chapter 3 supplementary material

| Trait                      | LG | Position (cM) | lower CI | higher CI | LOD  | P-value | threshold | Variance explained | N samples |
|----------------------------|----|---------------|----------|-----------|------|---------|-----------|--------------------|-----------|
| Weight                     | 6  | 9.00          | 0.00     | 25.72     | 4.17 | 0.031   | 3.90      | 0.050              | 374       |
| Length                     | 6  | 10.00         | 0.00     | 25.42     | 3.85 | 0.063   | 3.99      | 0.046              | 375       |
| Absolute Thickness         | 6  | 20.11         | 5.22     | 31.63     | 3.83 | 0.079   | 4.05      | 0.046              | 373       |
| Height growth              | 17 | 31.78         | 28.76    | 32.99     | 4.16 | 0.028   | 3.93      | 0.050              | 376       |
| Width growth               | 17 | 64.40         | 30.57    | 67.15     | 4.02 | 0.053   | 4.03      | 0.048              | 376       |
| Aperture Position Radial   | 17 | 64.09         | 50.27    | 67.15     | 6.16 | 0.001   | 3.89      | 0.073              | 376       |
| Aperture Position Vertical | 6  | 10.77         | 0.00     | 21.32     | 3.03 | 0.279   | 3.89      | 0.036              | 376       |
|                            | 17 | 67.00         | 63.49    | 67.15     | 5.79 | < 0.001 |           | 0.068              |           |
| Aperture Size              | 12 | 73.22         | 61.34    | 73.43     | 3.12 | 0.242   | 3.96      | 0.037              | 376       |
|                            | 17 | 28.76         | 31.33    | 47.09     | 3.18 | 0.212   |           | 0.038              |           |
| Aperture Shape             | 6  | 18.59         | 0.75     | 27.69     | 4.36 | 0.023   | 4.05      | 0.052              | 376       |
| Overall Growth             | 17 | 31.78         | 28.76    | 46.64     | 3.48 | 0.123   | 4.06      | 0.042              | 376       |
| Convexity                  | 17 | 67.15         | 58.32    | 67.15     | 9.07 | <0.001  | 3.95      | 0.105              | 376       |
| Relative Thickness         | 2  | 13.26         | 10.46    | 55.26     | 3.27 | 0.18    | 3.97      | 0.039              | 373       |
|                            | 6  | 26.03         | 15.11    | 52.17     | 3.07 | 0.26    |           | 0.037              |           |
| PC1                        | 17 | 67.15         | 64.09    | 67.15     | 5.14 | 0.007   | 3.91      | 0.061              | 376       |
| PC3                        | 2  | 46.32         | 41.48    | 49.04     | 3.13 | 0.243   | 4.01      | 0.038              | 376       |
|                            | 5  | 20.33         | 4.90     | 32.61     | 3.26 | 0.193   |           | 0.039              |           |
|                            | 17 | 36.74         | 27.24    | 39.01     | 3.09 | 0.261   |           | 0.037              |           |
| PC4                        | 2  | 48.14         | 24.81    | 67.70     | 3.65 | 0.094   | 3.97      | 0.044              | 376       |
| PC7                        | 8  | 16            | 4.27     | 21.47     | 3.40 | 0.119   | 3.81      | 0.041              | 376       |

**Figure C.1:** Table of significant and suggestive QTL position, including their confidence intervals, LOD scores and p-values for each peak, the score needed to reach the significance ( $p = 0.05$ ) threshold. The variance explained shows the amount of variation the QTL is estimated to account for.

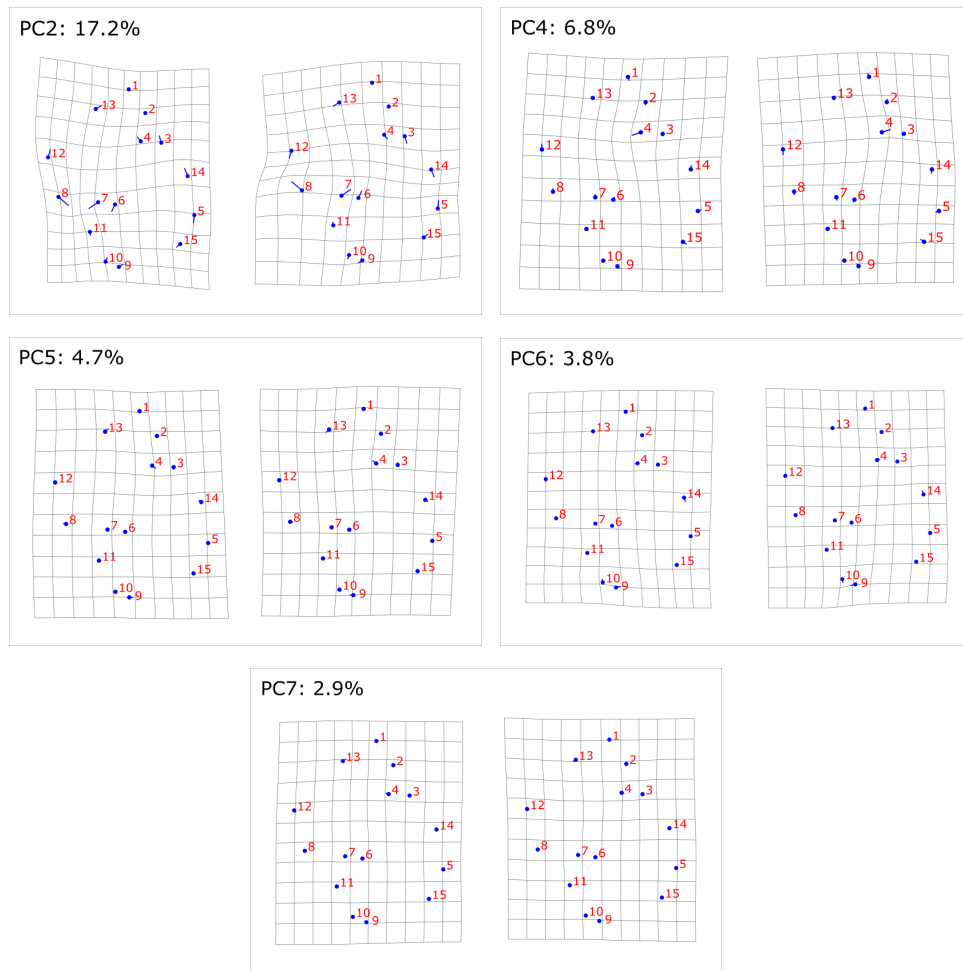


**Figure C.2:** Visualisations of the shape variation corresponding to the less informative principal components of the GM method, with their respective amount of variation explained. PC1 and PC3 can be found in figure 3.4.

|             | N marker | Length (cM) | Length (Mb) | Weight               | Length               | Thickness            | PC1                  | PC2                  | PC3                  | PC4                  | PC5                  | PC6                  | PC7                  |
|-------------|----------|-------------|-------------|----------------------|----------------------|----------------------|----------------------|----------------------|----------------------|----------------------|----------------------|----------------------|----------------------|
| <b>LG1</b>  | 2077     | 84.1        | 177.82      | 0.005 (0.023)        | 0.022 (0.034)        | 0.013 (0.026)        | 0.019 (0.035)        | 0.000 (0.000)        | 0.03 (0.036)         | 0.022 (0.028)        | <b>0.052 (0.047)</b> | 0.000 (0.000)        | 0.007 (0.022)        |
| <b>LG2</b>  | 2098     | 80.5        | 208.71      | 0.007 (0.027)        | 0.000 (0.000)        | 0.023 (0.033)        | <b>0.053 (0.044)</b> | 0.019 (0.032)        | <b>0.102 (0.058)</b> | <b>0.041 (0.036)</b> | <b>0.036 (0.037)</b> | 0.000 (0.000)        | 0.004 (0.021)        |
| <b>LG3</b>  | 1424     | 78.4        | 120.93      | 0.000 (0.000)        | 0.002 (0.023)        | 0.000 (0.000)        | 0.000 (0.000)        | 0.000 (0.000)        | 0.000 (0.000)        | 0.007 (0.02)         | 0.012 (0.023)        | 0.003 (0.024)        | 0.003 (0.017)        |
| <b>LG4</b>  | 1142     | 62.7        | 102.99      | 0.023 (0.036)        | 0.016 (0.032)        | 0.026 (0.039)        | 0.009 (0.02)         | 0.000 (0.000)        | 0.000 (0.000)        | <b>0.061 (0.048)</b> | 0.000 (0.000)        | 0.000 (0.000)        | 0.011 (0.02)         |
| <b>LG5</b>  | 1018     | 58.3        | 86.68       | 0.096 (0.084)        | <b>0.168 (0.098)</b> | 0.03 (0.04)          | 0.02 (0.029)         | 0.046 (0.046)        | <b>0.074 (0.053)</b> | <b>0.054 (0.047)</b> | 0.006 (0.022)        | 0.000 (0.000)        | 0.000 (0.000)        |
| <b>LG6</b>  | 1191     | 69.1        | 106.71      | <b>0.130 (0.072)</b> | <b>0.110 (0.065)</b> | <b>0.167 (0.079)</b> | 0.000 (0.000)        | 0.026 (0.031)        | 0.009 (0.018)        | 0.007 (0.019)        | <b>0.047 (0.042)</b> | <b>0.069 (0.047)</b> | 0.021 (0.036)        |
| <b>LG7</b>  | 1126     | 60.6        | 92.88       | 0.000 (0.000)        | 0.000 (0.000)        | 0.022 (0.04)         | 0.000 (0.000)        | <b>0.039 (0.038)</b> | 0.000 (0.000)        | 0.023 (0.027)        | 0.000 (0.000)        | 0.018 (0.028)        | 0.000 (0.000)        |
| <b>LG8</b>  | 682      | 66          | 43.46       | 0.000 (0.000)        | 0.000 (0.000)        | 0.011 (0.031)        | 0.008 (0.023)        | 0.008 (0.022)        | 0.024 (0.028)        | 0.01 (0.023)         | 0.000 (0.000)        | 0.008 (0.03)         | 0.019 (0.029)        |
| <b>LG9</b>  | 1081     | 65.5        | 73.91       | 0.000 (0.000)        | 0.000 (0.015)        | <b>0.044 (0.037)</b> | 0.014 (0.03)         | 0.000 (0.000)        | 0.000 (0.000)        | 0.000 (0.000)        | 0.000 (0.000)        | <b>0.086 (0.056)</b> | 0.01 (0.022)         |
| <b>LG10</b> | 1043     | 60.7        | 84.65       | 0.005 (0.02)         | 0.000 (0.000)        | 0.000 (0.000)        | 0.000 (0.000)        | 0.000 (0.000)        | 0.02 (0.029)         | 0.007 (0.02)         | 0.037 (0.042)        | 0.000 (0.000)        | 0.024 (0.033)        |
| <b>LG11</b> | 703      | 75.3        | 51.07       | 0.000 (0.000)        | 0.000 (0.000)        | 0.000 (0.000)        | 0.000 (0.000)        | 0.002 (0.021)        | 0.002 (0.017)        | 0.000 (0.000)        | 0.011 (0.025)        | 0.000 (0.000)        | 0.000 (0.000)        |
| <b>LG12</b> | 2145     | 73.4        | 187.86      | 0.000 (0.000)        | <b>0.101 (0.073)</b> | 0.088 (0.069)        | 0.037 (0.039)        | 0.039 (0.042)        | <b>0.161 (0.08)</b>  | <b>0.041(0.039)</b>  | 0.004 (0.02)         | <b>0.054 (0.043)</b> | <b>0.059 (0.042)</b> |
| <b>LG13</b> | 799      | 55.4        | 63.72       | 0.003 (0.021)        | 0.030 (0.037)        | 0.000 (0.000)        | 0.008 (0.023)        | 0.006 (0.022)        | 0.000 (0.000)        | 0.000 (0.000)        | 0.017 (0.023)        | 0.000 (0.000)        | 0.000 (0.000)        |
| <b>LG14</b> | 1050     | 34.6        | 75.03       | <b>0.064 (0.051)</b> | 0.027 (0.028)        | 0.009 (0.014)        | 0.002 (0.011)        | 0.001 (0.01)         | 0.000 (0.000)        | 0.000 (0.000)        | 0.007 (0.016)        | 0.009 (0.015)        | <b>0.035 (0.032)</b> |
| <b>LG15</b> | 726      | 68.1        | 56          | 0.000 (0.000)        | 0.000 (0.000)        | 0.000 (0.000)        | 0.035 (0.034)        | 0.000 (0.000)        | 0.004 (0.02)         | 0.000 (0.000)        | 0.000 (0.000)        | 0.000 (0.000)        | 0.019 (0.026)        |
| <b>LG16</b> | 508      | 70          | 32          | 0.000 (0.000)        | 0.010 (0.029)        | 0.000 (0.000)        | 0.000 (0.000)        | 0.024 (0.035)        | 0.003 (0.02)         | 0.000 (0.000)        | 0.000 (0.000)        | 0.012 (0.03)         | 0.008 (0.026)        |
| <b>LG17</b> | 1395     | 67.2        | 127.53      | <b>0.049 (0.046)</b> | 0.022 (0.037)        | <b>0.076 (0.062)</b> | <b>0.105 (0.064)</b> | 0.000 (0.000)        | 0.01 (0.021)         | 0.006 (0.024)        | <b>0.06 (0.049)</b>  | 0.04 (0.043)         | 0.000 (0.000)        |
|             |          |             | $h^2$       | <b>0.67 (0.086)</b>  | <b>0.592 (0.094)</b> | <b>0.65 (0.086)</b>  | <b>0.23 (0.09)</b>   | <b>0.12 (0.08)</b>   | <b>0.39 (0.09)</b>   | <b>0.28 (0.09)</b>   | <b>0.24 (0.09)</b>   | <b>0.23 (0.09)</b>   | <b>0.22 (0.08)</b>   |

**Figure C.3:** Variance partitioning table for the size parameters and the GM PCs. Numbers indicate the proportion of the total variation in each trait explained by each LG, with standard error values in brackets. Numbers in bold indicate that the LG contribution to variability is significant, and zeroes represent values which were too small to be estimated reliably. The  $h^2$  value gives the total heritability estimate of each trait for the whole genome.

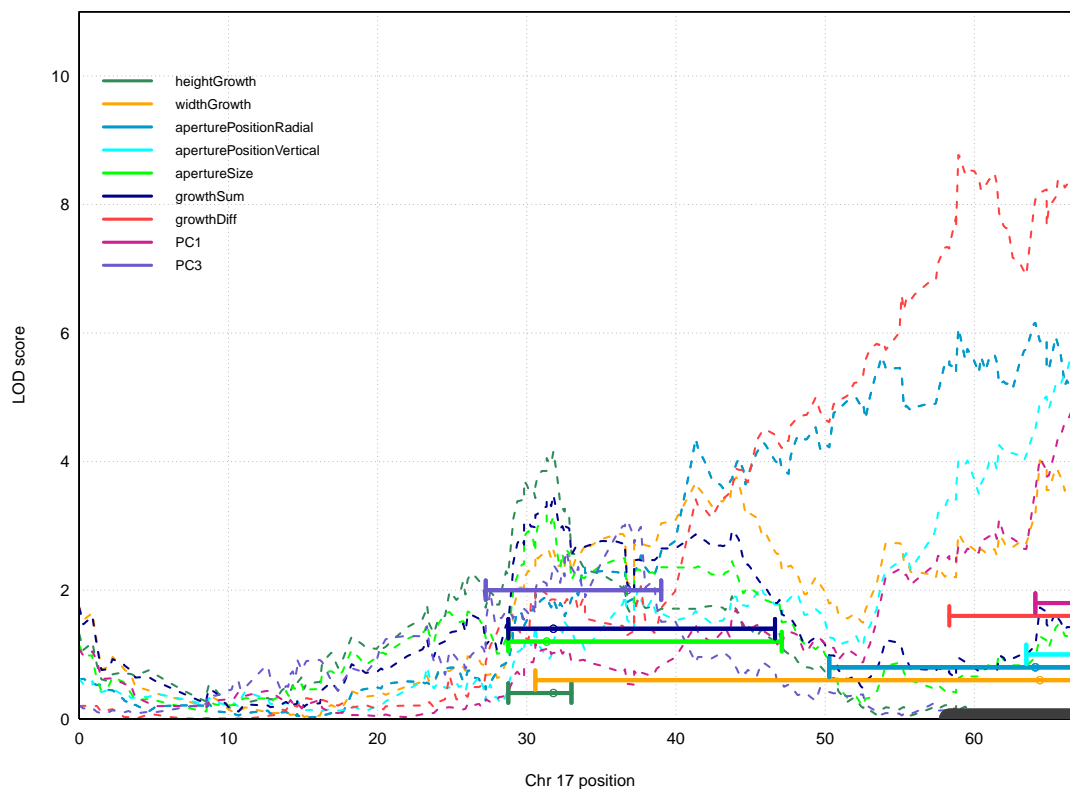


**Figure C.4:** Detailed view of the QTL peaks on LG 17 for the traits reaching a LOD score of at least 3, each with a 95% CI of their peak position indicated. The position of the suggested inversion is marked with a black line along the x-axis, and the QTL found suggest that there are loci involved in shape variation both within the inversion and outside of it.

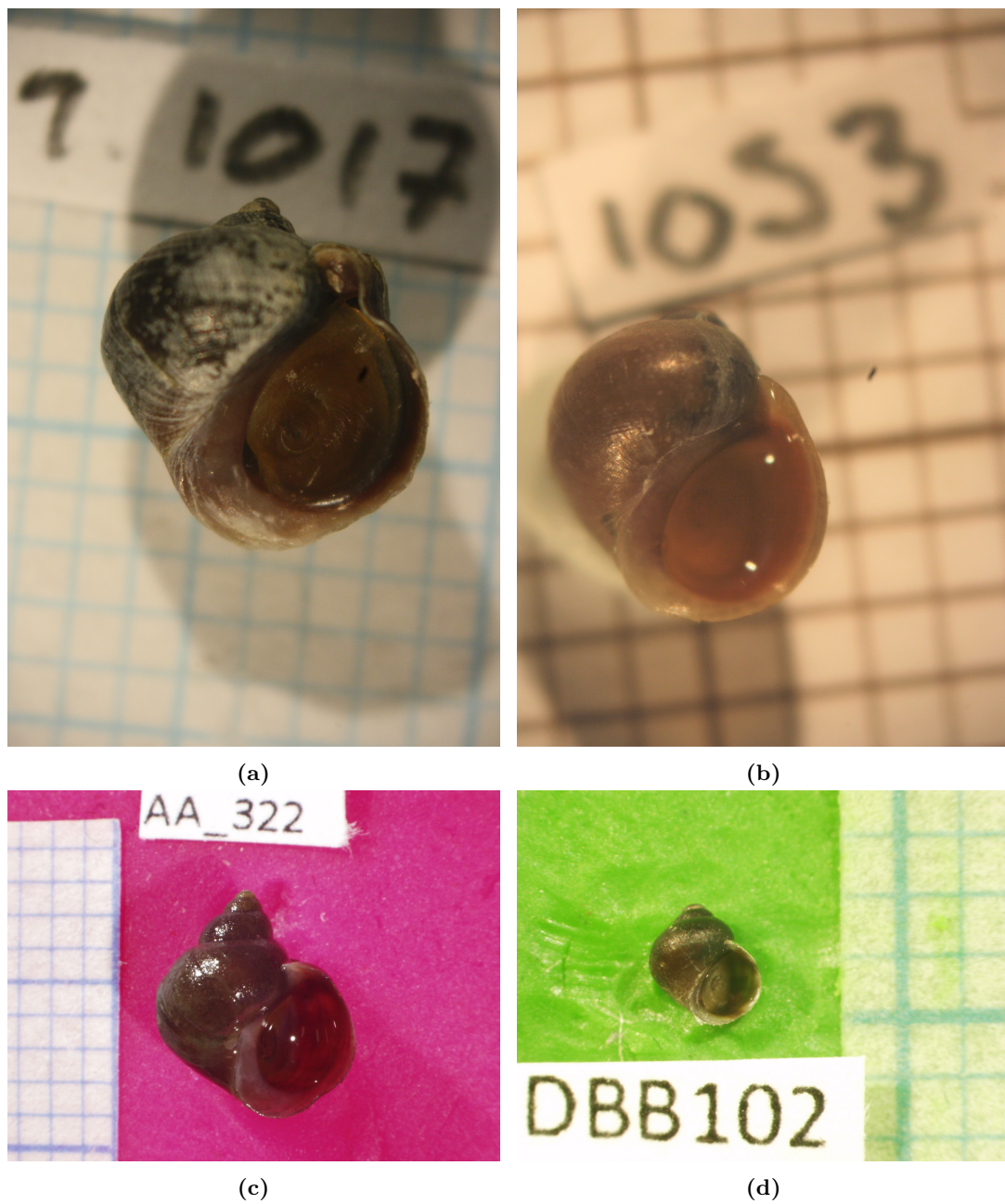


**Figure C.5:** Examples of four outliers in terms of convexity/concavity, top row from the F2 data set, bottom row from the pure ecotype data set. (a) and (c) showing concave growth patterns, the deformity of the aperture in (a) likely affects the inferred value of several parameters. (b) and (d) showing convex growth patterns.

|                            | Weight         | Length         | Thickness      | Height Growth  | Width Growth   | Overall Growth | Convexity      | Aperture Position Radial | Aperture Position Vertical | Aperture Size  | Aperture Shape | Relative Thickness | PC1       | PC3       |
|----------------------------|----------------|----------------|----------------|----------------|----------------|----------------|----------------|--------------------------|----------------------------|----------------|----------------|--------------------|-----------|-----------|
| Weight                     |                | 4.28E-10       | 0.004          | 0.013          | 0.573          | 0.123          | 0.013          | 0.373                    | 0.357                      | 0.176          | 0.056          | 0.374              | 0.653     | 0.116     |
| Length                     | 0.951 (0.04)   |                | 2.99E-04       | 3.17E-04       | 0.14           | 0.009          | 0.016          | 0.796                    | 0.832                      | 0.011          | 0.045          | 0.191              | 0.697     | 0.005     |
| Thickness                  | 0.551 (0.158)  | 0.632 (0.128)  |                | 0.159          | 0.948          | 0.467          | 0.089          | 0.322                    | 0.438                      | 0.665          | 0.298          | 1.58E-09           | 0.735     | 0.107     |
| Height Growth              | -0.488 (0.185) | -0.652 (0.146) | -0.283 (0.202) |                | 4.47E-06       | 3.33E-09       | 0.416          | 0.008                    | 0.001                      | 8.27E-09       | 0.077          | 0.556              | 0.080     | 5.207E-09 |
| Width Growth               | -0.117 (0.221) | -0.300 (0.210) | -0.014 (0.219) | 0.779 (0.202)  |                | 3.31E-09       | 0.013          | 1.96E-07                 | 1.89E-05                   | 7.40E-08       | 0.100          | 0.785              | 0.001     | 5.499E-05 |
| Overall Growth             | -0.314 (0.209) | -0.505 (0.182) | -0.150 (0.215) | 0.936 (0.026)  | 0.950 (0.021)  |                | 0.342          | 2.67E-05                 | 4.23E-05                   | 1.26E-09       | 0.069          | 0.656              | 0.007     | 2.572E-07 |
| Convexity                  | -0.490 (0.180) | -0.470 (0.176) | -0.359 (0.189) | 0.166 (0.206)  | -0.490 (0.161) | -0.193 (0.204) |                | 4.72E-04                 | 0.128                      | 0.57           | 0.898          | 0.807              | 0.019     | 0.437     |
| Aperture Position Radial   | 0.181 (0.211)  | -0.052 (0.211) | 0.197 (0.201)  | 0.492 (0.161)  | 0.859 (0.072)  | 0.726 (0.110)  | -0.657 (0.129) |                          | 1.44E-05                   | 2.16E-04       | 0.584          | 0.707              | 1.265E-04 | 0.011     |
| Aperture Position Vertical | -0.196 (0.221) | 0.044 (0.22)   | -0.163 (0.213) | -0.631 (0.146) | -0.787 (0.1)   | -0.753 (0.112) | 0.331 (0.197)  | -0.782 (0.098)           |                            | 4.08E-03       | 0.254          | 0.778              | 1.142E-05 | 0.007     |
| Aperture Size              | -0.277 (0.212) | -0.500 (0.181) | -0.089 (0.214) | 0.914 (0.053)  | 0.878 (0.057)  | 0.946 (0.036)  | -0.116 (0.209) | 0.655 (0.132)            | -0.57 (0.161)              |                | 0.009          | 0.801              | 0.014     | 3.042E-06 |
| Aperture Shape             | 0.494 (0.254)  | 0.514 (0.248)  | 0.272 (0.260)  | -0.397 (0.204) | -0.370 (0.207) | -0.404 (0.201) | 0.032 (0.247)  | -0.126 (0.230)           | -0.279 (0.223)             | -0.564 (0.159) |                | 0.508              | 0.593     | 0.051     |
| Relative Thickness         | 0.180 (0.205)  | 0.256 (0.195)  | 0.876 (0.051)  | -0.112 (0.192) | -0.053 (0.196) | -0.084 (0.193) | -0.051 (0.204) | 0.071 (0.189)            | -0.057 (0.200)             | -0.048 (0.193) | 0.151 (0.224)  |                    | 0.912     | 0.234     |

Figure C.6: Lower left values represent the genetic correlation between traits, numbers in brackets show the standard error, while upper right is the corresponding p-value.

|       | N marker | Length (cM) | Length (Mb) | Height Growth | Width Growth  | Overall Growth | Convexity     | Aperture Position Radial | Aperture Position Vertical | Aperture Size | Aperture Shape | Aperture Rotation | Relative Thickness |
|-------|----------|-------------|-------------|---------------|---------------|----------------|---------------|--------------------------|----------------------------|---------------|----------------|-------------------|--------------------|
| LG1   | 2077     | 84.1        | 177.82      | 0.024 (0.036) | 0.047 (0.046) | 0.037 (0.042)  | 0.046 (0.049) | 0.081 (0.056)            | 0.028 (0.037)              | 0.043 (0.044) | 0.024 (0.030)  | 0.018 (0.028)     | 0.036 (0.035)      |
| LG2   | 2098     | 80.5        | 208.71      | 0.087 (0.053) | 0.088 (0.049) | 0.09 (0.051)   | 0.071 (0.05)  | 0.032 (0.029)            | 0.069 (0.044)              | 0.038 (0.035) | 0.000 (0.000)  | 0.094 (0.053)     | 0.032 (0.03)       |
| LG3   | 1424     | 78.4        | 120.93      | 0.007 (0.021) | 0.000 (0.000) | 0.000 (0.000)  | 0.000 (0.000) | 0.000 (0.000)            | 0.000 (0.000)              | 0.000 (0.000) | 0.007 (0.024)  | 0.000 (0.000)     | 0.008 (0.019)      |
| LG4   | 1142     | 62.7        | 102.99      | 0.015 (0.026) | 0.021 (0.028) | 0.023 (0.029)  | 0.000 (0.000) | 0.015 (0.024)            | 0.02 (0.029)               | 0.041 (0.039) | 0 (0.026)      | 0.026 (0.034)     | 0.04 (0.039)       |
| LG5   | 1018     | 58.3        | 86.68       | 0.064 (0.047) | 0.067 (0.049) | 0.073 (0.049)  | 0.000 (0.000) | 0.05 (0.042)             | 0.026 (0.03)               | 0.135 (0.066) | 0.132 (0.081)  | 0.000 (0.000)     | 0.014 (0.023)      |
| LG6   | 1191     | 69.1        | 106.71      | 0.006 (0.015) | 0.001 (0.012) | 0.004 (0.014)  | 0.000 (0.000) | 0.000 (0.000)            | 0.02 (0.024)               | 0.001 (0.011) | 0.047 (0.038)  | 0.036 (0.039)     | 0.091 (0.062)      |
| LG7   | 1126     | 60.6        | 92.88       | 0.000 (0.000) | 0.000 (0.000) | 0.000 (0.000)  | 0.000 (0.000) | 0.000 (0.000)            | 0.000 (0.000)              | 0.000 (0.000) | 0.000 (0.000)  | 0.000 (0.000)     | 0.035 (0.045)      |
| LG8   | 682      | 66          | 43.46       | 0.024 (0.034) | 0.000 (0.000) | 0.012 (0.026)  | 0.000 (0.000) | 0.000 (0.000)            | 0.023 (0.029)              | 0.023 (0.034) | 0.007 (0.022)  | 0.000 (0.013)     | 0.000 (0.000)      |
| LG9   | 1081     | 65.5        | 73.91       | 0.000 (0.000) | 0.000 (0.000) | 0.000 (0.000)  | 0.000 (0.000) | 0.011 (0.024)            | 0.029 (0.032)              | 0.000 (0.000) | 0.01 (0.026)   | 0.000 (0.000)     | 0.063 (0.042)      |
| LG10  | 1043     | 60.7        | 84.65       | 0.005 (0.017) | 0.000 (0.000) | 0.000 (0.000)  | 0.025 (0.031) | 0.103 (0.061)            | 0.000 (0.000)              | 0.000 (0.000) | 0.000 (0.000)  | 0.000 (0.000)     | 0.008 (0.023)      |
| LG11  | 703      | 75.3        | 51.07       | 0.000 (0.000) | 0.000 (0.000) | 0.000 (0.000)  | 0.000 (0.000) | 0.000 (0.000)            | 0.012 (0.022)              | 0.000 (0.000) | 0.000 (0.000)  | 0.000 (0.000)     | 0.017 (0.027)      |
| LG12  | 2145     | 73.4        | 187.86      | 0.135 (0.071) | 0.127 (0.065) | 0.137 (0.069)  | 0.063 (0.054) | 0.114 (0.066)            | 0.094 (0.068)              | 0.132 (0.064) | 0.098 (0.06)   | 0.084 (0.061)     | 0.044 (0.045)      |
| LG13  | 799      | 55.4        | 63.72       | 0.012 (0.02)  | 0.000 (0.000) | 0.000 (0.000)  | 0.018 (0.028) | 0.000 (0.000)            | 0.000 (0.000)              | 0.000 (0.000) | 0.000 (0.000)  | 0.000 (0.000)     | 0.000 (0.000)      |
| LG14  | 1050     | 34.6        | 75.03       | 0.000 (0.000) | 0.000 (0.000) | 0.000 (0.000)  | 0.004 (0.016) | 0.022 (0.022)            | 0.021 (0.024)              | 0.000 (0.000) | 0.000 (0.000)  | 0.011 (0.019)     | 0.000 (0.000)      |
| LG15  | 726      | 68.1        | 56          | 0.003 (0.019) | 0.02 (0.025)  | 0.015 (0.024)  | 0.006 (0.022) | 0.015 (0.024)            | 0.000 (0.000)              | 0.036 (0.03)  | 0.006 (0.021)  | 0.005 (0.020)     | 0.002 (0.018)      |
| LG16  | 508      | 70          | 32          | 0.036 (0.039) | 0.000 (0.000) | 0.004 (0.025)  | 0.000 (0.000) | 0.004 (0.02)             | 0.000 (0.000)              | 0.000 (0.000) | 0.000 (0.000)  | 0.014 (0.026)     | 0.007 (0.021)      |
| LG17  | 1395     | 67.2        | 127.53      | 0.000 (0.000) | 0.074 (0.055) | 0.000 (0.000)  | 0.133 (0.06)  | 0.162 (0.076)            | 0.056 (0.044)              | 0.000 (0.000) | 0.03 (0.035)   | 0.051 (0.043)     | 0.168 (0.086)      |
| $h^2$ |          |             |             | 0.565 (0.091) | 0.573 (0.09)  | 0.434 (0.09)   | 0.400 (0.095) | 0.529 (0.091)            | 0.579 (0.096)              | 0.572 (0.09)  | 0.31 (0.10)    | 0.242 (0.09)      | 0.452 (0.09)       |

Figure C.7: Variance partitioning table for the growth related shape parameters. Numbers indicate the proportion of the total variation in each trait explained by each LG, with standard error values in brackets. Numbers in bold indicate that the LG contribution to variability is significant, and zeroes represent values which were too small to be estimated reliably. The  $h^2$  value gives the total heritability estimate of each trait for the whole genome.

# Appendix D

## Chapter 4 supplementary material

| Shape parameters                                   | Extreme Crab | Crab   | Intermediate | Wave   | Extreme Wave |
|--|--------------|--------|--------------|--------|--------------|
| $\log(g_w)$  | -2.714       | -2.451 | -2.188       | -1.910 | -1.631       |
| $\log(g_h)$  | -2.628       | -2.350 | -2.071       | -1.777 | -1.482       |
| $r_0$  | 0.178        | 0.199  | 0.219        | 0.241  | 0.263        |
| $h_0$  | 0.634        | 0.615  | 0.597        | 0.577  | 0.557        |
| $a_0$  | 0.185        | 0.240  | 0.296        | 0.355  | 0.414        |
| $c$  | 1.995        | 1.686  | 1.425        | 1.192  | 0.998        |
| $c_0$  | 0.368        | 0.405  | 0.422        | 0.423  | 0.413        |
| $\Theta$   | 17.048       | 16.082 | 15.117       | 14.095 | 13.072       |
| Circlipse area                                     | 0.160        | 0.244  | 0.334        | 0.434  | 0.538        |
| Relative foot area                                 | 0.040        | 0.149  | 0.306        | 0.510  | 0.744        |
| Length of small model (mm)                         | 4.54         | 4.17   | 3.86         | 3.61   | 3.41         |
| Foot area scaled to small model (mm <sup>2</sup> ) | 0.826        | 2.587  | 4.558        | 6.651  | 8.656        |

**Figure D.1:** A summary of the shape parameter values used for the shell models in chapter 4 (see chapter 2 for full description). The length is for the smallest size shell model, having of total volume 12 mm<sup>3</sup>. The estimated aperture (circlipse) area is calculated as  $\pi a_0(a_0 + c_0)/2$  from which the foot size is estimated according to the linear equation in figure 4.7b.

We used the drag forces to infer the preferred orientation of the shell models in the simulations (figure 4.8). However, it is also interesting to look at the drag coefficient,  $c_d$ , to understand in which direction the shell is the most streamlined, as this did not always coincide with the lowest forces the shell experienced, which we observed both in the simulations (figure 4.8 compared to figure D.2) and in the experiment with real shells (figure 4.11c compared to figure 4.11c). This further suggests that looking at more than one measure of drag is needed to understand the full story, and shows how useful it is to do highly controlled simulations to detangle the different effects of shape and orientation on various hydrodynamical properties.

We noted some interesting interaction of shell size with shape and flow speed in the simulation (figure D.3a). The drag coefficient was lower for the wave shapes of the smallest size, and crab shapes of the large size (size factor 4), corresponding to the common size of them respectively in nature, and this trend was generally consistent across orientations. For

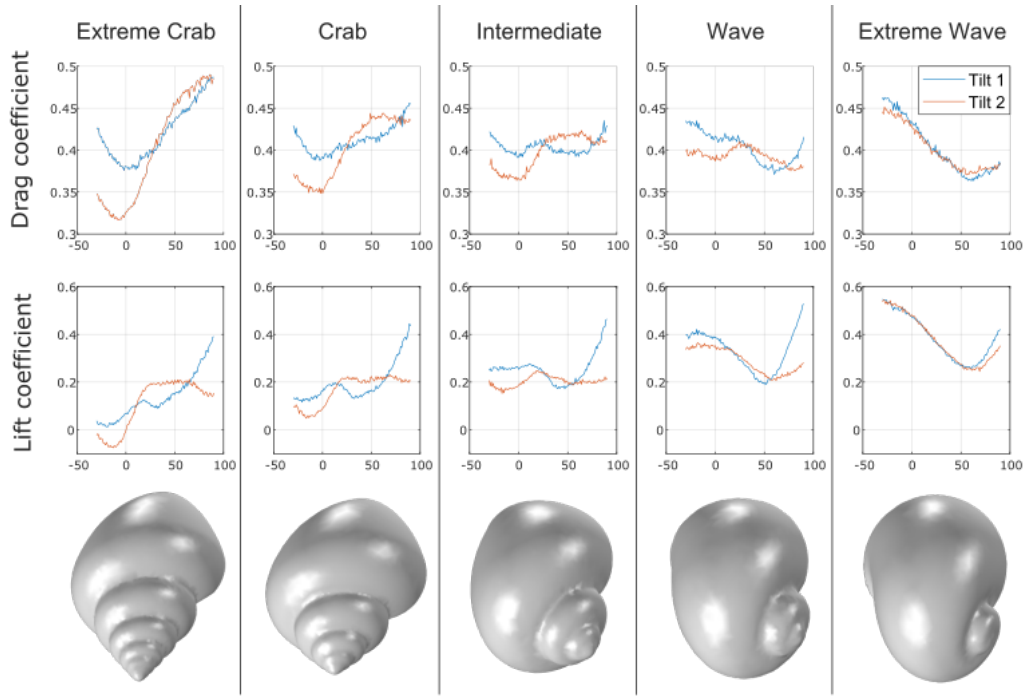


**Figure D.2:** The drag and lift coefficients calculated for the alignment simulations. Compare with the drag and lift forces for the same simulations (figure 4.8).

all shapes the extra large size had the highest drag coefficients, possibly having something to do with size limiting factors on rocky shores. However, these trends are small compared to the overall variability, and would need further study to understand general size limiting factors, and if and how this interact with different shapes.

The trend of the lift forces across flow speed differed for the different size categories (figure D.3b). For the smallest size, the lift remained stable across the different speeds, while for the three larger sizes there was a decreasing trend with higher speeds. This could be due to a change in flow pattern around the shells at different sizes and how this interacts with e.g. the boundary layer of the flow, i.e. the relative amount of water flowing underneath the shell or above it, which could potentially affect the lift to vary with flow speed. However, more analysis is needed to confirm this.

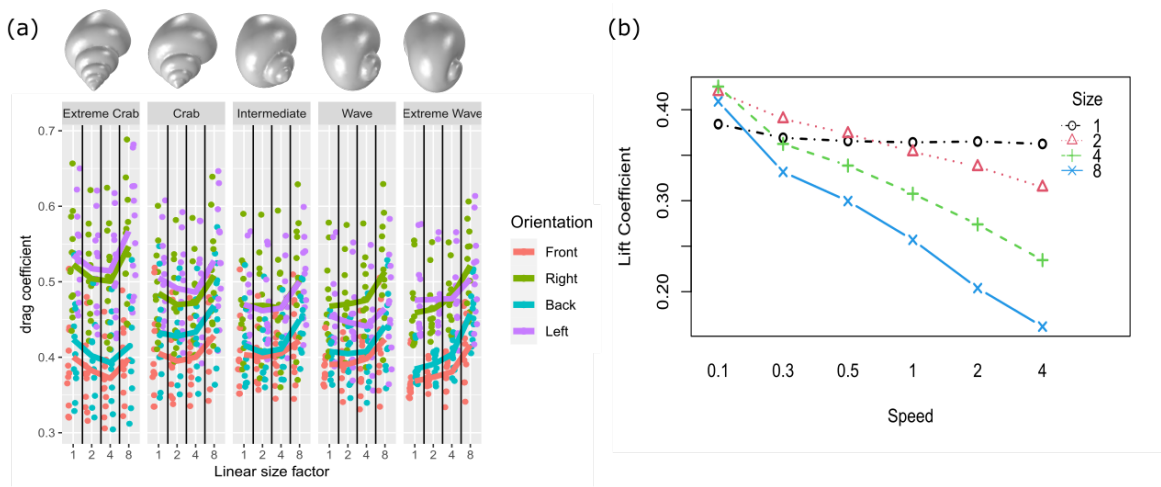


**Figure D.3:** Effects of shell size. (a) The varying trends of drag coefficients across size categories for the different shapes. (b) Interaction between shell size and flow speed for the lift coefficient in the simulations.

|                     | Df  | Sum Sq | Mean Sq | F value | Pr(>F)      |
|---------------------|-----|--------|---------|---------|-------------|
| shape               | 4   | 0.0967 | 0.0242  | 32.014  | < 2e-16 *** |
| rotation            | 3   | 1.6052 | 0.5351  | 708.514 | < 2e-16 *** |
| size                | 1   | 0.1584 | 0.1584  | 209.704 | < 2e-16 *** |
| shape:rotation      | 12  | 0.1985 | 0.0165  | 21.901  | < 2e-16 *** |
| shape:size          | 4   | 0.0185 | 0.0046  | 6.114   | 7.4e-05 *** |
| rotation:size       | 3   | 0.0049 | 0.0016  | 2.181   | 0.0888 .    |
| shape:rotation:size | 12  | 0.0186 | 0.0016  | 2.053   | 0.0177 *    |
| Residuals           | 920 | 0.6948 | 0.0008  |         |             |

---  
 Signif. codes: 0 '\*\*\*' 0.001 '\*\*' 0.01 '\*' 0.05 '.' 0.1 ' ' 1

(a) Results of an ANOVA comparing the residual drag coefficient values after a linear regression against flow speed, see figure 4.9b.

|                     | Df  | Sum Sq | Mean Sq | F value  | Pr(>F)     |
|---------------------|-----|--------|---------|----------|------------|
| shape               | 4   | 1.400  | 0.3500  | 263.627  | <2e-16 *** |
| rotation            | 3   | 6.768  | 2.2558  | 1698.973 | <2e-16 *** |
| size                | 1   | 0.393  | 0.3928  | 295.810  | <2e-16 *** |
| shape:rotation      | 12  | 0.786  | 0.0655  | 49.349   | <2e-16 *** |
| shape:size          | 4   | 0.010  | 0.0026  | 1.939    | 0.1019     |
| rotation:size       | 3   | 0.007  | 0.0023  | 1.750    | 0.1552     |
| shape:rotation:size | 12  | 0.026  | 0.0022  | 1.620    | 0.0806 .   |
| Residuals           | 920 | 1.222  | 0.0013  |          |            |

---  
 Signif. codes: 0 '\*\*\*' 0.001 '\*\*' 0.01 '\*' 0.05 '.' 0.1 ' ' 1

(b) Results of an ANOVA comparing the drag forces scaled by shell volume values, after a linear regression against flow speed, see figure 4.9c.

|                     | Df  | Sum Sq | Mean Sq | F value   | Pr(>F)      |
|---------------------|-----|--------|---------|-----------|-------------|
| shape               | 4   | 772.9  | 193.21  | 51561.569 | < 2e-16 *** |
| rotation            | 3   | 22.8   | 7.59    | 2026.591  | < 2e-16 *** |
| size                | 1   | 1.3    | 1.28    | 340.350   | < 2e-16 *** |
| shape:rotation      | 12  | 2.4    | 0.20    | 54.153    | < 2e-16 *** |
| shape:size          | 4   | 0.1    | 0.02    | 5.282     | 0.00033 *** |
| rotation:size       | 3   | 0.0    | 0.01    | 3.360     | 0.01830 *   |
| shape:rotation:size | 12  | 0.1    | 0.01    | 1.820     | 0.04095 *   |
| Residuals           | 920 | 3.4    | 0.00    |           |             |

---  
 Signif. codes: 0 '\*\*\*' 0.001 '\*\*' 0.01 '\*' 0.05 '.' 0.1 ' ' 1

(c) Results of an ANOVA comparing the drag forces scaled by shell volume values, after a linear regression against flow speed, see figure 4.9c.

**Figure D.4:** Comparison of the relative effects of shape, rotation, and size, as well as all interactions on the drag forces of the fluid dynamics simulations. For visualisations of the variation related to shape and rotation see figure 4.9.

|                     | Df  | Sum Sq | Mean Sq | F value | Pr(>F)       |
|---------------------|-----|--------|---------|---------|--------------|
| shape               | 4   | 8.442  | 2.111   | 157.440 | < 2e-16 ***  |
| rotation            | 3   | 16.391 | 5.464   | 407.571 | < 2e-16 ***  |
| size                | 1   | 1.288  | 1.288   | 96.086  | < 2e-16 ***  |
| shape:rotation      | 12  | 1.934  | 0.161   | 12.023  | < 2e-16 ***  |
| shape:size          | 4   | 0.596  | 0.149   | 11.108  | 8.38e-09 *** |
| rotation:size       | 3   | 0.693  | 0.231   | 17.244  | 6.71e-11 *** |
| shape:rotation:size | 12  | 0.510  | 0.043   | 3.173   | 0.000185 *** |
| Residuals           | 920 | 12.333 | 0.013   |         |              |

---  
 Signif. codes: 0 '\*\*\*' 0.001 '\*\*' 0.01 '\*' 0.05 '.' 0.1 ' ' 1

(a) Results of an ANOVA comparing the lift coefficient values, see figure 4.10a.

|                     | Df  | Sum Sq | Mean Sq | F value | Pr(>F)       |
|---------------------|-----|--------|---------|---------|--------------|
| shape               | 4   | 8.913  | 2.228   | 105.600 | < 2e-16 ***  |
| rotation            | 3   | 27.130 | 9.043   | 428.564 | < 2e-16 ***  |
| size                | 1   | 1.857  | 1.857   | 87.981  | < 2e-16 ***  |
| shape:rotation      | 12  | 3.479  | 0.290   | 13.739  | < 2e-16 ***  |
| shape:size          | 4   | 0.890  | 0.223   | 10.548  | 2.33e-08 *** |
| rotation:size       | 3   | 1.050  | 0.350   | 16.588  | 1.67e-10 *** |
| shape:rotation:size | 12  | 0.699  | 0.058   | 2.762   | 0.00106 **   |
| Residuals           | 920 | 19.413 | 0.021   |         |              |

---  
 Signif. codes: 0 '\*\*\*' 0.001 '\*\*' 0.01 '\*' 0.05 '.' 0.1 ' ' 1

(b) Results of an ANOVA comparing the lift forces scaled by shell volume values, after a linear regression against flow speed, see figure 4.9c.

|                     | Df  | Sum Sq | Mean Sq | F value | Pr(>F)       |
|---------------------|-----|--------|---------|---------|--------------|
| shape               | 4   | 248.54 | 62.14   | 272.982 | < 2e-16 ***  |
| rotation            | 3   | 129.93 | 43.31   | 190.268 | < 2e-16 ***  |
| size                | 1   | 21.72  | 21.72   | 95.428  | < 2e-16 ***  |
| shape:rotation      | 12  | 154.19 | 12.85   | 56.450  | < 2e-16 ***  |
| shape:size          | 4   | 42.10  | 10.52   | 46.237  | < 2e-16 ***  |
| rotation:size       | 3   | 3.97   | 1.32    | 5.809   | 0.000621 *** |
| shape:rotation:size | 12  | 6.21   | 0.52    | 2.272   | 0.007690 **  |
| Residuals           | 920 | 209.41 | 0.23    |         |              |

---  
 Signif. codes: 0 '\*\*\*' 0.001 '\*\*' 0.01 '\*' 0.05 '.' 0.1 ' ' 1

(c) Results of an ANOVA comparing the drag forces scaled by shell volume values, after a linear regression against flow speed, see figure 4.9c.

**Figure D.5:** Comparison of the relative effects of shape, rotation, and size, as well as all interactions on the lift forces of the fluid dynamics simulations. For visualisations of the variation related to shape and rotation see figure 4.10a-c.

```

                Df Sum Sq Mean Sq F value    Pr(>F)
shape            4  50.48  12.620 269.389 < 2e-16 ***
rotation        3  70.77  23.590 503.543 < 2e-16 ***
size            1  12.06  12.061 257.442 < 2e-16 ***
shape:rotation  12   7.54   0.628  13.408 < 2e-16 ***
shape:size      4   1.61   0.403   8.597 8.21e-07 ***
rotation:size   3   2.75   0.916  19.543 2.74e-12 ***
shape:rotation:size 12   2.69   0.224   4.785 1.20e-07 ***
Residuals     920  43.10   0.047
---
Signif. codes:  0 '***' 0.001 '**' 0.01 '*' 0.05 '.' 0.1 ' ' 1

```

**Figure D.6:** ANOVA results for the lift to drag force ratio using the factors shape, rotation, and size, as well as all interaction terms. For visualisation of the variation related to shape and rotation see figure 4.10d.

```

                Df Sum Sq Mean Sq  F value Pr(>F)
shape            4  772.9  193.21 36902.51 <2e-16 ***
rotation        3   22.8   7.59 1450.43 <2e-16 ***
shape:rotation  12    2.4   0.20   38.76 <2e-16 ***
Residuals     940    4.9   0.01
---
Signif. codes:  0 '***' 0.001 '**' 0.01 '*' 0.05 '.' 0.1 ' ' 1

```

(a) Results of an ANOVA comparing the residual drag coefficient values for 3D printed shell models after a linear regression against flow speed, see figure 4.12a.

```

                Df Sum Sq Mean Sq  F value Pr(>F)
shape            4  772.9  193.21 36902.51 <2e-16 ***
rotation        3   22.8   7.59 1450.43 <2e-16 ***
shape:rotation  12    2.4   0.20   38.76 <2e-16 ***
Residuals     940    4.9   0.01
---
Signif. codes:  0 '***' 0.001 '**' 0.01 '*' 0.05 '.' 0.1 ' ' 1

```

(b) Results of an ANOVA comparing the residual drag coefficient values for real shells after a linear regression against flow speed, see figure 4.12b.

**Figure D.7:** ANOVA tables for the drag coefficients in the flume experiment. Visualisations can be found in figure 4.12.

## Appendix E

# Quantitative measures and 3D shell models reveal interactions between bands and their position on growing *Cepaea* shells

Presented in its accepted form for publication.

Jackson, H. J., Larsson J., and Davison A. (2021). Quantitative measures and 3D shell models reveal interactions between bands and their position on growing *Cepaea* shells. *Ecology and Evolution*, 11(11): 6634-6648. doi: 10.1002/ece3.7517.

H. J. Jackson<sup>1\*</sup>, J. Larsson<sup>2</sup>, A. Davison<sup>1</sup>

<sup>1</sup>School of Life Sciences, University of Nottingham, Nottingham, UK

<sup>2</sup>Department of Animal and Plant Sciences, University of Sheffield, Sheffield, UK

\*Correspondence: hannah.jackson1@nottingham.ac.uk

**Contributions:** H.J. and A.D. conceptualised the project and curated the data. J.L. created the 3D analysis software. All authors contributed to the formal analysis and methodology. H.J. produced the original draft, and all authors provided input on subsequent versions.

## Abstract

The nature of shell growth in gastropods is useful because it preserves the ontogeny of shape, colour and banding patterns, making them an ideal system for understanding how inherited variation develops and is established and maintained within a population. However, qualitative scoring of inherited shell characters means there is a lack of knowledge regarding the mechanisms that control fine variation. Here, we combine empirical measures of quantitative variation and 3D modelling of shells to understand how bands are placed and interact. By comparing five-banded *Cepaea* individuals to shells lacking individual bands, we show that individual band absence has minor but significant impacts upon the position of remaining bands, implying that the locus controlling band presence/absence mainly acts after position is established. Then, we show that the shell grows at a similar rate, except for the region below the lower-most band. This demonstrates that wider bands of *Cepaea* are not an artefact of greater shell growth on the lower shell; they begin wider and grow at the same rate as other bands. Finally, we show that 3D models of shell shape and banding pattern, inferred from 2D photos using ShellShaper software, are congruent with empirical measures. This work therefore establishes a method that may be used for comparative studies of quantitative banding variation in snail shells, and extraction of growth parameters and morphometrics. In the future, studies that link the banding phenotype to the network of shell matrix proteins involved in biomineralization and patterning may ultimately aid in understanding the diversity of shell forms found in molluscs.

## Introduction

The nature of shell growth in gastropods is useful because it preserves the ontogeny of shape, colour and banding patterns, making them an ideal system for understanding how inherited variation develops and is established and maintained within a population (Johnson et al., 2019). This is particularly beneficial when considering animal colouration and patterning, both of which have been critical in understanding the key principles of evolution (Cuthill et al., 2017, Richards et al., 2013).

Historically, the foremost gastropod species in understanding colour polymorphism and band patterning has been the European land snail *Cepaea nemoralis*, and its sister taxon *C. hortensis* (Jones et al., 1977, Ożgo, 2011), partly due to their ease of collection. Also useful has been the ability to record morph frequencies, whether yellow, pink or brown, with varying numbers of bands, from zero to five (Cain & Sheppard, 1950, Cain & Sheppard, 1952, Jones et al., 1977). A further reason is the apparent simplicity of the Mendelian inheritance of the shell colour and banding loci, many of which are inherited together in a 'supergene' (Cook, 1967, Jones et al., 1977). As a result, studies on the shell polymorphism of the snail *Cepaea* have played a crucial role in establishing the role of natural selection in maintaining morphological variation, with the genus becoming a pre-eminent model for ecological genetics, alongside the peppered moth (Cook & Saccheri, 2013, Grant et al., 1996, Majerus et al., 2000, Walton & Stevens, 2018).

In the present day, one of the continuing benefits of working with *Cepaea* is an ability to compare the frequencies of shell morphs in historic collections against modern day samples, to infer the potential impact of natural selection and/or drift in changing shell morph frequencies (Cameron, 1992, Arthur et al., 1993, Cook et al., 1999, Ożgo & Schilthuizen, 2012, Cameron et al., 2013, Ożgo et al., 2017). Of particular use, the "Evolution Megalab" project digitised a large set of 20th century samples. These records, and others deposited in museums, are now being used with modern surveys to produce an increasing number of comparative papers (Silvertown et al., 2011, Cameron & Cook, 2012, Worthington et al., 2012, Cameron & Cook, 2013). New studies on the genetics and genomics (Richards et al., 2013, Mann & Jackson, 2014, Kerkvliet et al., 2017, Saenko et al., 2021) mean that *Cepaea*

snails are poised once again to become a powerful system. The findings from this single genus should lead the way in understanding the diverse variety of shell patterns that are found in the wider group of snails and molluscs to which they belong.

Unfortunately, a traditional focus on the qualitative scoring of the shell characters of *Cepaea* has resulted in a lack of knowledge regarding the mechanisms that control fine variation. For example, the ground colour of *Cepaea* has traditionally been grouped into one of three categories, yellow, pink, or brown. This was necessary for field-based classifications, but recent spectroscopy and psychophysical modelling of avian visual systems has shown that the colour variation is continuously distributed, albeit around three clusters which roughly correspond to the qualitative colour groupings of yellow, pink and brown (Davison et al., 2019). Although further studies are necessary, the observation of continuous variation in colour is intriguing because the traditional theory is that, provided observed variation results from frequency-dependent selection, the underlying supergene that determines colour has evolved to prevent phenotypes from “dissolving” into continuous trait distributions. These findings raised questions about the nature of the selection that acts upon the polymorphisms.

With interest in quantitative variation in *Cepaea* colour (Davison et al., 2019), it seems appropriate to reconsider variation within and between banding patterns, which has received little attention since Rotarides (1926), who established that the proportion of shell covered by band is correlated with variation within habitat types. This, and subsequent work using similar methods (Ozgo & Komorowska, 2009) have tended to focus on the proportion of the shell that is banded, and the potential effect on natural selection (Neiber & Hausdorf, 2015, Neiber et al., 2016). How the position and widths of bands might be established during shell growth has been neglected, but could provide useful insight into how banding patterns vary within individual shells over time.

In banding notation (Cain, 1988), bands are numbered 1 to 5 from the top of the shell down, with modifications to recognise band fusions and interruptions (**Figure 1a**). A five-banded snail with bands fused on the lower part of the shell is thus 123(45), and a mid-banded is 00300. However, as with colour, the qualitative scoring of bands masks complexities. For example, a five-banded individual may possess five wide bands which are close to fused with little ground colour visible between them, or it may possess five narrow bands, with considerable visible colour between the gaps. These individuals would be scored as having the same phenotype, yet the large differences between them may affect thermoregulation, visibility to predators and resistance to crushing forces (Staikou, 1999, Cook, 2008, Ozgo & Schilthuizen, 2012, Rosin et al., 2013, Surmacki et al., 2013). Bands are deeply integrated into the shell matrix, unlike colour which has no structural elements (Budd et al., 2014, Williams, 2017). In *Cepaea*, bands are present in all three layers of shell, and their presence in the central calcareous prismatic layer is likely responsible for the increased crushing resistance displayed by banded shells relative to their unbanded counterparts (Rosin et al., 2013).

How is band position determined? The main shell loci have been characterised but not yet identified. A locus *B* determines band presence/absence, locus *U* suppresses all bands except band 3 (to make a mid-banded snail 00300), and another locus suppresses bands 1 and 2. Several other loci, including spread band *S* and punctate *I* (or ‘interrupted’) loci modify the nature of the band phenotype. Individuals may also have unpigmented bands, a phenotype known as hyalozonate, where bands are present and visible, but lack the usual pigmentation, suggesting that whilst these processes may interact, the laying down of bands and the pigmentation of these bands occur independently of one another. There are also likely other loci, or environmental factors which act during growth, that exert a multifactorial effect on the phenotype, including modifiers of band width, band fusion, band colour, suppression of individual bands, and the timing of band expression (e.g. bands only

on last whorl). However, these loci are not useful in understanding how bands are placed, because they mainly specify presence/absence, or character, rather than position.

To begin to understand the genetic mechanisms underpinning pattern variation in *Cepaea*, a first step is to re-evaluate the description of the banding phenotype by quantification of variation in banding patterns both between and within phenotypes, and throughout shell growth. Here, we combine empirical measures of quantitative variation within and between bands, and 3D shell models, to understand how bands are placed and interact with one another. By comparing fully banded individuals against shells lacking individual bands, we infer that the locus that controls band absence mainly acts after band position is established. We also show that the lower bands are not wider as an artefact of greater shell growth on the lower shell. They grow at the same rate as all other bands, but are wider from their first formation. Finally, we show that the same measures may be taken from a photograph, and a 3D model inferred. Validation of these methods for shell pattern quantification provides a baseline for future analysis of shell patterning and ornamentation in gastropods. As we move towards identifying the genes involved in setting the patterns, these findings may together be used to develop a model for band placement in snail shells, set in the general context of understanding shell growth parameters.

## Materials and Methods

### *Snails*

Individuals of both species, *Cepaea nemoralis* and *C. hortensis*, were collected by volunteers and on fieldtrips across Europe. Snails were euthanised by freezing at  $-80^{\circ}\text{C}$  upon arrival at the University of Nottingham, and subsequently thawed and bodies extracted from their shell.

Shell banding and colour phenotypes were first scored qualitatively, using the scheme described in Murray (1963), with some minor deviations where necessary (Davison et al., 2019). The main phenotypes of importance to this study were five-banded, 12345, and mid-banded, 00300 (**Figure 1b**). These were used to understand the impact of band absence on the position and width of band 3. In a single Spanish population, shells lacking the second band, phenotype 10345, were relatively common. This population also included some shells in which band 2 was only present in the very last part of the shell, just before the lip. Here, we describe this feature as “.”, distinct from the mark used to represent punctate “:.” e.g. 1.345. These shells were used to understand the impact of the absence of band 2, and also a partial suppression of band 2, upon the positions of the remaining bands.

### *Shell measurements*

To measure the positions and widths of the bands on the *Cepaea* shells, a ~1 mm strip of electrical tape was wrapped around the last whorl of individual adult shells, from the suture to the umbilicus (**Figure 1a**). The tape was attached parallel to any growth lines, and placed ~3 mm back from the shell lip, necessary because banding phenotype often differs close to the lip. Band start and end position was then recorded by marking the tape with a super-fine permanent marker under a dissection microscope. Tape was removed from the shell, and the distances between marks measured using Vernier callipers under a dissection microscope.

The individual measures of band position were converted into proportions, standardising against the distance between the suture and the umbilicus, to enable comparison between shells of different sizes. The mid-point of the band was used to define band position, with band width considered separately. Individual measures were not used if

bands were ill-defined or fused. Shell height, width and weight were also measured, to enable tests for associations with size, and shell shape (width/height).

#### *Interactions between bands and band-gaps*

We first checked whether other shell parameters influence band position and width. Statistical models were created, using height, weight, shape, and band position and width data, in R version 3.6.2. All full models included fixed effects of shell shape (obtained by dividing shell height by shell width), shell height (used as a proxy for shell size), and shell weight (as a proxy for shell thickness), as well as a random effect of population to remove this as a confounding variable. For model selection, a full set of models including every combination of fixed effects was generated. These models were ranked according to their Akaike Information Criterion (AIC). From a full model set, models with a value within 2 AICs of the best fitting model (value closest to zero) were considered to be equally supported, and so these were averaged. Full coefficients are quoted in the final averaged model, meaning that any terms not appearing in a given component model were assigned a coefficient of zero before averaging.

The null hypothesis was that if the deposition of pigment in each band is independent of others, then absence of individual bands in the adult shell will not impact upon the position and width of other bands. Mann-Whitney U tests were therefore performed to determine whether the position and width of band 3 varied in mid-banded individuals (00300) compared with five-banded individuals (12345) in *Cepaea nemoralis*. Similarly, multivariate Kruskal-Wallis tests, followed by Dunn's pairwise tests with Benjamini-Hochberg adjustment, were carried out to determine whether partial or complete absence of band 2 impacted upon the position and width of the remaining bands.

Bands are established in juvenile snails, usually becoming progressively wider with each whorl of the shell. Band width is necessarily constrained by the edges – the point of contact with the suture and towards the umbilicus – and likely also interactions with other bands, and the gaps between bands. Therefore, to understand how bands grow in width and interact with one another, the edges, and the gaps between bands, we tested all possible correlations between individual band width and band-gap, focussing on the width of the gap immediately above or below each band. If bands increase in width together, a positive relationship will result between focal band width and the widths other bands at the level of an individual snail. The corollary was an expectation for a positive relationship between individual band-gap width and other band-gap widths, and a negative relationship between band width and band-gap width.

#### *Comparison between species and colour*

Differences in the position and width of each band between species were tested using five-banded snails and generalised linear mixed effects models (GLMMs). Each band was modelled separately. Species was fitted as the sole fixed factor, with a random effect for population in each model. The fixed term of species was removed in each model, testing the effect of deletion by comparison of Akaike Information Criterion (AIC). The AIC of the GLMM including the fixed effect was compared with that of a generalised linear model without the random terms to provide an approximate test of the importance of population, as per Davison et al. (2019). As genes for colour and banding patterns of shells may be in linkage disequilibrium (Cook, 2005), GLMMs were repeated with colour as the sole fixed factor.

#### *Shell growth and use of 3D models*

Bands 3, 4, and 5 on a *Cepaea* shell are typically wider than bands 1 and 2. One explanation is that the wider bands are simply an artefact of greater relative growth on the lower part of

the whorl. Therefore, two complementary methods were used to understand how band width varies with growth of the final whorl.

Shell segments were removed with a small circular saw, in 90° increments until an entire whorl had been removed, at each of five points, measurements of band width and position were taken as described above. In addition, shells were mounted on a flat surface with their apertures facing up, columella parallel to the surface. A photograph was also taken at each stage, ensuring that all bands were visible around the aperture. An updated version of the ShellShaper software (<https://github.com/jslarsson/ShellShaper>; Supplementary Methods) was used to build 3D models of shells, including the positions of bands, obtained by user-defined landmarks from each of the 2D images as per Larsson et al. (2020). Models were based on three-dimensional logarithmic helicospiral growth, although using only circular apertures and no shell thickness. Band position and width were defined for a predetermined number of bands on any given shell. Widths and positions were then extracted from the model and analysed.

To determine whether growth rate was influenced by the position on the shell, GLMMs were performed on mid-banded and five-banded shells, with the response variable of growth rate, and a fixed effect of shell section, with a random factor of ID included to mitigate the potential differences between individuals. Least square means with Tukey adjustments for multiple comparisons were performed to allow direct comparison of shell areas to one another.

Comparative analysis was performed on the two methods using a Bland-Altman plot to analyse agreement between the two methods, using the average of paired measurements of five banded individuals for reference. Differences in measurements from each method at constant locations and stages of growth across shells were analysed, and the measurement bias and 95% upper and lower confidence intervals found.

## Results

Band measurements were taken for 440 individuals, 271 *Cepaea nemoralis* and 169 *C. hortensis*, across 40 populations, distributed throughout the UK and mainland Europe (**Supplementary Table 1**). Shell shape, height, or weight did not impact upon the relative position or width of any of the five-bands (**Tables 1, 2**). In each of the 10 final averaged models generated, one for each position and width of each band, no predictors were significant. Ten similar models were generated to test for associations of band position and width with shell ground colour. The sole fixed factor of colour was not a significant predictor of variance in any of the 10 models.

### *Effect of missing bands*

Mann Whitney U tests demonstrated that, in *Cepaea nemoralis*, when other bands are absent, the mid-band was shifted towards the top of the shell, albeit only ~0.9% closer ( $W = 6867.5$ ,  $P = 0.0107$ ; **Figure 2a**). In comparison, the mean difference between first and second measures of the same band was 0.17%, ranging between 0.004% and 0.7%. The absence of other bands did not impact upon the variability in position of the band of a mid-banded individual; Kolmogorov-Smirnov tests demonstrated that distributions were equal when shifted to centre around a single mean, suggesting that variance in band position remained constant in both phenotypes ( $D=0.08$ ,  $P=0.9$ ). The width of the bands also did not change in the absence of other bands ( $W = 8831$ ,  $P = 0.7$ ; **Figure 2a**). Gaussian finite mixture modelling of the distribution of widths indicated that the width of band 3 in five-banded individuals is not multimodal. Both the best model (X, univariate normal, BIC -295.4;  $P = 0.04$  compared to second best model) and the next best models resolved a single

cluster. As with band position, the distribution of band widths in mid-banded snails did not differ from the distribution of individuals with five-bands.

Similarly, Kruskal-Wallis tests indicated that when band 2 was missing or partially suppressed (**Figure 2b**), both bands 1 and 3 were in different positions across the three phenotypes ( $H = 18.05$ ,  $df = 2$ ,  $P = 0.0001$ ;  $H = 17.1$ ,  $df = 2$ ,  $P = 0.0002$ ). Specifically, bands 1 and 3 were ~2.4% closer to each other when band 2 was absent (**Figure 2b**). Pairwise Dunn's tests with Benjamini-Hochberg adjustments indicate that this difference was only present between the 12345 and 10345 phenotypes for both bands one and three ( $Z = -4.1$ ,  $P = 0.000007$ ;  $Z = -4.2$ ,  $P = 0.0001$ ), with the partially suppressed phenotype intermediate and non-significantly different from the bands 1 and 3 in 10345 (10345;  $Z = -1.4$ ,  $P = 0.2$ ;  $Z = 1.9$ ,  $P = 0.06$ ), and 12345 ( $Z = 0.6$ ,  $P = 0.5$ ;  $Z = 0.09$ ,  $P = 0.9$ ). Band 4 was in a consistent position, but band 5 was shifted upward, by ~1.8%, in the absence of band 2 ( $Z = -3.0$ ,  $P = 0.0009$ ); band 5 was in the same position in shells of phenotype 12345 and 1.345.

Kruskal-Wallis tests indicated that band 1 did not differ in width across the three phenotypes ( $H = 1.2$ ,  $df = 2$ ,  $P = 0.6$ ), whereas band 3 width did differ ( $H = 23.1$ ,  $df = 2$ ,  $P = 0.00001$ ). Pairwise Dunn's tests with Benjamini-Hochberg adjustments indicated that there was no difference between any of the phenotypes in band 1 ( $Z = 1.02$ ,  $P = 0.3$ ;  $Z = 1.1$ ,  $P = 0.3$ ;  $Z = -0.1$ ,  $P = 0.9$ ). The width of band 3 differed between 12345 and 10345 phenotypes ( $Z = -4.8$ ,  $P = 0.000005$ ), with band 3 narrower when band 2 was absent. No difference in the width of band 3 was observed between the other phenotypes ( $Z = 2.3$ ,  $P = 0.06$ ;  $Z = 0.05$ ,  $P = 0.96$ ). The width of band 2 varied significantly between the partially suppressed phenotype and 12345 individuals ( $H = 20.6$ ,  $P = 0.000006$ ).

#### *Interactions between bands and band-gaps*

When individual bands were larger, the corresponding gaps above the band tended to be smaller (**Figure 3**), with band 4 showing the strongest relationship ( $R = -0.5$ ,  $P < 2.2e-16$ ), and band 5 the weakest ( $R = -0.2$ ,  $P = 0.005$ ). The same relationship was found between the individual bands and the gap width below (**Figure 3**); except that band 2 showed the strongest relationship ( $R = -0.6$ ,  $P < 2.2e-16$ ) and band 1 did not show any correlation with the band below ( $R = -0.01$ ,  $P = 0.8$ ).

In testing all comparisons between band widths and band-gap widths, most relationships were in the expected direction, except for some of the gap-gap comparisons (**Figure 4**); there were unexpected negative correlations between gaps 1/2 ( $R = -0.2$ ,  $P = 0.004$ ), 1/5 ( $R = -0.2$ ,  $P = 0.003$ ), 2/6 ( $R = -0.3$ ,  $P = 0.000003$ ), 3/6 ( $R = -0.2$ ,  $P = 0.003$ ), and 5/6 ( $R = -0.5$ ,  $P < 2.2e-16$ ).

#### *Comparison between species*

The bands had broadly similar positions and widths in the two species, with some minor, significant differences in magnitude (**Figure 5**). In *C. nemoralis*, band 1 was ~1% towards the base of the shell, whereas band 5 was ~3% closer to the top ( $X^2 = 4.4$ ,  $df = 1$ ,  $P = 0.04$ ;  $X^2 = 12.6$ ,  $df = 1$ ,  $P = 0.0004$ ). *C. nemoralis* individuals also had slightly narrower bands in positions 1 and 4 compared with *C. hortensis* ( $X^2 = 18.05$ ,  $df = 1$ ,  $P = 0.00002$ ;  $X^2 = 21.8$ ,  $df = 1$ ,  $P = 0.00003$ ).

#### *Shell growth and use of 3D models*

Bland-Altman plots of paired shell measurements (**Figure 6**) showed that neither the tape or computer-based method resulted in measurements which were consistently larger or smaller than the other, thus, the differences in the plots shows data points scattered evenly above and below zero. There was no consistent bias between the two methods (Bias = 0.005), and 95% of the data fell between the upper and lower limits of agreement of -2.04 and 2.05. This confirmed that whilst data is variable, the model is able to reproduce the 3D

shape from a 2D photo, and also, that ShellShaper is able to extract band-measurement data from a 2D image, whilst retaining information revealed by manual measurements.

Models fitted with fixed effect of shell region, and random effects for distance along the last whorl, and individual, demonstrated that regions of shell in both mid-banded and five-banded shells grow at different rates (Figure 6;  $X^2 = 119.7$ ,  $df = 10$ ,  $P < 0.0001$ ;  $X^2 = 84.9$ ,  $df = 2$ ,  $P < 0.0001$ ). Pairwise comparisons show that this difference is exclusively between all shell regions and the region between the last band and the umbilicus. The bottommost area grows at a faster rate than other areas of the shell, which all increase in size at an equal rate throughout growth (Tables 3, 4). The relative proportions of the shell covered by each region changed along the whorl, as the lowermost region of the shell expanded more rapidly than the others. All other shell regions remained at equal proportions relative to one another throughout growth (Figure 7). Models were repeated with distance along the last whorl as the sole fixed factor, with random effects for shell region and individual. These demonstrated that there is no difference in growth rates in areas of the shell across the length of the last whorl in five banded or mid banded snails (mid-banded: chi-squared = 0,  $df = 10$ ,  $P = 1$ ; five-banded: chi-squared = 0,  $df = 10$ ,  $P = 1$ ). Expansion per quarter whorl in every shell section remains constant throughout the growth of the entire last whorl.

#### *Allometric shell growth*

In order to produce the convex spires seen in globose species such as *Cepaea*, allometric growth is necessary. The type of allometry needed for this requires an increase in height of a complete whorl being greater than the increase in width of the same whorl. To confirm the required type of allometry was present in growing shells, a basic allometry test was used to determine whether that the growth in width was smaller than the growth of the height in the shells measured with Shell Shaper. Wilcoxon Signed-rank tests indicate that the increase in whorl height is greater than the increase in whorl width ( $V = 465$ ,  $P = 0.00000009$ ), confirming the allometric growth parameters necessary to produce a convex spire.

## **Discussion**

In the past, the banding phenotype of *Cepaea* snails has typically been scored as a qualitative character, even though shells with the same number of bands may have a quite different outward appearance. Here, we developed a method to describe quantitative variation in the banding patterns of both species, and then use these findings to test the interactions within and between bands and other shell characters. Broadly, we found that the precise position of bands depends upon the presence or absence of other bands, although the size of the effect is small. These findings give a first hint of the pathway that defines the positions and pigmentation of bands in the shell. By comparing the method with inferences from a 3D model, we show that the same quantitative measures may be applied to a 2D photo of a shell. Overall, the findings provide a starting point for exploration of how bands are placed in *Cepaea*, and the origins of fine variation in banding pattern.

#### *Pigmentation of individual bands is independent*

If the deposition of pigment in each band is independent of other bands, then one argument is that absence of individual bands in the adult shell should not impact upon the position or width of other bands. However, if there are fewer bands, then the absolute position of the remaining bands becomes of less importance, provided they do not overlap. Band position might then vary slightly, or the width might show greater variation in the absence of other bands. For example, a predator will tend to see a single mid-band, irrespective of the precise position on the shell. In comparison, in a five-banded snail, the mid-band must be distinct

from the other bands (unless there is a genetically coded band fusion), which reduces the range of possible positions.

In comparisons between the position of the third band in mid-banded and five-banded shells, we found that the band positions were broadly the same. This was also true of comparisons between the positions of the first and third bands in individuals where the second band was present or absent. Bands occupied more or less the same shell space as the corresponding band in a fully banded snail and did not cross over into the space which the other bands normally occupy. Yet, there were some small but significant differences in position. For example, the second and third bands were typically found at 16.6% and 27.0% of the distance from the suture (**Figure 2 inset**); in mid-banded snails, the third band was slightly closer, 26.1%, to the suture. Similarly, the first and third bands were typically found 9.1% and 27.0% (as before) from the suture. When band 2 was missing, bands 1 and 3 were closer together, 10.2 % and 25.6% from the suture. Shells with a band 2 that was only present on the last part of the shell were intermediate for the position of bands 1 and 3. In comparison, we did not find any difference in the widths of any of the bands when other bands were absent, nor any evidence that the differences are influenced by shape or ground colour of the shell. These results therefore show that while the approximate position of the bands is the same, there is a very limited degree of lability in their placement that is contingent upon the presence or absence of other bands.

There are two main explanations for these findings. The first is that the position of all five bands is established and maintained early in shell development, even in the absence of individual bands. The spatial signal for the five bands is likely present in a molecular sense, but the pigmentation is lacking for individual bands. This would imply that the locus for band absence acts late in the pathway that establishes bands. An alternative explanation is that individual band positions are established independently of each other, such that if one band is not present, then this does not impact upon the position of others. In this case, individual band position would have to be defined relative to a fixed character, such as the suture. In our opinion this second explanation is less credible because we found evidence that the bands do interact, at least to a small degree. Bands differed slightly in position when other bands are absent, including evidence that even late stage band expression can interfere with the position (**Figure 2**). More generally, if bands do not interact, it is difficult to understand why instances of mis-positioning of bands were not more common. It should also be noted that an analysis of hyalozonate patterns similar to those displaying fully pigmented bands could shed light on the relationship between pattern establishment and pigmentation. Does ground colour pigmentation in band position show similar variations in position and widths as the fully pigmented bands? Or, is the position of hyalozonate banding more tightly controlled, serving as a template for pigment adhesion, allowing an amount of variation?

To further explore how bands are placed and interact with one another and shell edges, we investigated correlations between the band widths and the gaps between bands. This was also partly motivated by wanting to understand the reason that bands 3, 4 and 5 are consistently wider than bands 1 and 2. The temptation might be to put the differences down to natural selection, but the default explanation must be non-adaptive. For example, perhaps the top-most bands are narrow because they are constrained by the suture edge. Alternatively, the bottom-most bands might be wider because their expansion is correlated with growth of the expanding whorl on the lower part of the shell, and band widening is simply an artefact of the deposition of new shell material.

Broadly speaking, the results showed that bands expand in width at the same rate. Where bands were wider in adult shells, the corresponding gap above and below each band was narrower (**Figure 3**). There were some unexpected slight negative correlations between the first gap (next to the suture) and the first band with other band-gaps, as well as negative

correlations between the last gap (next to the umbilicus) and some other band-gaps. As the negative correlations mainly involved edges, then perhaps the band-gaps at the edges indirectly exert some effect to maintain a narrow gap between the band and the edge?

Moreover, the projections that were taken from manual measurements (**Figure 3**) and those inferred from 3D models (**Figure 7**) confirmed that all of the regions of the shell expand at the same rate, with the exception of the lowermost part of the shell, the final band-gap before the umbilicus (**Figure 7, Tables 3, 4**). The widths of the bands are significantly correlated for bands 3, 4 and 5 ( $R = -0.2, -0.3, -0.4$ , all  $P < 0.001$ ; **Figure 4**) – as an individual band gets wider, then the last band-gap gets proportionately narrower – but there is no such relationship for bands 1 and 2 ( $R = -0.01, -0.1$ , neither significant). Overall, the relative difference between bands is unexpectedly small.

Although all bands and the gaps between them become progressively wider, the last gap (i.e. the gap between the end of the final band and the umbilicus) expands at a faster rate than the rest of the whorl. This implies that the lower bands are not simply wider as an artefact of shell material deposition during growth, but rather that the lower bands start wider, and so remain wider throughout growth. The consistency of growth rates across all bands, and therefore the gaps between them, suggests that the widths of all bands are under similar mechanisms of control/constraint, irrelevant of their position on the shell. The increased growth rate of the lowermost part of the shell is perhaps simply due to the relative downward movement of the aperture in the allometric growth necessary to produce shells with a globose spire, such as *Cepaea*. It is perhaps also likely that the final band-gap becomes larger with shell growth due to a change in the generating curve in the final growth stages of the shell, where the angle of the aperture of an adult shell is further from vertical than in juveniles.

#### *3D models to infer band position and shell shape parameters*

The initial method used to measure bands used electrical tape and a dissecting microscope. This means that it was straightforward, but also laborious, difficult to scale, and limited in the data that was collected. These issues were resolved using ShellShaper software. By taking a 2D photo of a shell with the aperture facing upwards, ShellShaper was used to take the same band position measures, and also to make 3D reconstructions of the shell (**Figure 7**). Whilst the measurements were varied (95% limits of agreement of ~2% in either direction, there was very limited bias between the two methods, suggesting that neither method consistently under or overestimated the size of a shell segment. Whilst larger sections of the shell (i.e. those towards the umbilicus) appear to produce more variable results when comparing the two methods (**Figure 6**), this may simply be due to the very different nature of the two methods, and inevitable slight differences in exact measurement position or angle of an area which grows more rapidly than the rest of the shell. The overarching patterns remain constant between the two methods, despite small discrepancies in exact measurements of individual segments.

Using ShellShaper has the advantage that the method may be applied to species with smaller shells, and those with more bands than *Cepaea*. The method also generates a shell model that can be used for further analyses, including the extraction of growth parameters that will allow for investigations of the similarities and differences within and between many different species of gastropods. Using Shell Shaper for such comparisons would allow high-throughput data collection, allowing the collection of much larger datasets in both comparative and species specific studies. Whilst Shell Shaper allows comparison of bands in a context similar to traditional geometric morphometrics, the version used here works on the assumption of circular apertures, limiting its use in understanding how band patterns might change in relation to the shape of the aperture or other shell characters. Continual development and increasing sophistication of 3D models produced by

ShellShaper, means that such analysis with the use of varying aperture shapes is a possibility in the future. Complementary methods devised by others (e.g. Liew & Schilthuizen, 2016) may also be used for the same function, and be more suitable, especially when there is great variability in shell form. Other methods require complex, time consuming, and expensive techniques, such as CT scanning. Shell Shaper has the advantage that a 3D structure can be generated from a single 2D photograph of the shell, which allows for relatively high throughput. Whilst other methods include options such as producing models with non-circular apertures and external shell ornamentation, the ease of inclusion of analysis of banding position and size in ShellShaper provides added advantages not present in other methods.

#### *Inter-species variation*

The banding patterns were broadly similar in the two species of *Cepaea*, albeit with some small differences. For example, bands 1 and 4 were narrower in *C. nemoralis*, and band 1 was closer to band 2, and band 5 closer to band 4. These results indicate that control of band deposition mechanisms are only subtly diverged in the two species. Such slight differences in phenotype are unlikely to be detectable to avian predators, although this requires experimental confirmation (Delhey et al., 2015, Davison et al., 2019). Understanding the variation, or lack thereof, present in these banding patterns does however provide a starting point in establishing the underpinning genetic mechanism, including in relation to other species.

#### *Reaction Diffusion Mechanism*

The underlying mechanisms behind both the formation, and the control of the position and widths of the bands, in *Cepaea* remain unexplored. Although the reaction-diffusion model has been hypothesised to be of importance in pattern formation in other organisms (Kondo, 2002, Gravan & Lahoz-Beltra, 2004), the interpretation of the models underlying shell pigmentation is limited to mathematical modelling of hypothetical signalling events (Budd et al., 2014). The models assume that pigmentation is caused by localised excitation and inhibition operating along a line of cells at the mantle edge during biomineralisation. It is not currently known whether the cells involved in pigment secretion are organised in this manner. The precise identity of the molecules involved in molluscan pigmentation also remains relatively uncertain (Budd et al., 2014). To date, there is no definitive evidence that the banding in *Cepaea* is under the control of the reaction-diffusion model.

In several land snail species, including *Cepaea*, the same pigmentation patterns can be observed on both the shell and the mantle (Emberton, 1963). The presence of bands on the mantle suggests that the system controlling pigmentation may not be controlled by the simple “line of cells” as first assumed. It should be noted also that physical cues in marine gastropod shells possessing varices (thickened protrusions of shell) do not appear to be the main mechanism used to position new shell structures. Instead, it has been suggested that positional information of these structures is created by a Turing-like system, but with previous shell structures providing some fine-tuning feedback (Webster & Palmer, 2019).

Whilst it may be hypothesised that Turing’s reaction-diffusion model plays a role in the formation of shell patterns in molluscs, identification of the genes is a first step before testing whether the interacting substances are necessary in defining the patterns. We envisage two converging routes by which this may be made possible, either taking a gene mapping and pattern-led approach (Cossins et al., 2006, Harper et al., 2011, Peichel & Marques, 2017), or else by comparing spatial gene expression (Landgrebe et al., 2002, Ståhl et al., 2016, Adamson et al., 2017).

It will certainly be interesting to investigate gene expression in relation to the wide diversity of shell phenotypes. For example, it is conceivable that unbanded *Cepaea* still

contain the spatial molecular markers that correspond to bands, but that they are not pigmented – if that is the case then any subtractive method (comparing gene expression in banded versus unbanded snails) will not work. To date, proteomic and transcriptomic studies have begun to identify both novel and co-opted ancient genes involved in biomineralisation and shell deposition (Clark et al., 2010, Jackson et al., 2010, Joubert et al., 2010, Marie et al., 2013, Mann & Jackson, 2014), which may ultimately assist in elucidating the formation and maintenance of variation within and between banding phenotypes in *Cepaea*.

Overall, by establishing a method for quantitatively measuring variation in an established banding pattern, and beginning to characterise pigments present in the bands, this work provides a baseline for further studies on the *Cepaea* banding polymorphism. This is true both from the perspective of understanding the presence and maintenance of variation in these banding patterns, and ultimately, the underpinning genetics involved. A next step must be to identify the component parts and evolutionary origins of the supergene in *Cepaea nemoralis* and *C. hortensis*. A recent genome assembly is a first step towards achieving this aim (Saenko et al., 2021).

**Acknowledgements:** This work was supported by the University of Nottingham; the Biotechnology and Biological Sciences Research Council [grant number BB/M008770/1] funded a studentship to Hannah Jackson. Jenny Larsson was funded by a studentship from the Leverhulme Centre for Advanced Biological Modelling. Thanks to Roger Butlin, Sean Stankowski, and Robert Cameron for useful discussions and feedback.

**Data accessibility:** All data for this manuscript are supplied in the Supplementary Information..

**Conflict of Interest statement:** The authors have no conflict of interest to declare.

## References

- Adamson, K. J., Wang, T., Rotgans, B. A., Kruangkum, T., Kuballa, A. V., Storey, K. B. & Cummins, S. F. 2017. Genes and associated peptides involved with aestivation in a land snail. *General and Comparative Endocrinology* **246**: 88-98.
- Arthur, W., Phillips, D. & Mitchell, P. 1993. Long-term stability of morph frequency and species distribution in a sand-dune colony of *Cepaea*. *Proceedings of the Royal Society B: Biological Sciences* **251**: 159-163.
- Budd, A., McDougall, C., Green, K. & Degnan, B. M. 2014. Control of shell pigmentation by secretory tubules in the abalone mantle. *Frontiers in Zoology* **11**.
- Cain, A. J. 1988. The scoring of polymorphic colour and pattern variation and its genetic basis in molluscan shells. *Malacologia* **28**: 1-15.
- Cain, A. J. & Sheppard, P. M. 1950. Selection in the polymorphic land snail *Cepaea nemoralis*. *Heredity* **4**: 275-294.
- Cain, A. J. & Sheppard, P. M. 1952. The effects of natural selection on body colour in the land snail *Cepaea nemoralis*. *Heredity* **6**: 217-231.
- Cameron, R. A. D. 1992. Change and stability in *Cepaea* populations over 25 years: A case of climatic selection. *Proceedings of the Royal Society B: Biological Sciences* **248**: 181-187.
- Cameron, R. A. D. & Cook, L. M. 2012. Habitat and the shell polymorphism of *Cepaea nemoralis* (L.): Interrogating the Evolution Megalab database. *Journal of Molluscan Studies* **78**: 179-184.

- Cameron, R. A. D. & Cook, L. M. 2013. Temporal morph frequency changes in sand-dune populations of *Cepaea nemoralis* (L.). *Biological Journal of the Linnean Society* **108**: 315-322.
- Cameron, R. A. D., Cook, L. M. & Greenwood, J. J. D. 2013. Change and stability in a steep morph-frequency cline in the snail *Cepaea nemoralis* (L.) over 43 years. *Biological Journal of the Linnean Society* **108**: 473-483.
- Clark, M. S., Thorne, M. A. S., Vieira, F. A., Cardoso, J. C. R., Power, D. M. & Peck, L. S. 2010. Insights into shell deposition in the Antarctic bivalve *Laternula elliptica*: Gene discovery in the mantle transcriptome using 454 pyrosequencing. *BMC Genomics* **11**: 362.
- Cook, L. M. 1967. The genetics of *Cepaea nemoralis*. *Heredity* **22**: 397-410.
- Cook, L. M. 2005. Disequilibrium in some *Cepaea* populations. *Heredity* **94**: 497-500.
- Cook, L. M. 2008. Variation with habitat in *Cepaea nemoralis*: The Cain & Sheppard diagram. *Journal of Molluscan Studies* **74**: 239-243.
- Cook, L. M., Cowie, R. H. & Jones, J. S. 1999. Change in morph frequency in the snail *Cepaea nemoralis* on the Marlborough downs. *Heredity* **82**: 336-1999.
- Cook, L. M. & Saccheri, I. J. 2013. The peppered moth and industrial melanism: Evolution of a natural selection case study. *Heredity* **110**: 207-212.
- Cossins, A., Fraser, J., Hughes, M. & Gracey, A. 2006. Post-genomic approaches to understanding the mechanisms of environmentally induced phenotypic plasticity. *Journal of Experimental Biology*: 2328-2336.
- Cuthill, I. C., Allen, W. L., Arbuckle, K., Caspers, B., Chaplin, G., Hauber, M. E., Hill, G. E., Jablonski, N. G., Jiggins, C. D., Kelber, A., Mappes, J., Marshall, J., Merrill, R., Osorio, D., Prum, R., Roberts, N. W., Roulin, A., Rowland, H. M., Sherratt, T. N., Skelhorn, J., Speed, M. P., Stevens, M., Stoddard, M. C., Stuart-Fox, D., Talas, L., Tibbetts, E. & Caro, T. 2017. The biology of color. *Science* **357**: eaan0221.
- Davison, A., Jackson, H. J., Murphy, E. W. & Reader, T. 2019. Discrete or indiscrete? Redefining the colour polymorphism of the land snail *Cepaea nemoralis*. *Heredity* **123**: 162-175.
- Delhey, K., Delhey, V., Kempenaers, B. & Peters, A. 2015. A practical framework to analyze variation in animal colors using visual models. *Behavioral Ecology* **26**: 367-375.
- Emberton, L. R. B. 1963. Relationships between pigmentation of shell and of mantle in the snails *Cepaea nemoralis* (L.) and *Cepaea hortensis* (Mull.). *Proceedings of the Zoological Society of London* **140**: 273-293.
- Grant, B. S., Owen, D. F. & Clarke, C. A. 1996. Parallel rise and fall of melanic peppered moths in America and Britain. *Journal of Heredity* **87**: 351-357.
- Gravan, C. & Lahoz-Beltra, R. 2004. Evolving morphogenetic fields in the zebra skin pattern based on Turing's morphogen hypothesis. *International Journal of Applied Mathematics and Computer Science* **14**: 351-361.
- Harper, M. A., Chen, Z., Toy, T., Machado, I. M. P., Nelson, S. F., Liao, J. C. & Lee, C. J. 2011. Phenotype sequencing: Identifying the genes that cause a phenotype directly from pooled sequencing of independent mutants. *PLoS ONE* **6**: e16517.
- Jackson, D. J., McDougall, C., Woodcroft, B., Moase, P., Rose, R. A., Kube, M., Reinhardt, R., Rokhsar, D. S., Montagnani, C., Joubert, C., Piquemal, D. & Degnan, B. M. 2010. Parallel Evolution of Nacre Building Gene Sets in Molluscs. *Molecular Biology and Evolution* **27**: 591-608.
- Johnson, A. B., Fogel, N. S. & Lambert, J. D. 2019. Growth and morphogenesis of the gastropod shell. *Proceedings of the National Academy of Sciences* **116**: 6878-6883.
- Jones, J. S., Leith, B. H. & Rawlings, P. 1977. Polymorphism in *Cepaea*: A Problem with Too Many Solutions? *Annual Review of Ecology and Systematics* **8**: 109-143.

- Joubert, C., Piquemal, D., Marie, B., Manchon, L., Pierrat, F., Zanella-Cléon, I., Cochennec-Laureau, N., Gueguen, Y. & Montagnani, C. 2010. Transcriptome and proteome analysis of *Pinctada margaritifera* calcifying mantle and shell: Focus on biomineralization. *BMC Genomics* **11**: 613.
- Kerkvliet, J., de Boer, T., Schilthuizen, M. & Kraaijeveld, K. 2017. Candidate genes for shell colour polymorphism in *Cepaea nemoralis*. *PeerJ* **5**: e3715.
- Kondo, S. 2002. The reaction-diffusion system: A mechanism for autonomous pattern formation in the animal skin. *Genes to Cells*: 535-541.
- Landgrebe, J., Welzl, G., Metz, T., Van Gaalen, M. M., Ropers, H., Wurst, W. & Holsboer, F. 2002. Molecular characterisation of antidepressant effects in the mouse brain using gene expression profiling. *Journal of Psychiatric Research* **36**: 119-129.
- Larsson, J., Westram, A. M., Bengmark, S., Lundh, T. & Butlin, R. K. 2020. A developmentally descriptive method for quantifying shape in gastropod shells. *Journal of the Royal Society Interface* **17**: 20190721.
- Liew, T.-S. & Schilthuizen, M. 2016. A method for quantifying, visualising, and analysing gastropod shell form. *PLOS ONE* **11**: e0157069.
- Majerus, M. E. N., Brunton, C. F. A. & Stalker, J. 2000. A bird's eye view of the peppered moth. *Journal of Evolutionary Biology* **13**: 155-159.
- Mann, K. & Jackson, D. J. 2014. Characterization of the pigmented shell-forming proteome of the common grove snail *Cepaea nemoralis*. *BMC Genomics* **15**: 249.
- Marie, B., Jackson, D. J., Ramos-Silva, P., Zanella-Cleon, I., Guichard, N. & Marin, F. 2013. The shell-forming proteome of *Lottia gigantea* reveals both deep conservations and lineage-specific novelties. *FEBS J* **280**: 214-32.
- Murray, J. 1963. The inheritance of some characters in *Cepaea hortensis* and *Cepaea nemoralis* (Gastropoda). *Genetics* **48**: 605-15.
- Neiber, M. T. & Hausdorf, B. 2015. Molecular phylogeny reveals the polyphyly of the snail genus *Cepaea* (Gastropoda: Helicidae). *Molecular Phylogenetics and Evolution* **93**: 143-149.
- Neiber, M. T., Sagorny, C. & Hausdorf, B. 2016. Increasing the number of molecular markers resolves the phylogenetic relationship of '*Cepaea*' *vindobonensis* (Pfeiffer 1828) with *Caucasotachea Boettger* 1909 (Gastropoda: Pulmonata: Helicidae). *Journal of Zoological Systematics and Evolutionary Research* **54**: 40-45.
- Ożgo, M. 2011. Rapid evolution in unstable habitats: A success story of the polymorphic land snail *Cepaea nemoralis* (Gastropoda: Pulmonata). *Biological Journal of the Linnean Society* **102**: 251-262.
- Ożgo, M. & Komorowska, A. 2009. Shell banding polymorphism in *Cepaea vindobonensis* in relation to habitat in southeastern Poland. *Malacologia* **51**: 81-88.
- Ożgo, M., Liew, T. S., Webster, N. B. & Schilthuizen, M. 2017. Inferring microevolution from museum collections and resampling: Lessons learned from *Cepaea*. *PeerJ* **5**: e3938.
- Ożgo, M. & Schilthuizen, M. 2012. Evolutionary change in *Cepaea nemoralis* shell colour over 43 years. *Global Change Biology* **18**: 74-81.
- Peichel, C. L. & Marques, D. A. 2017. The genetic and molecular architecture of phenotypic diversity in sticklebacks. *Philosophical Transactions of the Royal Society B: Biological Sciences* **372**: 20150486.
- Richards, P. M., Liu, M. M., Lowe, N., Davey, J. W., Blaxter, M. L. & Davison, A. 2013. RAD-Seq derived markers flank the shell colour and banding loci of the *Cepaea nemoralis* supergene. *Molecular Ecology* **22**: 3077-3089.
- Rosin, Z. M., Kobak, J., Lesicki, A. & Tryjanowski, P. 2013. Differential shell strength of *Cepaea nemoralis* colour morphs - Implications for their anti-predator defence. *Naturwissenschaften* **100**: 843-851.

- Rotarides, M. 1926. Über die Bandvariation von *Cepaea vindobonensis* Fer. *Zoologischer Anzeiger* **67**: 28-44.
- Saenko, S. V., Groenenberg, D. S. J., Davison, A. & Schilthuizen, M. 2021. The draft genome sequence of the grove snail *Cepaea nemoralis*. *G3: Genes, Genomes, Genetics in press*: jkaa071.
- Silvertown, J., Cook, L., Cameron, R., Dodd, M., McConway, K., Worthington, J., Skelton, P., Anton, C., Bossdorf, O., Baur, B., Schilthuizen, M., Fontaine, B., Sattmann, H., Bertorelle, G., Correia, M., Oliveira, C., Pokryszko, B., Ožgo, M., Stalažs, A., Gill, E., Rammul, Ü., Sólymos, P., Féher, Z. & Juan, X. 2011. Citizen science reveals unexpected continental-scale evolutionary change in a model organism. *PLoS ONE* **6**: e18927.
- Ståhl, P. L., Salmén, F., Vickovic, S., Lundmark, A., Navarro, J. F., Magnusson, J., Giacomello, S., Asp, M., Westholm, J. O., Huss, M., Mollbrink, A., Linnarsson, S., Codeluppi, S., Borg, Å., Pontén, F., Costea, P. I., Sahlén, P., Mulder, J., Bergmann, O., Lundeberg, J. & Frisén, J. 2016. Visualization and analysis of gene expression in tissue sections by spatial transcriptomics. *Science* **353**: 78-82.
- Staikou, A. E. 1999. Shell temperature, activity and resistance to desiccation in the polymorphic land snail *Cepaea vindobonensis*. *Journal of Molluscan Studies* **65**: 171–184.
- Surmacki, A., Ożarowska-Nowicka, A. & Rosin, Z. M. 2013. Color polymorphism in a land snail *Cepaea nemoralis* (Pulmonata: Helicidae) as viewed by potential avian predators. *Naturwissenschaften* **100**: 533-540.
- Walton, O. C. & Stevens, M. 2018. Avian vision models and field experiments determine the survival value of peppered moth camouflage. *Communications Biology* **1**: 118.
- Webster, N. & Palmer, A. R. 2019. How do gastropods grow synchronized shell sculpture? Effect of experimental varix manipulations on shell growth by *Ceratostoma foliatum* (Muricidae: Ocenebrinae). *Invertebrate Biology* **138**: 74-88.
- Williams, S. T. 2017. Molluscan shell colour. *Biol Rev Camb Philos Soc* **92**: 1039-1058.
- Worthington, J. P., Silvertown, J., Cook, L., Cameron, R., Dodd, M., Greenwood, R. M., Mcconway, K. & Skelton, P. 2012. Evolution MegaLab: A case study in citizen science methods. *Methods in Ecology and Evolution* **3**: 303-309.

**Table 1. Outcome of statistical tests for the impact of shell shape, height, or weight relative position of bands.**

| Predictors    | Band 1 position model |                      |                       | Band 2 position model |             |                      | Band 3 position model |                     |             | Band 4 position model |                       |                     | Band 5 position model |                      |                       |                     |
|---------------|-----------------------|----------------------|-----------------------|-----------------------|-------------|----------------------|-----------------------|---------------------|-------------|-----------------------|-----------------------|---------------------|-----------------------|----------------------|-----------------------|---------------------|
|               | Coefficient           | 2.5% CI <sup>a</sup> | 97.5% CI <sup>a</sup> | Weight <sup>b</sup>   | Coefficient | 2.5% CI <sup>a</sup> | 97.5% CI <sup>a</sup> | Weight <sup>b</sup> | Coefficient | 2.5% CI <sup>a</sup>  | 97.5% CI <sup>a</sup> | Weight <sup>b</sup> | Coefficient           | 2.5% CI <sup>a</sup> | 97.5% CI <sup>a</sup> | Weight <sup>b</sup> |
| Intercept     | <b>8.09212</b>        | 3.86712              | 12.31713              | -                     | 7.876642    | -13.7114             | 29.46473              | -                   | 18.64554    | -6.41917              | 43.71026              | -                   | <b>45.5849</b>        | 37.20569             | 53.9642               | -                   |
| Shape         | 1.65226               | -3.53767             | 6.842186              | 0.45                  | 12.206665   | -16.6317             | 41.04508              | 1                   | 11.4931     | -21.8597              | 44.84585              | 1                   | 2.3748                | -7.10486             | 11.85438              | 0.32                |
| Weight        | 0.12911               | -0.2449              | 0.503126              | 0.53                  | 0.330858    | -0.80643             | 1.468149              | 0.58                | 0.99644     | -2.72146              | 4.714346              | 0.71                | -                     | -                    | -                     | -                   |
| Height        | -0.02484              | -0.44134             | 0.091652              | 0.24                  | 0.081127    | -1.13012             | 1.292376              | 0.62                | 0.03748     | -1.30824              | 1.383211              | 0.58                | -0.2097               | -0.54152             | 0.122188              | 0.77                |
| Height:Shape  | -                     | -                    | -                     | -                     | -0.238209   | -1.85698             | 1.380563              | 0.14                | -0.2024     | -1.97129              | 1.566495              | 0.11                | -                     | -                    | -                     | -                   |
| Height:Weight | -                     | -                    | -                     | -                     | -0.004941   | -0.05364             | 0.043757              | 0.1                 | -0.01163    | -0.09578              | 0.07252               | 0.13                | -                     | -                    | -                     | -                   |
| Shape:Weight  | -                     | -                    | -                     | -                     | -           | -                    | -                     | -                   | -0.41312    | -4.54664              | 3.720394              | 0.1                 | -                     | -                    | -                     | -                   |

From a full model subset, models within two Akaike Information Criterion (AIC) of the best model were selected, means of the coefficients were taken.

All of the terms listed were included in all of the full models for each band position model

Coefficients in bold indicate those for which the 95% confidence interval does not include zero (therefore the effect of the predictor is not significant)

<sup>a</sup>Confidence Interval

<sup>b</sup>The sum of weights from models in which the variable in question appears in the final averaged model.

**Table 2. Outcome of statistical tests for the impact of shell shape, height, or weight relative width of bands.**

| Predictors    | Band 1 width model |                      |                       | Band 2 width model  |                |                      | Band 3 width model    |                     |               | Band 4 width model   |                       |                     | Band 5 width model |                      |                       |                     |
|---------------|--------------------|----------------------|-----------------------|---------------------|----------------|----------------------|-----------------------|---------------------|---------------|----------------------|-----------------------|---------------------|--------------------|----------------------|-----------------------|---------------------|
|               | Coefficient        | 2.5% CI <sup>a</sup> | 97.5% CI <sup>a</sup> | Weight <sup>b</sup> | Coefficient    | 2.5% CI <sup>a</sup> | 97.5% CI <sup>a</sup> | Weight <sup>b</sup> | Coefficient   | 2.5% CI <sup>a</sup> | 97.5% CI <sup>a</sup> | Weight <sup>b</sup> | Coefficient        | 2.5% CI <sup>a</sup> | 97.5% CI <sup>a</sup> | Weight <sup>b</sup> |
| Intercept     | <b>3.64178</b>     | 1.36071              | 5.920491              | -                   | <b>3.66466</b> | 2.231354             | 5.097974              | -                   | <b>9.0729</b> | 3.36438              | 14.78446              | -                   | <b>8.8122</b>      | 5.24962              | 12.37944              | -                   |
| Shape         | -0.69108           | -3.48987             | 2.107718              | 0.32                | -              | -                    | -                     | -                   | -0.61887      | -4.50273             | 3.264984              | 0.18                | -6.41179           | -33.1891             | 20.36552              | 0.21                |
| Weight        | 0.02701            | -0.11889             | 0.172911              | 0.24                | 0.11351        | -0.2041              | 0.431125              | 0.45                | 0.11229       | -0.32187             | 0.546444              | 0.34                | -1.35367           | -7.58921             | 4.881867              | 0.39                |
| Height        | -                  | -                    | -                     | -                   | 0.01142        | -0.05438             | 0.07723               | 0.2                 | -0.1498       | -0.45856             | 0.158956              | 0.56                | -0.02817           | -0.16895             | 0.112605              | 0.47                |
| Height:Shape  | -                  | -                    | -                     | -                   | -              | -                    | -                     | -                   | -             | -                    | -                     | -                   | -                  | -                    | -                     | -                   |
| Height:Weight | -                  | -                    | -                     | -                   | -              | -                    | -                     | -                   | 0.1107        | -0.10496             | 0.326377              | 0.56                | -                  | -                    | -                     | -                   |
| Shape:Weight  | -                  | -                    | -                     | -                   | -              | -                    | -                     | -                   | -             | -                    | -                     | -                   | -0.05204           | -0.26841             | 0.164324              | 0.18                |
|               | -                  | -                    | -                     | -                   | -              | -                    | -                     | -                   | 2.98324       | -9.43401             | 15.4005               | 0.18                | -                  | -                    | -                     | -                   |

From a full model subset, models within two Akaike Information Criterion (AIC) of the best model were selected, means of the coefficients were taken.

All of the terms listed were included in all of the full models for each band position model, but several model averages include a reduced model with no fixed factors

Coefficients in bold indicate those for which the 95% confidence interval does not include zero (therefore the effect of the predictor is not significant)

<sup>a</sup>Confidence Interval

<sup>b</sup>The sum of weights from models in which the variable in question appears in the final averaged model.

**Table 3.** Pairwise comparisons of proportionate differences in growth rates between areas of shell in mid banded individuals. Data generated by construction of 3D Shell Shaper models.

| Comparison   | Estimate | SE   | df    | t-ratio | p-value |
|--------------|----------|------|-------|---------|---------|
| gap 1 band 3 | 1.95     | 1.05 | 36.89 | 1.86    | 0.165   |
| gap 1 gap 2  | -1.33    | 1.05 | 36.89 | -1.26   | 0.425   |
| band 3 gap 2 | -3.28    | 1.05 | 36.89 | -3.12   | 0.009   |

**Table 4.** Pairwise comparisons of proportionate differences in growth rates between regions of shell in five banded individuals. Data generated by construction of 3D Shell Shaper models. Only significant comparisons included.

| Comparison   | Estimate | SE   | df     | t-ratio | p-value |
|--------------|----------|------|--------|---------|---------|
| gap 1 gap 6  | -3.43    | 0.79 | 141.62 | -4.32   | 0.0014  |
| band 1 gap 6 | -3.18    | 0.79 | 141.62 | -4.01   | 0.0046  |
| gap 2 gap 6  | -3.32    | 0.79 | 141.62 | -4.18   | 0.0025  |
| band 2 gap 6 | -3.10    | 0.79 | 141.62 | -3.90   | 0.0067  |
| gap 3 gap 6  | -3.67    | 0.79 | 141.62 | -4.62   | 0.0004  |
| band 3 gap 6 | -3.15    | 0.79 | 141.62 | -3.97   | 0.0053  |
| gap 4 gap 6  | -4.05    | 0.79 | 141.62 | -5.10   | 0.0001  |
| band 4 gap 6 | -3.38    | 0.79 | 141.62 | -4.26   | 0.0018  |
| gap 5 gap 6  | -3.65    | 0.79 | 141.62 | -4.60   | 0.0005  |
| band 5 gap 6 | -3.06    | 0.79 | 141.62 | -3.85   | 0.0080  |

Supplementary tables can be found at <https://doi.org/10.1002/ece3.7517>

**Figure 1. a)** *Cepaea* shell showing shell characters and illustrating position for measurement of bands. **b)** Banding phenotypes considered in this study, from left: five bands (12345), missing second band (10345), partial missing second band (1.345), mid-band (00300).

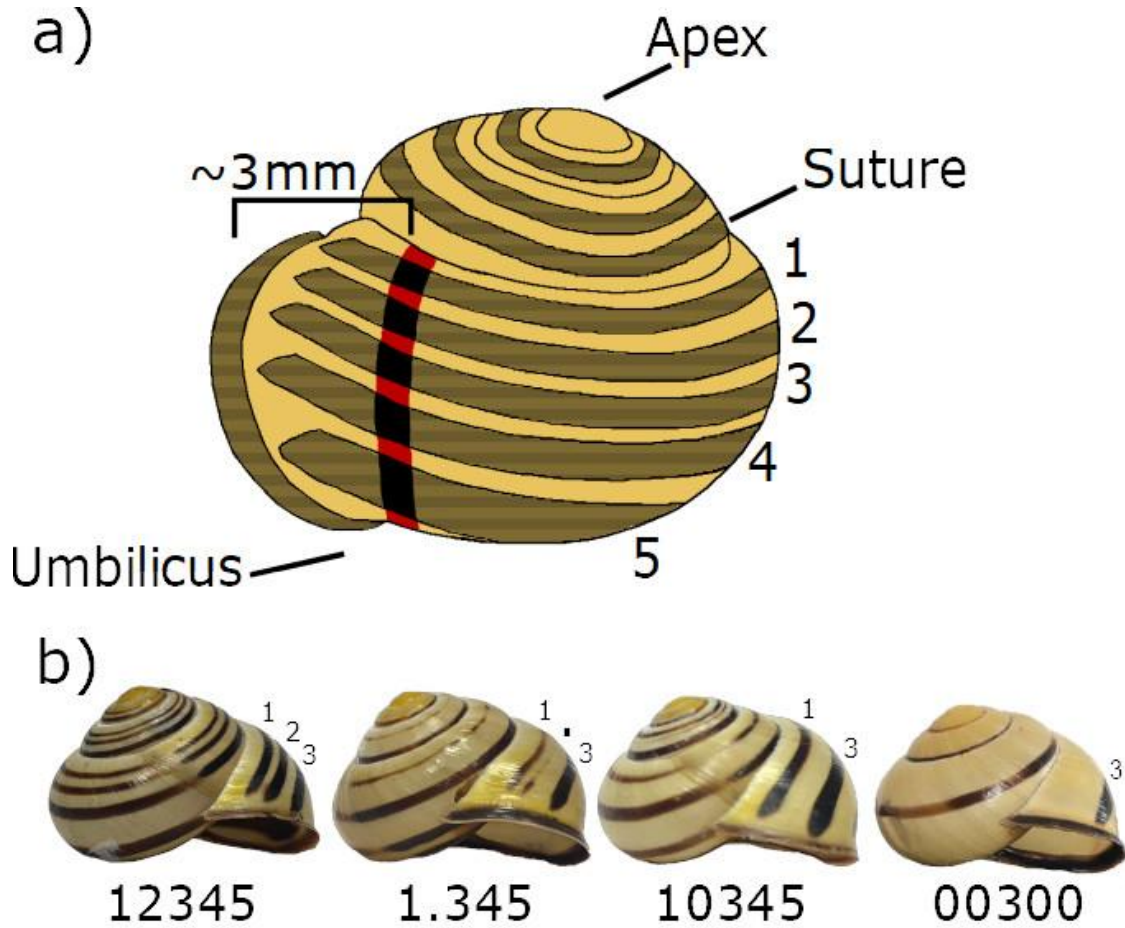


**Figure 2.** Band positions and widths in different phenotypes. **a)** Band 3 in mid-banded (00300) individuals is shifted ~ 0.9% upwards compared with the same band in five-banded (12345) snails. The width of band 3 does not differ between the same phenotypes. **b)** In shells in which band 2 is missing (10345), bands 1 and 3 are ~2.4% closer together. There are also some differences in band width, especially band 3.  $P < 0.05$ , \*;  $P < 0.0001$ , \*\*\*. Inset: summary of band positions in different phenotypes.

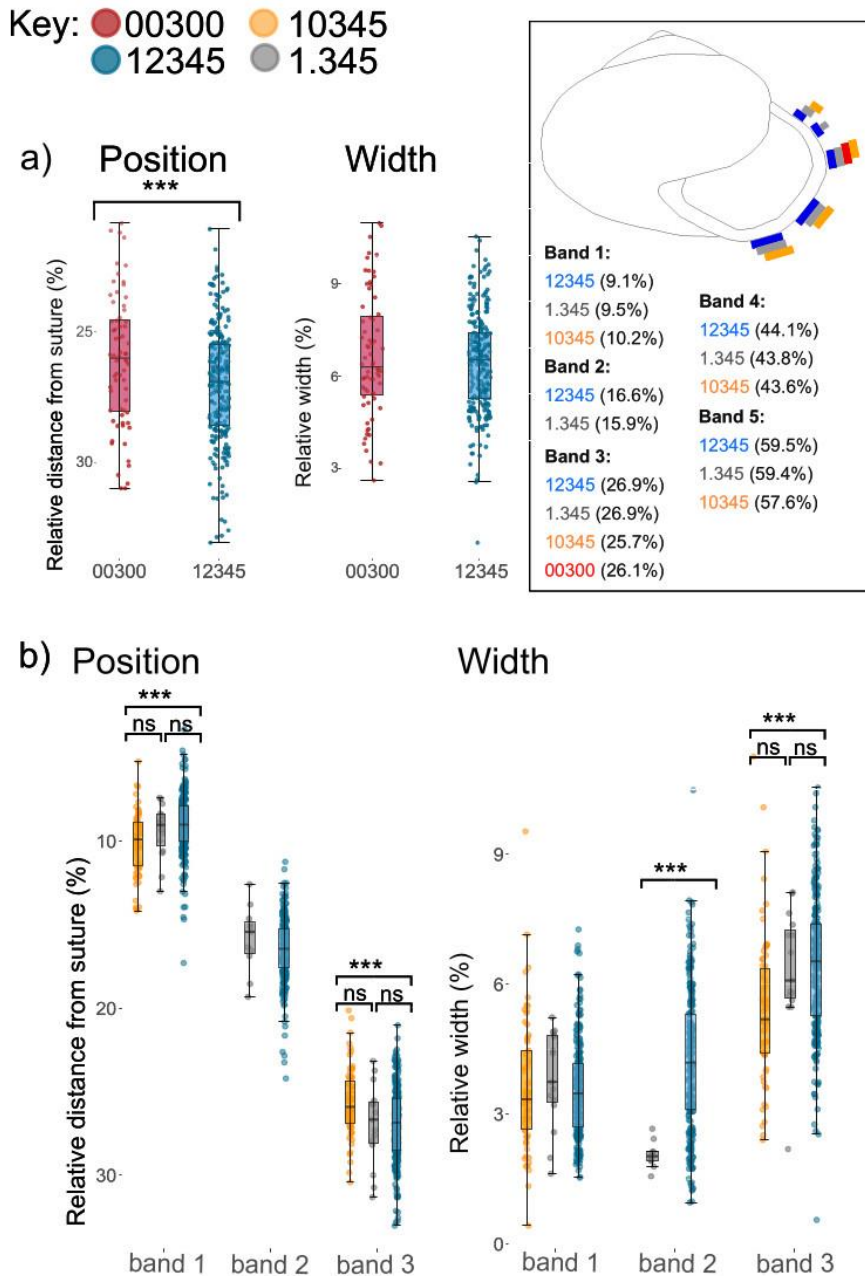


**Figure 3.** The relationship between the width of a band and the widths of the gap above and below in five banded *C. nemoralis*. Most of the correlations are significantly negative, as expected if bands expand in width by occupying the gaps in-between.

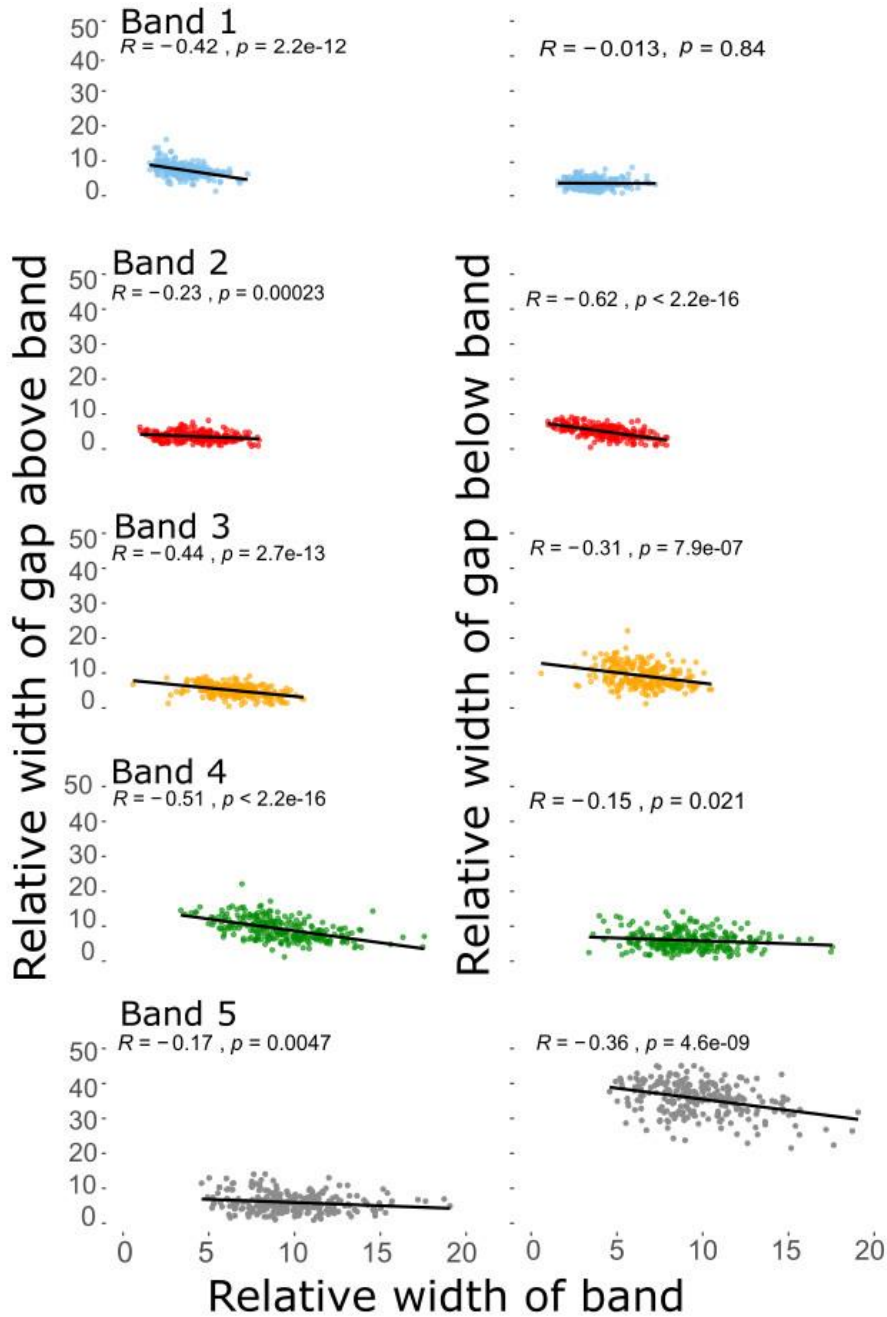




**Figure 5.** Between species comparison of the position (left) and width (right) of each of the five bands in five-banded individuals.

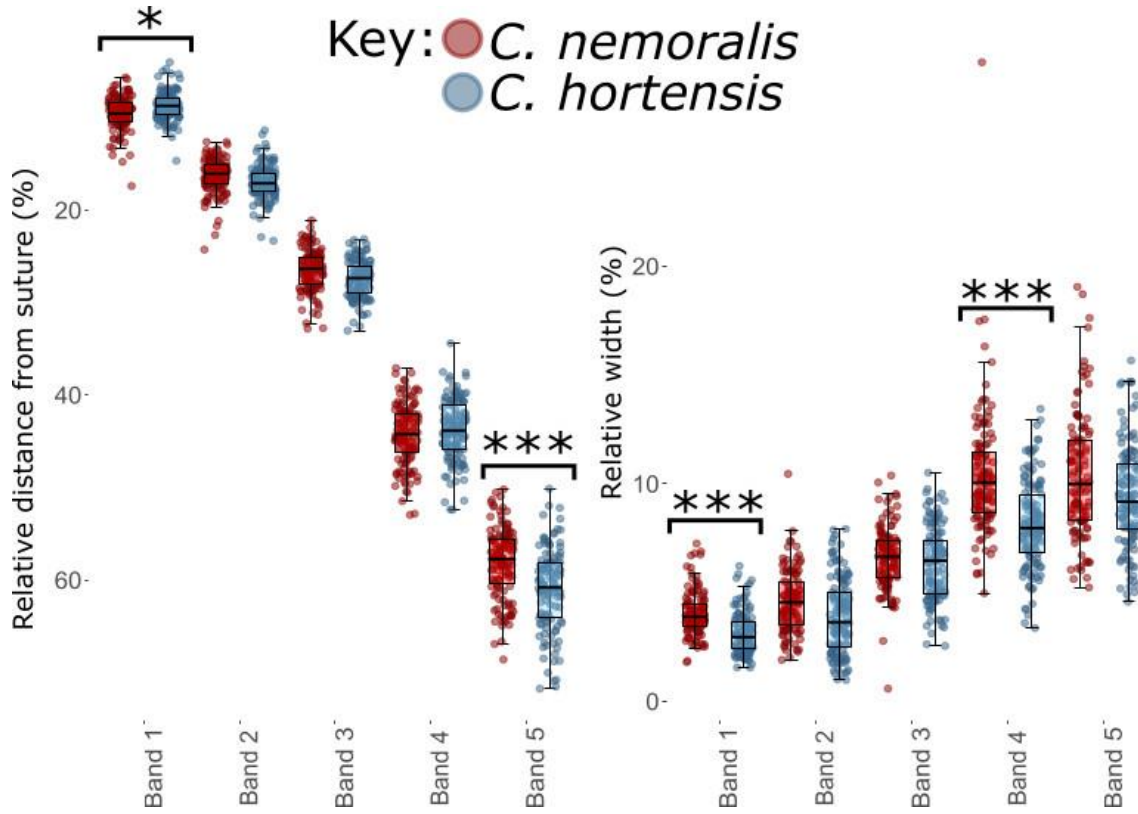
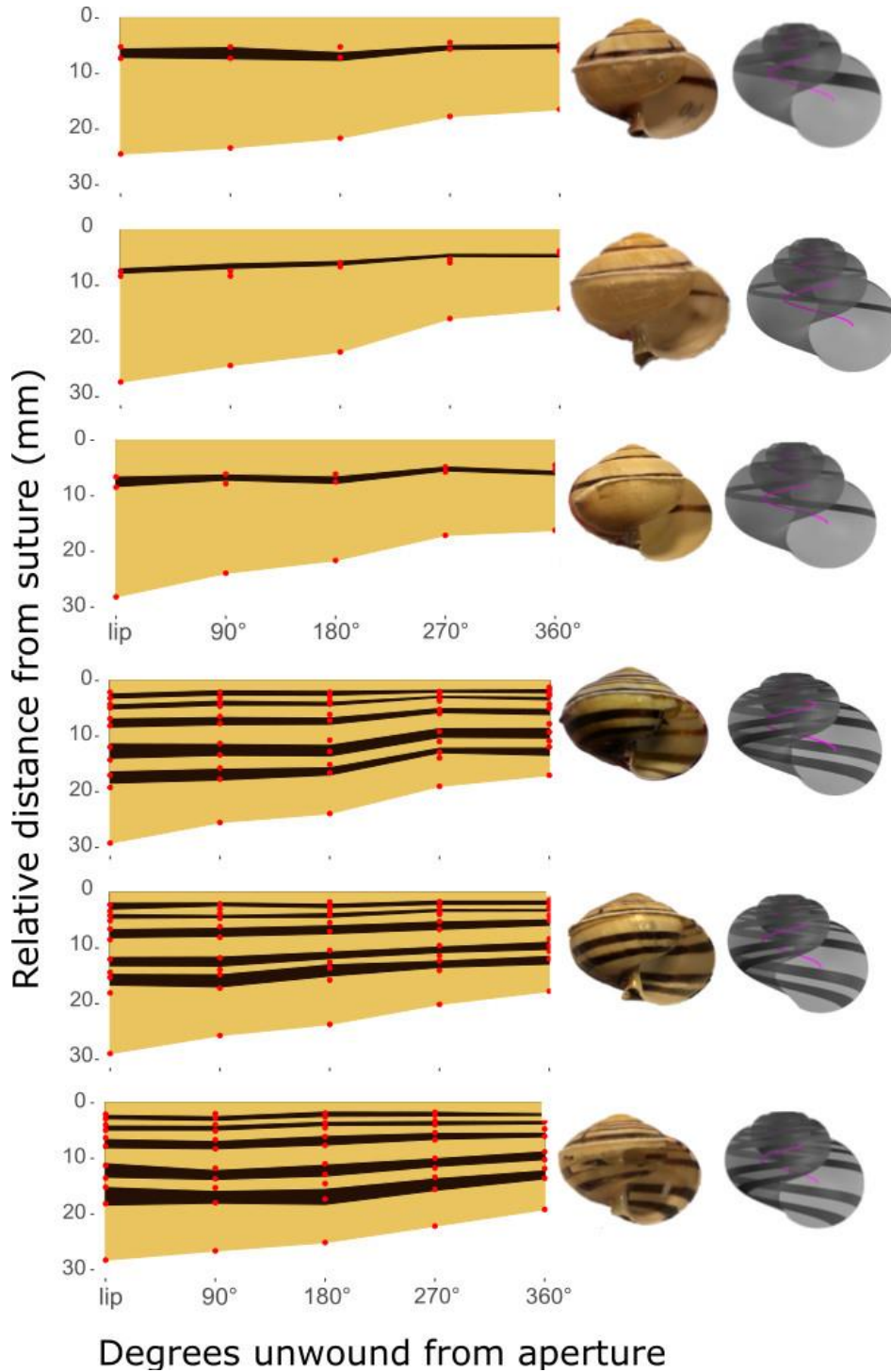
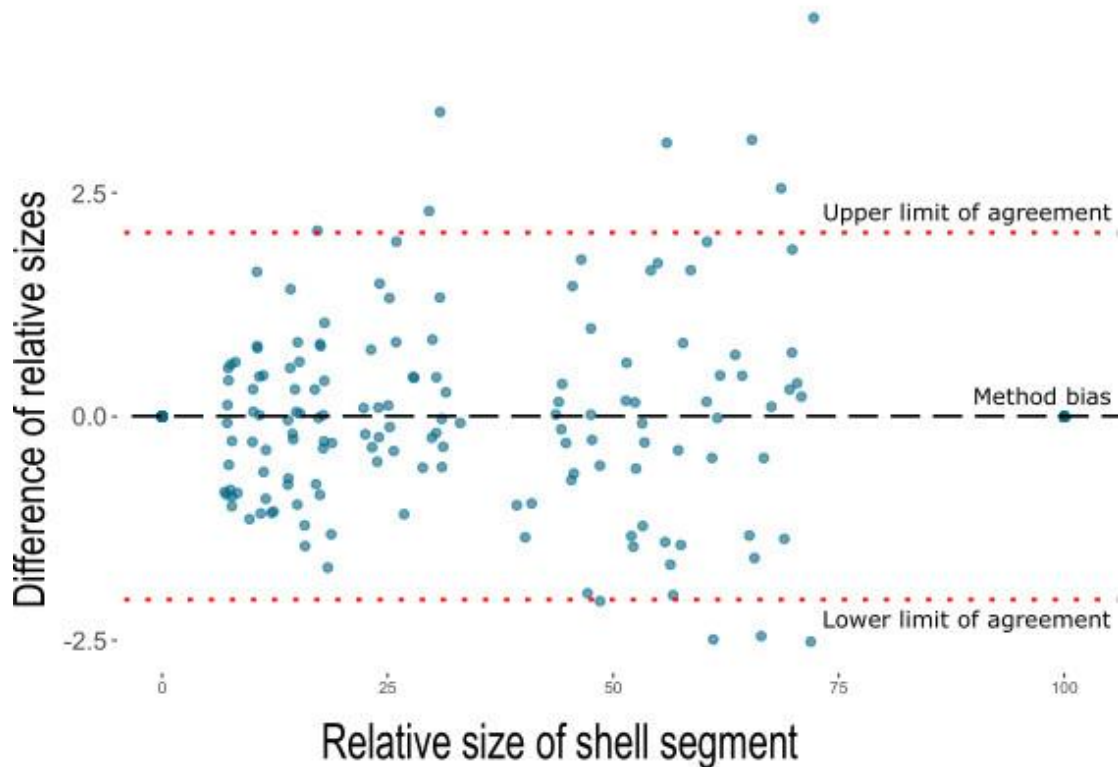


**Figure 6.** Projection of band position and width over last whorl of shell, using mid-banded (top three), and five-banded (bottom three) individuals. Manual (red points) and ShellShaper (dark shading) inferred measures show the same patterns. Also shown is a photo of each shell, and a 3D model generated by ShellShaper.



**Supplementary Figure 1.** Bland-Altman plot of relative widths of shell sections of five banded individuals. X axis represents the average measure of width of shell segment taken by the two methods, and the y-axis represents the difference of measurements from this average. The line of bias (black dashed lined) and the 95% limits of agreement (red dotted lines) are shown.



# ShellShaper user guide

## Banded version for circular apertures

Jenny Larsson  
jslarsson1@sheffield.ac.uk

2020-11-24

ShellShaper is a program for extracting information about shape and banding position in snail shells from standardised photographs. Shells in the images need to be in the correct orientation and this banded version currently only works when apertures are circular.

## 1 Preparation

- You need to have access to MATLAB ([www.mathworks.com](http://www.mathworks.com), version R2018b or later). Including the curve fitting toolbox, and image processing toolbox. You do not need to be proficient in MATLAB to use ShellShaper.
- The ShellShaper program files can be found here:  
<https://github.com/jslarsson/ShellShaper>
- Preferably save the downloaded ShellShaper folder as a subfolder of your MATLAB folder.
- Prepare one folder to include the shell photos you want to analyse, and create one folder for the output.

## 2 Setup

1. Start MATLAB
2. Change directory to the folder where you saved the ShellShaper scripts and open the following file:

```
ShellShaperBands.m
```

3. Change all paths of folders and files to ones that are correct for your file setup. All folders need to have been created before running the program. Make sure the paths are correct and does not overwrite already existing files unless that is your intention, MATLAB will overwrite files without asking for permission.
4. You can choose to only analyse a subset of the images by changing the 'startNumber' and 'lastNumber', they will be numbered alphabetically as found in the folder. This is useful for when there are more images than you can reasonably process in one go.
5. There are two settings for visuals. You can choose if you want the internal spiral to be visible, and if the colour scheme should represent orange *Cepaea* shells, or be greyscale, see figure 1f.

### 3 Running the program

Run the program by either pressing F5 or the big green arrow button in the tool strip. Make sure to do the above setup first, and that the current directory is set to the folder containing the ShellShaper scripts.

1. First the program will ask you to input the maximum number of bands found in the group of shells in your analysis.
2. A new window opens containing an image from the selected image folder, and a dialogue box pops up asking you to select the numbers of all bands that are present in this particular specimen, starting from the top by the suture and numbered clockwise.
3. Click on the image to position the first point at the apex, you can drag points around after initial placement. Press Enter when done.
4. Position the right and left extreme points of the latest whorls similar to figure 1b, pressing Enter will let you position the next one.
5. Position and resize the circle, see figure 1b, press Enter.
6. Position the aperture end points, one at the suture and one at the columella, press Enter.
7. Place the start and end points for each of the present bands in clockwise order starting from the suture, see figure 1c. Press Enter after each is positioned.
8. To get the scale correct, find a known distance by moving the endpoints of the line L, press Enter, and input the value in the dialogue box, see figure 1d.
9. There will be a pink shell model on top of the original image, see figure 1e, as well as a second window opening with a grey or orange shell model by itself, see figure 1f. A dialogue window will open on top of the image asking if the model is good enough. You have 2 options:
  - Yes** This saves images of model and model on original image and the relevant parameters, and lets you go to next one.
  - No** This will let you reposition all the objects to find a better approximation. This will also let you rotate the model to inspect it further and save other orientations as images. Press Enter to see the updated models, if it looks good enough, then press yes in the pop-up instead, otherwise press no again and reposition the points again.
10. The name and number of the image just analysed is shown in the command prompt, and the result is saved to the .txt-file. The next image in the folder will open automatically, repeat step 2-9 for each image.
11. When 'lastNumber' has been reached, the program will close the image windows and output 'Done!' in the command prompt.

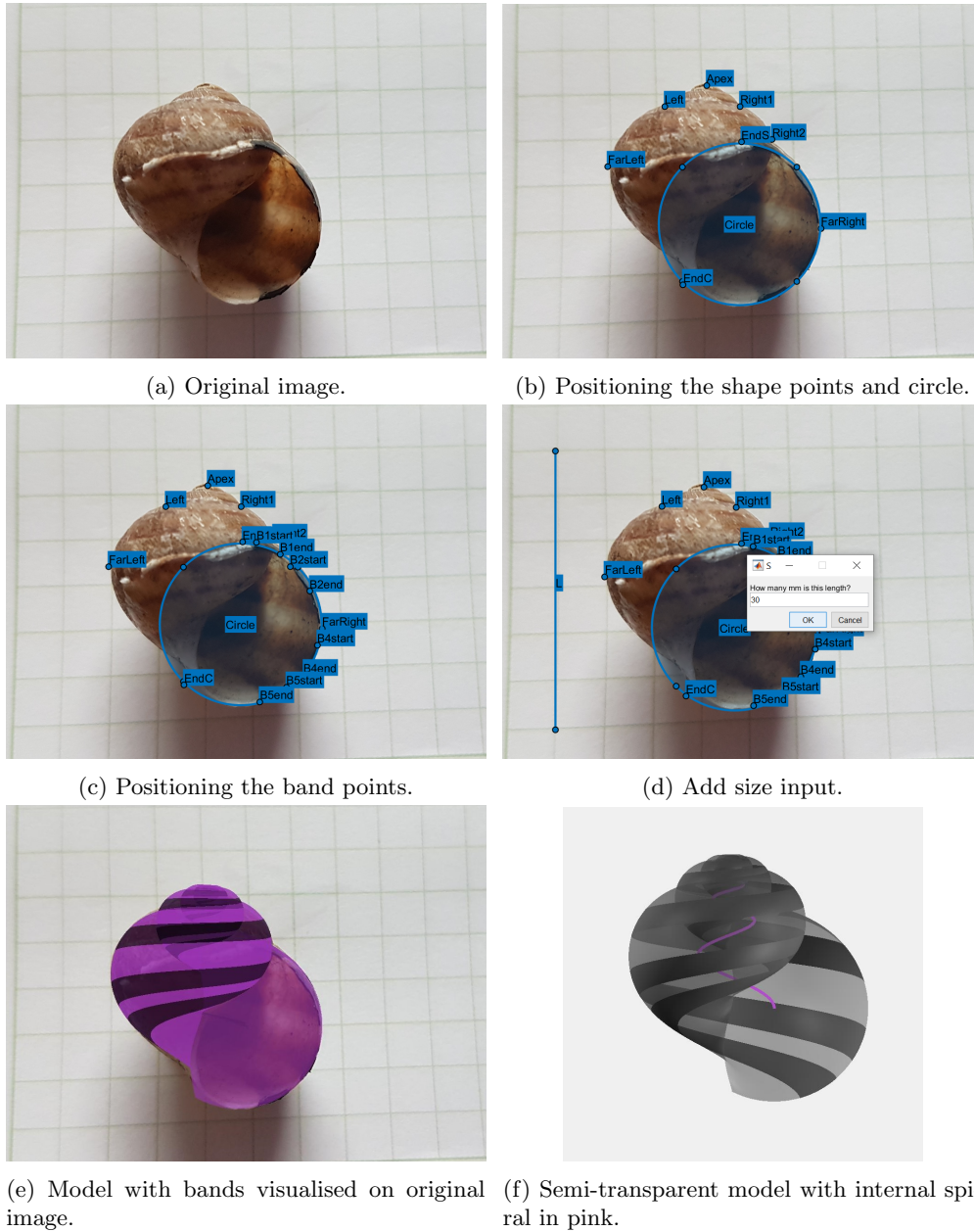


Figure 1: Example of procedure. Input image (a), interactive positioning of objects (b)-(d), output images (e)-(f).

## Appendix F

# Genetic variation for adaptive traits is associated with polymorphic inversions in *Littorina saxatilis*

Presented in its accepted form for publication.

Koch, E. L., Morales, H., Larsson, J., Westram, A. M., Faria, R., Lemmon, A. R., Lemmon, E. M., Johannesson, K., and Butlin, R. K. (2021). Genetic variation for adaptive traits is associated with polymorphic inversions in *Littorina saxatilis*. *Evolution Letters*, 5(3):196-213. doi: 10.1002/evl3.227.

Data and scripts are available at doi: 10.5061/dryad.zgmsbccb4.

E.L. Koch<sup>1</sup>, H. Morales<sup>2,7</sup>, J. Larsson<sup>1</sup>, A. M. Westram<sup>1,3</sup>, R. Faria<sup>1,4</sup>, A. R. Lemmon<sup>5</sup>, E. M. Lemmon<sup>6</sup>, K. Johannesson<sup>7\*</sup>, R. K. Butlin<sup>1,7\*</sup>

<sup>1</sup>Department of Animal and Plant Sciences, University of Sheffield, Sheffield, UK

<sup>2</sup>Evolutionary Genetics Section, University of Copenhagen, Copenhagen, Denmark

<sup>3</sup>IST Austria, Klosterneuburg, Austria

<sup>4</sup>CIBIO-InBIO, Centro de Investigação em Biodiversidade e Recursos Genéticos, Universidade do Porto, Vairão, Portugal

<sup>5</sup>Department of Scientific Computing, Florida State University, Tallahassee, Florida

<sup>6</sup>Department of Biological Science, Florida State University, Tallahassee, Florida

<sup>7</sup>Department of Marine Sciences, University of Gothenburg, Strömstad, Sweden

\*These authors contributed equally

Correspondence: e.koch@sheffield.ac.uk

**Contributions:** R.K.B. and K.J. conceived the study. K.J., A.M.W., R.K.B., J.L., A.R.L., and E.M.L. collected data. E.L.K., H.M., J.L., and R.F. analyzed data. E.L.K. drafted the initial version of the manuscript, and all authors contributed to later versions of the manuscript.

**Abstract**

Chromosomal inversions have long been recognized for their role in local adaptation. By suppressing recombination in heterozygous individuals, they can maintain co-adapted gene complexes and protect them from homogenizing effects of gene flow. However, to fully understand their importance for local adaptation we need to know their influence on phenotypes under divergent selection. For this, the marine snail *Littorina saxatilis* provides an ideal study system. Divergent ecotypes adapted to wave action and crab predation occur in close proximity on intertidal shores with gene flow between them. Here, we used F2 individuals obtained from crosses between the ecotypes to test for associations between genomic regions and traits distinguishing the Crab/Wave adapted ecotypes, including size, shape, shell thickness and behaviour. We show that most of these traits are influenced by two previously detected inversion regions that are divergent between ecotypes. We thus gain a better understanding of one important underlying mechanism responsible for the rapid and repeated formation of ecotypes: divergent selection acting on inversions. We also found that some inversions contributed to more than one trait suggesting that they may contain several loci involved in adaptation, consistent with the hypothesis that suppression of recombination within inversions facilitates differentiation in the presence of gene flow.

**Impact Summary**

Chromosomal inversion polymorphisms, segments of chromosomes that are flipped in orientation and occur in reversed order in some individuals, have long been recognized to play an important role in local adaptation. They can reduce recombination in heterozygous individuals and thus help to maintain sets of locally adapted alleles. In a wide range of organisms, populations adapted to different habitats differ in frequency of inversion arrangements. However, getting a full understanding of the importance of inversions for adaptation requires confirmation of their influence on traits under divergent selection. Here, we studied a marine snail, *Littorina saxatilis*, that has evolved ecotypes adapted to wave exposure or crab predation. These two types occur in close proximity on different parts of the shore. Gene flow between them exists in contact zones. However, they exhibit strong phenotypic divergence in several traits under habitat-specific selection, including size, shape and behaviour. We used crosses between these ecotypes to identify genomic regions that explain variation in these traits. We could show that previously detected inversion regions contribute to adaptive divergence. Some inversions influenced multiple traits suggesting that they contain sets of locally adaptive alleles. Our study also identified regions without known inversions that are important for phenotypic divergence. Thus, we provide a more complete overview of the importance of inversions in relation to the remaining genome.

## Introduction

Understanding the mechanisms that promote phenotypic diversification is of central interest in evolutionary biology. Some of the differences we observe in nature may not be caused by genetic divergence but by environmental effects. However, in many cases there is evidence for heritability of traits contributing to local adaptation (Hereford 2009), confirming that populations are genetically adapted to their native habitats (Savolainen et al. 2013). Genetic differentiation can even occur over very small geographical scales (Slatkin 1987) where differentially adapted populations are within dispersal range of each other. While some isolating mechanisms, like assortative mating (Servedio and Boughman 2017) or phenological differences, may contribute to keeping locally adapted entities apart, in many cases some level of gene flow exists (Lenormand 2002; Smadja and Butlin 2011), for instance, in contact zones with frequent hybridisation (Wu et al. 2008; Harrison and Larson 2016; Schaefer et al. 2016; Chhatre et al. 2018). These examples have raised questions about the mechanisms maintaining and promoting genetic differentiation despite the homogenising effects of gene flow (Felsenstein 1981; Pinho and Hey 2010).

Theoretical studies have found that certain genetic architectures favour local adaptation and protect locally-advantageous alleles (Feder et al. 2012; Yeaman 2013; Rafajlović et al. 2016). Adaptation by fewer loci of large effect should proceed faster and be more resistant to gene flow under selection-migration balance (Yeaman and Otto 2011; Yeaman and Whitlock 2011). Furthermore, it is expected that selection in different habitats is multivariate with many traits involved and potentially many contributing genetic loci. However, recurrent recombination is expected to break down advantageous allele combinations. If local adaptation is based on alleles at multiple loci, reduced recombination between them should be under positive selection in the presence of gene flow (Lenormand and Otto 2000) and can favour local adaptation (Kirkpatrick and Barton 2006). Thus, there should be selection for locally-adapted alleles to be tightly linked, either by being physically close on the same chromosome or in regions of low recombination (Bürger and Akerman 2011; Yeaman and Whitlock 2011; Aeschbacher et al. 2017). In light of this, chromosomal inversions have received great interest for their potential role in local adaptation and speciation in the presence of ongoing gene flow (Feder and Nosil 2009; Smadja and Butlin 2011; Feder et al. 2012; Ravinet et al. 2017). Inversions are known to suppress recombination by impeding cross-overs during meiosis in heterozygous individuals or leading to gametic imbalance and embryo abortion (Kirkpatrick 2010). Inversions can thus maintain sets of locally adapted alleles and prevent exchange with other genetic backgrounds, forming barriers to gene flow that might contribute to reproductive isolation (Rieseberg 2001; Navarro and Barton 2003; Faria et al. 2019b).

Over the past years there has been accumulating evidence that inversion polymorphisms contribute to local adaptation in a wide range of taxa (Hoffmann and Rieseberg 2008; Wellenreuther and Bernatchez 2018). Alternative arrangements often differ in frequencies between ecotypes (Twyford and Friedman 2015; Hanson et al. 2017; Christmas et al. 2019).

Although these patterns are intriguing, and consistent with expectations from theory (Charlesworth and Barton 2018), the exact mechanisms are often not fully understood. Since selection acts on phenotypes, a full understanding of the specific role of chromosomal rearrangements for adaptation necessarily requires establishing the link between inversions and phenotypes under divergent selection in locally adapted populations. Empirical support for selection on inversions is often based on covariance with environmental variables, either by frequency fluctuations over seasons (Butlin and Day 1989; Ayala et al. 2011) or environmental clines (Ayala et al. 2014; Kapun et al. 2016a). Cases where these clines are replicated with consistent patterns across continents provide strong support (Kapun et al. 2016a; Mérot et al. 2018). However, confirming a direct causal influence is often challenging (Hoffmann et al. 2004; Kirkpatrick and Kern 2012). The exact features that make inversions important for local adaptation, suppression of recombination and maintenance of large regions in linkage disequilibrium, also pose a substantial challenge for studying their content and identifying targets of selection. Using QTL and association mapping studies showed that they contribute to desiccation resistance in *Anopheles* (Ayala et al. 2019), fitness variation and divergence in monkeyflowers (Lowry and Willis 2010; Lee et al. 2016; Coughlan and Willis 2019), migratory behaviour in cod (Sinclair-Waters et al. 2018), mimicry in *Heliconius* butterflies (Joron et al. 2011), body size in *Drosophila* (Kapun et al. 2016b; Durmaz et al. 2018), and life-history traits in seaweed flies (Butlin and Day 1985; Mérot et al. 2020). In most cases the exact loci inside an inversion responsible for phenotypic variation could not be identified. Only a few studies have been successful in getting more insights, e.g. finding linked colour pattern loci within an inversion in *Heliconius* (Joron et al. 2011; Edelman et al. 2019), or ecologically important QTLs in *Boechera stricta* (Lee et al. 2017).

When studying inversion polymorphism in wild populations an additional challenge is imposed by potentially strong confounding effects of the environment on phenotypes. Most phenotypes are plastic, i.e. influenced by the environment, which can lead to differences even in the absence of genetic differentiation. Furthermore, inversion frequency clines can also result from neutral, demographic processes and reflect patterns of colonization and range expansion (Klopfstein et al. 2006). Making robust conclusions about the role of inversions in local adaptation requires disentangling these effects from causal effects of inversions. It is therefore crucial to complement studies in the field with controlled lab experiments.

Here, we explored the role of inversions in phenotypic divergence in a well-studied system, the marine snail *Littorina saxatilis*. This species has evolved divergent ecotypes associated with distinct shore habitats multiple times (Johannesson et al. 1993; Panova et al. 2006; Rolán-Alvarez 2007; Butlin et al. 2014). Snails living on wave-exposed rocks and those occurring in crab-rich habitats differ in a range of traits including size, shell shape and behaviour (Johannesson et al. 2010; Johannesson 2016). “Wave” snails are characterized by globular shells (Johannesson 1986) and a wide aperture, potentially adapted to prevent dislodgment by wave action (Le Pennec et al. 2017). In contrast, “Crab” snails are less exposed

to wave action but experience predation pressure from crabs. They are two to three times larger and have thicker shells (even when controlled for size) with narrower apertures that impede crabs from either cracking the shell or pulling snails out (Johannesson 1986; Boulding et al. 2017). In addition, Wave snails are bolder, i.e. more anxious to crawl out and remain attached to the surface, while Crab snails are wary and stay longer inside their shell after disturbance (Johannesson and Johannesson 1996). Phenotypes change across transition zones from one habitat to the next (Johannesson et al. 2010; Le Pennec et al. 2017; Westram et al. 2018). Previous studies have found them to persist, at least partially, in lab-reared individuals (Johannesson and Johannesson 1996) suggesting a genetic basis. Although there is some evidence for assortative mating between ecotypes (Johannesson et al. 2008; Perini et al. 2020) ongoing gene flow between them is common (Panova et al. 2006; Westram et al. 2018). Recently, it was shown that the *L. saxatilis* genome contains multiple large inversions (regions of high linkage disequilibrium (LD); Faria et al. 2019a), with many of them showing frequency differences between the ecotypes and significant clinal patterns across the hybrid zones. Moreover, genetic differentiation between ecotypes has accumulated in genomic regions containing these putative inversions (Westram et al. 2018; Morales et al. 2019). However, the influence of these inversions on phenotypic divergence is mostly unknown.

To investigate the influence of inversions on local adaptation we applied a powerful approach using more than 380 lab-reared individuals resulting from crosses between the two divergent ecotypes. This strategy allowed us to remove confounding environmental effects and homogenize the genomic background of individuals. We used QTL mapping to test for associations between genomic regions and phenotypic traits distinguishing ecotypes. Furthermore, we applied variance partitioning across linkage groups to test whether chromosomes harbouring inversions that differ in frequency between ecotypes contributed disproportionately to phenotypic variation. By using complementary approaches, we were able to capture different aspects of the genetic architecture of local adaptation beyond inversions and identify additional regions important for phenotypic divergence.

## Methods

### *Sample collection and crossing*

Crossing was performed between Crab and Wave ecotype individuals collected on the Swedish West Coast at Ängklåvebukten (58.8697°, 11.1197°), where both ecotypes occur in close proximity (see also Westram et al. 2018). The parental female snails were brought into the lab as juveniles and raised in isolation until maturity to prevent uncontrolled matings. The parental males were brought in as adults (more details in Supporting Information Appendix S1). Two virgin Crab-females were crossed with two Wave-males resulting in two F1-families (Figure I in Appendix S1). Three males and three females of each F1-family were then crossed reciprocally with an individual from the other family (see Supporting Information, Appendix Figure I). Unfortunately, genotypic data showed that offspring did not all belong to the

expected families, potentially due to contamination from different tanks or non-virginity of F1 females. To avoid parental misassignments, we evaluated relationships within the F2 and relationships to the presumed parents based on genomic data, following VanRaden (2008) as implemented in the Rpackage “AGHmatrix” (Amadeu et al. 2016), and adjusted the pedigree accordingly since misclassification of individuals as full-sibs can lead to inflation of linkage maps (Supporting Information Appendix S1). This resulted in a total of 386 individuals divided into 13 F2-families (eight full-sib families and one half-sib family that included five full-sib groups, see Appendix S1, Table II) that were used for linkage map construction and phenotyping.

### *Genotyping*

DNA was extracted from a small piece of foot tissue using a CTAB protocol (Panova et al. 2016). We performed targeted re-sequencing at Florida State University’s Center for Anchored Phylogenomics ([www.anchoredphylogeny.com](http://www.anchoredphylogeny.com)) as described in Faria et al. (2019a) and Westram et al. (2018), using a total of 25,000 (120 bp) enrichment probes. The majority of probes (20,000) were drawn from those that were informative in Westram et al. (2018). Novel probe regions (5000) were added to extend the existing linkage map, selecting one probe per contig from randomly drawn genomic contigs from the *L. saxatilis* reference genome as in Westram et al. (2018). Details of probes are provided in Table S8. Raw reads were processed as described in Faria et al. (2019a); details in Appendix S1.

### *Phenotypes*

Phenotypes measured included weight, shell length, shell thickness (mean of three measurements per snail), relative thickness (size-independent), shell shape, shell colour, and boldness behaviour that were previously found to differ between ecotypes (Johannesson et al. 2010). Size-independent parameters for shell shape were obtained based on a growth model (Larsson et al. 2020). We included Height and Width growth, describing the shape of the shell, as well as the position (radial position in Larsson et al. 2020), size and shape (aperture extension in Larsson et al. 2020) of the aperture (Fig. 1). This previous study showed an association with environmental variables describing Crab/Wave habitats. Colour was recorded as RAL categories (<https://www.ralcolor.com>) by visual matching to colour cards by one of us (KJ). To obtain a continuous variable, we converted RAL categories to rgb-colour values (<https://rgb.to/ral>). For boldness behaviour, snails were disturbed to induce retraction and time recorded until an individual crawled out (following Johannesson and Johannesson 1996). Observations were terminated after 15 minutes and individuals that had not emerged during that time were given a random value drawn from the tail of the distribution (log normal distribution of all observational times). Individual behaviours were tested three times on separate days and the average values (log of time) were used as Bold Score (lower values indicate bolder individuals, i.e. less time until emergence). Measurements took place in three months (December 2014, March 2015, June 2015). Except for boldness and thickness, each

phenotype was measured once (month of measurement was included in subsequent analyses). Sex of F2-individuals was determined by dissection.

#### *Linkage map construction*

A linkage map was generated using LepMap3. We used 386 F2-individuals (see Supporting Information Appendix S1) with 22,095 markers and combined all families for construction of one linkage map. The “ParentCall2” module was used (with options `removeNonInformative=1`, `halfSibs=1`) to calculate the most accurate parental genotype posteriors and to obtain missing parental information from offspring. We used the LepMap3 filtering module to remove markers with significant segregation distortion (`dataTolerance = 0.01`). Markers were grouped into Linkage Groups (LG) with the “SeparateChromosomes2” module, using a LOD score limit of 16 and `sizeLimit=100`. We set `lodLimit=16` since this resulted in 17 LGs as was expected based on chromosome number (García-Souto et al. 2018). Additional singular markers that could not be assigned in this step were subsequently added using the “joinSingles2all” (using `lodLimit=16`, `lodDifference=2`) function with 21 iterations. After assignments of markers to different LG, we ran the “OrderMarker2” module for each LG six times and selected the run with highest likelihood score. “OrderMarkers2” orders the markers within each LG by maximizing the likelihood of the data given the order. Markers not showing strong linkage with others that cannot be placed in the right order with certainty are placed to the ends of the LG. Therefore, we manually removed isolated markers causing long gaps (> 2cM) at the end of each LG. We then ran the “OrderMarker2” module again. The final map contained phased chromosomal marker data with imputed missing genotypes (using parameter `outputPhasedData = 1`, `hyperPhaser=1`). Phased data were converted for QTL mapping using Lep-MAP's `map2genotypes.awk` script. For subsequent QTL analysis we averaged female- and male-specific marker positions (option `sexAveraged=1` in the “OrderMarker2” module). To transfer the positions of the previously detected putative inversions, we used the positions of markers within these regions (see Faria et al. 2019a) that were in common with our new map. We used the minimum and maximum positions of these markers to define the boundaries of inverted regions in our map. Please note that this is only an approximation since some markers within the LD clusters of the previous map were not included in our data set (Supporting Information, Table S1).

#### *QTL mapping*

QTL mapping was performed in rQTL (Arends et al. 2010; Broman et al. 2019) using Haley-Knott-regression implemented in the “scan1” function. We included batch (month of measurement) and sex as covariates and ran QTL scans for all phenotypic traits. A genome-wide significance threshold (0.95 quantile) was assessed by 10,000 permutations. Sex was analysed as a binary trait (without covariates). Confidence intervals for the position of a QTL were inferred using the “lod\_int” function. The three `rgb` values for colour were analysed as a multivariate trait using the Rpackages “ShapeQTL” (Navarro 2015) and rQTL (Arends et al.

2010; Broman et al. 2019). To confirm the co-localization of QTLs and inverted regions we further tested the effect of inversion genotypes on phenotypes directly using linear mixed models (Rpackages “lme4” and “lmerTest” (Bates et al. 2015; Kuznetsova et al. 2017)) with phenotype as response variable, sex, batch and inversion genotype as fixed effects and family as random effect. We used type I ANOVA tests to infer significance of inversion effects, i.e. after correcting for sex and batch effects. Complete results are in Supporting Information Table S7 and Fig S5. Inversion genotypes of F1 parents and F2 progeny were inferred using clusters detected in a principal component analysis (PCA) of SNPs in putatively inverted regions following an approach described in Faria et al. (2019a). For a detailed description see Appendix S1. Genotypes of F1 parents and F2 individuals can be found in Supporting Information Table S2.

#### *Chromosome partitioning, regional heritability, and genetic correlations*

QTL analysis may fail to find regions associated with phenotypic variation if a trait is highly polygenic and each locus has an effect below the detection threshold (Manolio et al. 2009; Rockman 2012). Quantitative genetic approaches that rely on comparing phenotypes of individuals with different degrees of relatedness can estimate overall heritability but do not give any information about the genetic loci involved. However, by using genomic markers and information on their position in a linkage map for calculating relationships it is possible to partition genetic variance across the genome and identify specific regions important for phenotypic variation. Regions can be whole chromosomes (Yang et al. 2010; Robinson et al. 2013) or smaller regions (Nagamine et al. 2012; Riggio et al. 2013). This approach was first applied successfully to estimate SNP-based heritability for human height (Yang et al. 2010) but also to several natural populations (Robinson et al. 2013; Bérénos et al. 2015; Santure et al. 2015; Wenzel et al. 2015). By integrating variance due to rare and common alleles as well as many loci with only small effects into a single estimate of additive variance it potentially allows the identification of regions that cannot be detected by QTL analysis.

Relationships between individuals were based on genomic relationships inferred from genetic marker data using the same marker set as in the linkage map. Pairwise genomic relationship matrices were calculated using the method proposed by Yang et al. (2010) as implemented in the Rpackage “AGHmatrix”. Marker assignment to chromosomes (linkage groups, LGs) was based on the linkage map presented here. Chromosome partitioning was performed following the procedure described in Robinson et al. (2013). Briefly, relationships between individuals were estimated separately by using only genetic markers from a specific region and these different relationship matrices were then included in one model. We used linear mixed models (also known as “animal models”, see Kruuk 2004; Wilson et al. 2010) including the fixed effects of sex and batch (month of measurement) and random additive genetic effects which were divided into two parts, regional genomic and whole genomic additive

genetic effects. For this, we calculated pairwise genomic relationship matrices using 1) all markers, 2) all markers excluding those of the focal LG, and 3) markers exclusively from the focal LG. First, we ran a model including the genomic relationships based on all markers (**model A**): Phenotype  $\sim$  batch + sex + additive genetic effects (based on all markers). Next, we fitted three models for each LG:

**Model B:** including a relatedness matrix based on all markers except those on the focal LG: Phenotype  $\sim$  batch + sex + additive genetic effects (all markers excluding focal LG)

**Model C:** including a relatedness matrix based on all markers except those on the focal LG and a second relatedness matrix using only markers from the focal LG. Phenotype  $\sim$  batch + sex + additive genetic effects (all markers excluding focal LG) + additive genetic effects (markers of focal LG)

**Model D:** including relatedness using all markers plus a second relatedness matrix using only markers from the focal LG. Phenotype  $\sim$  batch + sex + additive genetic effects (all markers) + additive genetic effects (markers of focal LG).

We then compared log-likelihoods of the different models using likelihood ratio tests with one degree of freedom. We tested whether a LG explained significant variation in a trait by comparing the log likelihood of model **model C** (genome-wide excluding focal LG plus second relatedness matrix based on focal LG) with the log likelihood of the **model B** (genome-wide excluding focal LG). Under a polygenic architecture with many contributing loci that are evenly distributed across the genome we expect that variance explained increases with length of the LG. To identify certain LGs that deviate from this expectation and explain more variance than expected based on their length we compared whether **model D** (genome-wide plus focal LG) was significantly better than **model A** (genome-wide model) (Robinson et al. 2013).

Next, we refined variance partitioning to smaller regions. Each chromosome was divided into regions of 200 adjacent markers based on our linkage map. Variance partitioning and significance assessment was conducted analogously to chromosome partitioning.

Pairwise genetic correlations were inferred using bivariate animal models using relationships estimated from all markers. Significance was assessed by likelihood-ratio tests comparing the model with correlation to a model where the correlation was set to zero (Wilson et al. 2010).

Models were run in Asreml 3 (Gilmour et al. 2009) implemented in Asreml-R (Butler et al. 2009).

## Results

### *Linkage map*

The final linkage map consisted of 18,949 markers across 17 Linkage Groups (LG) with a total length of 1129.8 cM. Lengths of LGs ranged between 34.6 and 84.1 cM. These LGs corresponded well to those of the previously published map (Westram et al. 2018) (Supporting Information Table S3). LG numbering was adjusted to maintain consistency with previous *Littorina* studies. Consistent with the expectation of suppressed recombination when parents are heterozygous for alternative arrangements (see genotypes Table S2), we found that many markers within these regions (e.g. inversions 6.1/2 and inversion 14.1/2) shared the same position in our QTL map (Fig. S1). However, in most cases markers from inversion regions showed some recombination and not all of them were in complete LD because some F1 parents were inversion homozygotes (Fig. S1, see also Table S1). For other inversions (e.g. 1.1, 4.1, 9.1, 11.1), we expected little recombination suppression since most parental individuals were homozygous (Table S2).

### *QTL mapping: QTLs map to inversion regions*

Most of the studied traits showed suggestive peaks (LOD > 3) in the QTL analysis (Fig. 2, Supporting Information, Table S4). We detected a significant QTL for weight (LOD = 4.17,  $P = 0.031$ ) on LG 6. Shell thickness and length showed an almost identical pattern (Fig. 2A) but with slightly lower LOD (thickness 3.83,  $P = 0.06$ ; length: 3.85,  $P = 0.08$ ) that did not pass the significance threshold ( $P = 0.05$ ). We found significant QTLs for the shape parameters: Height Growth (LOD = 4.16,  $P = 0.028$ ) and Aperture Position (LOD = 6.16,  $P = 0.001$ ) on LG 17, as well as for aperture shape on LG 6 (LOD = 4.36,  $P = 0.023$ ; Fig. 2B, C). Other shape parameters showing suggestive peaks (LOD > 3) were Width Growth on LG 17 (LOD = 4.02,  $P = 0.053$ ) and Aperture Size on LG 17 (LOD = 3.18,  $P = 0.21$ ) and LG 12 (LOD = 3.12,  $P = 0.21$ ). Colour (based on rgb-values) showed significant peaks on LG 6 and LG 17 (Fig. 2D). In contrast, no significant QTL could be detected for relative shell thickness (one suggestive peak on LG 2, LOD = 3.41,  $P = 0.14$ ) or for Bold Score (Fig. S2). However, we detected a highly significant QTL for sex on LG 12 (LOD=26,  $P < 0.001$ , Fig. 2E).

All significant and most suggestive QTLs mapped to regions on LG 6 and LG 17. Closer inspection revealed that QTLs and their confidence intervals often overlapped with regions that were previously described as putative inversions (Supporting Information Table S1) and showed some suppression of recombination in our linkage map (Fig. 3, Fig. S1). QTLs for weight, shell thickness, length, Aperture Shape and colour fell into the inversion region on LG 6 (Fig. 3A). QTLs for Width Growth and Aperture Position fell in the putative inversion region on LG 17. However, the QTL peak for Height Growth and colour on LG 17 were outside the inversion (Fig. 3B). We tested the effects of inversions directly by genotyping F2 individuals for inversion arrangements. In general, we found the results of the QTL analysis to be confirmed: traits that showed significant QTL peaks in inversion regions (weight and Aperture

Shape on LG 6 and Width Growth and Aperture Position on LG 17) were significantly influenced by the genotype of that respective inversion (Table S7, Fig. S5). Interestingly, these results were also consistent with the localisation of QTLs for Aperture Size, colour and Height Growth outside the inversion on LG 17 (Fig. 3B): No significant effect of inversion 17.1 on these traits could be detected (Table S7). We could also see that other inversions, e.g. inversion 1.1 and inversions on LG 12 (Table S7) showed significant associations with phenotypes although no significant QTL peaks could be detected.

Variance explained by significant QTLs ranged from 4.3 to 7.4 % (see also Table S4). However, these estimates are upwardly biased since only significant QTLs are considered and effects of QTLs in low recombination regions are generally overestimated (Noor et al. 2001; Roesti 2018).

*Linkage groups with inversions contributed disproportionately but non-inverted regions were important as well*

Based on our chromosome partitioning analysis, several LGs contributed significantly to phenotypic variation (Supporting Information Table S5, Fig. 4), individual LGs explaining up to 16% of the total variance. Size related phenotypes (weight, shell length, thickness) were predominantly influenced by LG 6 whereas shape parameters (Height and Width Growth, aperture size, aperture position) were influenced by LG 5, 12 and 17 (Fig. 4). Summing point estimates of LG-specific variances resulted in lower numbers than heritability ( $h^2$ ) estimates obtained from a model that included markers from all LGs combined (Table S5). Some inconsistencies can be expected given that  $h^2$  estimates for each LG are surrounded by large standard errors (Fig. 4A). In some cases, statistical power for LG-specific  $h^2$  might have been too low resulting in zero estimates, which were probably underestimations.

Results of variance partitioning and QTL analysis showed generally a good concordance. In most cases LGs harbouring QTLs were found to explain significant proportions of variance in the respective phenotype. LG 6 and 17, which showed a clustering of several QTLs, were also found to explain variance in more than one trait (Table S5, Fig. 4B): LG 6 for weight, thickness and shell length, LG 17 for Width Growth and aperture position. However, some LGs without any significant QTLs, not even suggestive peaks, explained high proportions of variance in several traits, namely LG 5 and 12. Consistent with this result, we found that inversions of LG 12 had significant influence on several traits (Table S7) when we tested inversion genotype effects directly. Interestingly, LG 14, a strong candidate for being involved in ecotype divergence (Westram et al. 2018), but without a QTL peak in our analysis, was found to contribute to variation in weight (Fig. 4) and inversion 14.1/2 showed significant effects on size related traits thickness, weight, and shell length. Variance partitioning showed that several LGs contributed significantly more to trait variation than expected based on their length. These LGs included those with a clustering of QTLs in inverted regions (LG 6 and LG

17) but also LG 5 and LG 12 (Fig. 4, Fig. 5). Although larger LGs (e.g. LG 12, 2, 5) often contributed significantly to phenotypic variation, almost all traits deviated from the expected polygenic pattern (Fig. 4A, Table S5).

*Regional heritability mapping: Accumulation of outlier regions*

Results of regional heritability mapping (RHM) were mainly consistent with variance partitioning across LGs. Significant regions were predominantly found on chromosomes that contributed significantly to trait variation and were almost always adjacent, with all regions of one LG often showing similar estimates, namely on inversion regions on LG 6, LG 12, LG 14, LG 17 (Fig. 5, Fig. S3). Such a pattern is expected when closely related individuals are studied since there was not much opportunity for recombination to break down linked regions on the same chromosome, particularly in inverted regions where recombination is suppressed RHM estimates should be similar. However, RHM could in some cases provide additional insights. Linkage group 2 explained a significant amount of variance in Height and Width growth (Fig. 5, Fig. S3). RHM suggested that the influence of LG 2 is not due to a cumulative effect of many loci that are evenly distributed across this LG but showed an accumulation of significant regions in the middle, outside known inversions (Fig. 5).

*Genetic covariances and adaptation*

We found that most of the studied traits showed significant genetic correlations (Fig. 6, Table S3). Traits falling into the same category form modules with high intercorrelation, e.g. size-related measures weight, thickness and length, as well as shape and aperture related measures, Width Growth, Height Growth and aperture variables. Interestingly, genetic correlations were almost always consistent with trait associations that characterise ecotypes in the field (see Fig. 1A),(Johannesson et al. 2010; Larsson et al. 2020). Wave shape (large Height and Width growth) was genetically correlated with larger apertures and a smaller total size. In contrast, larger individuals tended to show smaller and narrower apertures (Fig. 1B), whereas smaller snails have larger and rounder apertures. We could also find genetic correlations between very different trait types. Bold Score showed a positive correlation with shell length (Fig. 8, Table S3). Since time until coming out of the shell was measured this means that larger individuals needed longer until they crawled out of their shell after disturbance. Relative thickness and coloration (sum of rgb-colour values, i.e. lower values for darker shells) did not show significant correlations with other traits. However, the estimated correlation coefficients were mostly consistent with ecotype differences: positive correlations between relative thickness and size, Bold Score and coloration (bolder individuals have a darker shell), and Bold Score and relative thickness (bolder individuals have thinner shells). Phenotypic correlations based on all individuals (Fig. S4. A) as well as phenotypic correlations for each family separately (Fig. S4 B-J) did not show strong differences.

## Discussion

This study contributes to our understanding of the role of inversion polymorphisms in local adaptation by confirming their influence on traits under divergent selection. Using lab-reared F2 individuals from crosses between *Littorina saxatilis* ecotypes allowed us to avoid confounding environmental effects and enabled us to identify genomic regions important for phenotypic divergence between ecotypes. We show that traits that have diverged between ecotypes are significantly influenced by genomic regions previously described as putative inversions (Faria et al. 2019a). QTL analysis revealed a clustering of significant loci in these regions and we detected a significant association between inversion genotypes and traits. However, since power to detect candidate loci depends on LD between markers and causal loci, these regions are prone to exhibit significant QTLs. An approach combining QTL analysis with variance partitioning across chromosomes may thus help us to better evaluate the contribution of inversion regions compared to the remaining genome. Candidate LGs with inversions containing loci for ecotype divergence (based on genomic differentiation (Morales et al. 2019) or showing significant clines (Westram et al. 2018)) contributed disproportionately to phenotypic divergence. However, we also detected regions outside inversions that seem to be important for phenotypic variation. Notably, we found that phenotypic trait associations that characterise ecotypes in the field are genetically correlated and in many cases candidate LGs with inversions contributed significantly to more than one trait. Although exact insights into underlying mechanisms are not possible at present, this result suggests that inversions contain sets of co-adapted alleles that facilitated the rapid and repeated formation of these ecotypes.

### *Inversions are involved in local adaptation and under divergent selection*

Previous studies have characterized phenotypic divergence between snails collected in the Crab and Wave habitats including size, shape and behavioural differences and found them to persist under lab conditions, at least in part (Johannesson et al. 2010; Johannesson 2016). In contrast, overall genetic differentiation between these ecotypes is low (Panova et al. 2006; Westram et al. 2018; Morales et al. 2019). However, a consistent pattern was an accumulation of outliers in putatively inverted regions on LGs 6, 14, and LG 17 at this particular Swedish site (Westram et al. 2018) and elevated divergence in these regions in several European populations (including Sweden, Spain, UK, and France) (Morales et al. 2019). Genotyping the parental and F2 individuals confirmed that inversions were segregating. For two of these strong candidate regions (LG 6 and LG 17) we detected significant associations with several traits. Since selection acts on phenotypes, gaining a deeper understanding of the process leading to phenotypic divergence and local adaptation requires establishing the link between observed phenotypic and genetic differentiation. Our results thus complement these previous studies and confirm the role of inversions in ecotype divergence and local adaptation. They also add evidence that observed frequency clines of inversions across the habitat transition zone are not solely the product of neutral processes, e.g. isolation by

distance, genome-wide barrier effects, or hitchhiking with a beneficial allele outside the inversion (Kirkpatrick and Barton 2006; Westram et al. 2018).

We found that LG 6 had a strong influence on all size-related measures (weight, thickness, shell length). Size almost universally shows a positive correlation with reproductive output and thus often appears under positive selection (Blanckenhorn 2000). However, faster growth rate may trade-off with reaching sexual maturity later. If mortality in the wave habitat is higher or higher for large individuals that get more easily dislodged, alleles promoting sexual maturity early but retarding growth might be under positive selection (Janson 1983). In contrast, Crab snails may be under selection to increase size rapidly to escape predation, with reproduction starting later (Boulding et al. 2017) resulting in Crab snails having higher growth rates (Janson 1982) and being two to three times larger than Wave snails at maturity. Our finding of a QTL for size, a classic example of a highly polygenic trait, makes *L. saxatilis* rather exceptional, and might have facilitated evolution of differently sized ecotypes (Reid 1996; Johannesson et al. 2010). Influence of inversions on adult size has also been described in *Drosophila* (Kapun and Flatt 2019) and seaweed flies (Butlin et al. 1982) and might be due to the combined effect of multiple small effect loci within inversions.

LG 17 showed clear QTL peaks for several parameters describing shell shape and aperture size and position. Shape is under divergent selection in the two different habitats. Under wave action globular shells as well as a larger foot area help snails to remain attached to the rock surface and decrease the risk of dislodgment (Le Pennec et al. 2017). In contrast, under crab predation, narrower apertures protect snails from being pulled out and high-spined shells allow them to retract further inside the shell (Johannesson 1986; Boulding et al. 2017).

Interestingly, an inverted region on LG 14 that exhibited a high number of non-neutral SNPs in cline analyses (Westram et al. 2018) showed some influence on weight but not on other traits studied despite segregation of the inversion in the F2. We should keep in mind that adaptation to the different habitats may include more traits than those measured here, and may involve, for instance, important physiological traits (Sokolova and Pörtner 2003; Panova and Johannesson 2004).

Colour categories (black and beige) had been shown to vary clinally across the contact zone at the Swedish site. SNPs associated with these colours were found on LG 5 and LG 9 (Westram et al. 2018). In contrast, here we found a clear association with LG 6 and LG 17 for colour traits. The way we analysed colour as a continuous variable (rgb-value) might explain this discrepancy. However, variation in colour was not high among F2 individuals, which might have limited our precision for estimating relevant effects. Consequently, the high estimates obtained for colour in variance partitioning (Table S5, Fig. 4) should be interpreted with caution.

*Insights into genetic architecture of local adaptation by using complementary approaches*

A classical question is whether adaptation is mainly due to some large effect loci or mainly polygenic. Polygenic architecture may be common and often QTL or association studies fail to detect significant loci for heritable traits if each individual locus has only a small effect (“missing heritability”) (Pritchard and Di Rienzo 2010; Rockman 2012). In our case we had the *a priori* expectation that inversion regions previously identified as enriched for genetic differentiation should have a strong influence on phenotypic divergence. A QTL scan was thus a useful approach and indeed confirmed our expectation for some traits. Most significant peaks in our QTL analysis mapped to inverted regions on LG 6 and 17 that were strong candidates for local adaptation in previous studies. However, inversions, large blocks with little to no recombination, may lead to a detection bias towards these regions (Noor et al. 2001; Roesti 2018). Even without a clustering of important loci in these regions, statistical power for any association analysis between genetic markers and phenotypes is increased. Combining QTL mapping with variance partitioning across LGs might help in two ways. First, it can circumvent this detection bias by showing that candidate chromosomes with inversions explain high amounts of phenotypic variance. In addition, it gives a more nuanced overview than focusing on inversion regions only. It can help to identify genomic regions containing many loci of effects that are too small to be detected individually (Riggio et al. 2013). This higher sensitivity resulted in significant results for many traits without significant peaks in the QTL analysis. We can thus give a more comprehensive picture, which also allows a better evaluation of the importance of inversions in relation to the remaining genomic background. Testing effects of inversion genotypes directly mainly confirmed results of the QTL analysis and variance partitioning and provided additional support for the effects of the different arrangements on phenotypes (Fig. S5, Table S7). Interestingly, some inversions showed significant effects although no QTL in these regions was detected. This could indicate that, in these cases, position effects potentially influencing gene expression are more important than allelic content. Alternatively, testing for genotypes directly may integrate effects of all loci within the inversion region and may thus increase the statistical power similar to variance partitioning.

Almost all traits show clear deviations from the pattern expected under a purely polygenic architecture, where variance explained should increase with chromosomal length (Fig. 4A). This indicates presence of large effect loci or a non-uniform distribution of loci and clustering in certain regions. In line with our expectation and QTL analysis (see Fig. 2 and Fig. 3), LG 6 and LG 17 that harbour inversions involved in genetic ecotype differentiation were clearly identified as outliers in variance partitioning for several traits (Fig. 4). However, some discrepancies exist for LG 5 and 12. Neither showed significant peaks in the QTL analysis, but both clearly stood out in variance partitioning. This may suggest that contribution of these LGs to phenotypic variance is due to a clustering of many loci of small effects that cannot be detected individually by QTL analysis but only by variance partitioning that integrates the effect of the whole LG.

Particularly interesting is LG 12 that most likely includes a sex-determination locus. *Littorina saxatilis* does not seem to have heteromorphic sex chromosomes (García-Souto et al. 2018) and the exact sex determining mechanism is unknown. In other systems, inversions are involved in the evolution of sex chromosomes (Rice 1987; Lenormand 2003; Connallon et al. 2018) as they can suppress recombination and maintain sets of alleles under sexually antagonistic selection. Coupling of alleles with sex-specific benefits to the sex determining locus can ultimately lead to the evolution of sex chromosomes. Some of the traits associated with LG 12 (Height and Width Growth and Aperture Size) showed differences between sexes (Larsson et al. 2020). However, it is unknown whether and how they influence fitness in males and females.

Regional heritability mapping (RHM), where each linkage group is divided into equally sized smaller regions was used to get more information at a finer scale. In the case of Height and Width Growth we could show in this way that high variance explained by LG 2 is not solely caused by its length and a simple cumulative effect of many loci evenly distributed along the LG. RHM showed an accumulation of regions contributing disproportionately to phenotypic variance in the centre of this LG consistent with an enrichment of Crab/Wave outliers that was found before (Morales et al. 2019). Other mechanisms than inversions can lead to high linkage disequilibrium and clusters of loci contributing to divergence (Rafajlović et al. 2016; Burri 2017; Roesti 2018). Low recombination and clustering of adaptive loci may be under positive selection in situations of divergent selection with gene flow. Accumulation of differentiated loci close to the centromere during speciation with gene flow had also been described (Carneiro et al. 2009) and might be an explanation for the clustering of candidate regions in the centre of LG 2. However, in our experiment the ability to reliably detect clusters of adaptive loci is limited by strong LD between regions on the same LG. Since we worked with a F2-cross there had not been much opportunity for recombination and adjacent regions show often the same estimate.

#### *Genetic correlations facilitated ecotype evolution and contributed to adaptation*

Using bivariate animal models for estimation of genetic correlation provided insights into the extent to which different traits share a genetic basis and may thus be prevented from evolving independently. Genetic correlations among traits may either increase or decrease the rate of adaptation, depending on the direction of maximum genetic variance relative to selection acting on the different traits (Lande and Arnold 1983; Hansen and Houle 2008; Stinchcombe et al. 2014). They can prevent adaptation if a correlated trait evolves in a direction that disfavours adaptation or they can increase and facilitate evolution if multivariate selection is in line with genetic covariances. We could show that features that characterise ecotypes in the field are genetically correlated in a way that facilitates adaptation. For example, thicker shells, elongate shape and narrower apertures are features that are genetically correlated and are all under positive selection in the Crab habitat. This may explain the success of *L.*

*saxatilis* in rapidly evolving locally adapted populations multiple times (Johannesson et al. 2010; Butlin et al. 2014; Ravinet et al. 2016).

Genetic correlations alone do not provide any information on whether they are caused by pleiotropic effects, strong linkage between loci or which regions in the genome contribute to them. Here, the QTL analysis gave additional insights by showing that some inversions influence several traits (Fig. 4B). If adaptation depends on alleles at several loci, reduced recombination between them will be positively selected under gene flow. An inversion containing several loci can thus serve as a toolkit for adaptation to different habitats and both facilitate and accelerate formation of locally adapted ecotypes if the alleles combined inside an inversion are in line with the selection pressures associated with a certain habitat. Inversion polymorphisms in an ancestral population, potentially maintained by balancing selection (Faria et al. 2019b), could thus lead to a rapid and repeated formation of ecotypes as was found in sticklebacks (Roesti et al. 2015) and saltmarsh beetles (Van Belleghem et al. 2018).

Although this hypothesis of beneficial recombination suppression has been very popular and is in line with the frequent observation of inversions involved in ecotype formation and speciation (Kirkpatrick and Barton 2006; Ortiz-Barrientos et al. 2016; Charlesworth and Barton 2018; Wellenreuther et al. 2019), empirical evidence remains elusive given the complexity of detecting at least two adaptive loci inside an inversion (but see for example Fuller et al. 2017; Lee et al. 2017; Coughlan and Willis 2019). Here we argue that our observation of some inversions explaining variation in more than one trait is suggestive for adaptive recombination suppression. However, without knowing the exact genetic basis and identification of responsible genes we cannot confirm that this is caused by multiple loci inside the inversion. Specific mechanisms by which inversions can influence phenotypes are diverse. They can have a strong and direct influence on phenotypes when genes at breakpoints are disrupted. Independent of allelic contents, directionality of an inversion can influence phenotypes by rearranging regulatory regions and changing gene expression (Lavington and Kern 2017; Huang et al. 2018; Said et al. 2018). It is thus also possible that observed associations with several traits are caused by pleiotropic effects.

Genetic covariances can also help us to disentangle the causative drivers of phenotypic clines observed in nature. Two potential problems when analysing clines are high confounding of environmental factors and also identifying the target of selection when many traits change simultaneously. It is possible that some of the phenotypic clines observed in *L. saxatilis* could be the result of indirect selection acting on other traits. We found evidence that colour was influenced by an inversion on LG 6 that contribute to many other traits under divergent selection. Thus, colouration might be co-segregating with other traits directly targeted by selection, potentially explaining the large amount of colour polymorphism in this species (Johannesson and Butlin 2017).

The exact mechanisms by which inversions influence phenotypes are still unknown. Measuring gene expression, testing whether transcript abundance for reads mapped to inversion regions differs between karyotypes, may help to test whether allelic content or directionality are more important for phenotypic variation. While tight linkage between alleles within an inversion might have facilitated adaptation to Crab/Wave habitats, it also means a reduced evolutionary flexibility since some traits cannot evolve independently. For instance, a high genetic correlation between shape and aperture size found here indicates that evolution of forms with narrow apertures but the globular wave shape might be unlikely or limited. In contrast, correlation between size measures and shape is lower meaning they can evolve independently. *Littorina saxatilis* shows a large range of differently adapted ecotypes with different shapes and sizes (Reid 1996; Johannesson et al. 2010). It remains an open question how widespread specific inversions are, and whether the same ancestral inversion polymorphism was repeatedly involved in ecotype development.

### **Acknowledgments**

We are very grateful to Irena Senčić for technical assistance and to Michelle Kortyna and Sean Holland at the Center for Anchored Phylogenomics for assistance with data collection. RKB was funded by the Natural Environment Research Council and by the European Research Council. KJ was funded by the Swedish Research Councils VR and Formas (Linnaeus grant: 217-2008-1719). JL was funded by a studentship from the Leverhulme Centre for Advanced Biological Modelling. AMW was funded by the European Union's Horizon 2020 research and innovation program under Marie Skłodowska-Curie grant agreement no. 797747. RF was funded by the European Union's Horizon 2020 research and innovation programme under the Marie Skłodowska-Curie grant agreement No. 706376 and by FEDER Funds through the Operational Competitiveness Factors Program - COMPETE and by National Funds through FCT - Foundation for Science and Technology within the scope of the project "Hybrabbid" (PTDC/BIA-EVL/30628/2017- POCI-01-0145-FEDER-030628). We are grateful to other members of the *Littorina* research group for helpful discussions. We thank Claire Mérot and an anonymous referee for insightful comments on an earlier version.

### **Conflict of interest**

The authors declare no conflicts of interest.

### **Data archiving**

Data and scripts are available from the Dryad Digital Repository (<https://doi.org/10.5061/dryad.zgmsbccb4>).

## References

- Aeschbacher, S., J. P. Selby, J. H. Willis, and G. Coop. 2017. Population-genomic inference of the strength and timing of selection against gene flow. *Proc. Natl. Acad. Sci.* 114:7061–7066.
- Amadeu, R. R., C. Cellon, J. W. Olmstead, A. A. F. Garcia, M. F. R. Resende, and P. R. Muñoz. 2016. AGHmatrix: R package to construct relationship matrices for autotetraploid and diploid species: A blueberry example. *Plant Genome* 9.
- Arends, D., P. Prins, R. C. Jansen, and K. W. Broman. 2010. R/qt1: High-throughput multiple QTL mapping. *Bioinformatics* 26:2990–2992.
- Ayala, D., M. C. Fontaine, A. Cohuet, D. Fontenille, R. Vitalis, and F. Simard. 2011. Chromosomal inversions, natural selection and adaptation in *Anopheles funestus*. *Mol. Biol. Evol.* 28:745–758.
- Ayala, D., A. Ullastres, and J. González. 2014. Adaptation through chromosomal inversions in *Anopheles*. *Front. Genet.* 5:1–10.
- Ayala, D., S. Zhang, M. Chateau, C. Fouet, I. Morlais, C. Costantini, M. W. Hahn, and N. J. Besansky. 2019. Association mapping desiccation resistance within chromosomal inversions in the African malaria vector *Anopheles gambiae*. *Mol. Ecol.* 28:1333–1342.
- Bates, D., M. Mächler, B. Bolker, and S. Walker. 2015. Fitting linear mixed-effects models using lme4. *J. Stat. Softw.* 67.
- Béréos, C., P. A. Ellis, J. G. Pilkington, S. H. Lee, J. Gratten, and J. M. Pemberton. 2015. Heterogeneity of genetic architecture of body size traits in a free-living population. *Mol. Ecol.* 24:1810–1830.
- Blanckenhorn, W. U. 2000. The Evolution of Body Size: What Keeps Organisms Small. *Q. Rev. Biol.* 75:385–407.
- Boulding, E. G., M. J. Rivas, N. González-Lavín, E. Rolán-Alvarez, and J. Galindo. 2017. Size selection by a gape-limited predator of a marine snail: Insights into magic traits for speciation. *Ecol. Evol.* 7:674–688.
- Broman, K. W., D. M. Gatti, P. Simecek, N. A. Furlotte, P. Prins, Ś. Sen, B. S. Yandell, and G. A. Churchill. 2019. R/qt2: Software for Mapping Quantitative Trait Loci with High-Dimensional Data and Multiparent Populations. *Genetics* 211:495–502.
- Bürger, R., and A. Akerman. 2011. The effects of linkage and gene flow on local adaptation: A two-locus continent-island model. *Theor. Popul. Biol.* 80:272–288.
- Burri, R. 2017. Interpreting differentiation landscapes in the light of long-term linked selection. *Evol. Lett.* 1:118–131.
- Butler, D. G., B. R. Cullis, A. R. Gilmour, and B. J. Gogel. 2009. Analysis of mixed models for S language environments: ASReml-R reference manual. Brisbane, DPI Publ.
- Butlin, R. K., and T. H. Day. 1985. Adult size, longevity and fecundity in the seaweed fly, *Coelopa frigida*. *Heredity* 54:107–110.
- Butlin, R. K., and T. H. Day. 1989. Environmental correlates of inversion frequencies in natural populations of seaweed flies (*Coelopa frigida*). *Heredity* 62:223–232.
- Butlin, R. K., I. L. Read, and T. H. Day. 1982. The effects of a chromosomal inversion on adult size and male mating success in the seaweed fly, *Coelopa frigida*. *Heredity* 49:51–62.
- Butlin, R. K., M. Saura, G. Charrier, B. Jackson, C. André, A. Caballero, J. A. Coyne, J. Galindo, J. W. Grahame, J. Hollander, P. Kempainen, M. Martínez-Fernández, M. Panova, H. Quesada, K. Johannesson, and E. Rolán-Alvarez. 2014. Parallel evolution of local adaptation and reproductive isolation in the face of gene flow. *Evolution* 68:935–949.
- Carneiro, M., N. Ferrand, and M. W. Nachman. 2009. Recombination and speciation: Loci near centromeres are more differentiated than loci near telomeres between subspecies of the European rabbit (*Oryctolagus cuniculus*). *Genetics* 181:593–606.
- Charlesworth, B., and N. H. Barton. 2018. The spread of an inversion with migration and selection. *Genetics* 208:377–382.
- Chhatre, V. E., L. M. Evans, S. P. DiFazio, and S. R. Keller. 2018. Adaptive introgression and maintenance of a trispecies hybrid complex in range-edge populations of *Populus*. *Mol. Ecol.*

- 27:4820–4838.
- Christmas, M. J., A. Wallberg, I. Bunikis, A. Olsson, O. Wallerman, and M. T. Webster. 2019. Chromosomal inversions associated with environmental adaptation in honeybees. *Mol. Ecol.* 28:1358–1374.
- Connallon, T., C. Olito, L. Dutoit, H. Papoli, F. Ruzicka, and L. Yong. 2018. Local adaptation and the evolution of inversions on sex chromosomes and autosomes. *Philos. Trans. R. Soc. B Biol. Sci.* 373.
- Coughlan, J. M., and J. H. Willis. 2019. Dissecting the role of a large chromosomal inversion in life history divergence throughout the *Mimulus guttatus* species complex. *Mol. Ecol.* 28:1343–1357.
- Durmaz, E., C. Benson, M. Kapun, P. Schmidt, and T. Flatt. 2018. An inversion supergene in *Drosophila* underpins latitudinal clines in survival traits. *J. Evol. Biol.* 31:1354–1364.
- Edelman, N. B., P. B. Frandsen, M. Miyagi, B. Clavijo, J. Davey, R. B. Dikow, G. García-Accinelli, S. M. Van Belleghem, N. Patterson, D. E. Neafsey, R. Challis, S. Kumar, G. R. P. Moreira, C. Salazar, M. Chouteau, B. A. Counterman, R. Papa, M. Blaxter, R. D. Reed, K. K. Dasmahapatra, M. Kronforst, M. Joron, C. D. Jiggins, W. Owen McMillan, F. Di Palma, A. J. Blumberg, J. Wakeley, D. Jaffe, and J. Mallet. 2019. Genomic architecture and introgression shape a butterfly radiation. *Science* 366:594–599.
- Faria, R., P. Chaube, H. E. Morales, T. Larsson, A. R. Lemmon, E. M. Lemmon, M. Rafajlović, M. Panova, M. Ravinet, K. Johannesson, A. M. Westram, and R. K. Butlin. 2019a. Multiple chromosomal rearrangements in a hybrid zone between *Littorina saxatilis* ecotypes. *Mol. Ecol.* 28:1375–1393.
- Faria, R., K. Johannesson, R. K. Butlin, and A. M. Westram. 2019b. Evolving Inversions. *Trends Ecol. Evol.* 34:239–248.
- Feder, J. L., S. P. Egan, and P. Nosil. 2012. The genomics of speciation-with-gene-flow. *Trends Genet.* 28:342–350.
- Feder, J. L., and P. Nosil. 2009. Chromosomal inversions and species differences: When are genes affecting adaptive divergence and reproductive isolation expected to reside within inversions? *Evolution* 63:3061–3075.
- Felsenstein, J. 1981. Skepticism Towards Santa Rosalia, or Why are There so Few Kinds of Animals? *Evolution* 35:124.
- Fuller, Z. L., G. D. Haynes, S. Richards, and S. W. Schaeffer. 2017. Genomics of natural populations: Evolutionary forces that establish and maintain gene arrangements in *Drosophila pseudoobscura*. *Mol. Ecol.* 26:6539–6562.
- García-Souto, D., S. Alonso-Rubido, D. Costa, J. M. Eirín-López, E. Rolán-álvarez, R. Faria, J. Galindo, and J. J. Pasantes. 2018. Karyotype characterization of nine periwinkle species (Gastropoda, littorinidae). *Genes (Basel)*. 9:1–11.
- Gilmour, A. R., B. J. Gogel, B. R. Cullis, and R. Thompson. 2009. ASReml user guide release 3.0.
- Hansen, T. F., and D. Houle. 2008. Measuring and comparing evolvability and constraint in multivariate characters. *J. Evol. Biol.* 21:1201–1219.
- Hanson, D., J. Hu, A. P. Hendry, and R. D. H. Barrett. 2017. Heritable gene expression differences between lake and stream stickleback include both parallel and antiparallel components. *Heredity* 119:339–348.
- Harrison, R. G., and E. L. Larson. 2016. Heterogeneous genome divergence, differential introgression, and the origin and structure of hybrid zones. *Mol. Ecol.* 25:2454–2466.
- Hereford, J. 2009. A Quantitative Survey of Local Adaptation and Fitness Trade-Offs. *Am. Nat.* 173:579–588.
- Hoffmann, A. A., and L. H. Rieseberg. 2008. Revisiting the Impact of Inversions in Evolution: From Population Genetic Markers to Drivers of Adaptive Shifts and Speciation? *Annu. Rev. Ecol. Evol. Syst.* 39:21–42.
- Hoffmann, A. A., C. M. Sgrò, and A. R. Weeks. 2004. Chromosomal inversion polymorphisms and

- adaptation. *Trends Ecol. Evol.* 19:482–488.
- Huang, Y. C., V. D. Dang, N. C. Chang, and J. Wang. 2018. Multiple large inversions and breakpoint rewiring of gene expression in the evolution of the fire ant social supergene. *Proc. R. Soc. B Biol. Sci.* 285.
- Janson, K. 1982. Genetic and environmental effects on the growth rate of *Littorina saxatilis*. *Mar. Biol.* 69:73–78.
- Janson, K. 1983. Selection and migration in two distinct phenotypes of *Littorina saxatilis* in Sweden. *Oecologia* 59:58–61.
- Johannesson, B. 1986. Shell morphology of *Littorina saxatilis* Olivi: The relative importance of physical factors and predation. *J. Exp. Mar. Bio. Ecol.* 102:183–195.
- Johannesson, B., and K. Johannesson. 1996. Population differences in behaviour and morphology in the snail *Littorina saxatilis*: Phenotypic plasticity or genetic differentiation? *J. Zool.* 240:475–493.
- Johannesson, K. 2016. What can be learnt from a snail? *Evol. Appl.* 9:153–165.
- Johannesson, K., and R. K. Butlin. 2017. What explains rare and conspicuous colours in a snail? A test of time-series data against models of drift, migration or selection. *Heredity* 118:21–30.
- Johannesson, K., J. N. Havenhand, P. R. Jonsson, M. Lindegarth, A. Sundin, and J. Hollander. 2008. Male discrimination of female mucous trails permits assortative mating in a marine snail species. *Evolution* 62:3178–3184.
- Johannesson, K., B. Johannesson, and E. Rolan-Alvarez. 1993. Morphological Differentiation and Genetic Cohesiveness Over a Microenvironmental Gradient in the Marine Snail *Littorina saxatilis*. *Evolution* 47:1770.
- Johannesson, K., M. Panova, P. Kempainen, C. André, E. Rolan-Alvarez, and R. K. Butlin. 2010. Repeated evolution of reproductive isolation in a marine snail: Unveiling mechanisms of speciation. Pp. 1735–1747 in *Philosophical Transactions of the Royal Society B: Biological Sciences*.
- Joron, M., L. Frezal, R. T. Jones, N. L. Chamberlain, S. F. Lee, C. R. Haag, A. Whibley, M. Becuwe, S. W. Baxter, L. Ferguson, P. A. Wilkinson, C. Salazar, C. Davidson, R. Clark, M. A. Quail, H. Beasley, R. Glithero, C. Lloyd, S. Sims, M. C. Jones, J. Rogers, C. D. Jiggins, and R. H. French-Constant. 2011. Chromosomal rearrangements maintain a polymorphic supergene controlling butterfly mimicry. *Nature* 477:203–206.
- Kapun, M., D. K. Fabian, J. Goudet, and T. Flatt. 2016a. Genomic Evidence for Adaptive Inversion Clines in *Drosophila melanogaster*. *Mol. Biol. Evol.* 33:1317–1336.
- Kapun, M., and T. Flatt. 2019. The adaptive significance of chromosomal inversion polymorphisms in *Drosophila melanogaster*. *Mol. Ecol.* 28:1263–1282.
- Kapun, M., C. Schmidt, E. Durmaz, P. S. Schmidt, and T. Flatt. 2016b. Parallel effects of the inversion In(3R)Payne on body size across the North American and Australian clines in *Drosophila melanogaster*. *J. Evol. Biol.* 29:1059–1072.
- Kirkpatrick, M. 2010. How and why chromosome inversions evolve. *PLoS Biol.* 8:e1000501.
- Kirkpatrick, M., and N. Barton. 2006. Chromosome inversions, local adaptation and speciation. *Genetics* 173:419–434.
- Kirkpatrick, M., and A. Kern. 2012. Where's the money? inversions, genes, and the hunt for genomic targets of selection. *Genetics* 190:1153–1155.
- Klopfstein, S., M. Currat, and L. Excoffier. 2006. The fate of mutations surfing on the wave of a range expansion. *Mol. Biol. Evol.* 23:482–490.
- Kruuk, L. E. B. 2004. Estimating genetic parameters in natural populations using the “animal model.” *Philos. Trans. R. Soc. B Biol. Sci.* 359:873–890.
- Kuznetsova, A., P. B. Brockhoff, and R. H. B. Christensen. 2017. lmerTest Package: Tests in Linear Mixed Effects Models. *J. Stat. Softw.* 82:1–26.
- Lande, R., and S. J. Arnold. 1983. The Measurement of Selection on Correlated Characters. *Evolution* 37:1210.

- Larsson, J., A. M. Westram, S. Bengmark, T. Lundh, and R. K. Butlin. 2020. A developmentally descriptive method for quantifying shape in gastropod shells. *J. R. Soc. Interface* 17:20190721.
- Lavington, E., and A. D. Kern. 2017. The effect of common inversion polymorphisms In(2L)t and In(3R)Mo on patterns of transcriptional variation in *Drosophila melanogaster*. *G3 Genes, Genomes, Genet.* 7:3659–3668.
- Le Pennec, G., R. K. Butlin, P. R. Jonsson, A. I. Larsson, J. Lindborg, E. Bergström, A. M. Westram, and K. Johannesson. 2017. Adaptation to dislodgement risk on waveswept rocky shores in the snail *Littorina saxatilis*. *PLoS One* 12:1–15.
- Lee, C. R., B. Wang, J. P. Mojica, T. Mandáková, K. V. S. K. Prasad, J. L. Goicoechea, N. Perera, U. Hellsten, H. N. Hundley, J. Johnson, J. Grimwood, K. Barry, T. Fairclough, J. W. Jenkins, Y. Yu, D. Kudrna, J. Zhang, J. Talag, W. Golser, K. Ghattas, M. E. Schranz, R. Wing, M. A. Lysak, J. Schmutz, D. S. Rokhsar, and T. Mitchell-Olds. 2017. Young inversion with multiple linked QTLs under selection in a hybrid zone. *Nat. Ecol. Evol.* 1:0119.
- Lee, Y. W., L. Fishman, J. K. Kelly, and J. H. Willis. 2016. A segregating inversion generates fitness variation in yellow monkeyflower (*Mimulus guttatus*). *Genetics* 202:1473–1484.
- Lenormand, T. 2002. Gene flow and the limits to natural selection. *Trends Ecol. Evol.* 17:183–189.
- Lenormand, T. 2003. The evolution of sex dimorphism in recombination. *Genetics* 163:811–822.
- Lenormand, T., and S. P. Otto. 2000. The evolution of recombination in a heterogeneous environment. *Genetics* 156:423–438.
- Lowry, D. B., and J. H. Willis. 2010. A widespread chromosomal inversion polymorphism contributes to a major life-history transition, local adaptation, and reproductive isolation. *PLoS Biol.* 8.
- Manolio, T. A., F. S. Collins, N. J. Cox, D. B. Goldstein, L. A. Hindorff, D. J. Hunter, M. I. McCarthy, E. M. Ramos, L. R. Cardon, A. Chakravarti, J. H. Cho, A. E. Guttmacher, A. Kong, L. Kruglyak, E. Mardis, C. N. Rotimi, M. Slatkin, D. Valle, A. S. Whittemore, M. Boehnke, A. G. Clark, E. E. Eichler, G. Gibson, J. L. Haines, T. F. C. Mackay, S. A. McCarrroll, and P. M. Visscher. 2009. Finding the missing heritability of complex diseases. *Nature* 461:747–753.
- Mérot, C., E. L. Berdan, C. Babin, E. Normandeau, M. Wellenreuther, and L. Bernatchez. 2018. Intercontinental karyotype-environment parallelism supports a role for a chromosomal inversion in local adaptation in a seaweed fly. *Proc. R. Soc. B Biol. Sci.* 285.
- Mérot, C., V. Llaurens, E. Normandeau, L. Bernatchez, and M. Wellenreuther. 2020. Balancing selection via life-history trade-offs maintains an inversion polymorphism in a seaweed fly. *Nat. Commun.* 11.
- Morales, H. E., R. Faria, K. Johannesson, T. Larsson, M. Panova, A. M. Westram, and R. K. Butlin. 2019. Genomic architecture of parallel ecological divergence: Beyond a single environmental contrast. *Sci. Adv.* 5.
- Nagamine, Y., R. Pong-Wong, P. Navarro, V. Vitart, C. Hayward, I. Rudan, H. Campbell, J. Wilson, S. Wild, A. A. Hicks, P. P. Pramstaller, N. Hastie, A. F. Wright, and C. S. Haley. 2012. Localising Loci underlying Complex Trait Variation Using Regional Genomic Relationship Mapping. *PLoS One* 7:e46501.
- Navarro, A., and N. H. Barton. 2003. Accumulating postzygotic isolation genes in parapatry: A new twist on chromosomal speciation. *Evolution* 57:447–459.
- Navarro, N. 2015. R/shapeQTL: shape QTL mapping experiment with R. Retrieved from [github.com/nnavarro/shapeQTL](https://github.com/nnavarro/shapeQTL).
- Noor, M. A. F., A. L. Cunningham, and J. C. Larkin. 2001. Consequences of recombination rate variation on quantitative trait locus mapping studies: Simulations based on the *Drosophila melanogaster* genome. *Genetics* 159:581–588.
- Ortiz-Barrientos, D., J. Engelstädter, and L. H. Rieseberg. 2016. Recombination Rate Evolution and the Origin of Species. *Trends Ecol. Evol.* 31:226–236.
- Panova, M., H. Aronsson, A. Cameron, P. Dahl, A. Godhe, U. Lind, O. Ortega-Martinez, R. Pereyra, S. V. M. Tesson, T. BlombergKerstin, A.-L. WrangeAnders, T. SV, A.-L. Wrange, A. Blomberg, and K. Johannesson. 2016. DNA extraction protocols for whole-genome sequencing in marine

- organisms. Pp. 13–44 in S. J. Bourlat, ed. *Marine Genomics, Methods and Protocols*. Springer, New York.
- Panova, M., J. Hollander, and K. Johannesson. 2006. Site-specific genetic divergence in parallel hybrid zones suggests nonallopatric evolution of reproductive barriers. *Mol. Ecol.* 15:4021–4031.
- Panova, M., and K. Johannesson. 2004. Microscale variation in Aat (aspartate aminotransferase) is supported by activity differences between upper and lower shore allozymes of *Littorina saxatilis*. *Mar. Biol.* 144:1157–1164.
- Perini, S., M. Rafajlović, A. M. Westram, K. Johannesson, and R. K. Butlin. 2020. Assortative mating, sexual selection, and their consequences for gene flow in *Littorina*. *Evolution* 1–16.
- Pinho, C., and J. Hey. 2010. Divergence with Gene Flow: Models and Data. *Annu. Rev. Ecol. Evol. Syst.* 41:215–230.
- Pritchard, J. K., and A. Di Rienzo. 2010. Adaptation - Not by sweeps alone. *Nat. Rev. Genet.* 11:665–667.
- Rafajlović, M., A. Emanuelsson, K. Johannesson, R. K. Butlin, and B. Mehlig. 2016. A universal mechanism generating clusters of differentiated loci during divergence-with-migration. *Evolution* 70:1609–1621.
- Ravinet, M., R. Faria, R. K. Butlin, J. Galindo, N. Bierne, M. Rafajlović, M. A. F. Noor, B. Mehlig, and A. M. Westram. 2017. Interpreting the genomic landscape of speciation: a road map for finding barriers to gene flow. *J. Evol. Biol.* 30:1450–1477.
- Ravinet, M., A. Westram, K. Johannesson, R. Butlin, C. André, and M. Panova. 2016. Shared and nonshared genomic divergence in parallel ecotypes of *Littorina saxatilis* at a local scale. *Mol. Ecol.* 25:287–305.
- Reid, D. G. 1996. *Systematics and Evolution of Littorina*. Ray Society.
- Rice, W. R. 1987. The accumulation of sexually antagonistic genes as a selective agent promoting the evolution of reduced recombination between primitive sex chromosomes. *Evolution* 41:911–914.
- Rieseberg, L. H. 2001. Chromosomal rearrangements and speciation. *Trends Ecol. Evol.* 16:351–358.
- Riggio, V., O. Matika, R. Pong-Wong, M. J. Stear, and S. C. Bishop. 2013. Genome-wide association and regional heritability mapping to identify loci underlying variation in nematode resistance and body weight in Scottish Blackface lambs. *Heredity* 110:420–429.
- Robinson, M. R., A. W. Santure, I. DeCauwer, B. C. Sheldon, and J. Slate. 2013. Partitioning of genetic variation across the genome using multimarker methods in a wild bird population. *Mol. Ecol.* 22:3963–3980.
- Rockman, M. V. 2012. The QTN program and the alleles that matter for evolution: All that’s gold does not glitter. *Evolution* 66:1–17.
- Roesti, M. 2018. Varied genomic responses to maladaptive gene flow and their evidence. *Genes (Basel)*. 9.
- Roesti, M., B. Kueng, D. Moser, and D. Berner. 2015. The genomics of ecological vicariance in threespine stickleback fish. *Nat. Commun.* 6.
- Rolán-Alvarez, E. 2007. Sympatric speciation as a by-product of ecological adaptation in the Galician *Littorina saxatilis* hybrid zone. *J. Molluscan Stud.* 73:1–10.
- Said, I., A. Byrne, V. Serrano, C. Cardeno, C. Vollmers, and R. Corbett-Detig. 2018. Linked genetic variation and not genome structure causes widespread differential expression associated with chromosomal inversions. *Proc. Natl. Acad. Sci.* 115:5492–5497.
- Santure, A. W., J. Poissant, I. De Cauwer, K. Van Oers, M. R. Robinson, J. L. Quinn, M. A. M. Groenen, M. E. Visser, B. C. Sheldon, and J. Slate. 2015. Replicated analysis of the genetic architecture of quantitative traits in two wild great tit populations. *Mol. Ecol.* 24:6148–6162.
- Savolainen, O., M. Lascoux, and J. Merilä. 2013. Ecological genomics of local adaptation. *Nat. Rev. Genet.* 14:807–820.
- Schaefer, J., D. Duvernell, and D. C. Campbell. 2016. Hybridization and introgression in two

- ecologically dissimilar *Fundulus* hybrid zones. *Evolution* 70:1051–1063.
- Servedio, M. R., and J. W. Boughman. 2017. The Role of Sexual Selection in Local Adaptation and Speciation. *Annu. Rev. Ecol. Evol. Syst.* 48:85–109.
- Sinclair-Waters, M., I. R. Bradbury, C. J. Morris, S. Lien, M. P. Kent, and P. Bentzen. 2018. Ancient chromosomal rearrangement associated with local adaptation of a postglacially colonized population of Atlantic Cod in the northwest Atlantic. *Mol. Ecol.* 27:339–351.
- Slatkin, M. 1987. Gene Flow and the Geographic Structure of Natural Populations. *Science* 236:787–792.
- Smadja, C. M., and R. K. Butlin. 2011. A framework for comparing processes of speciation in the presence of gene flow. *Mol. Ecol.* 20:5123–5140.
- Sokolova, I. M., and H. O. Pörtner. 2003. Metabolic plasticity and critical temperatures for aerobic scope in a eurythermal marine invertebrate (*Littorina saxatilis*, Gastropoda: Littorinidae) from different latitudes. *J. Exp. Biol.* 206:195–207.
- Stinchcombe, J. R., A. K. Simonsen, and M. W. Blows. 2014. Estimating uncertainty in multivariate responses to selection. *Evolution* 68:1188–1196.
- Twyford, A. D., and J. Friedman. 2015. Adaptive divergence in the monkey flower *Mimulus guttatus* is maintained by a chromosomal inversion. *Evolution* 69:1476–1486.
- Van Belleghem, S. M., C. Vangestel, K. De Wolf, Z. De Corte, M. Möst, P. Rastas, L. De Meester, and F. Hendrickx. 2018. Evolution at two time frames: Polymorphisms from an ancient singular divergence event fuel contemporary parallel evolution. *PLoS Genet.* 14:1–26.
- VanRaden, P. M. 2008. Efficient methods to compute genomic predictions. *J. Dairy Sci.* 91:4414–4423.
- Wellenreuther, M., and L. Bernatchez. 2018. Eco-Evolutionary Genomics of Chromosomal Inversions. *Trends Ecol. Evol.* 33:427–440.
- Wellenreuther, M., C. Mérot, E. Berdan, and L. Bernatchez. 2019. Going beyond SNPs: The role of structural genomic variants in adaptive evolution and species diversification. *Mol. Ecol.* 28:1203–1209.
- Wenzel, M. A., M. C. James, A. Douglas, and S. B. Piertney. 2015. Genome-wide association and genome partitioning reveal novel genomic regions underlying variation in gastrointestinal nematode burden in a wild bird. *Mol. Ecol.* 24:4175–4192.
- Westram, A. M., M. Rafajlović, P. Chaube, R. Faria, T. Larsson, M. Panova, M. Ravinet, A. Blomberg, B. Mehlig, K. Johannesson, and R. Butlin. 2018. Clines on the seashore: The genomic architecture underlying rapid divergence in the face of gene flow. *Evol. Lett.* 2:297–309.
- Wilson, A. J., D. Réale, M. N. Clements, M. M. Morrissey, E. Postma, C. A. Walling, L. E. B. Kruuk, and D. H. Nussey. 2010. An ecologist's guide to the animal model. *J. Anim. Ecol.* 79:13–26.
- Wu, C. A., D. B. Lowry, A. M. Cooley, K. M. Wright, Y. W. Lee, and J. H. Willis. 2008. *Mimulus* is an emerging model system for the integration of ecological and genomic studies. *Heredity* 100:220–230.
- Yang, J., B. Benyamin, B. P. McEvoy, S. Gordon, A. K. Henders, D. R. Nyholt, P. A. Madden, A. C. Heath, N. G. Martin, G. W. Montgomery, M. E. Goddard, and P. M. Visscher. 2010. Common SNPs explain a large proportion of the heritability for human height. *Nat. Genet.* 42:565–569.
- Yeaman, S. 2013. Genomic rearrangements and the evolution of clusters of locally adaptive loci. *Proc. Natl. Acad. Sci.* 110.
- Yeaman, S., and S. P. Otto. 2011. Establishment and maintenance of adaptive genetic divergence under migration, selection, and drift. *Evolution* 65:2123–2129.
- Yeaman, S., and M. C. Whitlock. 2011. The genetic architecture of adaptation under migration-selection balance. *Evolution* 65:1897–1911.

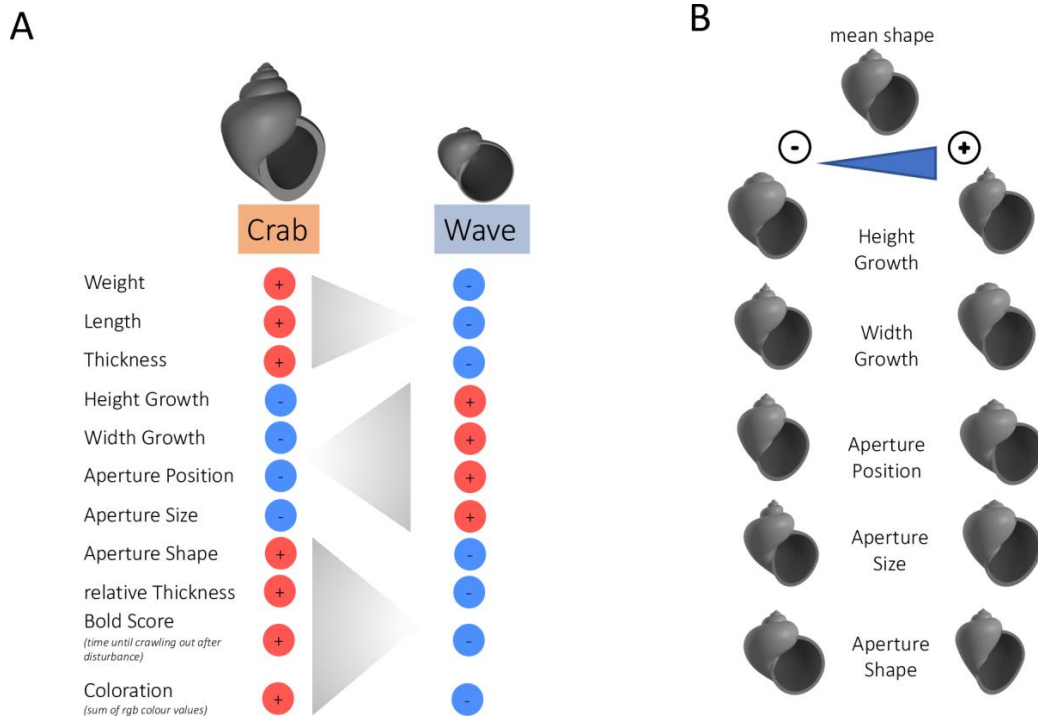


**Figure 1: (A).** Traits analysed in this study and their association with ecotypes in the field. The Crab ecotype occurs in boulder fields and is exposed to Crab predation, whereas the Wave type can be found on rocky shores under wave exposure. Red + indicates that larger values are associated with the respective ecotype, blue – indicates smaller values. **(B)** Illustration of the different shape parameters analysed in this study. Parameters are obtained based on a growth model (Larsson et al. 2020). The shape at the top represents the mean value of the whole F2 set. Each of the other shapes is varied for one parameter of interest, while all other parameters are held constant. The overall characteristic Crab and Wave shapes are shown in **(A)**.

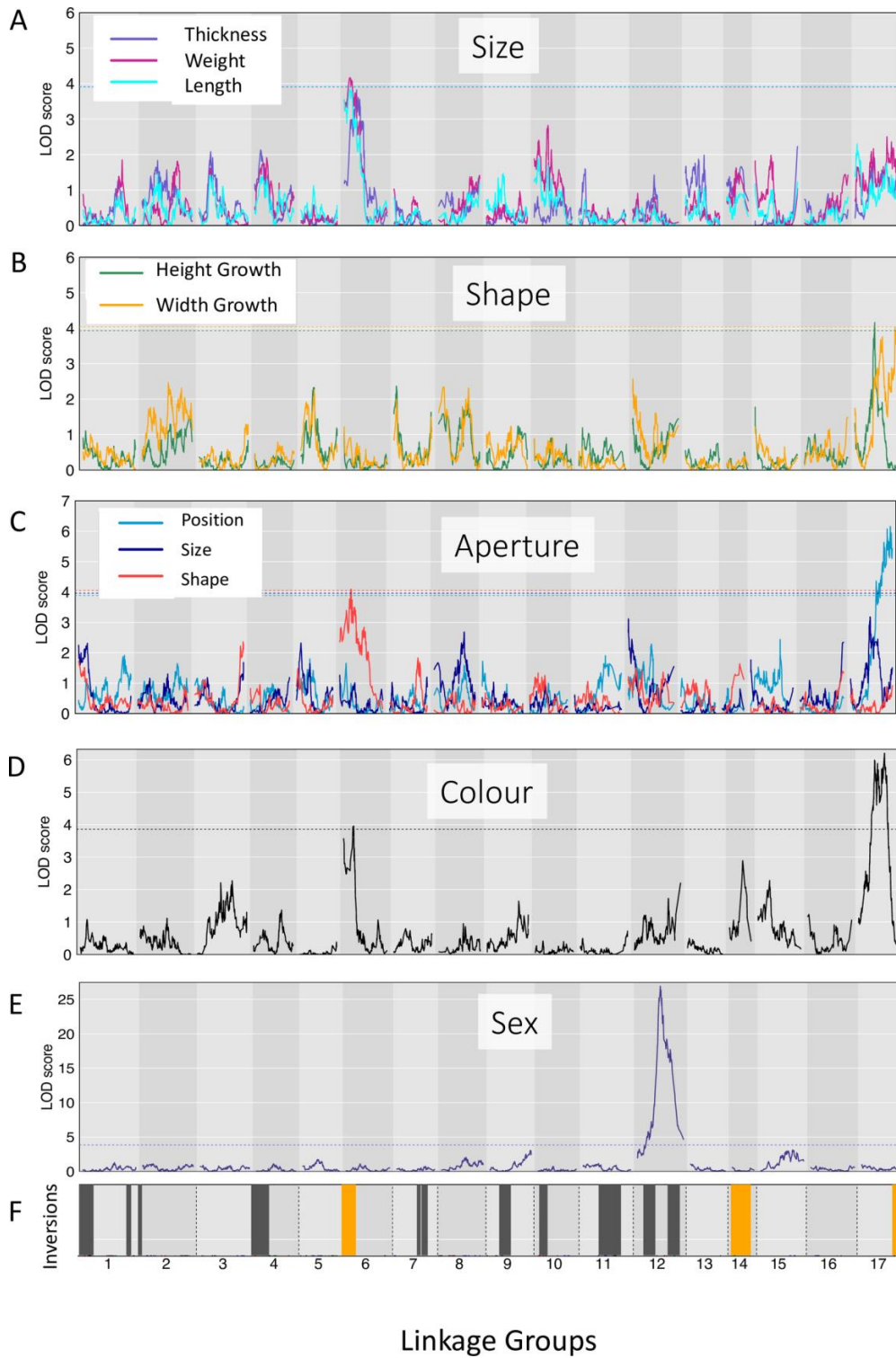


**Figure 2:** QTL scans for: weight, shell thickness and shell length (**A**); size independent parameters describing shell shape: Width and Height growth (**B**); for Aperture Size, Shape, and Position (**C**), shell colour (rgb values) analysed as a multivariate trait (**D**), and sex analysed

as binary trait **(E)**. Dashed lines indicate genome wide significant thresholds ( $P = 0.05$ ). Positions of putative inversion regions ( $\pm 2$  cM) based on Faria et al. (2019a) **(F)**. The positions are based on markers in common with the previous linkage map (based on a Crab/Crab cross). The exact positions of the inverted regions can thus only be approximated since markers at the utmost boundaries of the inversions were not always present in our map (see Supporting Information Table S1). Regions that showed an elevated proportion of non-neutral SNPs based on cline analysis in the hybrid zone (Westram et al. 2018) and that overlap with inversions are indicated in orange.

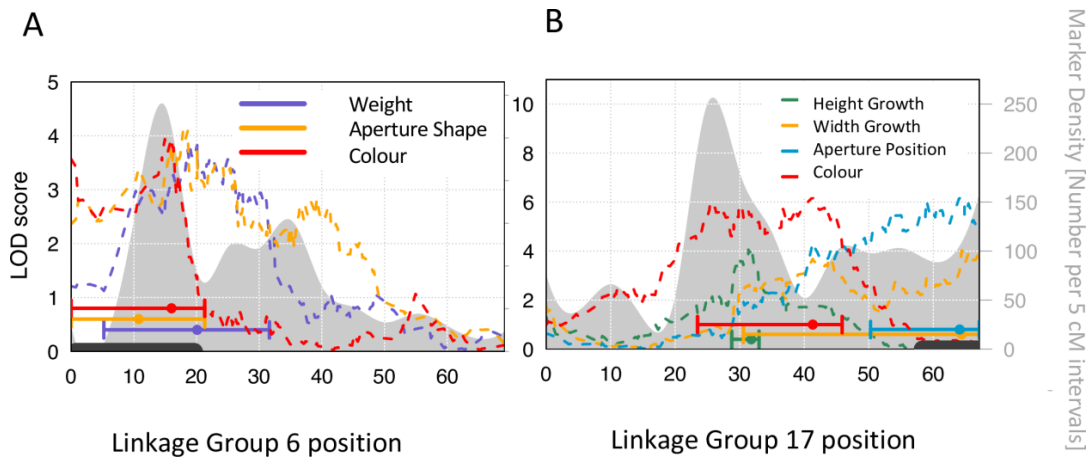


**Figure 3:** LOD scores for traits with significant QTLs ( $P$ -value for Width Growth = 0.053) on linkage group 6 **(A)** and 17 **(B)** with the 95 % confidence interval (bars with CI) of their position. Position along the linkage group is given on the x-axis and LOD-scores (dashed lines) on the left y-axis. Grey density plots give the marker density (number of markers per 5cM intervals) along the linkage group (right y-axis). Locations of inversions that were detected previously (Faria et al 2019a) are shown by grey bars along the x-axis. Regions of suppressed recombination with high marker density often coincide with previously described inversions. On both linkage groups a clustering of QTLs within inverted regions is observed. On LG 17 we also see a cluster outside the inversion region consisting of QTLs for colour, Height Growth and Aperture Size (not significant, LOD = 3.12,  $P = 0.24$ ).

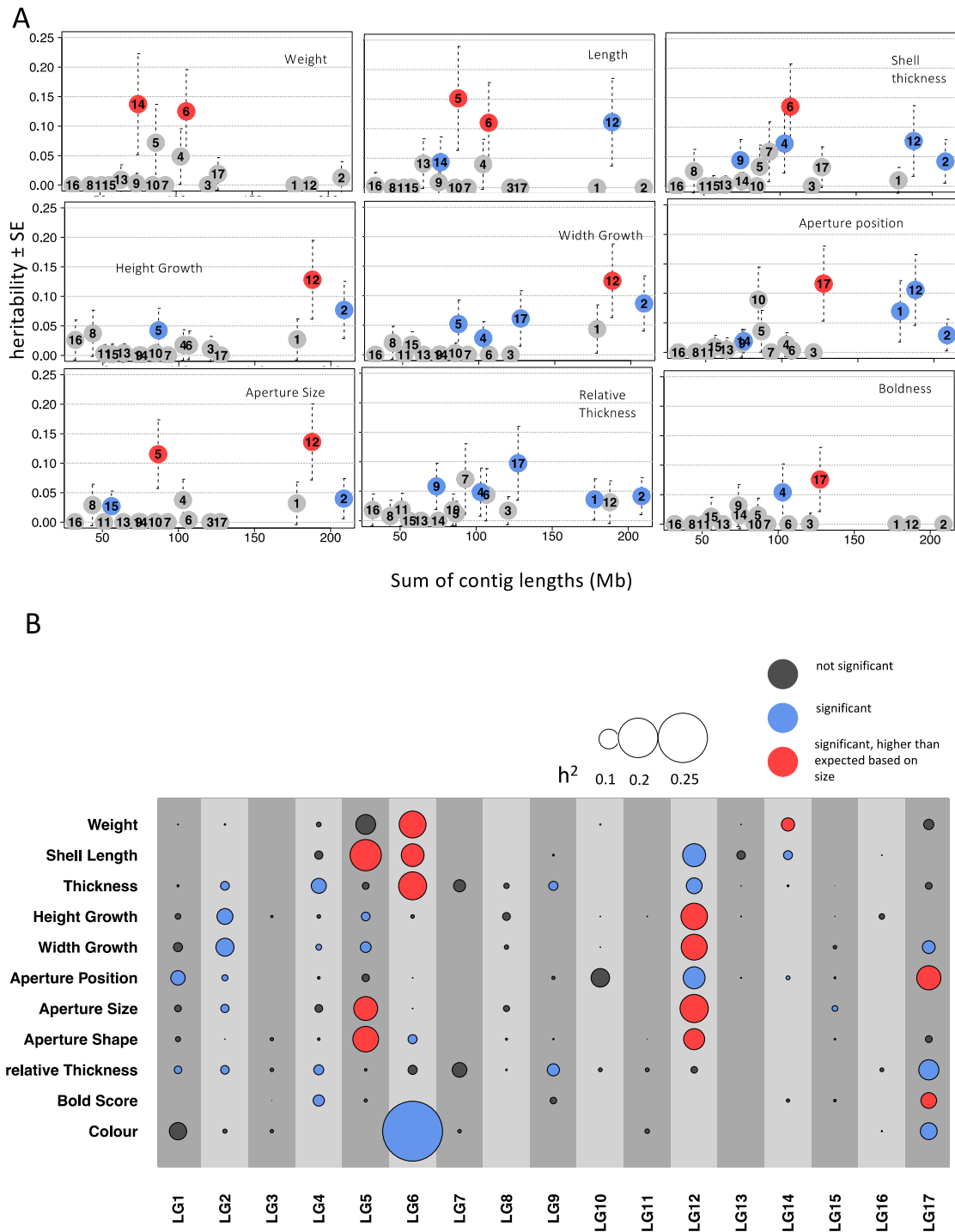


**Figure 4:** (A) Examples for proportion of phenotypic variance explained by different linkage groups (LG) ± standard error (SE) relative to sum of contig length that are assigned to each LG (proportional to chromosome length). If a trait is completely polygenic and loci are evenly distributed across chromosomes, a positive correlation between linkage group length and

variance explained is expected. Deviations from polygenicity can be caused by large effect loci or clustering of loci. **(B)** Overview of LG-specific heritability for all traits studied here. Circle size is proportional to LG specific heritability estimates. LGs explaining significant amounts of phenotypic variance are shown in blue; those explaining more phenotypic variance than expected based on their length in red.

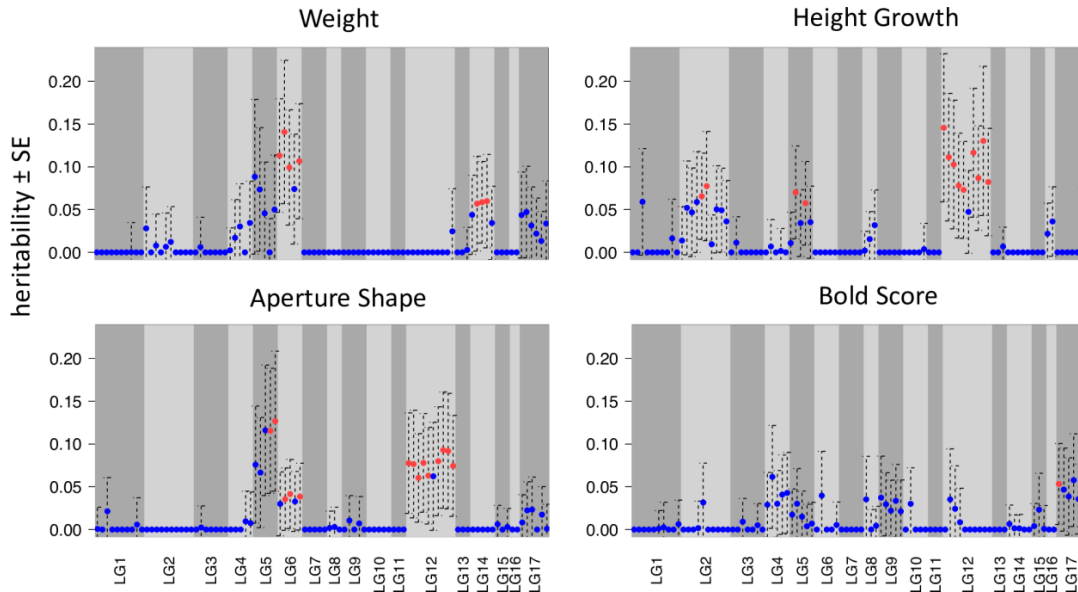


**Figure 5:** Examples for regional heritability  $\pm$  standard error (SE) mapping of different traits. Each region consisted of 200 adjacent markers. Significant estimates are shown in red. Other traits can be found in Supporting Information Figure S3.

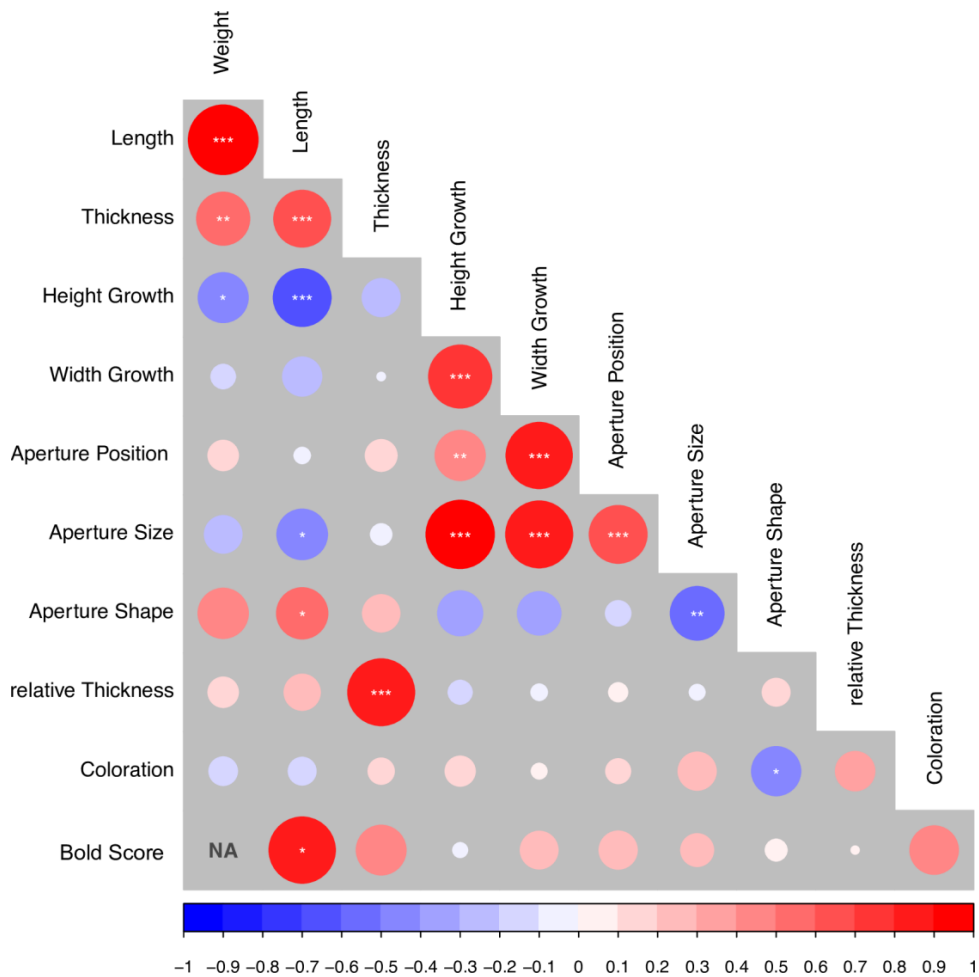


**Figure 6:** Genetic correlations between different traits estimated by bivariate animal models. Circle sizes are proportional to correlation coefficients. Significance was inferred from comparisons with models where correlation was set to zero using likelihood-ratio tests. Due to lack of model convergence no estimates for correlation between weight and Bold Score can be reported. Significance: \*P < 0.05; \*\*P < 0.01; \*\*\*P<0.001. Phenotypic correlations for the whole F2 as well as for each family separately are shown in Supporting Information Figure S4.

## Appendix S1

### *Crossing and confirmation of relationships between individuals*

Crossing was performed between Crab and Wave ecotype individuals collected on the Swedish West Coast at Ängklåvebukten (58.8697°, 11.1197°), where both ecotypes occur in close proximity (see also Westram et al. 2018). The parental female snails were brought into the lab as juveniles and raised in isolation until maturity to prevent uncontrolled matings. The parental males were brought in as adults. Two virgin Crab-females were crossed with two Wave-males resulting in two F1-families (Figure I). Three males and three females of each F1-family were then crossed reciprocally with an individual from the other family to produce six F2-families. F1 and F2 generations were raised in large tanks provided with flow-through sea water from 40 m depth at ambient temperature (5-15 degrees depending on season) and salinity (approx. 30 psu) filtered through sand-filters. Snails grazed the biofilm of microalgae growing inside the tanks under the illumination of daylight lamps. Generation time in the lab was around 6-12 months depending on water temperature.

We performed targeted re-sequencing as described in Faria et al. (2019) and Westram et al. (2018), using a total of 25,000 (120 bp) enrichment probes (Supporting Information Table S8), 20,000 that were informative in previous experiments and 5000 novel probe regions chosen from random contigs of the *Littorina saxatilis* genome assembly that were not placed on the existing genetic map, with the intention of extend the linkage map coverage. Raw reads were processed as described in Faria et al (2019). In short, the pipeline consisted in read-trimming with Trimmomatic v. 0.36 (Bolger et al. 2014), quality control with FastQC v0.11.5 (Andrews 2010), read-mapping with BWA v0.7.15 (Li and Durbin 2009), PCR duplicate removal and InDel re-alignment with Picard v. 1.138 (<http://broadinstitute.github.io/picard/>) and SNP calling with GATK UnifiedGenotyper v3.7-0 (Depristo et al. 2011). We aggressively filtered the resulting genotypes to retain a set of high confidence SNPs with vcftools (Danecek et al. 2011) and vcfliib from vcfliib (<https://github.com/vcfliib/vcfliib>). The final set of SNPs consisted of 22,759 sites with an average depth of 44X (SD=22X) across individuals, a minimum individual depth of 8X, a minimum base and mapping qualities of 40, a maximum missingness per individual of 0.5% (average = 0.14%), a maximum missingness per site of 17% (average = 0.12%) and a minor allele frequency higher than 5%.

Inversion genotypes of F1 parents and F2 offspring (after confirming their relationships, see below) were inferred using the genotypes (extracted from vcf -file using vcftools) of the same marker data that were used for linkage map construction. SNPs with unknown map position and more than 1000 bp away from mapped SNPs in the previous linkage map were removed, as in Westram et al. (2018). The original map position of the remaining SNPs was then replaced by their position in our map. A principal component analyses (PCA) using the SNPs located within each putatively inverted region (with boundaries defined according to our map) was implemented with the R package PCADAPT (Luu et al. 2017) including all individuals,

as in Faria et al. (2019). Groups of individuals across the PC1 (without intermediates) were identified using the R function “KMEANS” and confirmed/adjusted visually. For each inversion, the number of groups observed for each F1 couple and their offspring varied between one, two or three, representing a cross between two homozygotes for one arrangement, a cross between a homozygote for one arrangement and a heterozygote, and a cross between two inversion heterozygotes, respectively. The only exception was observed for the complex inversion LGC6.1/2 where six groups of genotypes were observed, as expected for the presence of three possible arrangements in the analysed individuals. The inversion genotyping consistency was subsequently confirmed by comparing the genotypes of offspring and their (known) parents. The most likely inversion genotype of each unknown parent was inferred based on the distribution of its offspring and mate genotypes. A second PCA was subsequently implemented, where genotypes from the two crab parents of the crab linkage map and 28 individuals from the crab end of the transect of the same source population obtained from Westram et al. (2018) and Faria et al. (2019) were also included. The goal of this second PCA was to identify the most common arrangement in the crab ecotype (R) and to genotype the F1 parents and F2 offspring individuals as RR, RA or AA (and RB, AB, and BB for LGC6.1/2), where A (and B) are alternative arrangements. The only exception was observed for LGC12.2, where R and A are equally frequent in the crab ecotype, and each arrangement was classified as R or A in a random manner.

Confirmation that individuals of each presumed family are true full sibs is crucial for linkage map construction. False classification of more distantly related individuals as full-sibs would inflate the map since the number of recombination events would have been much higher than assumed.

We calculated genomic relationships among presumed F2 individuals following VanRaden (2008), as implemented in the Rpackage “AGHmatrix” (Amadeu et al. 2016). We also tested relationships using the IBD module in LepMap 3 (Rastas 2017). To avoid using genotypes that were curated by our input pedigree (this module takes the output of the “ParentCall2” module in LepMap 3 and not vcf-files directly) we set raw=1 in “ParentCall2” to prevent LepMap using pedigree information while producing proper input format for the IBD module. The results were consistent with the genomic relationships obtained from the method by VanRaden (2008).

We tested the relationship of all individuals of a presumed family with their presumed parents and to each other. For each family we expected that individuals were either full-sibs, in line with the original crossing scheme, half-sibs, potentially caused by using non-virgin females that stored sperm of previous matings, or unrelated, presumably due to contamination from other tanks. Identifying individuals that share the same father and mother is the most reliable way to identify full-sibs. Unfortunately, genetic data for F1 parents were not always available (Table I) since these individuals died before DNA collection or the true parent was not

sequenced. In these cases, we could only test relationship with one potential parent or with other F2 individuals.

In all cases, the presumed families consisted of several genetic sub-groups (Figure II-VII) indicating that not all of them were true full-sibs. For some of the identified sub-groups we found that both presumed parents were wrong and true parents could not be identified. Sometimes they showed intermediate relationships with the intended parents suggesting that they were offspring of other F1-individuals (avuncular relationship to planned parent). We assumed the identified subgroups to be full-sibs if they formed a cluster based on their genomic relationships and their within-subgroup relationships were within a range that was reasonable for full-sibs (compared to the most reliable full-sib families where we could confirm that both parents were correct, Figure II). On this basis, we split the originally presumed families into sub-groups that we identified as full-sib families. In total we obtained eight full-sib families and one half-sib family that consisted of five full-sib families. We therefore set  $\text{halfSib}=1$  when running the "ParentCall2" module in LepMap3 to use this information. In cases where we could not identify the correct parents, we assigned placeholder parental IDs (e.g. "mother\_fam8.1"). LepMap3 can construct linkage maps even without complete parental data, but a pedigree in the right format is required to identify families. Individuals that did not show close relationships with other F2 or F1 individuals, or could not be classified without doubt, were excluded. The final numbers of F2 individuals per family are given in Table II.

The presumed family 8.1 consisted of two groups of closely related individuals (Figure III). Combining relatedness among offspring with relationship data to the presumed mother showed that one of these full-sib groups was indeed the offspring of the planned mother while the other was not. Individuals within this second group were not related to any of the candidate parents. We excluded them.

We proceeded in the same way with the other potential families, shown in Fig III-VII. Table II shows how the presumed families were split into subgroups.

Family 8-2 consisted of two clusters (Figure IV). One of the clusters was sired by the planned father whereas the other, much smaller cluster was not. Genetic data for the potential mother was not available. Individuals not closely related to the planned father were excluded.

Family 8-3 (Figure V) included a cluster where both of the presumed parents were correct (family 83.1). Another cluster showed an intermediate relationship to the presumed parents, which can occur if the true parents were related to the presumed ones (avuncular relationship). The relationship between individuals within this cluster was within the range (Figure II) that we observed for the family 83.1, which we knew to be a true full-sib family since both parents were correct. We therefore decided to classify this cluster (family 83.2) as

a full-sib family and assigned place holder parental IDs (e.g. "Mother\_83.2") as their parent IDs in the pedigree. Individuals in the other clusters were excluded, because they either did not show a close relationship to presumed parents making it therefore unclear whether they were descendants of the originally crossed F1-families or the potential full-sib family was too small.

Family 9-1 (Figure VI) consisted of two main clusters. Most of the individuals were offspring of the presumed mother. Genetic data for the father was not available. Two individuals that were not offspring of the presumed mother were excluded. We observed that the relationship to the mother of individuals of one cluster was higher (fam 91.1), presumably due to inbreeding when the mother mated with her brother before the planned cross took place. We divided Family 9-1 therefore into two full-sib families and assigned placeholder IDs for the two fathers.

Family 9-2 consisted of three clusters (Figure VII). Individuals of the first cluster (three individuals) were unrelated to both presumed parents and were excluded. Another cluster consisted of individuals that were indeed offspring of the presumed parents and were thus classified as a full-sib family. Individuals of the last cluster were offspring of the presumed mother but unrelated to the potential father. Relationships within this cluster were high (Figure II). We therefore decided to classify it as a full-sib family (fam92.1).

Family 9-3 (Figure VIII) included a few individuals that were unrelated to the presumed parents and were thus excluded. The presumed father was correct for all remaining individuals. These individuals were related to the presumed mother, but not as closely as expected for a parent-offspring relationship (Figure VIII B, please note the difference in relatedness to candidate father and mother). It seemed likely that they were offspring of another female of the same F1 family. Relationships within this large cluster showed a high variation (Figure II). When we first classified them as full-sibs we obtained linkage maps that were inflated. We therefore thought it likely that they represented offspring of several females and we therefore split the large cluster into five smaller clusters, each of them representing a full-sib family. Relationships within these clusters were then within the range of the other full-sib families (Figure II) and we did not obtain inflated linkage maps.

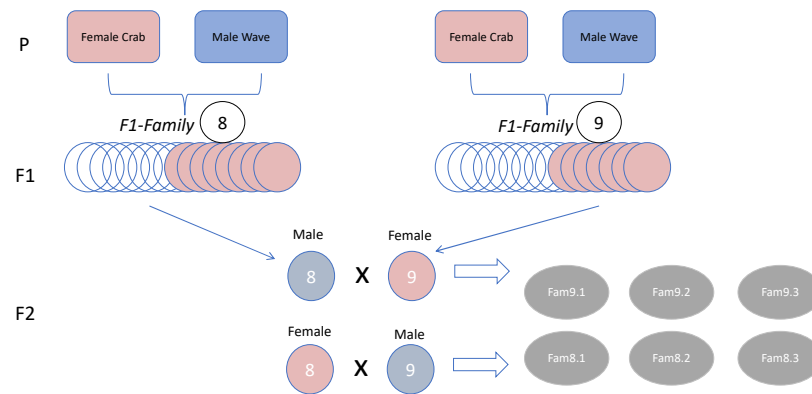


**Figure I** Crossing design to produce F2- individuals for QTL analysis. Parental individuals (adapted to crab predation and wave exposure) were collected at the Swedish West Coast at Ångklåvbukten.

**Table I** Genetic data for potential parents of F2-families available

|        | FAM_8-1 | FAM_8-2 | FAM_8-3 | FAM_9-1 | FAM_9-2 | FAM_9-3 |
|--------|---------|---------|---------|---------|---------|---------|
| Mother | yes     | no      | yes     | yes     | yes     | yes     |
| Father | no      | yes     | yes     | no      | yes     | yes     |

**Table II:** Number of individuals included for each of the identified full-sib families. The full-sib families marked with \* are half-sib families to each other

|         | identified fullsib-families | N  | Mother  | Father  |
|---------|-----------------------------|----|---------|---------|
| FAM_8-1 | fam81-1                     | 42 | I23015  | unknown |
| FAM_8-2 | fam82-1                     | 41 | unknown | I23006  |
| FAM_8-3 | fam83-1                     | 43 | I23004  | I23003  |
|         | fam83-2                     | 13 | unknown | unknown |
| FAM_9-1 | fam91-1                     | 35 | I23007  | unknown |
|         | fam91-2                     | 23 | I23007  | unknown |
| FAM_9-2 | fam92-1                     | 17 | I23009  | unknown |
|         | fam92-2                     | 41 | I23009  | I23010  |
| FAM_9-3 | fam93-1*                    | 25 | unknown | I23014  |
|         | fam93-2*                    | 32 | unknown | I23014  |
|         | fam93-3*                    | 23 | unknown | I23014  |
|         | fam93-4*                    | 29 | unknown | I23014  |
|         | fam93-5*                    | 22 | unknown | I23014  |

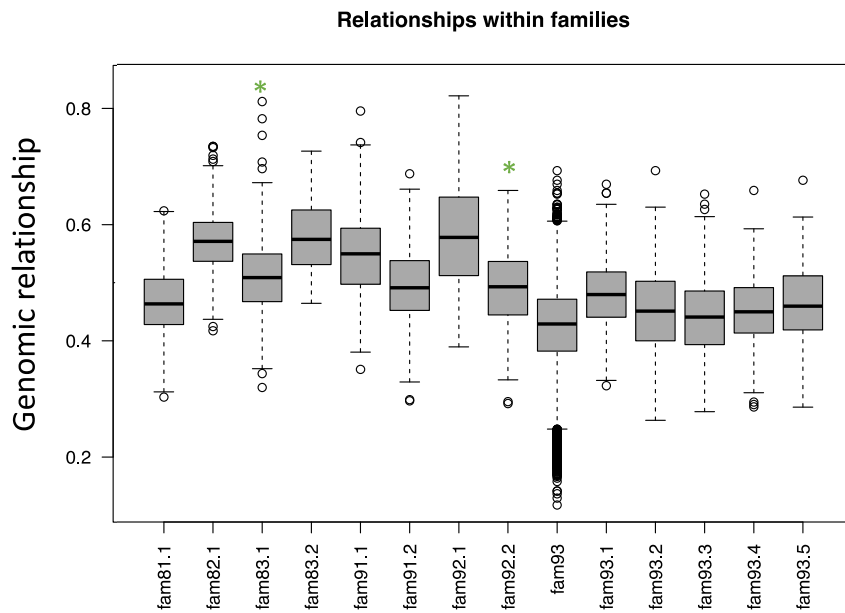


**Figure II:** Relationships between individuals within the identified full-sib clusters and halfsib-family fam93. Green stars indicate those families where we could confirm that both presumed parents were correct and thus represent the most reliable ones.

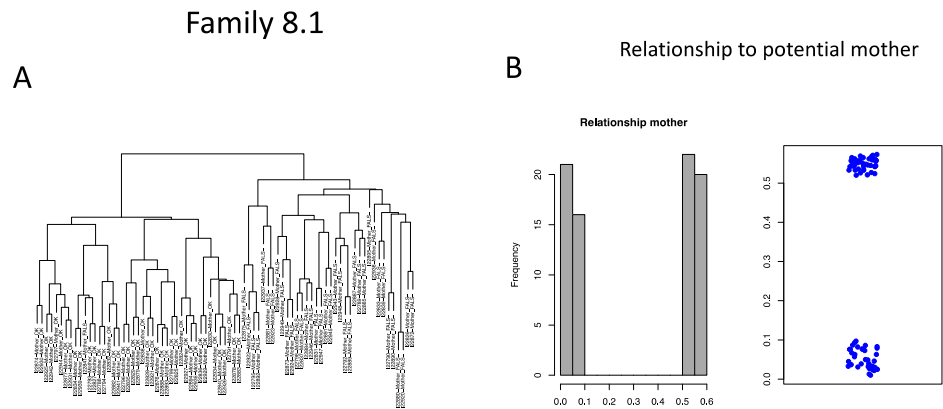


**Figure III** Relationship within the presumed family 8.1. Relationship between individuals based on additive genetic relationships (A) and the relationship to presumed mother (B). Labeling in (A) as ‘OK’ or ‘FALSE’ is based

on information whether the presumed mother was correct (relationship >0.4 obtained from IBD module in LepMap which corresponds roughly to 0.2 in genomic relationships using the method proposed by VanRaden (2008) as implemented in the Rpackage “AGHmatrix”(Amadeu et al. 2016)) or false (< 0.2 IBD module LepMap; < 0 genomic relationships). Genetic data for the potential father was not available.

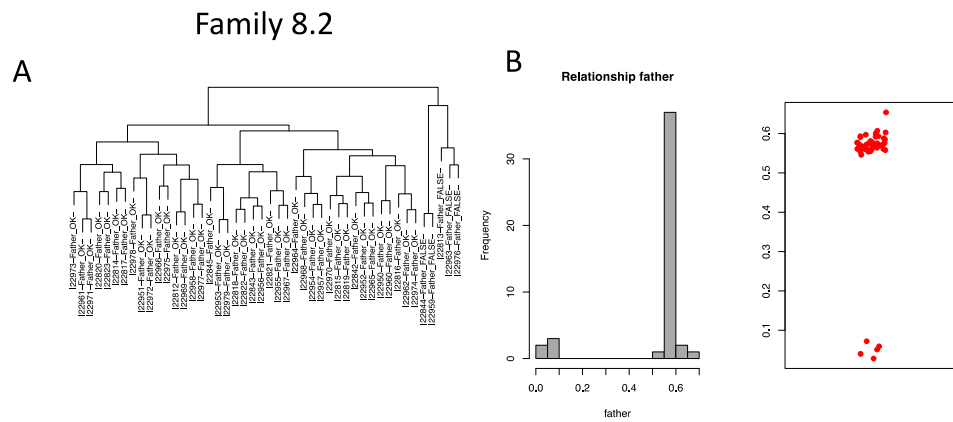


**Figure IV** Relationship within the presumed family 8.2. Relationship between individuals (A) and the relationship to presumed father (B). Labeling in (A) consists of information whether the presumed father was correct (relationship >0.4) or false (< 0.2). Genetic data for the potential mother was not available.

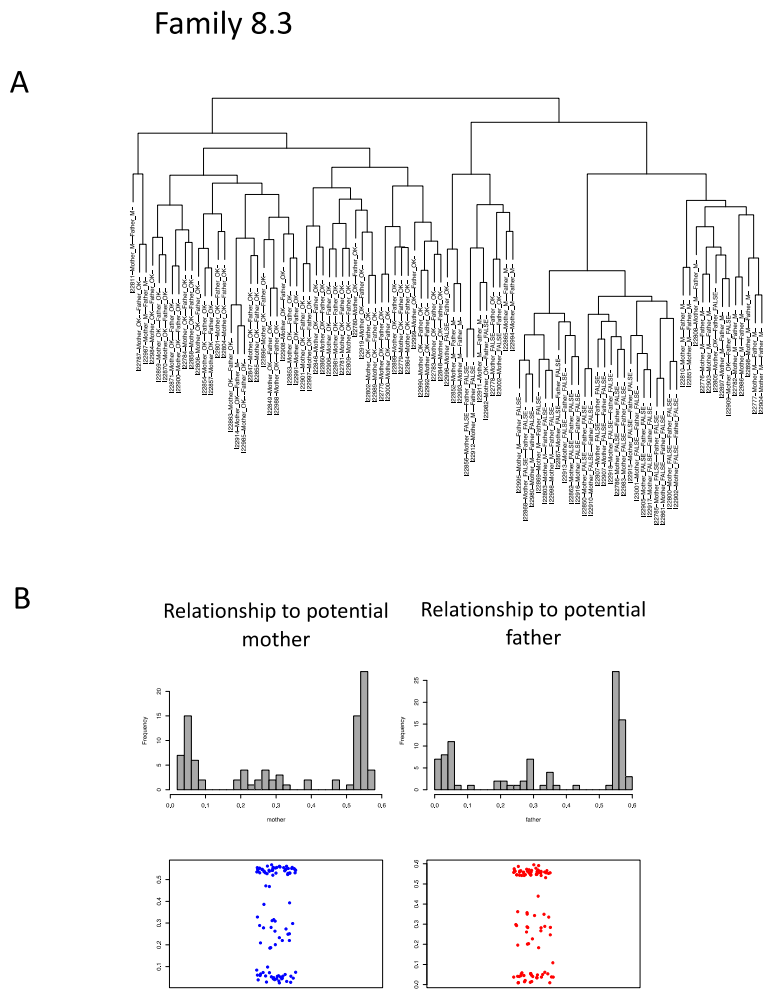
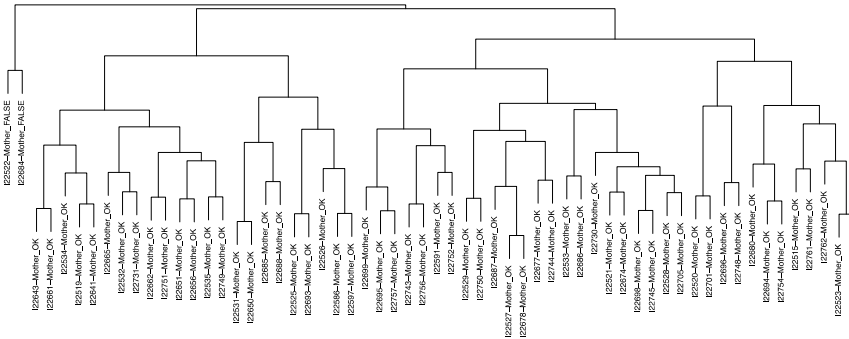


**Figure V** Relationship within the presumed family 8.3. Relationship between individuals (A) and the relationship to presumed parents (B). Labeling in (A) consists of information whether the presumed parents were correct (relationship >0.4) or false (< 0.2). M indicates an intermediate relationship (0.2-0.4), which can occur if the true parent was a fullsib to the presumed one.

A Family 9.1



B

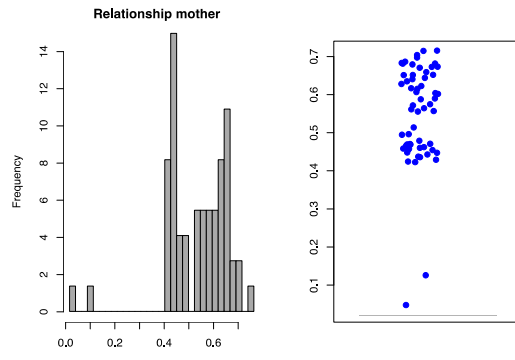
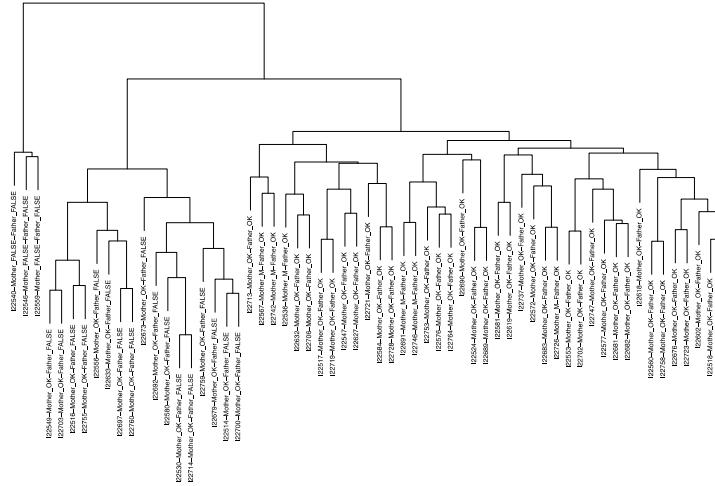


**Figure VI** Relationship within the presumed family 9.1. Relationship between individuals (A) and the relationship to presumed mother(B). Labeling in (A) consists of information whether the presumed mother was correct (relationship >0.4) or false (< 0.2). The two clusters represent maternal half-sib families. One of these families is likely to be the result of inbreeding (mating of the mother with her brother) as is indicated by elevated relationship with the mother. There was no genetic data for the presumed father available.

A Family 9.2



B

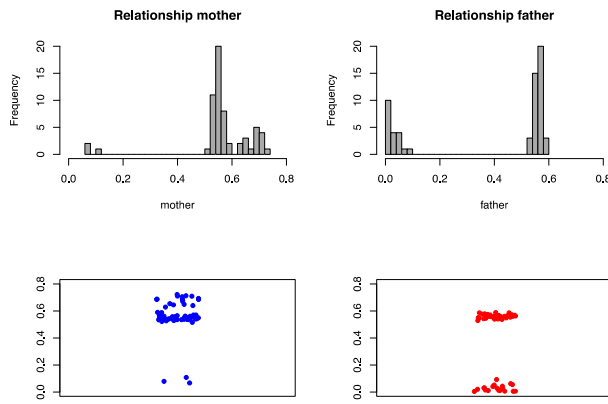


**Figure VII** Relationship within the presumed family 9.2. Relationship between individuals (A) and the relationship to presumed parents(B). Labeling in (A) consists of information whether the presumed parents were correct (relationship >0.4) or false (<0.2). Two of the clusters represent maternal half-sib families. One of these families is likely to be the result of inbreeding (mating of the mother with her brother) as is indicated by elevated relationship with the mother.

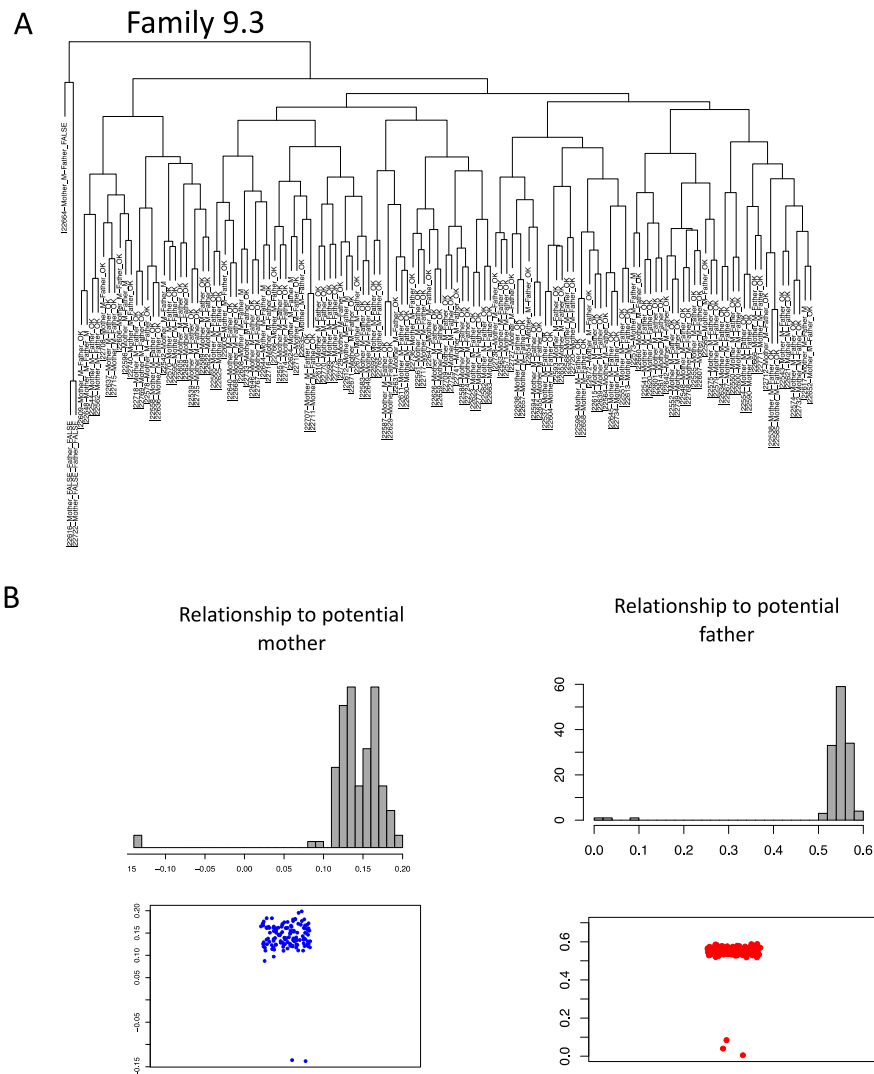


**Figure VIII** Relationship within the presumed family 9.3. Relationship between individuals (A) and the relationship to presumed parents (B). Labeling in (A) consists of information whether the presumed parents were correct (relationship  $>0.4$ ) or false ( $<0.2$ ). M indicates an intermediate relationship ( $0.2-0.4$ ), which can occur if the true parent was a fullsib to the presumed one. Here, the true mothers of the different clusters are likely to be sister of the presumed one.

## References

- Amadeu, R. R., C. Cellon, J. W. Olmstead, A. A. F. Garcia, M. F. R. Resende, and P. R. Muñoz. 2016. AGHmatrix: R package to construct relationship matrices for autotetraploid and diploid species: A blueberry example. *Plant Genome* 9.
- Andrews, S. 2010. FastQC: A quality control tool for high throughput sequence data. Retrieved from <https://www.bioinformatics.babraham.org.uk/projects/fastqc/>.
- Bolger, A. M., M. Lohse, and B. Usadel. 2014. Trimmomatic: A flexible trimmer for Illumina sequence data. *Bioinformatics* 30:2114–2120.

- Danecek, P., A. Auton, G. Abecasis, C. A. Albers, E. Banks, M. A. DePristo, R. E. Handsaker, G. Lunter, G. T. Marth, S. T. Sherry, G. McVean, and R. Durbin. 2011. The variant call format and VCFtools. *Bioinformatics* 27:2156–2158.
- DePristo, M. A., E. Banks, R. Poplin, K. V. Garimella, J. R. Maguire, C. Hartl, A. A. Philippakis, G. Del Angel, M. A. Rivas, M. Hanna, A. McKenna, T. J. Fennell, A. M. Kernytsky, A. Y. Sivachenko, K. Cibulskis, S. B. Gabriel, D. Altshuler, and M. J. Daly. 2011. A framework for variation discovery and genotyping using next-generation DNA sequencing data. *Nat. Genet.* 43:491–501.
- Faria, R., P. Chaube, H. E. Morales, T. Larsson, A. R. Lemmon, E. M. Lemmon, M. Rafajlović, M. Panova, M. Ravinet, K. Johannesson, A. M. Westram, and R. K. Butlin. 2019. Multiple chromosomal rearrangements in a hybrid zone between *Littorina saxatilis* ecotypes. *Mol. Ecol.* 28:1375–1393.
- Li, H., and R. Durbin. 2009. Fast and accurate short read alignment with Burrows-Wheeler transform. *Bioinformatics* 25:1754–1760.
- Luu, K., E. Bazin, and M. G. B. Blum. 2017. pcadapt: an R package to perform genome scans for selection based on principal component analysis. *Mol. Ecol. Resour.* 17:67–77.
- Rastas, P. 2017. Lep-MAP3: Robust linkage mapping even for low-coverage whole genome sequencing data. *Bioinformatics* 33:3726–3732.
- VanRaden, P. M. 2008. Efficient methods to compute genomic predictions. *J. Dairy Sci.* 91:4414–4423.
- Westram, A. M., M. Rafajlović, P. Chaube, R. Faria, T. Larsson, M. Panova, M. Ravinet, A. Blomberg, B. Mehlig, K. Johannesson, and R. Butlin. 2018. Clines on the seashore: The genomic architecture underlying rapid divergence in the face of gene flow. *Evol. Lett.* 2:297–309.

Table S1: Transferring positions of putatively inverted regions (Faria et al.2019, Table 1, doi:10.1111/mec.14972) to the new map. We used markers inside the identified LD clusters that were present in our data set and used their minimum/maximum positions to define the boundaries of the potentially inverted regions.

| Inversion       | position of putative<br>inversions in previous<br>map |       | position of common<br>markers in previous map |         | position of common<br>markers in QTL map |         |
|-----------------|---|-------|---|---------|--|---------|
|                 | start   | end   | minimum                                       | maximum | minimum                                  | maximum |
| <b>inv1.1</b>   | 0   | 2.1   | 0.66  | 0.97    | 0.00                                     | 20.69   |
| <b>inv1.2</b>   | 75.53   | 80.95 | 75.53   | 77.23   | 77.10                                    | 80.92   |
| <b>inv2.1</b>   | 0.34  | 14.21 | 0.34  | 11.50   | 0.54                                     | 2.67    |
| <b>inv4.1</b>   | 1.03  | 1.51  | 1.36  | 1.51    | 0.00                                     | 24.40   |
| <b>inv6.1/2</b> | 0   | 29.3  | 0.00  | 29.30   | 0.75                                     | 19.65   |
| <b>inv7.1</b>   | 36.01   | 37.74 | 36.01   | 37.45   | 40.80                                    | 42.62   |
| <b>inv7.2</b>   | 42.08   | 51.37 | 42.08   | 49.16   | 48.09                                    | 53.91   |
| <b>inv9.1</b>   | 18.64   | 41.82 | 19.27   | 41.82   | 23.16                                    | 37.71   |
| <b>inv10.1</b>  | 0.58  | 3.12  | 0.87  | 3.12    | 10.54                                    | 19.66   |
| <b>inv11.1</b>  | 52.32   | 52.91 | 52.60   | 52.91   | 33.37                                    | 65.01   |
| <b>inv12.1</b>  | 3.32  | 29.63 | 5.88  | 29.63   | 18.27                                    | 33.41   |
| <b>inv12.2</b>  | 48.71   | 60.24 | 48.71   | 58.56   | 57.09                                    | 72.46   |
| <b>inv14.1</b>  | 0.39  | 11.71 | 1.55  | 11.71   | 6.82                                     | 29.26   |
| <b>inv14.2</b>  | 8.81  | 11.71 | 10.24   | 11.71   | 6.82                                     | 29.26   |
| <b>inv14.3</b>  | 11.71   | 34.94 | 13.14   | 34.94   | 20.61                                    | 34.59   |
| <b>inv17.1</b>  | 46.99   | 62.32 | 46.99   | 61.74   | 58.32                                    | 66.06   |

Table S2A: Inversion genotypes of F1 individuals. R and A (B for overlapping inversion on LG6) indicate alternative alleles. Arrangement R is more common in the Crab ecotype, except for LGC12.2 where the frequency of both arrangements is very similar. For details about inversion genotyping see Appendix S1. Heterozygous individuals where suppressed recombination is expected are shown in green. Please note that genetic data was not available for all parents due to errors

|           | I23003   | I23004 | I23006 | I23007 | I23009 | I23010 | I23014 | I23015 |
|-----------|--|--------|--------|--------|--------|--------|--------|--------|
| LGC1.1    | RR   | RA     | RR     | RR     | RR     | RA     | RA     | RR     |
| LGC1.2    | RA   | RR     |
| LGC2.1    | RA   | RA     | RA     | RA     | RA     | RA     | RA     | RA     |
| LGC4.1    | RR   | RR     | RR     | RR     | RA     | RR     | RR     | RR     |
| LGC6.1/2  | RA   | RA     | RA     | RA     | RA     | RB     | RA     | RA     |
| LGC7.1    | RR   | RR     | RR     | RR     | RR     | RA     | RA     | RA     |
| LGC7.2    | RR   | RR     | RR     | RR     | RR     | RR     | RR     | RR     |
| LGC9.1    | RR   | RR     | RR     | RR     | RR     | RR     | RR     | RR     |
| LGC10.1   | RR   | RR     | RA     | RR     | RA     | RR     | RR     | RR     |
| LGC11.1   | RR   | RR     | RR     | RR     | RR     | RR     | RR     | RR     |
| LGC12.1   | RR   | RA     | RR     | RA     | RR     | RR     | RA     | RA     |
| LGC12.2   | RA   | RR     | RA     | RA     | RA     | RA     | AA     | RA     |
| LGC14.1/2 | AA   | RA     | RA     | AA     | RA     | RA     | RA     | RA     |
| LGC14.3   | too few loci two infer anything but looking at patterns of LGC14.1 it should be all RR |        |        |        |        |        |        |        |
| LGC17.1   | RR   | RR     | RR     | RR     | RR     | RA     | RA     | RA     |

Table S2B: Inversion genotypes of parents of the different F2 families. For details how individuals were assigned to families see Appendix S1

|         | identified fu | N  | Mother  | Father  | inv1.1 |        | inv1.2 |        | inv2.1 |        | inv4.1 |        | inv6.1/2 |          | inv7.1   |        | inv7.2 |        |        |
|---------|---------------|----|---------|---------|--------|--------|--------|--------|--------|--------|--------|--------|----------|----------|----------|--------|--------|--------|--------|
|         |               |    |         |         | Mother | Father | Mother | Father | Mother | Father | Mother | Father | Mother   | Father   | Mother   | Father | Mother | Father |        |
| FAM_8-1 | fam81-1       | 42 | I23015  | unknown | homoR  | homoR  | homo R | homo R | hetero | hetero | hetero | homo R | hetero   | heteroRA | heteroRA | hetero | homo R | homo R | homo R |
| FAM_8-2 | fam82-1       | 41 | unknown | I23006  | homoR  | homoR  | homo R | homo R | hetero | hetero | hetero | homo R | homo R   | homoB    | heteroRA | homo R | homo R | homo R | homo R |
| FAM_8-3 | fam83-1       | 43 | I23004  | I23003  | hetero | hetero | homo R | homo R | hetero | hetero | hetero | homo R | homo R   | heteroRA | heteroRA | homo R | homo R | homo R | homo R |
|         | fam83-2       | 13 | unknown | unknown | homoR  | homoR  | homo R | homo R | hetero | hetero | hetero | homo R | homo R   | homoB    | heteroRA | homo R | homo R | homo R | homo R |
| FAM_9-1 | fam91-1       | 35 | I23007  | unknown | homoR  | homoR  | homo R | homo R | hetero | hetero | hetero | homo R | homo R   | heteroRA | heteroRA | homo R | homo R | homo R | homo R |
|         | fam91-2       | 23 | I23007  | unknown | homoR  | homoR  | homo R | homo R | hetero | hetero | hetero | homo R | homo R   | heteroRA | heteroRA | homo R | homo R | homo R | homo R |
| FAM_9-2 | fam92-1       | 17 | I23009  | unknown | homoR  | homoR  | homo R | homo R | hetero | hetero | hetero | hetero | hetero   | heteroRA | heteroRA | homo R | homo R | homo R | homo R |
|         | fam92-2       | 41 | I23009  | I23010  | homoR  | hetero | homo R | homo R | hetero | hetero | hetero | hetero | hetero   | heteroRA | heteroRB | homo R | hetero | homo R | homo R |
| FAM_9-3 | fam93-1       | 25 | unknown | I23014  | homoR  | hetero | hetero | homo R | hetero | hetero | homo R | homo R | heteroRA | heteroRA | homo R   | hetero | homo R | homo R | homo R |
|         | fam93-2       | 32 | unknown | I23014  | homoR  | hetero | hetero | homo R | hetero | hetero | homo R | homo R | heteroRA | heteroRA | homo R   | hetero | homo R | homo R | homo R |
|         | fam93-3       | 23 | unknown | I23014  | homoR  | hetero | hetero | homo R | hetero | hetero | homo R | homo R | heteroRA | heteroRA | homo R   | hetero | homo R | homo R | homo R |
|         | fam93-4       | 29 | unknown | I23014  | homoR  | hetero | hetero | homo R | hetero | hetero | homo R | homo R | heteroRA | heteroRA | homo R   | hetero | homo R | homo R | homo R |
|         | fam93-5       | 22 | unknown | I23014  | homoR  | hetero | hetero | homo R | hetero | hetero | homo R | homo R | heteroRA | heteroRA | homo R   | hetero | homo R | homo R | homo R |

|         | identified fu | N  | Mother  | Father  | inv9.1 |        | inv10.1 |        | inv11.1 |        | inv12.1 |        | inv12.2 |        | inv14.1/2 |        | inv17.1 |        |
|---------|---------------|----|---------|---------|--------|--------|---------|--------|---------|--------|---------|--------|---------|--------|-----------|--------|---------|--------|
|         |               |    |         |         | Mother | Father | Mother  | Father | Mother  | Father | Mother  | Father | Mother  | Father | Mother    | Father | Mother  | Father |
| FAM_8-1 | fam81-1       | 42 | I23015  | unknown | homo R | homo R | homo R  | homo R | homo R  | homo R | hetero  | homo R | hetero  | hetero | hetero    | hetero | hetero  | hetero |
| FAM_8-2 | fam82-1       | 41 | unknown | I23006  | homo R | homo R | homo R  | hetero | homo R  | homo R | hetero  | homo R | homo A  | hetero | homo R    | hetero | homo A  | homo R |
| FAM_8-3 | fam83-1       | 43 | I23004  | I23003  | homo R | homo R | homo R  | homo R | homo R  | homo R | hetero  | homo R | homo R  | hetero | hetero    | homo R | homo R  | homo R |
|         | fam83-2       | 13 | unknown | unknown | homo R | homo R | homo R  | homo R | homo R  | homo R | hetero  | homo R | hetero  | homo A | hetero    | homo R | homo R  | homo R |
| FAM_9-1 | fam91-1       | 35 | I23007  | unknown | homo R | homo R | homo R  | homo R | homo R  | homo R | hetero  | homo R | hetero  | hetero | homo R    | hetero | homo R  | hetero |
|         | fam91-2       | 23 | I23007  | unknown | homo R | homo R | homo R  | homo R | homo R  | homo R | hetero  | hetero | hetero  | homo A | homo R    | hetero | homo R  | homo R |
| FAM_9-2 | fam92-1       | 17 | I23009  | unknown | homo R | homo R | hetero  | homo R | homo R  | homo R | homo R  | homo R | hetero  | hetero | hetero    | hetero | hetero  | hetero |
|         | fam92-2       | 41 | I23009  | I23010  | homo R | homo R | hetero  | homo R | homo R  | homo R | homo R  | homo R | hetero  | hetero | hetero    | hetero | hetero  | homo R |
| FAM_9-3 | fam93-1       | 25 | unknown | I23014  | homo R | homo R | homo R  | homo R | homo R  | homo R | hetero  | hetero | hetero  | homo A | hetero    | hetero | hetero  | hetero |
|         | fam93-2       | 32 | unknown | I23014  | homo R | homo R | homo R  | homo R | homo R  | homo R | hetero  | hetero | hetero  | homo A | hetero    | hetero | hetero  | hetero |
|         | fam93-3       | 23 | unknown | I23014  | homo R | homo R | homo R  | homo R | homo R  | homo R | hetero  | hetero | hetero  | homo A | hetero    | hetero | hetero  | hetero |
|         | fam93-4       | 29 | unknown | I23014  | homo R | homo R | homo R  | homo R | homo R  | homo R | hetero  | hetero | hetero  | homo A | hetero    | hetero | hetero  | hetero |
|         | fam93-5       | 22 | unknown | I23014  | homo R | homo R | homo R  | homo R | homo R  | homo R | hetero  | hetero | hetero  | homo A | hetero    | hetero | hetero  | hetero |

Table S2C: Inversion genotypes of F2 individuals

| snail_ID | Fam     | father  | mother | inv1.1 | inv1.2 | inv2.1 | inv4.1 | inv6.1/2 | inv7.1 | inv10.1 | inv12.1 | inv12.2 | inv14.1 | inv17.1 |
|----------|---------|---------|--------|--------|--------|--------|--------|----------|--------|---------|---------|---------|---------|---------|
| 122788   | fam81_1 | Fat81_1 | I23015 | homoR  | homoR  | hetero | homoR  | homoRR   | homoR  | homoR   | hetero  | hetero  | homoA   | homoA   |
| 122791   | fam81_1 | Fat81_1 | I23015 | homoR  | homoR  | hetero | hetero | homoRR   | homoR  | homoR   | homoR   | hetero  | hetero  | hetero  |
| 122793   | fam81_1 | Fat81_1 | I23015 | homoR  | hetero | homoR  | homoR  | homoRR   | homoR  | homoR   | homoR   | homoA   | hetero  | homoA   |
| 122794   | fam81_1 | Fat81_1 | I23015 | homoR  | homoR  | hetero | homoR  | heteroRA | hetero | homoR   | hetero  | hetero  | hetero  | homoA   |
| 122796   | fam81_1 | Fat81_1 | I23015 | homoR  | hetero | hetero | homoR  | heteroRA | homoR  | homoR   | hetero  | hetero  | hetero  | homoA   |
| 122797   | fam81_1 | Fat81_1 | I23015 | homoR  | homoR  | homoA  | homoR  | heteroRA | homoR  | homoR   | homoR   | homoR   | homoA   | homoA   |
| 122799   | fam81_1 | Fat81_1 | I23015 | homoR  | homoR  | hetero | hetero | heteroRA | homoR  | homoR   | hetero  | hetero  | homoA   | hetero  |
| 122824   | fam81_1 | Fat81_1 | I23015 | homoR  | hetero | homoA  | hetero | heteroRA | homoR  | homoR   | hetero  | homoR   | homoR   | homoA   |
| 122825   | fam81_1 | Fat81_1 | I23015 | homoR  | hetero | hetero | hetero | heteroRA | homoR  | homoR   | hetero  | homoA   | hetero  | hetero  |
| 122827   | fam81_1 | Fat81_1 | I23015 | homoR  | hetero | homoR  | homoR  | heteroRA | homoR  | homoR   | hetero  | homoA   | homoR   | hetero  |
| 122828   | fam81_1 | Fat81_1 | I23015 | homoR  | homoR  | hetero | hetero | heteroRA | homoR  | homoR   | homoR   | hetero  | homoA   | homoA   |
| 122829   | fam81_1 | Fat81_1 | I23015 | homoR  | homoR  | hetero | homoR  | homoRR   | hetero | homoR   | hetero  | homoA   | hetero  | hetero  |
| 122830   | fam81_1 | Fat81_1 | I23015 | homoR  | hetero | homoR  | homoR  | homoRR   | hetero | homoR   | homoR   | hetero  | homoA   | hetero  |
| 122832   | fam81_1 | Fat81_1 | I23015 | homoR  | hetero | hetero | homoR  | homoRR   | homoR  | homoR   | homoR   | hetero  | hetero  | hetero  |
| 122834   | fam81_1 | Fat81_1 | I23015 | homoR  | hetero | hetero | hetero | heteroRA | hetero | homoR   | hetero  | hetero  | hetero  | homoR   |
| 122835   | fam81_1 | Fat81_1 | I23015 | homoR  | homoR  | homoR  | homoR  | homoRR   | homoR  | homoR   | hetero  | hetero  | hetero  | homoR   |
| 122836   | fam81_1 | Fat81_1 | I23015 | homoR  | homoR  | hetero | homoR  | homoAA   | hetero | homoR   | homoR   | hetero  | hetero  | hetero  |
| 122838   | fam81_1 | Fat81_1 | I23015 | homoR  | homoR  | hetero | homoR  | homoAA   | hetero | homoR   | hetero  | hetero  | hetero  | homoA   |
| 122840   | fam81_1 | Fat81_1 | I23015 | homoR  | homoR  | homoR  | hetero | heteroRA | hetero | homoR   | homoR   | hetero  | hetero  | homoA   |
| 122874   | fam81_1 | Fat81_1 | I23015 | homoR  | hetero | hetero | hetero | homoAA   | homoR  | homoR   | hetero  | hetero  | hetero  | homoA   |
| 122876   | fam81_1 | Fat81_1 | I23015 | homoR  | homoR  | homoR  | homoR  | heteroRA | homoR  | homoR   | hetero  | hetero  | hetero  | hetero  |
| 122877   | fam81_1 | Fat81_1 | I23015 | homoR  | homoR  | homoA  | hetero | heteroRA | homoR  | homoR   | hetero  | hetero  | homoA   | homoR   |
| 122878   | fam81_1 | Fat81_1 | I23015 | homoR  | homoR  | hetero | hetero | heteroRA | homoR  | homoR   | hetero  | homoR   | homoA   | homoA   |
| 122879   | fam81_1 | Fat81_1 | I23015 | homoR  | homoR  | homoR  | homoR  | heteroRA | homoR  | homoR   | hetero  | hetero  | homoA   | hetero  |
| 122882   | fam81_1 | Fat81_1 | I23015 | homoR  | homoR  | hetero | homoR  | homoRR   | hetero | homoR   | hetero  | hetero  | homoR   | homoR   |
| 122883   | fam81_1 | Fat81_1 | I23015 | homoR  | homoR  | hetero | hetero | heteroRA | hetero | homoR   | homoR   | homoR   | hetero  | hetero  |
| 122888   | fam81_1 | Fat81_1 | I23015 | homoR  | homoR  | hetero | hetero | heteroRA | homoR  | homoR   | homoR   | hetero  | hetero  | homoR   |
| 122893   | fam81_1 | Fat81_1 | I23015 | homoR  | homoR  | hetero | hetero | homoAA   | homoR  | homoR   | homoR   | hetero  | hetero  | homoR   |
| 122894   | fam81_1 | Fat81_1 | I23015 | homoR  | homoR  | homoA  | hetero | heteroRA | hetero | homoR   | homoR   | hetero  | hetero  | homoA   |
| 122921   | fam81_1 | Fat81_1 | I23015 | homoR  | hetero | hetero | hetero | heteroRA | homoR  | homoR   | hetero  | hetero  | hetero  | homoR   |
| 122925   | fam81_1 | Fat81_1 | I23015 | homoR  | hetero | hetero | hetero | heteroRA | homoR  | homoR   | hetero  | hetero  | homoA   | hetero  |
| 122926   | fam81_1 | Fat81_1 | I23015 | homoR  | hetero | homoR  | hetero | homoRR   | hetero | homoR   | homoR   | homoR   | hetero  | homoA   |
| 122927   | fam81_1 | Fat81_1 | I23015 | homoR  | hetero | hetero | hetero | homoRR   | hetero | homoR   | homoR   | hetero  | hetero  | hetero  |
| 122929   | fam81_1 | Fat81_1 | I23015 | homoR  | homoR  | homoA  | hetero | heteroRA | hetero | homoR   | homoR   | hetero  | homoR   | hetero  |
| 122930   | fam81_1 | Fat81_1 | I23015 | homoR  | hetero | hetero | hetero | homoRR   | homoR  | homoR   | hetero  | hetero  | homoR   | hetero  |
| 122931   | fam81_1 | Fat81_1 | I23015 | homoR  | homoR  | homoA  | homoR  | heteroRA | hetero | homoR   | hetero  | homoR   | homoA   | hetero  |
| 122934   | fam81_1 | Fat81_1 | I23015 | homoR  | hetero | hetero | homoR  | heteroRA | hetero | homoR   | homoR   | hetero  | hetero  | homoA   |
| 122936   | fam81_1 | Fat81_1 | I23015 | homoR  | homoR  | homoA  | hetero | heteroRA | hetero | homoR   | hetero  | hetero  | hetero  | hetero  |
| 122939   | fam81_1 | Fat81_1 | I23015 | homoR  | homoR  | hetero | hetero | homoRR   | homoR  | homoR   | hetero  | hetero  | homoA   | hetero  |
| 122941   | fam81_1 | Fat81_1 | I23015 | homoR  | hetero | homoA  | homoR  | homoRR   | homoR  | homoR   | hetero  | hetero  | hetero  | homoR   |
| 122942   | fam81_1 | Fat81_1 | I23015 | homoR  | homoR  | homoR  | hetero | heteroRA | homoR  | homoR   | hetero  | homoA   | homoA   | hetero  |
| 122944   | fam81_1 | Fat81_1 | I23015 | homoR  | hetero | hetero | homoR  | heteroRA | homoR  | homoR   | hetero  | homoR   | homoA   | homoR   |
| 122812   | fam82_1 | I23006  | I23005 | homoR  | homoR  | homoA  | homoR  | heteroAB | homoR  | homoR   | hetero  | homoA   | hetero  | hetero  |
| 122814   | fam82_1 | I23006  | I23005 | homoR  | homoR  | homoA  | homoR  | heteroAB | homoR  | homoR   | hetero  | homoA   | hetero  | hetero  |
| 122815   | fam82_1 | I23006  | I23005 | homoR  | homoR  | homoA  | homoR  | heteroAB | homoR  | homoR   | hetero  | homoA   | homoR   | hetero  |
| 122816   | fam82_1 | I23006  | I23005 | homoR  | hetero | hetero | homoR  | heteroAB | homoR  | homoR   | hetero  | hetero  | homoR   | hetero  |
| 122817   | fam82_1 | I23006  | I23005 | homoR  | homoR  | homoA  | homoR  | heteroRB | homoR  | homoR   | hetero  | homoA   | hetero  | hetero  |
| 122818   | fam82_1 | I23006  | I23005 | homoR  | homoR  | hetero | homoR  | heteroRB | homoR  | homoR   | hetero  | homoR   | hetero  | hetero  |
| 122819   | fam82_1 | I23006  | I23005 | homoR  | homoR  | homoA  | homoR  | heteroAB | homoR  | hetero  | hetero  | homoA   | homoR   | hetero  |
| 122820   | fam82_1 | I23006  | I23005 | homoR  | homoR  | homoA  | homoR  | heteroAB | homoR  | homoR   | hetero  | hetero  | hetero  | hetero  |
| 122821   | fam82_1 | I23006  | I23005 | homoR  | homoR  | hetero | homoR  | heteroRB | homoR  | hetero  | homoR   | hetero  | homoR   | hetero  |
| 122822   | fam82_1 | I23006  | I23005 | homoR  | homoR  | homoA  | homoR  | heteroRB | homoR  | hetero  | hetero  | homoA   | homoR   | hetero  |
| 122823   | fam82_1 | I23006  | I23005 | homoR  | homoR  | hetero | homoR  | heteroAB | homoR  | homoR   | hetero  | hetero  | hetero  | hetero  |
| 122842   | fam82_1 | I23006  | I23005 | homoR  | homoR  | homoA  | homoR  | heteroAB | homoR  | hetero  | hetero  | homoA   | hetero  | hetero  |
| 122843   | fam82_1 | I23006  | I23005 | homoR  | hetero | hetero | homoR  | heteroRB | homoR  | homoR   | hetero  | homoA   | hetero  | hetero  |
| 122845   | fam82_1 | I23006  | I23005 | homoR  | homoR  | homoA  | homoR  | heteroRB | homoR  | hetero  | homoR   | hetero  | hetero  | hetero  |
| 122950   | fam82_1 | I23006  | I23005 | homoR  | hetero | hetero | homoR  | heteroAB | homoR  | homoR   | hetero  | hetero  | homoR   | hetero  |
| 122951   | fam82_1 | I23006  | I23005 | homoR  | homoR  | hetero | homoR  | heteroAB | homoR  | homoR   | homoR   | hetero  | homoA   | homoR   |
| 122952   | fam82_1 | I23006  | I23005 | homoR  | hetero | hetero | homoR  | heteroAB | homoR  | hetero  | hetero  | hetero  | homoR   | hetero  |
| 122953   | fam82_1 | I23006  | I23005 | homoR  | homoR  | homoA  | homoR  | heteroAB | homoR  | hetero  | homoR   | hetero  | hetero  | hetero  |
| 122954   | fam82_1 | I23006  | I23005 | homoR  | hetero | hetero | homoR  | heteroRB | homoR  | hetero  | hetero  | homoA   | homoR   | hetero  |
| 122955   | fam82_1 | I23006  | I23005 | homoR  | homoR  | homoA  | homoR  | heteroAB | homoR  | homoR   | homoR   | hetero  | homoR   | hetero  |
| 122956   | fam82_1 | I23006  | I23005 | homoR  | homoR  | homoA  | homoR  | heteroRB | homoR  | hetero  | hetero  | hetero  | hetero  | hetero  |
| 122957   | fam82_1 | I23006  | I23005 | homoR  | homoR  | hetero | homoR  | heteroRB | homoR  | homoR   | hetero  | homoA   | hetero  | hetero  |
| 122958   | fam82_1 | I23006  | I23005 | homoR  | homoR  | hetero | homoR  | heteroAB | homoR  | homoR   | hetero  | homoA   | hetero  | hetero  |
| 122960   | fam82_1 | I23006  | I23005 | homoR  | homoR  | hetero | homoR  | heteroAB | homoR  | homoR   | hetero  | hetero  | hetero  | hetero  |
| 122961   | fam82_1 | I23006  | I23005 | homoR  | homoR  | homoA  | homoR  | heteroRB | homoR  | homoR   | hetero  | hetero  | homoR   | hetero  |
| 122962   | fam82_1 | I23006  | I23005 | homoR  | hetero | hetero | homoR  | heteroRB | homoR  | hetero  | hetero  | homoA   | hetero  | hetero  |
| 122964   | fam82_1 | I23006  | I23005 | homoR  | homoR  | homoA  | homoR  | heteroRB | homoR  | homoR   | hetero  | hetero  | homoR   | hetero  |
| 122965   | fam82_1 | I23006  | I23005 | homoR  | hetero | hetero | homoR  | heteroAB | homoR  | hetero  | hetero  | homoA   | hetero  | hetero  |
| 122966   | fam82_1 | I23006  | I23005 | homoR  | homoR  | homoA  | homoR  | heteroRB | homoR  | homoR   | hetero  | homoA   | hetero  | hetero  |
| 122967   | fam82_1 | I23006  | I23005 | homoR  | hetero | hetero | homoR  | heteroRB | homoR  | homoR   | hetero  | homoA   | homoR   | hetero  |
| 122968   | fam82_1 | I23006  | I23005 | homoR  | homoR  | hetero | homoR  | heteroRB | homoR  | homoR   | homoR   | homoA   | homoR   | hetero  |
| 122969   | fam82_1 | I23006  | I23005 | homoR  | homoR  | homoA  | homoR  | heteroAB | homoR  | homoR   | homoR   | homoA   | hetero  | hetero  |
| 122970   | fam82_1 | I23006  | I23005 | homoR  | homoR  | homoA  | homoR  | heteroAB | homoR  | hetero  | hetero  | homoA   | homoR   | hetero  |
| 122971   | fam82_1 | I23006  | I23005 | homoR  | homoR  | homoA  | homoR  | heteroAB | homoR  | homoR   | hetero  | homoA   | homoR   | hetero  |
| 122972   | fam82_1 | I23006  | I23005 | homoR  | hetero | hetero | homoR  | heteroAB | homoR  | homoR   | homoR   | hetero  | hetero  | hetero  |
| 122973   | fam82_1 | I23006  | I23005 | homoR  | homoR  | homoA  | homoR  | heteroRB | homoR  | homoR   | hetero  | hetero  | homoR   | hetero  |
| 122974   | fam82_1 | I23006  | I23005 | homoR  | hetero | hetero | homoR  | heteroRB | homoR  | hetero  | hetero  | hetero  | homoR   | hetero  |
| 122975   | fam82_1 | I23006  | I23005 | homoR  | homoR  | hetero | homoR  | heteroRB | homoR  | homoR   | hetero  | hetero  | homoR   | hetero  |
| 122977   | fam82_1 | I23006  | I23005 | homoR  | homoR  | homoA  | homoR  | heteroAB | homoR  | homoR   | hetero  | hetero  | homoA   | hetero  |
| 122978   | fam82_1 | I23006  | I23005 | homoR  | homoR  | homoA  | homoR  | heteroRB | homoR  | homoR   | homoR   | hetero  | homoR   | hetero  |
| 122979   | fam82_1 | I23006  | I23005 | homoR  | homoR  | homoA  | homoR  | heteroAB | homoR  | hetero  | hetero  | hetero  | homoR   | hetero  |
| 122775   | fam83_1 | I23003  | I23004 | homoR  | hetero | hetero | homoR  | heteroRA | homoR  | homoR   | homoR   | hetero  | homoR   | homoR   |
| 122779   | fam83_1 | I23003  | I23004 | homoR  | hetero | hetero | homoR  | heteroRA | homoR  | homoR   | hetero  | hetero  | homoR   | homoR   |
| 122780   | fam83_1 | I23003  | I23004 | homoR  | homoR  | homoR  | homoR  | heteroRA | homoR  | homoR   | homoR   | hetero  | homoR   | homoR   |
| 122781   | fam83_1 | I23003  | I23004 | homoR  | hetero | hetero | homoR  | heteroRA | homoR  | homoR   | hetero  | hetero  | homoR   | homoR   |
| 122783   | fam83_1 | I23003  | I23004 | homoR  | homoR  | hetero | homoR  | homoAA   | homoR  | homoR   | homoR   | hetero  | hetero  | homoR   |
| 122784   | fam83_1 | I23003  | I23004 | homoR  | homoR  | homoA  | homoR  | homoRR   | homoR  | homoR   | hetero  | hetero  | homoR   | homoR   |
| 122801   | fam83_1 | I23003  | I23004 | homoR  | hetero | hetero | homoR  | homoRR   | homoR  | homoR   | hetero  | hetero  | hetero  | homoR   |
| 122802   | fam83_1 | I23003  | I23004 | homoR  | hetero | homoR  | homoR  | homoAA   | homoR  | homoR   | hetero  | hetero  | homoR   | homoR   |
| 122804   | fam83_1 | I23003  | I23004 | hetero | homoR  | hetero | homoR  | heteroRA | homoR  | homoR   | hetero  | hetero  | hetero  | homoR   |
| 122806   | fam83_1 | I23003  | I23004 | homoR  | homoR  | homoA  | homoR  | homoRR   | homoR  |         |         |         |         |         |



|        |         |          |         |        |        |        |        |          |        |        |        |        |        |        |
|--------|---------|----------|---------|--------|--------|--------|--------|----------|--------|--------|--------|--------|--------|--------|
| 122749 | fam91_2 | Fat91_2  | 123007  | homoR  | homoR  | hetero | homoR  | heteroRA | homoR  | homoR  | hetero | homoA  | hetero | homoR  |
| 122751 | fam91_2 | Fat91_2  | 123007  | homoR  | homoR  | hetero | homoR  | homoAA   | homoR  | homoR  | hetero | hetero | hetero | homoR  |
| 122514 | fam92_1 | Fat92_1  | 123009  | homoR  | hetero | homoA  | hetero | heteroRA | homoR  | homoR  | homoR  | homoR  | homoR  | homoR  |
| 122516 | fam92_1 | Fat92_1  | 123009  | homoR  | hetero | homoA  | homoR  | heteroRA | homoR  | hetero | homoR  | hetero | hetero | homoR  |
| 122530 | fam92_1 | Fat92_1  | 123009  | homoR  | homoR  | hetero | homoA  | homoAA   | homoR  | hetero | homoR  | hetero | hetero | hetero |
| 122549 | fam92_1 | Fat92_1  | 123009  | homoR  | hetero | hetero | hetero | homoRR   | homoR  | hetero | homoR  | hetero | hetero | homoR  |
| 122556 | fam92_1 | Fat92_1  | 123009  | homoR  | homoR  | hetero | homoR  | homoRR   | homoR  | hetero | homoR  | homoA  | homoR  | homoR  |
| 122580 | fam92_1 | Fat92_1  | 123009  | homoR  | homoR  | homoA  | homoA  | homoRR   | homoR  | hetero | homoR  | hetero | homoA  | hetero |
| 122633 | fam92_1 | Fat92_1  | 123009  | homoR  | homoR  | hetero | homoR  | homoAA   | homoR  | hetero | homoR  | homoR  | hetero | homoR  |
| 122673 | fam92_1 | Fat92_1  | 123009  | homoR  | hetero | hetero | homoR  | heteroRA | homoR  | homoR  | homoR  | hetero | hetero | hetero |
| 122679 | fam92_1 | Fat92_1  | 123009  | homoR  | homoR  | homoA  | hetero | heteroRA | homoR  | homoR  | homoR  | hetero | homoR  | hetero |
| 122692 | fam92_1 | Fat92_1  | 123009  | homoR  | homoR  | hetero | hetero | heteroRA | homoR  | hetero | homoR  | hetero | homoA  | hetero |
| 122697 | fam92_1 | Fat92_1  | 123009  | homoR  | homoR  | homoA  | hetero | heteroRA | homoR  | hetero | homoR  | homoR  | homoR  | hetero |
| 122700 | fam92_1 | Fat92_1  | 123009  | homoR  | homoR  | homoA  | hetero | homoRR   | homoR  | homoR  | homoR  | hetero | hetero | homoR  |
| 122703 | fam92_1 | Fat92_1  | 123009  | homoR  | hetero | hetero | homoR  | homoRR   | homoR  | hetero | homoR  | hetero | homoR  | homoR  |
| 122714 | fam92_1 | Fat92_1  | 123009  | homoR  | homoR  | hetero | homoA  | heteroRA | homoR  | hetero | homoR  | hetero | hetero | homoR  |
| 122755 | fam92_1 | Fat92_1  | 123009  | homoR  | hetero | homoA  | homoR  | homoAA   | homoR  | hetero | homoR  | hetero | hetero | homoR  |
| 122759 | fam92_1 | Fat92_1  | 123009  | homoR  | hetero | homoR  | homoA  | heteroRA | homoR  | hetero | homoR  | hetero | hetero | homoR  |
| 122760 | fam92_1 | Fat92_1  | 123009  | homoR  | homoR  | hetero | hetero | heteroRA | homoR  | hetero | homoR  | homoR  | homoR  | homoR  |
| 122517 | fam92_2 | 123010   | 123009  | homoR  | homoR  | hetero | homoR  | heteroRB | hetero | hetero | homoR  | hetero | hetero | hetero |
| 122518 | fam92_2 | 123010   | 123009  | homoR  | homoR  | homoA  | homoR  | heteroRB | hetero | hetero | homoR  | homoA  | hetero | homoR  |
| 122524 | fam92_2 | 123010   | 123009  | homoR  | homoR  | homoA  | homoR  | heteroRA | hetero | hetero | homoR  | hetero | hetero | homoR  |
| 122536 | fam92_2 | 123010   | 123009  | homoR  | homoR  | homoA  | homoR  | homoRR   | homoR  | homoR  | homoR  | hetero | hetero | hetero |
| 122547 | fam92_2 | 123010   | 123009  | hetero | homoR  | hetero | homoR  | heteroAB | hetero | hetero | homoR  | hetero | hetero | hetero |
| 122553 | fam92_2 | 123010   | 123009  | homoR  | homoR  | homoR  | homoR  | heteroRB | homoR  | homoR  | homoR  | hetero | homoA  | homoR  |
| 122560 | fam92_2 | 123010   | 123009  | homoR  | homoR  | homoA  | hetero | heteroAB | homoR  | hetero | homoR  | homoA  | hetero | hetero |
| 122567 | fam92_2 | 123010   | 123009  | hetero | homoR  | homoA  | homoR  | heteroRB | homoR  | homoR  | homoR  | hetero | hetero | homoR  |
| 122572 | fam92_2 | 123010   | 123009  | homoR  | homoR  | homoR  | homoR  | heteroRA | hetero | homoR  | homoR  | homoA  | hetero | hetero |
| 122576 | fam92_2 | 123010   | 123009  | hetero | homoR  | hetero | hetero | heteroRA | hetero | hetero | homoR  | homoR  | hetero | hetero |
| 122577 | fam92_2 | 123010   | 123009  | hetero | homoR  | homoR  | homoR  | homoRR   | hetero | homoR  | homoR  | homoA  | hetero | hetero |
| 122581 | fam92_2 | 123010   | 123009  | hetero | homoR  | hetero | homoR  | homoRR   | hetero | homoR  | homoR  | hetero | hetero | homoR  |
| 122584 | fam92_2 | 123010   | 123009  | hetero | homoR  | homoA  | hetero | heteroRB | homoR  | homoR  | homoR  | homoR  | homoA  | hetero |
| 122602 | fam92_2 | 123010   | 123009  | hetero | homoR  | homoA  | hetero | heteroRB | hetero | hetero | homoR  | homoA  | hetero | hetero |
| 122618 | fam92_2 | 123010   | 123009  | homoR  | hetero | hetero | homoR  | homoR    | homoR  | homoR  | homoR  | homoA  | homoR  | hetero |
| 122619 | fam92_2 | 123010   | 123009  | hetero | homoR  | homoR  | homoR  | homoRR   | hetero | homoR  | homoR  | hetero | homoR  | homoR  |
| 122627 | fam92_2 | 123010   | 123009  | hetero | homoR  | hetero | hetero | heteroAB | hetero | hetero | homoR  | homoA  | hetero | hetero |
| 122632 | fam92_2 | 123010   | 123009  | hetero | homoR  | homoA  | hetero | heteroRB | hetero | homoR  | homoR  | hetero | hetero | homoR  |
| 122676 | fam92_2 | 123010   | 123009  | hetero | homoR  | homoA  | homoR  | homoRR   | homoR  | hetero | homoR  | homoA  | hetero | homoR  |
| 122681 | fam92_2 | 123010   | 123009  | hetero | homoR  | homoR  | hetero | homoRR   | homoR  | homoR  | homoR  | hetero | homoR  | hetero |
| 122682 | fam92_2 | 123010   | 123009  | hetero | homoR  | hetero | homoR  | homoRR   | hetero | homoR  | homoR  | hetero | hetero | homoR  |
| 122683 | fam92_2 | 123010   | 123009  | hetero | homoR  | hetero | homoR  | heteroRB | hetero | homoR  | homoR  | homoA  | hetero | hetero |
| 122689 | fam92_2 | 123010   | 123009  | homoR  | homoR  | hetero | homoR  | heteroAB | homoR  | hetero | homoR  | hetero | homoR  | homoR  |
| 122690 | fam92_2 | 123010   | 123009  | hetero | homoR  | homoA  | homoR  | heteroAB | homoR  | homoR  | homoR  | hetero | hetero | hetero |
| 122691 | fam92_2 | 123010   | 123009  | hetero | homoR  | homoA  | homoR  | heteroRA | homoR  | homoR  | homoR  | hetero | homoR  | hetero |
| 122702 | fam92_2 | 123010   | 123009  | homoR  | hetero | hetero | homoR  | heteroRB | homoR  | homoR  | homoR  | hetero | homoA  | homoR  |
| 122706 | fam92_2 | 123010   | 123009  | homoR  | homoR  | homoA  | homoR  | heteroRB | homoR  | hetero | homoR  | hetero | hetero | hetero |
| 122713 | fam92_2 | 123010   | 123009  | hetero | homoR  | homoR  | homoR  | heteroRB | hetero | hetero | homoR  | homoR  | hetero | hetero |
| 122719 | fam92_2 | 123010   | 123009  | homoR  | homoR  | hetero | hetero | heteroRA | hetero | hetero | homoR  | hetero | hetero | hetero |
| 122721 | fam92_2 | 123010   | 123009  | homoR  | hetero | hetero | hetero | heteroAB | hetero | homoR  | homoR  | homoR  | homoA  | hetero |
| 122723 | fam92_2 | 123010   | 123009  | hetero | homoR  | hetero | hetero | homoRR   | hetero | hetero | homoR  | homoA  | homoR  | homoR  |
| 122726 | fam92_2 | 123010   | 123009  | hetero | homoR  | hetero | hetero | homoRR   | homoR  | homoR  | homoR  | hetero | hetero | hetero |
| 122728 | fam92_2 | 123010   | 123009  | homoR  | homoR  | homoA  | homoR  | heteroRA | homoR  | homoR  | homoR  | homoR  | homoA  | hetero |
| 122737 | fam92_2 | 123010   | 123009  | hetero | homoR  | hetero | homoR  | heteroAB | homoR  | homoR  | homoR  | hetero | hetero | hetero |
| 122742 | fam92_2 | 123010   | 123009  | hetero | homoR  | hetero | hetero | heteroRA | homoR  | homoR  | homoR  | homoR  | homoR  | hetero |
| 122746 | fam92_2 | 123010   | 123009  | homoR  | homoR  | homoA  | homoR  | heteroRB | hetero | homoR  | homoR  | homoA  | homoR  | hetero |
| 122747 | fam92_2 | 123010   | 123009  | homoR  | homoR  | homoR  | homoR  | homoRR   | hetero | homoR  | homoR  | homoA  | hetero | hetero |
| 122753 | fam92_2 | 123010   | 123009  | hetero | homoR  | homoA  | hetero | heteroRB | homoR  | hetero | homoR  | hetero | homoR  | hetero |
| 122758 | fam92_2 | 123010   | 123009  | homoR  | homoR  | homoR  | hetero | heteroAB | homoR  | hetero | homoR  | hetero | homoA  | hetero |
| 122763 | fam92_2 | 123010   | 123009  | homoR  | homoR  | homoA  | hetero | homoRR   | homoR  | hetero | homoR  | homoA  | hetero | hetero |
| 122764 | fam92_2 | 123010   | 123009  | hetero | homoR  | homoR  | homoR  | heteroAB | hetero | hetero | homoR  | homoR  | hetero | hetero |
| 122537 | fam93_1 | 123014   | Mot93_1 | hetero | homoR  | hetero | homoR  | homoRR   | homoR  | homoR  | homoA  | hetero | hetero | hetero |
| 122551 | fam93_1 | 123014   | Mot93_1 | hetero | homoR  | homoR  | homoR  | homoAA   | hetero | homoR  | homoA  | homoA  | homoR  | hetero |
| 122563 | fam93_1 | 123014   | Mot93_1 | hetero | hetero | hetero | homoR  | heteroRA | hetero | homoR  | hetero | homoA  | homoA  | homoR  |
| 122564 | fam93_1 | 123014   | Mot93_1 | homoR  | homoR  | homoA  | homoR  | homoRR   | homoR  | homoR  | homoA  | hetero | hetero | homoR  |
| 122568 | fam93_1 | 123014   | Mot93_1 | hetero | homoR  | homoR  | homoR  | homoRR   | homoR  | homoR  | homoR  | homoA  | hetero | homoR  |
| 122571 | fam93_1 | 123014   | Mot93_1 | hetero | homoR  | homoR  | homoR  | homoRR   | hetero | homoR  | hetero | hetero | hetero | hetero |
| 122593 | fam93_1 | 123014   | Mot93_1 | homoR  | hetero | homoA  | homoR  | homoRR   | homoR  | homoR  | homoA  | homoA  | hetero | hetero |
| 122594 | fam93_1 | 123014   | Mot93_1 | homoR  | homoR  | hetero | homoR  | heteroRA | hetero | homoR  | homoA  | homoA  | homoA  | hetero |
| 122598 | fam93_1 | 123014   | Mot93_1 | homoR  | homoR  | hetero | homoR  | homoRR   | homoR  | homoR  | homoA  | homoA  | hetero | hetero |
| 122604 | fam93_1 | 123014   | Mot93_1 | hetero | homoR  | homoR  | homoR  | heteroRA | hetero | homoR  | homoA  | hetero | homoA  | hetero |
| 122613 | fam93_1 | 123014   | Mot93_1 | hetero | homoR  | homoR  | homoR  | homoAA   | homoR  | homoR  | homoA  | hetero | hetero | hetero |
| 122615 | fam93_1 | 123014   | Mot93_1 | homoR  | hetero | hetero | homoR  | heteroRA | homoR  | homoR  | homoA  | homoA  | hetero | hetero |
| 122638 | fam93_1 | 123014   | Mot93_1 | hetero | homoR  | homoA  | homoR  | homoRR   | hetero | homoR  | homoA  | hetero | hetero | homoA  |
| 122639 | fam93_1 | 123014   | Mot93_1 | hetero | homoR  | hetero | homoR  | homoRR   | homoR  | homoR  | homoA  | hetero | hetero | homoR  |
| 122645 | fam93_1 | 123014   | Mot93_1 | hetero | homoR  | homoR  | homoR  | heteroRA | homoR  | homoR  | homoA  | homoA  | hetero | homoR  |
| 122653 | fam93_1 | 123014   | Mot93_1 | hetero | homoR  | homoA  | homoR  | homoRR   | homoR  | homoR  | homoA  | homoA  | hetero | homoR  |
| 122654 | fam93_1 | 123014   | Mot93_1 | homoR  | homoR  | hetero | homoR  | homoRR   | homoR  | homoR  | hetero | homoA  | hetero | hetero |
| 122655 | fam93_1 | 123014   | Mot93_1 | homoR  | homoR  | hetero | homoR  | heteroRA | hetero | homoR  | homoA  | homoA  | hetero | homoA  |
| 122657 | fam93_1 | 123014   | Mot93_1 | hetero | hetero | homoA  | homoR  | homoRR   | hetero | homoR  | hetero | homoA  | hetero | hetero |
| 122658 | fam93_1 | 123014   | Mot93_1 | hetero | homoR  | hetero | homoR  | homoRR   | hetero | homoR  | homoA  | homoA  | hetero | hetero |
| 122672 | fam93_1 | 123014   | Mot93_1 | homoR  | hetero | hetero | homoR  | heteroRA | homoR  | homoR  | homoA  | hetero | hetero | hetero |
| 122720 | fam93_1 | 123014   | Mot93_1 | homoR  | homoR  | hetero | homoR  | heteroRA | homoR  | homoR  | hetero | homoA  | hetero | hetero |
| 122727 | fam93_1 | 123014   | Mot93_1 | hetero | hetero | homoA  | homoR  | heteroRA | homoR  | homoR  | homoA  | hetero | hetero | homoR  |
| 122734 | fam93_1 | 123014   | Mot93_1 | hetero | homoR  | hetero | homoR  | homoRR   | homoR  | homoR  | homoA  | hetero | hetero | hetero |
| 122738 | fam93_1 | 123014   | Mot93_1 | homoR  | homoR  | hetero | homoR  | heteroRA | hetero | homoR  | homoA  | hetero | hetero | hetero |
| 122538 | fam93_2 | 123014   | Mot93_2 | hetero | hetero | hetero | homoR  | homoAA   | hetero | homoR  | hetero | homoA  | homoA  | homoA  |
| 122541 | fam93_2 | 123014   | Mot93_2 | homoR  | hetero | homoA  | homoR  | heteroRA | homoR  | homoR  | homoA  | hetero | homoR  | homoA  |
| 122543 | fam93_2 | 123014   | Mot93_2 | hetero | hetero | homoA  | homoR  | heteroRA | homoR  | homoR  | homoR  | hetero | homoA  | hetero |
| 122548 | fam93_2 | 123014   | Mot93_2 | hetero | homoR  | homoR  | homoR  | heteroRA | homoR  | homoR  | hetero | hetero | homoA  | hetero |
| 122550 | fam93_2 | 123014   | Mot93_2 | homoR  | homoR  | hetero | homoR  | homoRR   | homoR  | homoR  | hetero | homoA  | hetero | homoR  |
| 122552 | fam93_2 | 123014   | Mot93_2 | homoR  | hetero | homoR  | homoR  | heteroRA | hetero | homoR  | hetero | hetero | homoA  | homoA  |
| 122554 | fam93_2 | 123014   | Mot93_2 | homoR  | hetero | homoA  | homoR  | homoRR   | homoR  | homoR  | hetero | hetero | homoA  | homoR  |
| 122555 | fam93_2 | 123014   | Mot93_2 | homoR  | hetero | hetero | homoR  | homoAA   | hetero | homoR  | hetero | hetero | hetero | hetero |
| 122569 | fam93_2 | 123014</ |         |        |        |        |        |          |        |        |        |        |        |        |



Table S3: Correspondence of linkage groups (LG) of the previous linkage map (Westram et al., 2018, doi: 10.1002/evl3.74) and the map presented in this study. Given are the proportions (in %) of markers on common contigs of each LG in the new map (in rows) that were assigned to LGs in the previous map. All LGs in our new map corresponded well with one of the previous LGs.

|                       |    | Linkage groups previous map |       |       |       |       |       |       |      |      |       |       |       |       |       |       |       |       |
|-----------------------|----|-----------------------------|-------|-------|-------|-------|-------|-------|------|------|-------|-------|-------|-------|-------|-------|-------|-------|
|                       |    | 1                           | 2     | 3     | 4     | 5     | 6     | 7     | 8    | 9    | 10    | 11    | 12    | 13    | 14    | 15    | 16    | 17    |
| Linkage group QTL map | 1  | 0                           | 0     | 0     | 0.06  | 0     | 0.62  | 0     | 0    | 0    | 0     | 0     | 98.92 | 0     | 0     | 0.4   | 0     | 0     |
|                       | 2  | 0                           | 99.91 | 0.02  | 0.07  | 0     | 0     | 0     | 0    | 0    | 0     | 0     | 0     | 0     | 0     | 0     | 0     | 0     |
|                       | 3  | 99.72                       | 0.02  | 0.19  | 0.04  | 0     | 0     | 0.02  | 0    | 0    | 0     | 0     | 0     | 0     | 0     | 0.02  | 0     | 0     |
|                       | 4  | 0                           | 0     | 99.89 | 0     | 0     | 0.04  | 0     | 0    | 0.08 | 0     | 0     | 0     | 0     | 0     | 0     | 0     | 0     |
|                       | 5  | 0.5                         | 0     | 0.12  | 0     | 0     | 0.06  | 0     | 0    | 0    | 0     | 0     | 0     | 0     | 0     | 0     | 0     | 99.32 |
|                       | 6  | 0                           | 0.13  | 0     | 1.54  | 0     | 96.93 | 0     | 0    | 0    | 0     | 0     | 0     | 0     | 0     | 0     | 0     | 1.41  |
|                       | 7  | 0                           | 0     | 0.17  | 99.62 | 0     | 0.17  | 0     | 0    | 0    | 0     | 0     | 0     | 0     | 0     | 0     | 0.04  | 0     |
|                       | 8  | 0                           | 0     | 0     | 0     | 0     | 0     | 99.57 | 0    | 0    | 0     | 0     | 0.05  | 0     | 0     | 0.38  | 0     | 0     |
|                       | 9  | 0                           | 0     | 0     | 0     | 0     | 0     | 0     | 0    | 100  | 0     | 0     | 0     | 0     | 0     | 0     | 0     | 0     |
|                       | 10 | 0                           | 0.16  | 0     | 0     | 0     | 0     | 0     | 0    | 0    | 0     | 0     | 0     | 0     | 99.84 | 0     | 0     | 0     |
|                       | 11 | 0                           | 0.27  | 0     | 0.2   | 0     | 0     | 0     | 0    | 0    | 99.53 | 0     | 0     | 0     | 0     | 0     | 0     | 0     |
|                       | 12 | 0.09                        | 0     | 0     | 0.05  | 99.63 | 0.23  | 0     | 0    | 0    | 0     | 0     | 0     | 0     | 0     | 0     | 0     | 0     |
|                       | 13 | 0.21                        | 0     | 0     | 0     | 0     | 1.26  | 0     | 0    | 0    | 0     | 0     | 0     | 98.18 | 0     | 0.35  | 0     | 0     |
|                       | 14 | 0.49                        | 0     | 0     | 0     | 0     | 0     | 0     | 0    | 0    | 0     | 0     | 0     | 0     | 0     | 99.51 | 0     | 0     |
|                       | 15 | 0                           | 0     | 0     | 0.09  | 0     | 0     | 0     | 0    | 0    | 0     | 99.81 | 0     | 0     | 0     | 0     | 0     | 0.09  |
|                       | 16 | 0                           | 0     | 0     | 0.4   | 0     | 0     | 0     | 99.5 | 0    | 0     | 0     | 0     | 0     | 0     | 0.1   | 0     | 0     |
|                       | 17 | 0.62                        | 0     | 0     | 0     | 0     | 0     | 0     | 0    | 0    | 0     | 0.47  | 0     | 0     | 0     | 0.16  | 98.75 | 0     |

|               | Trait                                     | LG    | Position     |              |              | LOD          | P-value           | threshold   | variance explained | N observations |
|---------------|---|-------|--------------|--------------|--------------|--------------|-------------------|-------------|--------------------|----------------|
|               |   |       | (cM)         | lower CI     | higher CI    |              |                   |             |                    |                |
| <i>Size</i>   | shell thickness                           | 6     | 20.11        | 5.22         | 31.63        | 3.83         | 0.079             | 4.05        | 0.046              | 373            |
|               | weight                                    | 6     | <b>9.00</b>  | <b>0.00</b>  | <b>25.72</b> | <b>4.17</b>  | <b>0.031</b>      | <b>3.90</b> | <b>0.050</b>       | 374            |
|               | shell length                              | 6     | 10.00        | 0.00         | 25.42        | 3.85         | 0.063             | 3.99        | 0.046              | 375            |
| <i>Shape</i>  | height growth                             | 17    | <b>31.78</b> | <b>28.76</b> | <b>32.99</b> | <b>4.16</b>  | <b>0.028</b>      | <b>3.93</b> | <b>0.050</b>       | 376            |
|               | width growth                              | 17    | <b>64.40</b> | <b>30.57</b> | <b>67.15</b> | <b>4.02</b>  | <b>0.053</b>      | <b>4.03</b> | <b>0.048</b>       | 376            |
|               | aperture position radial                  | 17    | <b>64.09</b> | <b>50.27</b> | <b>67.15</b> | <b>6.16</b>  | <b>0.001</b>      | <b>3.89</b> | <b>0.073</b>       | 376            |
|               | aperture size                             | 12    | 73.22        | 61.34        | 73.43        | 3.12         | 0.242             | 3.96        | 0.037              | 376            |
|               |   | 17    | 28.76        | 31.33        | 47.09        | 3.18         | 0.212             |             | 0.038              |                |
|               | aperture shape (=extension)               | 6     | <b>18.59</b> | <b>0.75</b>  | <b>27.69</b> | <b>4.356</b> | <b>0.023</b>      | <b>4.05</b> | <b>0.052</b>       | 376            |
|               | relative thickness                        | 2     | 13.26        | 10.46        | 55.26        | 3.27         | 0.18              | 3.97        | 0.039              | 376            |
|               | 6   | 26.03 | 15.11        | 52.17        | 3.07         | 0.26         |                   | 0.037       |                    |                |
| <i>Colour</i> | rgb values analysed as multivariate trait | 6     | <b>16.02</b> | <b>0.00</b>  | <b>18.59</b> | <b>3.96</b>  | <b>0.04</b>       | <b>3.86</b> | <b>0.048</b>       | 373            |
|               |   | 17    | <b>41.32</b> | <b>23.46</b> | <b>45.87</b> | <b>6.20</b>  | <b>&lt; 0.001</b> |             | <b>0.074</b>       |                |
| <i>Sex</i>    | sex                                       | 9     | 63.97        | 52.45        | 65.47        | 3.06         | 0.246             | 3.84        | 0.038              | 367            |
|               |   | 12    | <b>37.05</b> | <b>35.68</b> | <b>37.96</b> | <b>26.91</b> | <b>&lt; 0.001</b> |             | <b>0.287</b>       |                |
|               |   | 15    | 50.59        | 29.92        | 67.50        | 3.12         | 0.229             |             | 0.038              |                |

Table S5: Results of variance partitioning across linkage groups. Shown are proportions of the total phenotypic variance explained by each linkage group (LG) with standard errors in brackets. Significant estimates are shown in bold. Size of each linkage group is given as number of markers (N marker) and length (based on our linkage map (cM) and summed length of assigned contigs in (Mb)).  $h^2$  gives heritability obtained from a model using markers from all LG. Cor gives the Spearman correlation between LG length and variance explained with significant estimates in bold.

|                    | LG1                  | LG2                  | LG3           | LG4                  | LG5                  | LG6                  | LG7           | LG8           | LG9                  | LG10          | LG11          | LG12                 | LG13           | LG14                 | LG15                | LG16            | LG17                 | $h^2$                | cor         |  |
|--------------------|----------------------|----------------------|---------------|----------------------|----------------------|----------------------|---------------|---------------|----------------------|---------------|---------------|----------------------|----------------|----------------------|---------------------|-----------------|----------------------|----------------------|-------------|--|
| N marker           | 2077                 | 2098                 | 1424          | 1142                 | 1018                 | 1191                 | 1126          | 682           | 1081                 | 1043          | 703           | 2145                 | 799            | 1050                 | 726                 | 508             | 1395                 |                      |             |  |
| Length (cM)        | 84.1                 | 80.5                 | 78.4          | 62.7                 | 58.3                 | 69.1                 | 60.6          | 66            | 65.5                 | 60.7          | 75.3          | 73.4                 | 55.4           | 34.6                 | 68.1                | 70              | 67.2                 |                      |             |  |
| Length (Mb)        | 177.82               | 208.71               | 120.93        | 102.99               | 86.68                | 106.71               | 92.88         | 43.46         | 73.91                | 84.65         | 51.07         | 187.86               | 63.72          | 75.03                | 56                  | 32              | 127.53               |                      |             |  |
| Weight             | 0.005 (0.023)        | 0.007 (0.027)        | 0.000 (0.000) | 0.023 (0.036)        | 0.095 (0.084)        | <b>0.130 (0.072)</b> | 0.009 (0.000) | 0.000 (0.000) | 0.000 (0.000)        | 0.005 (0.02)  | 0.000 (0.000) | 0.000 (0.000)        | 0.003 (0.021)  | <b>0.064 (0.051)</b> | 0.000 (0.000)       | 0.000 (0.000)   | <b>0.045 (0.046)</b> | 0.67 (0.086)         | 0.19        |  |
| Shell Length       | 0.022 (0.034)        | 0.006 (0.000)        | 0.002 (0.023) | 0.016 (0.032)        | <b>0.168 (0.098)</b> | <b>0.110 (0.065)</b> | 0.002 (0.000) | 0.000 (0.000) | 0.000 (0.000)        | 0.000 (0.000) | 0.000 (0.000) | <b>0.101 (0.073)</b> | 0.0297 (0.037) | 0.0238 (0.028)       | 0.000 (0.000)       | 0.00985 (0.029) | 0.0216 (0.037)       | <b>0.592 (0.094)</b> | <b>0.57</b> |  |
| Thickness          | 0.013 (0.016)        | 0.023 (0.023)        | 0.000 (0.000) | 0.025 (0.039)        | 0.03 (0.04)          | 0.167 (0.079)        | 0.022 (0.04)  | 0.011 (0.031) | 0.044 (0.037)        | 0.008 (0.000) | 0.000 (0.000) | 0.081 (0.059)        | 0.000 (0.000)  | 0.009 (0.014)        | 0.000 (0.000)       | 0.000 (0.000)   | 0.075 (0.063)        | <b>0.65 (0.086)</b>  | 0.32        |  |
| Height Growth      | 0.024 (0.036)        | <b>0.067 (0.053)</b> | 0.007 (0.021) | 0.015 (0.026)        | 0.064 (0.047)        | 0.006 (0.015)        | 0.000 (0.000) | 0.024 (0.034) | 0.000 (0.000)        | 0.005 (0.017) | 0.000 (0.000) | <b>0.135 (0.071)</b> | 0.012 (0.02)   | 0.000 (0.000)        | 0.003 (0.019)       | 0.036 (0.039)   | 0.000 (0.000)        | <b>0.965 (0.091)</b> | 0.24        |  |
| Width Growth       | 0.047 (0.046)        | 0.088 (0.049)        | 0.000 (0.000) | 0.021 (0.028)        | 0.067 (0.049)        | 0.001 (0.012)        | 0.000 (0.000) | 0.000 (0.000) | 0.000 (0.000)        | 0.000 (0.000) | 0.000 (0.000) | <b>0.127 (0.065)</b> | 0.000 (0.000)  | 0.000 (0.000)        | 0.02 (0.025)        | 0.000 (0.000)   | <b>0.074 (0.055)</b> | <b>0.573 (0.091)</b> | 0.5         |  |
| Aperture Position  | <b>0.081 (0.056)</b> | <b>0.082 (0.059)</b> | 0.000 (0.000) | 0.015 (0.024)        | <b>0.05 (0.042)</b>  | 0.000 (0.000)        | 0.000 (0.000) | 0.000 (0.000) | 0.011 (0.024)        | 0.103 (0.061) | 0.000 (0.000) | <b>0.114 (0.066)</b> | 0.000 (0.000)  | <b>0.022 (0.022)</b> | 0.015 (0.024)       | 0.004 (0.02)    | <b>0.162 (0.076)</b> | <b>0.529 (0.091)</b> | <b>0.57</b> |  |
| Aperture Size      | 0.043 (0.044)        | <b>0.038 (0.035)</b> | 0.000 (0.000) | 0.041 (0.039)        | <b>0.135 (0.066)</b> | 0.001 (0.011)        | 0.000 (0.000) | 0.023 (0.034) | 0.000 (0.000)        | 0.000 (0.000) | 0.000 (0.000) | <b>0.132 (0.064)</b> | 0.000 (0.000)  | 0.000 (0.000)        | <b>0.036 (0.03)</b> | 0.000 (0.000)   | 0.000 (0.000)        | <b>0.572 (0.09)</b>  | 0.42        |  |
| Aperture Shape     | 0.024 (0.030)        | 0.000 (0.000)        | 0.007 (0.024) | 0 (0.026)            | <b>0.132 (0.061)</b> | <b>0.047 (0.038)</b> | 0.008 (0.000) | 0.007 (0.022) | 0.01 (0.026)         | 0.000 (0.000) | 0.000 (0.000) | <b>0.098 (0.06)</b>  | 0.000 (0.000)  | 0.000 (0.000)        | 0.006 (0.021)       | 0.000 (0.000)   | 0.03 (0.035)         | <b>0.51 (0.10)</b>   | 0.38        |  |
| Relative Thickness | <b>0.036 (0.035)</b> | <b>0.032 (0.03)</b>  | 0.008 (0.019) | 0.04 (0.039)         | 0.014 (0.023)        | 0.091 (0.062)        | 0.035 (0.045) | 0.000 (0.000) | <b>0.063 (0.042)</b> | 0.008 (0.023) | 0.017 (0.027) | 0.044 (0.045)        | 0.000 (0.000)  | 0.000 (0.000)        | 0.002 (0.018)       | 0.007 (0.021)   | <b>0.168 (0.086)</b> | <b>0.452 (0.09)</b>  | <b>0.63</b> |  |
| Boldness           | 0.012 (0.026)        | 0.001 (0.000)        | 0.000 (0.000) | <b>0.087 (0.065)</b> | <b>0.021 (0.029)</b> | 0.007 (0.021)        | 0.000 (0.000) | 0.002 (0.02)  | 0.018 (0.029)        | 0.000 (0.000) | 0.005 (0.021) | 0.001 (0.000)        | 0.000 (0.000)  | 0.000 (0.000)        | 0.001 (0.024)       | 0.000 (0.000)   | 0.062 (0.054)        | <b>0.878 (0.074)</b> | 0.07        |  |
| Colour             | 0.084 (0.059)        | 0.02 (0.03)          | 0.016 (0.025) | 0.000 (0.000)        | 0.000 (0.000)        | <b>0.289 (0.088)</b> | 0.017 (0.025) | 0.000 (0.000) | 0.000 (0.000)        | 0.000 (0.000) | 0.022 (0.026) | 0.000 (0.000)        | 0.000 (0.000)  | 0.000 (0.000)        | 0.000 (0.000)       | 0.006 (0.026)   | <b>0.081 (0.052)</b> | <b>0.535 (0.091)</b> | 0.35        |  |

Table S6: Pairwise genetic correlations between traits estimated using bivariate animal model. Correlation coefficients are shown on the lower triangle with standard errors in brackets, P-values on the upper triangle. P-values were obtained from comparisons with models where correlation was set to zero using likelihood-ratio tests.

|                                     | Weight                | Length                | Thickness            | Height Growth         | Width Growth         | Aperture Position (radial) | Aperture Position (vertical) | Aperture Size         | Aperture Shape        | relative Thickness | Coloration    | Boldness     |
|-------------------------------------|-----------------------|-----------------------|----------------------|-----------------------|----------------------|----------------------------|------------------------------|-----------------------|-----------------------|--------------------|---------------|--------------|
| <b>Weight</b>                       |                       | <b>4.28E-10</b>       | <b>4.44E-03</b>      | <b>0.013</b>          | 0.573                | 0.373                      | 0.357                        | 0.176                 | 0.056                 | 0.374              | 0.427         | NA           |
| <b>Length</b>                       | <b>0.951 (0.04)</b>   |                       | <b>2.99E-04</b>      | <b>3.17E-04</b>       | 0.14                 | 0.796                      | 0.832                        | <b>0.011</b>          | <b>0.045</b>          | 0.191              | 0.438         | <b>0.017</b> |
| <b>Thickness</b>                    | <b>0.551 (0.158)</b>  | <b>0.632 (0.128)</b>  |                      | 0.159                 | 0.948                | 0.322                      | 0.438                        | 0.665                 | 0.298                 | <b>1.58E-09</b>    | 0.503         | 0.141        |
| <b>Height Growth</b>                | <b>-0.488 (0.185)</b> | <b>-0.652 (0.146)</b> | -0.283 (0.202)       |                       | 4.47E-06             | <b>8.30E-03</b>            | <b>1.06E-03</b>              | <b>8.27E-09</b>       | 0.077                 | 0.556              | 0.387         | 0.89         |
| <b>Width Growth</b>                 | -0.117 (0.221)        | -0.300 (0.210)        | -0.014 (0.219)       | <b>0.779 (0.202)</b>  |                      | <b>1.96E-07</b>            | <b>1.89E-05</b>              | <b>7.40E-08</b>       | 0.100                 | 0.785              | 0.807         | 0.364        |
| <b>Aperture Position (radial)</b>   | 0.181 (0.211)         | -0.052 (0.211)        | 0.197 (0.201)        | <b>0.492 (0.161)</b>  | <b>0.859 (0.072)</b> |                            | <b>1.44E-05</b>              | <b>2.16E-04</b>       | 0.584                 | 0.707              | 0.552         | 0.359        |
| <b>Aperture Position (vertical)</b> | -0.196 (0.221)        | 0.044 (0.22)          | -0.163 (0.213)       | <b>-0.631 (0.146)</b> | <b>-0.787 (0.1)</b>  | <b>-0.782 (0.098)</b>      |                              | <b>4.08E-03</b>       | 0.254                 | 0.778              | 0.273         | 0.312        |
| <b>Aperture Size</b>                | -0.277 (0.212)        | <b>-0.500 (0.181)</b> | -0.089 (0.214)       | <b>0.914 (0.053)</b>  | <b>0.878 (0.057)</b> | <b>0.655 (0.132)</b>       | <b>-0.57 (0.161)</b>         |                       | <b>9.50E-03</b>       | 0.801              | 0.14          | 0.492        |
| <b>Aperture Shape</b>               | 0.494 (0.254)         | <b>0.514 (0.248)</b>  | 0.272 (0.260)        | -0.397 (0.204)        | -0.370 (0.207)       | -0.126 (0.230)             | -0.279 (0.223)               | <b>-0.564 (0.159)</b> |                       | 0.508              | 0.026         | 0.822        |
| <b>relative Thickness</b>           | 0.180 (0.205)         | 0.256 (0.195)         | <b>0.876 (0.051)</b> | -0.112 (0.192)        | -0.053 (0.196)       | 0.071 (0.189)              | -0.057 (0.200)               | -0.048 (0.193)        | 0.151 (0.224)         |                    | 0.106         | 0.965        |
| <b>Coloration</b>                   | -0.159 (0.211)        | -0.151 (0.207)        | 0.134 (0.205)        | <b>0.177 (0.208)</b>  | <b>0.048 (0.204)</b> | <b>0.121 (0.206)</b>       | 0.228 (0.195)                | <b>0.285 (0.196)</b>  | <b>-0.473 (0.190)</b> | 0.303 (0.196)      |               | 0.133        |
| <b>Boldness</b>                     | NA                    | <b>0.862 (0.33)</b>   | 0.485 (0.327)        | -0.043 (0.325)        | 0.279 (0.301)        | 0.285 (0.303)              | -0.347 (0.335)               | 0.211 (0.302)         | 0.093 (0.393)         | 0.013 (0.302)      | 0.460 (0.293) |              |

Table S7: p-values for effects of inversions on phenotypes. p-values are adjusted for testing effects of each inversion on multiple traits (FDR correction). Significant ( $p < 0.05$ ) effects are shown in grey. Linear mixed models with phenotypic values as response and inversion genotypes as fixed effects (after correcting for batch and sex) were used to infer significance of inversion genotypes. Families were included as random effects.

|                           | Inversion |        |        |        |          |        |         |          |          |           |          |
|---------------------------|-----------|--------|--------|--------|----------|--------|---------|----------|----------|-----------|----------|
|                           | Inv1.1    | Inv1.2 | Inv2.1 | Inv4.1 | inv6.1/2 | inv7.1 | inv10.1 | inv12.1  | inv12.2  | inv14.1/2 | inv17.1  |
| <b>Thickness</b>          | 0.633     | 0.910  | 0.711  | 0.038  | 0.005    | 0.991  | 0.795   | 0.008    | 0.134    | 0.121     | 0.629    |
| <b>Weight</b>             | 0.633     | 0.818  | 0.926  | 0.494  | 0.020    | 0.991  | 0.852   | 0.138    | 0.962    | 0.001     | 0.073    |
| <b>ShellLength</b>        | 0.728     | 0.910  | 0.847  | 0.376  | 0.020    | 0.991  | 0.852   | 0.085    | 0.671    | 0.116     | 0.358    |
| <b>Bold Score</b>         | 0.983     | 0.446  | 0.714  | 0.633  | 0.962    | 0.991  | 0.852   | 0.387    | 0.671    | 0.354     | 0.133    |
| <b>HeightGrowth</b>       | 0.102     | 0.910  | 0.714  | 0.875  | 0.907    | 0.991  | 0.735   | 3.36E-04 | 0.088    | 0.958     | 0.910    |
| <b>WidthGrowth</b>        | 0.045     | 0.910  | 0.714  | 0.618  | 0.962    | 0.991  | 0.852   | 3.37E-04 | 0.030    | 0.958     | 0.009    |
| <b>Aperture Position</b>  | 0.008     | 0.910  | 0.711  | 0.603  | 0.962    | 0.991  | 0.735   | 0.008    | 0.134    | 0.116     | 1.98E-06 |
| <b>Aperture Size</b>      | 0.045     | 0.910  | 0.847  | 0.618  | 0.906    | 0.991  | 0.852   | 1.18E-04 | 6.27E-04 | 0.958     | 0.629    |
| <b>Aperture Shape</b>     | 0.045     | 0.910  | 0.711  | 0.633  | 0.005    | 0.991  | 0.735   | 0.106    | 0.007    | 0.563     | 0.133    |
| <b>relative Thickness</b> | 0.663     | 0.910  | 0.711  | 0.038  | 0.020    | 0.991  | 0.795   | 0.008    | 0.007    | 0.353     | 0.961    |
| <b>PC colour</b>          | 0.018     | 0.910  | 0.711  | 0.366  | 6.92E-05 | 0.991  | 0.735   | 0.903    | 0.028    | 0.958     | 0.961    |